Universitat Politècnica de Catalunya

Nanomaterials for controlling bacterial pathogens and resistance occurrence

LbL decoration of biopolymers and QQ enzymes onto active NPs

Targeted NCs for selective bacterial elimination

Advanced nanomaterials

Multilayer assemblies of biopolymers onto inert NPs

Hybrid metal/enzyme nanocoating for prevention of bacterial infections

In vivo biosafety

Live human cells

Biofilm prevention

Bacterial elimination

Aleksandra Ivanova

Nanomaterials for controlling bacterial pathogens and resistance occurrence

Aleksandra Asenova Ivanova

A thesis submitted in fulfilment of the requirements for degree of

Doctor of Philosophy

at the

Universitat Politècnica de Catalunya

Supervised by Dr. Tzanko Tzanov

Group of Molecular and Industrial Biotechnology (GBMI)

Department of Chemical Engineering

Universitat Politècnica de Catalunya

Terrassa (Barcelona)

2022

The work carried out during the thesis was financially supported by:

To my family,

"Hardship often prepares an ordinary person

for an extraordinary destiny"

Christopher Markus

"The energy of the mind is the essence of life"

Aristotle

Abstract

Infectious diseases are the leading cause of death worldwide, while the constantly raising antimicrobial resistance (AMR) is a major concern for the public health. During the infection establishment, bacterial pathogens communicate via expression of signaling molecules, controlled through a phenomenon called quorum sensing (QS). As a result of this, bacteria produce virulence factors and form resistant biofilms on living and non-living surfaces causing persistent infections. The infection complexity, especially in chronic diseases, requires the use of broad-spectrum antibiotics responsive for the appearance and the spread of drug resistant species. Infections caused by antibiotic-resistant pathogens are associated with high morbidity, mortality, and huge economic burden. Unlike the decrease over the past three decades of the number of novel marketed antimicrobial drugs, the number of antibiotic resistant bacterial strains steadily increases. Thus, there is an urgent need for development of alternative strategies to manage difficult-to-treat infections.

This thesis aims at the engineering of advanced nano-enabled materials and nanostructured coatings for controlling bacterial pathogenesis and resistance occurrence. To achieve this, biopolymers, antibiofilm and anti-infective enzymes, and inorganic compounds were nano-hybridized as alternative modalities to the conventional antibiotics. The nanoform was able to provide enhanced interaction with bacterial cell membranes and easier penetration into biofilms, increasing the antimicrobial efficacy at lower dosages, while preventing from development of antimicrobial resistance. Additionally, specific targeting moieties increased the nanomaterial's interaction with the pathogens, avoiding the drug resistance appearance and cytotoxicity.

The first part of the thesis describes the functionalization of biologically inert nanoparticles (NPs) with membrane disturbing antimicrobial aminocellulose (AM) and biocompatible hyaluronic acid (HA) in a layer-by-layer (LbL) fashion for elimination of medically relevant pathogens. The generated nanoentities demonstrated high potential to inhibit the biofilm formation, without affecting the human cell viability.

Further, the LbL technique was applied to decorate antimicrobial, but potentially toxic silver (Ag) nano-templates with biocompatible AM and quorum quenching (QQ) acylase in order to obtain safe antibacterial and antibiofilm nanomaterials. The deposition of acylase and AM on the Ag core interfered with the QS signaling and

bacterial pathogenesis, and enhanced the NPs interaction with the bacterial membrane. The integration of triple mechanisms of action in the hybrid nanoentities resulted in complete bacteria and biofilm eradication and improved biocompatibility of the AgNPs.

The thesis also describes the development of targeted nanocapsules (NCs) for selective elimination of *Staphylococcus aureus*. Herein, self-assembling nanoencapsulation technology using the biocompatible and biodegradable protein zein was applied for the generation of zein NCs loaded with bactericidal oregano essential oil (EO). An antibody specifically targeting *S. aureus* was covalently grafted on the NCs surface. The obtained targeted NCs demonstrated antibacterial selectivity in a mixed bacterial inoculum, and the treatment efficacy was validated in an *in vitro* coculture model of bacteria and mammalian cells.

Finally, high intensity ultrasound (US) process was employed for engineering of durable antibacterial/antibiofilm coating on urinary catheters. The simultaneous deposition of zinc oxide (ZnO) NPs and a matrix-degrading amylase enzyme improved the NPs adhesion on the silicone material, and prevented its bacterial colonization and biofilm formation *in vitro*. The hybrid nanostructured coating prevented the occurrence of early onset urinary tract infections (UTIs) and showed excellent biosafety in an *in vivo* animal model.

Key words: biopolymers, enzymes, essential oils, metal nanoparticles, Layer-by-Layer assembly, sonochemistry, bacteria targeting, antibacterial and antibiofilm properties, antibiotic resistance

Table of Contents

Abbreviation list

A

AAPH	2, 2-azobis (2-amidino-propane) dihydrochloride
A. baumannii	*Acinetobacter baumannii*
AIs	autoinducers
AIPs	auto-inducing peptides
pro-AIP	auto-inducing peptide precursor
Ag	silver
$AgNO_3$	silver nitrate
Agr	accessory gene regulator
A. tumefaciens	*Agrobacterium tumefaciens*
AHLs	acyl-homoserine lactones
AM	aminocellulose
AMR	antimicrobial resistance
ANOVA	a one way analysis of variance
ATCC	American type culture collection
A. melleus	*Aspergillus melleus*
Au	gold

B

B. cereus	*Bacillus cereus*
B. mycoides	*Bacillus mycoides*
B. subtilis	*Bacillus subtilis*
B. thuringiensis	*Bacillus thuringiensis*
BSA	bovine serum albumin

C

C_6-HSL	N-hexanoyl-L-homoserine lactone
CaO	calcium oxide
CAUTIs	catheters-associated urinary tract infections
C. albicans	*Candida albicans*
CECT	Spanish type culture collection
CFU	colony-forming unit
CO_2	carbon dioxide
C. violaceum	*Chromobacterium violaceum*
CVC	central venous catheters
CuO	copper oxide

D

DCFDA	2′, 7′-dichlorofluorescin diacetate
DCFHDA	dichlorodihydrofluorescein diacetate
DLS	dynamic light scattering
DMEM	Dulbecco's modified Eagle's medium
DMSO	dimethyl sulfoxide
DNA	deoxyribonucleic acid
DNase I	deoxyribonuclease I
DNS	3, 5-dinitrosalicylic acid

E

E. coli	*Escherichia coli*
eDNA	extracellular deoxyribonucleic acid
EDTA	ethylenediaminetetraacetic acid

EDX	energy dispersive X-ray
EE	encapsulation efficiency
E. faecalis	*Enterococcus faecalis*
EO	essential oils
EPM	extracellular polymeric matrix
EPS	exopolysaccharide
F	
Fe_3O_4	iron oxide
FITC	fluorescein isothiocyanate
H	
HA	hyaluronic acid
HCl	hydrochloric acid
HNO_3	nitric acid
HPLC	high-performance liquid chromatography
HRSEM	high resolution scanning electron microscopy
I	
ICP	inductively coupled plasma
IUPAC	International Union of Pure and Applied Chemistry
K	
K. pneumoniae	*Klebsiella pneumoniae*
L	
LB	Luria Bertani broth
LbL	layer-by-layer
M	

MBEC	Minimum Biofilm Eradication Concentration
MBIC	Minimum Biofilm Inhibitory Concentration
MDR	multidrug resistance
MgO	magnesium oxide
MIC	Minimum Inhibitory Concentration
MHB	Mueller Hinton broth
MRSA	multidrug resistant *Staphylococcus aureus*

N

NAMET	N-acetyl-L-methionine
NB	nutrient broth
NCs	nanocapsules
NPs	nanoparticles
NTA	nanoparticles tracking analysis

O

OD	optical density

P

P. aeruginosa	*Pseudomonas aeruginosa*
PB	phosphate buffer
PBS	phosphate buffered saline
PE	L-α-phosphatidylethanolamine
PI	propidium iodide
PMMA	poly (methacrylic acid)
Pt	platinum

Q

QCM-D	quartz crystal microbalance with dissipation
QQ	quorum quenching
QS	quorum sensing

R

RNA	ribonucleic acid
RIP	RNAIII inhibiting peptide
ROS	reactive oxygen species
RT	room temperature

S

SEM	scanning electron microscopy
S. aureus	*Staphylococcus aureus*
S. epidermidis	*Staphylococcus epidermidis*
STEM	scanning transmission electron microscope

T

TEM	transmission electron microscopy
Ti	titanium
TiO_2	titanium dioxide
TSB	tryptic soy broth

U

US	ultrasound
UTIs	urinary tract infections
UV	ultraviolet

Z

ZnO	zinc oxide

Figure, Scheme, and Table Captions

1 Introduction

In the past decades, the discovery of antibiotics has been a breakthrough in the management of infectious diseases.[1] However, the AMR is a natural evolutionary response whereby bacteria evoke mechanisms to overcome the antimicrobial therapies.[2] The AMR is now described as the "silent pandemic" of 21st century, associated with impaired treatment and prevention of infections caused by parasites, fungi, bacteria, and viruses.[3] The misuse and overuse of antibiotics led to the appearance of multidrug resistance (MDR) strains capable to withstand the effects of the conventional antimicrobials.[4] The high incidence of MDR is responsible for 700 000 deaths annually worldwide and is expected to grow to 10 million deaths by 2050.[5,6] Moreover, bacteria have affinity to attach and colonize surfaces, such as those of indwelling devices, tissues, and organs, forming microbial communities, called biofilms, which are up to 1000 times more resistant to the existing antibiotics than the free-floating cells.[7] In these communities, the bacterial cells are protected by multi-layered self-produced extracellular polymeric matrix (EPM), able to restrict the antibiotic penetration, causing severe chronic infections.[8] Frequently, the treatment of biofilm-related infections involves intensive antibiotic therapies, associated with side effects, such as inflammatory response or cytotoxicity.[9] Given the growing impact of antibiotic resistance, there is an urgent need to develop novel non-antibiotic antibacterial strategies with different mechanisms of action to outsmart the bacterial evolutionary mechanisms and resistance occurrence.

Significant attention has been posed to the nanotechnology as a novel emerging branch for engineering of non-conventional antibacterial chemotherapies to tackle the current challenges for managing the MDR and bacterial diseases.[10] Natural polymers and natural-occurring compounds have received considerable attention due to their antibacterial features and are suggested as powerful alternatives for controlling bacterial infections.[11,12] Furthermore, approaches which interfere with the bacterial pathogenesis-regulating QS system, make the bacteria more susceptible to antibacterial agents and the host immune system, reducing the risk of resistance development.[13] The nanoformulation of materials and their targeted delivery may overcome most of the limitations of the traditional bulk therapeutics with the same composition, and improve their antibacterial activity and therapeutic index.[14,15]

In this thesis, innovative highly efficient antibiotic-free nano-composites and nanocoatings were developed for prevention and reduction of bacterial

contamination and biofilm formation, minimizing the spread of drug resistance. This was achieved by an innovative platform of: i) hybrid assemblies of antibacterial and antifouling (bio)polymers onto inert NP template, ii) hybrid nano-assemblies of QQ enzymes/antibacterial polymers onto active NP template, iii) antibody-enabled NCs for targeted drug delivery and selective bacterial elimination, and iv) hybrid nanocomposite coatings of bactericidal metal/antibiofilm enzyme NPs for prevention of bacterial infections.

The rationale of these innovative nano-enabled materials and coatings for infection control was based on the synergy of:

> *Biopolymers* with intrinsic antimicrobial activity hybridized with inorganic and polymeric NPs able to eradicate the pathogens through unspecific interactions with bacterial cell membranes.

> *Anti-biofilm and anti-infective enzymes* to break down the QS signals in the extracellular space of Gram-negative, unlike conventional biocides, and inhibit the virulence and capacity of bacteria to establish biofilms. Combination of these enzymes with inorganic NPs, adding a new mechanism to their action- a membrane disturbing capacity due to the nanoform- will further reduce the possibility of resistance development.

> *Biofilm matrix-degrading enzymes* that degrade the adhesive components of the EPM weakening and dispersing the biofilm. Enzyme induced EPM degradation will significantly reduce the biofilm occurrence and increase the susceptibility of both Gram-negative and Gram-positive bacteria to antimicrobials.

> *Nano-sized* combination of the new antimicrobials *with targeting moieties* will allow the development of highly potent and specific targeted nanosystems able to address both evolutionary and cooperatively acquired AMR. Such therapeutic approach was expected to eliminate the targeted pathogen, exerting less selective pressure for resistance development, lowering the side effects to human cells and maintaining the microbiome balanced.

2 State-of-the-art

2.1 Antimicrobial resistance

AMR and the spread of drug-resistant pathogens with new resistance mechanisms have emerged as a major public health issue of the 21st century that threatens the effective prevention and treatment of bacterial infections.[16] Since the number of drug-resistant strains constantly increases, while novel and efficient antimicrobials are not entering the market, there is a serious concern about the dramatically growing number of untreatable infections.[16] AMR infections are the main reason for the increased morbidity and mortality in the healthcare facilities, longer hospital stays, and elevated financial burden worldwide.[17] Assessment of the future impact of AMR predicts almost 10 million deaths annually worldwide by 2050 if new antibiotic alternatives are not developed.[5] The antibiotic over usage is interconnected with the transmission of AMR to the humans via animal products as well. Diverse studies have reported that the antibiotic administration duration, the selected drug, and the indications are irrelevant in 30-50 % of the prescribed antibiotic therapies. Moreover, the antibiotics are applied as growth promoters in livestock.[18] The majority of nosocomial infections or hospital-acquired infections occurs after the patient received healthcare treatment.[19] The patient's exposure to the microorganisms in the hospital settings, to medical personnel or visitors, increases the risk of infections occurrence within 48 h after hospital admission, or in up to 30 days after surgery.[20] Besides, the risk of infections with MDR pathogen is increased in patients with compromised health conditions, such as cancer, diabetes, human immunodeficiency virus, and renal failure.[21,22] Some drug-resistant bacteria can infect children, immunodeficient patients, and elderly, causing worse clinical outcomes or death.[23]

Bacteria possess multiple mechanisms to evade the actions of antibiotics. This AMR can be intrinsic (naturally occurred) or acquired (caused by the mutations in the genetic materials).[24] The intrinsic form of resistance is inherent and specific class of antibiotics can be ineffective against certain bacterial specie.[23] The outer membrane of the cell wall in Gram-negative bacteria and the efflux pumps are the most common intrinsic drug resistant mechanisms.[22] Gram-negative bacteria demonstrate intrinsic resistance to glycopeptide antibiotics, e.g. vancomycin, due to its incapability to pass through the outer cell membrane.[22] For example, triclosan has been widely used against Gram-positive bacteria and some Gram-negative species; however, it is inactive against *Pseudomonas* due to its intrinsic resistance to this bactericidal agent.[18]

The antibiotics act against bacteria through obstructing certain targets, such as nucleic acid replication or protein and cell wall synthesis[25] (**Figure 2.1**). The bacterial pathogens can develop several acquired resistant mechanisms that can "neutralize" the antibiotic action, such as altering the drug target site and enzymatic degradation of the drugs.[26] The bacteria secrete enzymes, e.g. β-lactamases, phosphorylases, adenylases, and acetylases that can modify and destroy the antibiotic structure.

The antibiotics, depending on the class, act by binding to a specific site in the selected bacteria. The evocation of changes in the structure of the targeted site may cause drug disability for binding to the target.[27] Additionally, the bacteria have evoked multiple mutations that led to development of MDR, generally defined as "superbugs", associated with the occurrence of severe infections. This form of resistance is related to mutations in the bacterial genome, which mutations can be in the bacterial chromosomal deoxyribonucleic acid (DNA) or can be acquired genetically, and subsequently transferred to the next generation of bacteria.[24]
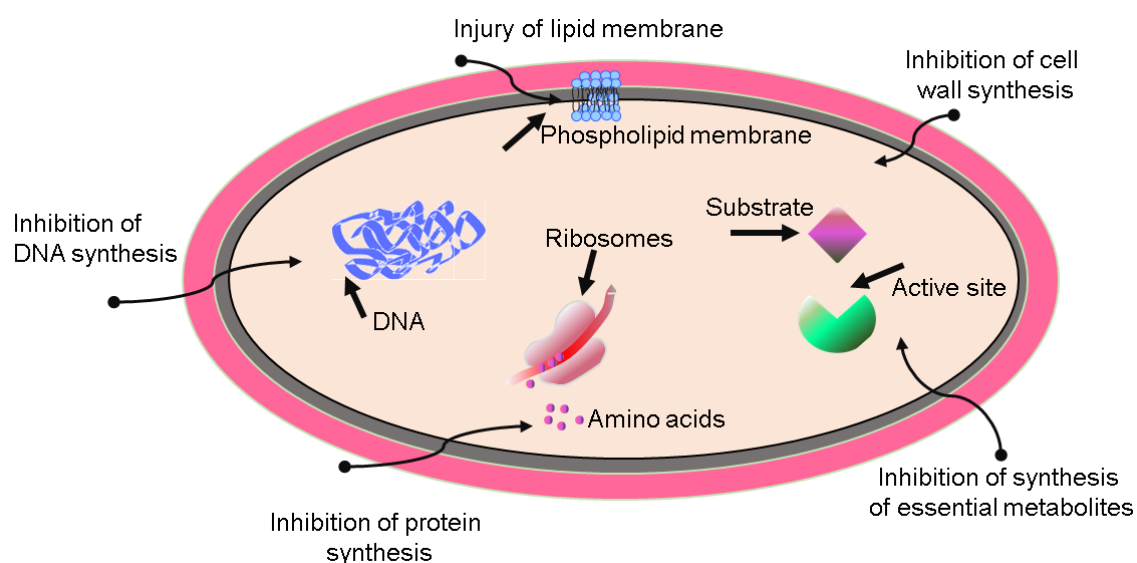
Figure 2. 1 Mechanisms of antibiotic action. Antibiotics are able to inhibit the cell wall synthesis or injure the bacterial cell membrane. Other targets are the synthesis of essential metabolites, DNA and protein synthesis.

S. aureus is one of the most common Gram-positive pathogens responsible for serious nosocomial infections, including skin, bloodstream, and surgical wound infections.

Staphylococci sp., producing penicillinase acount for more than 90 % of the patient isolates, making the penicillin no longer usable for treatment of staphylococcal infections.[28] Furthermore, the appearance of methicillin-resistant *S. aureus* (MRSA) strains is the main clinical problem and one of the leading cause for the high incidence of nosocomial infections. Meta analytical studies reported that MRSA bacteremia is associated with a significant increase in mortality and prolonged hospitalization among patients with bloodstream infections.[29] Methicillin-resistant staphylococci are sensitive only to small number of antibacterial agents and often are characterized with MDR to large number of antibiotics such as macrolides, β-lactams, lincosamides, aminoglycosides, and tetracycline.[30] The continuous growth of drug-resistance community-acquired MRSA and the decreased susceptibility of MRSA to the main antibiotic vancomycin used for staphylococcal infections is an urgent matter for the public healthcare.[18] Additionally, of great concern are the *Escherichia coli* and nontyphoidal *Salmonella* resistance to fluoroquinolones, impairing the treatment of UTIs and diarrhea, respectively. Currently, many species of tuberculosis, staphylococci, and pneumococci are insusceptible to most of the existing antibiotics, increasing the economic and human burden.[31]

2.2 Bacterial biofilms and quorum sensing system
2.2.1 Biofilms and biofilm-related bacterial resistance

Bacteria adhere on living or non-living surfaces forming communities of cells encased in self-produced EPM, called biofilms.[32] The bacterial transformation from planktonic to sessile mode of growth involves multiple and complex processes (**Figure 2.2**). During the first stage, the bacterial cells not adhered to the surface are susceptible to antibiotics. The free-floating bacteria interact with solid surfaces via pili, flagella, fimbriae, and production of exopolysaccharide (EPS), leading to bacterial attachment and formation of micro-colonies. The EPM substances secreted around the colonies comprise mainly polysaccharides (50-90 %), extracellular DNA (eDNA), lipids, and proteins. The pathogen proliferation and the secretion of EPM components result in establishment of three-dimensional mature biofilm structures. Subsequently, the morphology and topography of these biofilm structure alter and the pathogens disperse from the biofilm colonizing other solid surfaces.[32]
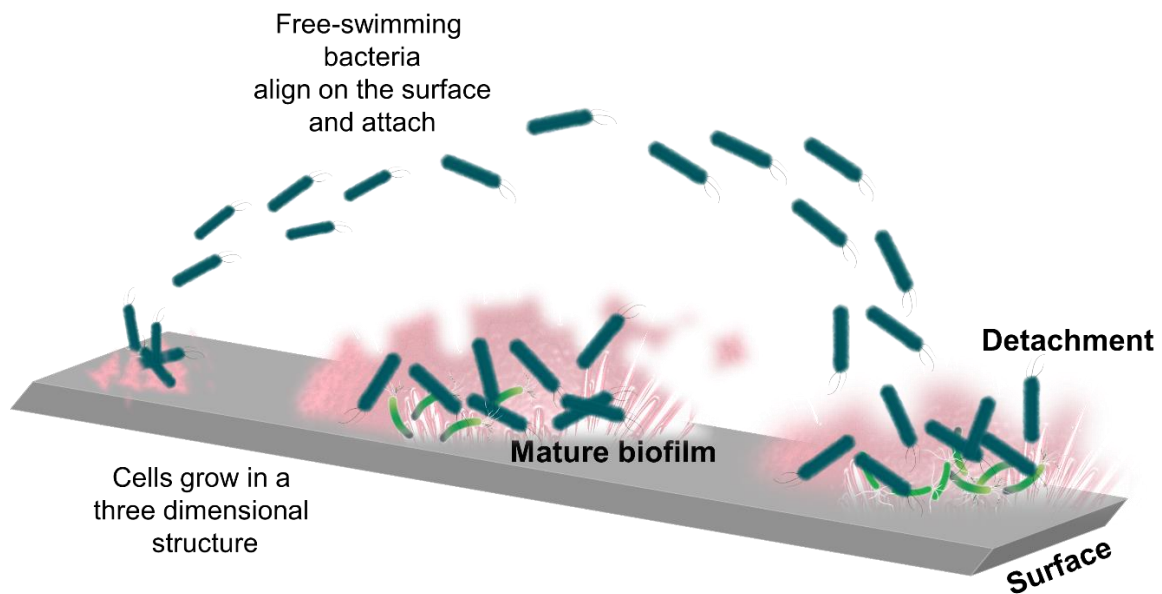
Figure 2. 2 Biofilm growth cycle. Initially the free-floating bacterial cells attach to a solid surface, and secrete matrix components, leading to formation of mature biofilm structure. Finally, parts of the established biofilm and bacteria are dispersed in the surrounded environment able to attach and colonize new surfaces and start the biofilm cycle again.

An increased percentage of bacterial planktonic cells is already resistant to most of the existing antibiotics; however, their biofilm-mode of growth is even more challenging for eradication by the available therapeutics. The formation of the densely packed EPM makes the cells within the biofilm 100 to 1000 times more insusceptible to antibacterials, than their free-floating counterparts.[33] The formation of biofilms is responsible for more than 60 % of infectious diseases such as cystic fibrosis, sepsis, otitis, endocarditis, chronic wounds, periodontitis, and dental caries.[34] The treatment of biofilm-associated infections involves the combination of various antibiotics at high dosages.[35] The Gram-negative *E. coli*, *Klebsiella pneumoniae*, *Pseudomonas aeruginosa* and *Proteus mirabilis*, and the Gram-positive *Enterococcus faecalis*, *S. aureus*, *Staphylococcus epidermidis*, as well as the yeast *Candida albicans*, are among the most common biofilm forming species found in severe and persistent nosocomial infections.[36] Several mechanisms, such as limited drug penetration, decelerated bacterial growth in the biofilm structure, and enzyme drug neutralization have been proposed for the high level of biofilm-related bacterial resistant nature.[32] *P. aeruginosa* is an opportunistic Gram-negative bacterium able to form drug resistant biofilms, responsible for cutaneous wound infections and chronic leg ulcers.[37] The alginate-producing *P.*

aeruginosa and mucoid-biofilms in the patient's lungs cause persistent and chronic infections, associated with increased morbidity and mortality.[38] The presence of EPM reduces the aminoglycosides and fluoroquinolones penetration, allowing the pathogen to respond to the stress via acquired defensive mechanisms. For example, the secretion of cephalosporinase AmpC enzymes in cystic fibrosis is responsible for the *P. aeruginosa* resistance to β-lactam.[32] Another study proposed that EPM could retard the drug penetration and trigger the expression of genes that induce drug resistance and genetic adaptation to various conditions.[39] In similar fashion, the biofilm matrix can limit the nutrient availability to the bacterial cells, decelerating the growth rate, and increasing the antibiotic resistance. Several antibiotics such as ampicillin and penicillin can act only when bacterial cells are growing. The Gram-negative *E. coli* and *P. aeruginosa* have demonstrated resistance to cetrimide and tobramycin, respectively due to the slow bacterial growth.[32] Despite growing in single strain biofilms, these bacterial species are also able to communicate and interact, forming even more resistant sessile structures. For example, the Gram-positive *S. aureus* colonizes chronic wounds and frequently forms mixed-species biofilm structures in infectious conditions.[40]

The frequent usage of indwelling devices, medical contact lenses, organ transplantation, and intervention therapies led to an increased occurrence of nosocomial infections heavily affecting the patients with serious illnesses. The most common infections in intensive care hospital facilities are the UTIs (40 %),[41] bloodstream infections (10.5 %), skin and soft tissue infections (6.7 %),[42] respiratory tract infections and pneumonia (22.8 %), surgical-site infections (15.7 %),[36] associated with drug resistant biofilms. For instance, patients with long-term inserted central venous catheters (CVC) have an increased risk of bloodstream infections. It has been reported that the bacterial pathogens colonized the CVC already after one day of catheterization.[36,43] Bacteria have affinity to attach to endotracheal tubes, forming drug resistant biofilms within 24 h causing ventilator-associated pneumonia, leading to prolonged hospitalization and increased mortality rates.[36] Surgical-site infections due to Staphylococcus sp. are frequently occurring within 30 days after the surgery.[44] The catheter-associated UTIs (CAUTIs) account for 80 % of all UTIs and are the main cause of prolonged hospitalization and increased risk of resistance occurrence. The bacterial pathogens have affinity for colonization of catheter's surface and can easily enter in contact with tissues and organs, leading to occurrence of UTIs. The bacteria can gain access to the

patient's body during the catheter insertion, or from the urethral meatus together with the catheter-urethral interface, or due to contamination of the drainage system. Upon insertion, the indwelling urinary catheters provide a suitable surface for pathogenic colonization. Furthermore, during the catheterization, the device may cause damage of the uroepithelial mucosa, favoring the bacteria to attach on new surfaces.[45] Several studies reported that the insertion of indwelling urinary catheter increased the risk of infection appearance by 10 % in the urethra, bladder or kidney, and 10-50 % of the patients have developed asymptomatic bacteriuria after the short-term catheterization (0-2 weeks).[36,46]

2.2.2 Quorum sensing systems in bacteria

Bacteria have the ability to "talk" in a cell density dependent manner through a process called QS.[47] It has been reported that the microbial pathogenesis and biofilm formation is under the control of the QS system. In QS, bacteria release signaling molecules-autoinducers (AIs)-into their surrounding that after reaching high concentrations are recognized by the intracellular receptors of Gram-negative or the membrane receptors of Gram-positive bacteria. The signals for cells communication are different in Gram-negative and Gram-positive bacteria. Gram-negative bacteria use acyl-homoserine lactones (AHLs),[48,49] while Gram-positive bacteria produce oligopeptides, termed autoinducing peptides (AIPs) (**Figure 2.3A**).[50] There is also a third QS signal type, AI-2, which is found in both bacteria, and have gained the interest as target to control multispecies infections.[51]

The QS signals of Gram-negative bacteria are produced by LuxI-type AHL synthases, using AHL precursors acyl-acyl carrier protein and S-adenosyl-methionine. The signals accumulate and saturate in the extracellular environment and when the concentrations are above the threshold level they pass through the cell membrane via diffusion.[52,53] Once in the cells, the AHLs conjugate to specific QS transcription regulators, frequently from the LuxR family, which in turn promote the target genes expression (**Figure 2.3A**).[53] Unlike the communication system in Gram-negative bacteria, the signals for Gram-positive bacteria are small AIPs that are post-translationally synthesized in the bacterial cells and subsequently exported through specific membrane bound transporters. When their concentration exceeds the threshold level, these peptides bind to a two-component histidine kinase sensor, which auto-phophorylates and in turns alter

the target genes expression and corresponding group related behaviors **(Figure 2.3B)**. The QS system in *S. aureus*, for example, is under the control of the accessory gene regulator (*agr*) locus which encodes the AIPs secretion.[54,55] The *agr* system regulates the expression of many toxins and degradative exoenzymes, predominantly controlled by P2 and P3 promoters, producing two divergent transcripts respectively RNAII and RNAIII.[56]The RNAII transcript is composed of four genes -*agrA, agrB, agrC* and *agrD* -encoding the production of AIP precursors, the signal maturation and its transduction by histidine kinase. The RNAIII is an intracellular effector molecule and is responsible for the upregulation of α-haemolysin and proteases, as well as for the downregulation of surface proteins, such as protein A among others. [57,58]

Except for the interspecies way of talking, bacteria possess the ability to "understand" the messages sent by other species present in the environment.[59] In this case, they use another type of QS molecules procured from 4, 5-dihydroxy-2, 3-pentanedione, also termed AI-2 interspecies signal. The synthesis of AI-2 signal, obtained from S-ribosylhomocysteine is catalyzed by the LuxS type synthase involved in the regulation of the AI-2 QS system in multiple bacterial species.[60] LuxS, for example controls the expression of over 400 genes involved in surface adhesion, motility and toxin production by *E. coli*. [61]
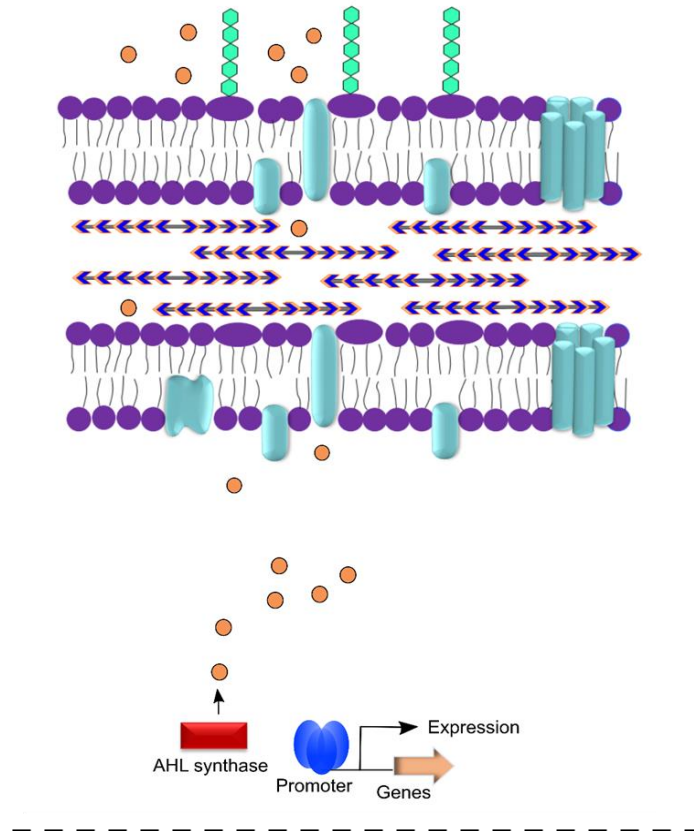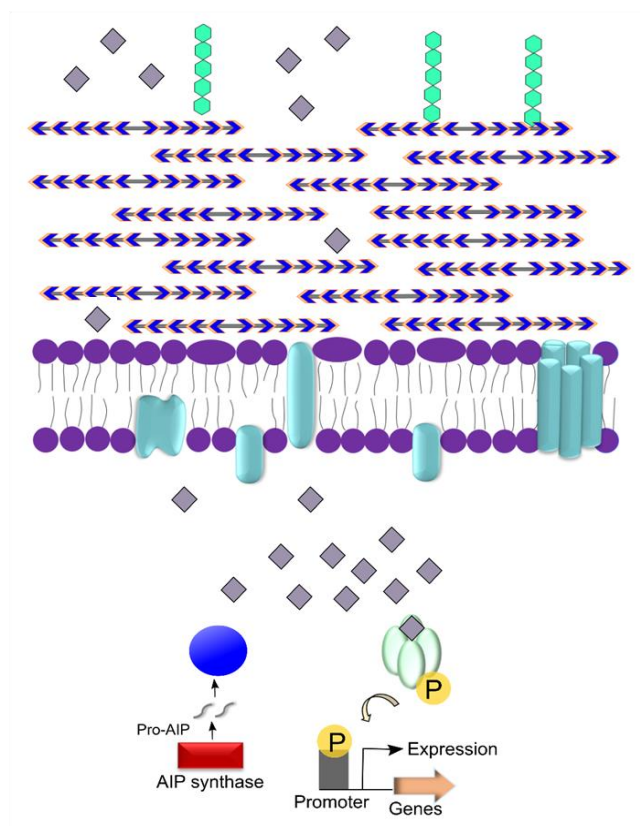
Figure 2. 3 QS signaling in Gram-negative (A) and Gram-positive bacteria (B). In Gram-negative bacteria, AHL QS signals (orange circles) are produced by AHL synthases (red rectangle) and secreted in the cells surrounding. When the concentration of AHLs in the

surrounding is above the threshold, the signals pass through the cell membrane via diffusion and activate specific AHL receptors (blue motif), promoting the target genes expression. In Gram-positive bacteria, small AIPs (grey pentagons) are post-translationally synthesized in the cells and exported through specific membrane bound transporters (light blue motif). At threshold level, AIPs bind to a two-component histidine kinase sensor, which auto-phosphorylates and alters the target genes expression.

2.3 Therapeutic strategies to manage bacterial infections and antibiotic resistance

The usage of antibiotics to treat and control bacterial infections has a huge impact on the public healthcare. However, the misuse or overuse of antimicrobial agents progressively led to development of drug resistance and occurrence of life-threatening infections.[62] The ability of bacteria to encase in self-produced EPM onto medical devices or living tissues is associated with severe bacterial infections with restricted antibiotic efficacy and resistance to the host defense mechanisms.[63] The current strategies to prevent and treat drug-resistant infections involve prolonged administration of aggressive combinations of antibiotics. However, these intensive therapies may provoke hypersensibility, cytotoxicity, inflammatory response or development of MDR bacterial strains.[64] Taking into consideration the failure of conventional antibiotics, the spread of AMR, drug resistant biofilms, and the small pipeline of novel therapies, there is an urgent need for development of new efficient antimicrobial alternatives with different mechanisms of action. Effective strategies for prevention and treatment of bacterial infections with lower risk of resistance appearance should integrate: i) bacterial eradication without creating selective pressure for development of new resistant mechanisms,[65] ii) prevention and elimination of biofilm formation,[66,67] iii) biocompatibility, protection of the beneficial strains and host environment,[68] iv) long-term stability.[69] Targeting the essential for bacterial pathogenesis QS system and biofilm matrix are viable alternatives to impair the bacterial virulence and biofilms formation.[70] Significant efforts have been directed to the application of natural and synthetic materials due to their broad-spectrum antibacterial activity and biocompatibility.[71] Taking into account the key factors involved in the drug resistance occurrence, the combination of different actives with complementary modes of action is a new paradigm for designing biosafety highly effective therapeutics. Thus, special attention is devoted to the nano-sized hybrid materials and targeted nanoentities as promising therapies for overcoming the current antibiotic challenges in treating infectious diseases without inducing toxicity to mammalian cells and beneficent flora.[72]

The nanomaterials possess several advantages over their bulk counterparts, such as enhanced antibacterial efficacy and lower risk of resistance development. Moreover, the development of nanostructured coatings onto medical devices, hindering the bacterial viability and mitigating the bacterial colonization, is an innovative approach for prevention and control of device-associated infections.[14]

2.3.1 Anti-virulent strategies-inhibition of bacterial pathogenesis

Targeting QS system is an attractive strategy to reduce the QS-controlled virulence factors expression and prevent biofilm formation, without affecting the bacterial growth, making the pathogens more susceptible to the antibiotics and host immune response.[73,74] Recently, numerous anti-QS compounds, altering the pathogenic behavior, without inhibiting the bacterial growth have been developed. Different strategies interfering QS process have been developed as new alternatives to tackle the antibiotic challenges in managing infectious diseases.

Table 2. 1 Common QS inhibitors and their application in infection control.

Compound	Mechanism of action	Main achievements
Adenosyl-homocysteine	Inhibition of AHL synthesis in P. aeruginosa	Attenuation of QS regulated toxins secretion and prevention of bacterial infections [75]
Lactonase	AHLs lactone ring hydrolysis	Inhibition of *Vibrio parahaemolyticus* biofilm growth and intestinal colonization in shrimp [76]
Acylase	AHLs amide bond hydrolysis	Coating of medical devices for controlling biofilm related urinary tract infections[77]
Flavanoids	Blocking the QS receptors	Suggested as alternatives to the traditional antibiotics for treatment of *P. aeruginosa* associated infectious diseases

Structural analogue of AHL signal	Blocking the QS receptors	Attenuation of *P. aeruginosa* pathogenesis through the decreased production of rhamnolipids, elastase and protease by the bacterium[78]
RNAIII-inhibiting peptide (RIP)	Inactivating staphylococcal TRAP/agr system	Grafting on urinary stents to counteract *S. aureus* urinary tract infections [79]
Curcumin with antibiotics	Synergistic mechanism of action	Development of combined therapy against bacterial pathogens [80]

For example, LuxI, HdtS and LuxM are identified as signal producers in Gram-negative bacteria.[81] In particular, LuxI has been found in many bacterial strains and has been investigated as a potential target to control toxins secretion and biofilm formation. It has been reported that compounds such as S-adenosylhomocysteine, butyryl-S-adenosyl methione and sinefungin inhibit the *in vitro* AHL synthesis in pathogenic *P. aeruginosa*.[75] Chang and co-authors have reported that trans-cinnamaldehyde was able to efficiently inhibit the AHL production by Rhl QS system in *P. aeruginosa*. In addition, trans-cinnamaldehyde could reduce the pyocyanin production in *P. aeruginosa* by up to 40 % without affecting the normal bacterial growth.[82]

Altering the QS signals in the extracellular environment is among the most promising anti-QS approaches, avoiding the need to penetrate the cells and reach the specific signal receptors. Several enzymes degrading the AIs have been reported until now. They are produced by bacterial strains such as *Bacillus* strain COT1, *Bacillus* sp. 240B1, *Agrobacterium tumefaciens, Arthrobacter* sp. IBN110, *Bacillus cereus*, *Bacillus mycoides*, *Rhodococcus*, *Anabaena*, *Ralstonia*, *Bacillus thuringiensis*, and *Streptomyces* sp.[83]

Bacillus sp. possess aiiA that encodes AHL-inactivating enzyme lactonase. Lactonase inhibits the QS regulated virulence in various Gram-negative pathogens via the hydrolysis of the AHLs lactone ring.[84] AHL lactonase, from metallo-β-lactamase superfamily has been identified recently and characterized by Tang *et al*. The enzyme has the ability to decompose AHLs with different side chain length, with or without oxo-group at the position C-3.[85] The lactonase did not affect the bacterial cells viability,

but has the ability to increase the bactericidal activity of antibiotics and reduce the sessile growth of *P. aeruginosa* and *Acinetobacter baumannii*.[86] The QS inhibition by lactonase has been utilized as a tool to boost the activity of gentamicin and ciprofloxacin towards the drug-resistant biofilm forms of *P. aeruginosa*.[87] Furthermore, the synergistic effect with ciprofloxacin has been demonstrated against *P. aeruginosa* PAO1 in a burn infection model on mice. Topical application of gels containing the anti-QS enzyme lactonase inhibited the spread of skin pathogens and reduced to minimum the mice mortality after the addition of lower antibiotic dosage.[88]

Some bacterial strains such as *Variovorax paradoxus and Ralstonia sp*. produce another AHL-degrading enzyme, named acylase. Acylase hydrolyzes the amide bond of the AHLs and interrupts the QS pathways in plant and human pathogens.[83] Acylase expression in pathogenic *P. aeruginosa* PAO1 significantly reduced the production of pyocyanin and elastase, declined the bacterium swarming motility and weakened its pathogensis *in vivo* in *C. elegans* infection model.[89] In our group, silicone urinary catheters have been coated with fungal acylase from *Aspergillus melleus* using the LbL technique. The acylase-coated catheters disrupted the AHLs based QS signaling and inhibited *P. aeruginosa* biofilm development *in vitro* under conditions simulating the real situation during catheterization.[90] Our group developed multi-enzymatic coatings on silicone catheters comprised of acylase and another hydrolytic enzyme amylase, which acts on the bacterial exopolysaccharides. The generated enzyme coatings demonstrated better antibiofilm activity depending on the outer layer (acylase *vs* amylase). The coatings with acylase as uppermost layer inactivated the QS signals and demonstrated higher antibiofilm activity against *P. aeruginosa* and *E. coli* single and dual species cultures. The enzymes multilayers could delay the *in vivo* biofilm formation in a catheterized rabbit model.[77]

Numerous components blocking the QS receptors have been described. Recently, it has been demonstrated that flavonoids can bind to the QS receptors and significantly reduce their ability to activate the corresponding genes expression in *P. aeruginosa*.[91] Yang *et al*. reported a structural analogue of AHL signal, named N-decanoyl-L-homoserine benzyl ester that blocks the cognate receptor in *P. aeruginosa* and counteracts the production of rhamnolipids, elastase and protease, without killing the bacterial cells. The receptor antagonist also potentiated the antibacterial activity on various antibiotics, lowering their therapeutic concentrations for *P. aeruginosa* infections.[78] Loughlin *et al*.

synthesized metachloro-thiolactone, and meta-bromo-thiolactone, and demonstrated their anti-virulent potential through the inhibition of pyocyanin production. The last one not only could downregulate the virulence factors expression and biofilm formation, but also could protect *C. elegans* and human lung epithelial cells from the virulent *P. aeruginosa*.[92] Geske *et al*. have developed AHLs analogues that can bind to the LuxR, TraR and LasR receptors in *Vibrio fischeri*, *A. tumefaciens* and *P. aeruginosa*, respectively.[93] In another investigation, Kim *et al*. evaluated the potential of 6-gingerol for controlling bacterial pathogenesis and infections occurrence. The authors confirmed that this anti-QS compound was effective and can repress the QS genes involved in the exoprotease, rhamnolipid and pyocyanin production in *P. aeruginosa* .[94]

Targeting the *agr* operon in Gram-positive bacteria has received noteworthy attention. Changing the amino acids or removing the side chain of the AIPs have been shown as efficient methods for designing analogues that block the *agr* receptors.[95] RIP is another promising inhibitor targeting the staphylococcal TRAP/*agr* system. Animal model of rats treated with RIP demonstrated its role in preventing methicillin-resistant *S. aureus* infections. RIP has also been shown to be very effective in controlling biofilm related staphylococcal infections caused by the use of ureteral stents, central orthopedic implants, and venous catheters. The RIP deposition onto surface of the medical devices resulted in suppression of *S. aureus* biofilm formation.[79] Other investigations have been carried out to demonstrate the synergism of curcumin with antibiotics against *P. aeruginosa*. Drastic decrease of virulent QS-genes expression and mini- mum inhibitory concentrations of gentamicin and azithromycin was obtained when the actives were applied simultaneously.[80] These finding are considered significant, because the decrease of the toxins production will increase host defense as well as the efficiency of the antimicrobials, which is a promising strategy for treatment of infectious diseases.

2.3.2 Biofilm-disrupting enzymes

The disruption of the biofilm structure integrity may increase the bacterial susceptibility to antibacterial agents. Thus, targeting the essential for the biofilms EPM is another promising strategy to manage bacterial pathogenesis. Dispersin B is one of the most studied enzymes able to degrade the poly-N-acetylglucosamine polysaccharide, playing key role in the *Actinobacillus actinomycetemcomitans* attachment to the surfaces and conducting the bacterial resistance to host immune cells and antibacterial agents.

Pavlukhina *et al*. developed LbL matrices of poly (allylamine hydrochloride) and poly (methacrylic acid) (PMMA), cross-linked with glutaraldehyde and pH-triggered removal of PMAA, generating a stable poly (allylamine hydrochloride) hydrogel matrix, employed for loading of matrix-degrading dispersin B. The presence of the enzyme in the coating led to $\geq$ 98 % biofilm inhibition of two *S. epidermidis* strains compared to mock-loaded coatings, without affecting the human osteoblast cells attachment and growth.[96] In another study, dispersin B and antibacterial triclosan were deposited on the surface of vascular catheters. The developed hybrid coating demonstrated synergistic antibacterial and antibiofilm activities against *S. aureus*, *S. epidermidis*, and *E. coli*, compared to the pristine catheters.[97] Deoxyribonuclease I (DNase I) is another widely used enzyme, degrading the eDNA in biofilm matrix, showing negative impact on the biofilm structure of medically relevant pathogens such as *P. aeruginosa*, *E. coli*, *S. aureus*, and *K. pneumonia*. The employment of very low concentration of DNase I increased the bacterial susceptibility to cefotaxime, rifampin, ampicillin, azithromycin, and levofloxacin and increased the antibiotic efficacy.[98] Alginate lyase cleaves β-glycosidic bonds of alginate, presented in the biofilm matrix of *P. aeruginosa* and reduces the bacterial colonization in the lungs of patients with cystic fibrosis. The application of the enzyme in combination with antibiotics showed enhanced the antibacterial efficacy for managing bacterial infections such as cystic fibrosis, caused by *P. aeruginosa* infections.[99] The α-amylases have been demonstrated very strong antibiofilm activity towards Gram-positive *S. aureus*. The enzyme hydrolyzes the α-1,4-glycosidic linkages in polysaccharides in biofilm structures and dispersed the *S. aureus* mature biofilms within less than 30 min of contact.[100]

2.3.3 Antimicrobial polymers, biopolymers, and natural compounds

The antimicrobial polymers and biopolymers appeared as new promising agents against bacterial contamination in the healthcare, food and textile industry with minimalized risk of resistance development.[101] Natural polyphenols (e.g. gallic acid, tannic acid, curcumin)[102,103] and polysaccharides (e.g. chitosan)[104] have demonstrated strong bactericidal activities and are considered as efficient antimicrobial agents able to synergistically potentiate the bactericidal activities of the existing drugs at very low concentrations.

Biocidal polymer architectures are obtained by the polymerization of antibacterial cationic, anionic or neutral monomers.[105] Of particular interest is the engineering of cationic polymers, acting as contact active agents due to their ability to interact with the negatively charged bacterial cell wall membrane, causing bacterial cell to burst.[104] Generally, the engineered positively charged polymers have demonstrated selectivity to bacteria over the mammalian cells, mimicking the host-defense antibacterial peptides.[106] Poly(ε-lysine) and chitosan exhibit strong antibacterial properties due to their cationic nature and the availability of amino-bearing groups.[105] Several studies have reported that chitosan interacts electrostatically with the lipopolysaccharide of Gram-negative bacteria, causing membrane disturbance and perforation, leading to cell death. Moreover, the chitosan reduces the bacterial adhesion by affecting the protein adsorption on the pathogen surface.[107] Similarly, poly(ε-lysine) interact electrostatically with the bacterial membrane, causing membrane disruption integrity, pores formation that promoting the DNA binding associated with the generation of reactive oxygen species (ROS), causing cell death.[105] AM is considered as an efficacious antibacterial active able to disrupt the bacterial membrane through electrostatic interactions leading to permeability of the cell membrane, osmotic damage, cytoplasmic leakage and cell death.[104,108] The synthetic polymers have been reported as low-density antibacterial agents with lessen risk of resistance development.[109] Quaternary ammonium polymers and polyhexamethylene biguanides have been demonstrated strong bacterial elimination due to the electrostatic interaction between the ammonium groups and bacterial cell membrane, causing membrane damage and cell lysis.[110,111] Besides the contact killing polymers, the antimicrobial materials can be biocide-releasing polymers. Compounds containing N-halamine groups are associated with slow release of the halogens that react with the thiol or amino groups of bacterial cells, causing cell death.[112] Furthermore, polymers able to deliver reactive nitrogen species such as nitric acid have shown broad antibacterial activity and are explored with variety of materials like titanium (Ti)[113] or polystyrene for biomedical and water treatment applications.[114] Phospho- and sulfo-containing polymers disturb the bacterial cell membrane. For example, the phosphonium containing polycationic agents demonstrated strong bactericidal properties.[115]

Recently, the potential of natural compounds as novel therapeutic agents to combat bacterial resistance and infectious diseases was confirmed. EOs, plant extracts, and their

derivatives are secreted as secondary metabolites, generally recognized as safe and are widely exploited for multi-purpose applications in the food and pharmaceutical industries. Nowadays, the EOs are employed to various medical conditions such as stress, cancer, and infectious diseases.[116] The EOs of thyme, oregano, clove, rosemary, and cinnamon possess high antibacterial properties against Gram-positive and Gram-negative bacteria. The strong antibacterial activity was associated with the presence of carvacrol, eugenol, cinnamic aldehyde, and thymol. These plant-derived components have demonstrated antibacterial potential against *Vibrio vulnificus*, *E. coli*, *Listeria monocytogenes*, and *Salmonella typhimurium*.[117] EOs from coriander, basil, and oregano showed very strong inhibition towards *S. aureus* and *P. aeruginosa* at very low concentrations.[118] The proposed mechanisms of antibacterial action of EOs are various. The EOs are able to destabilize the cell membrane integrity, causing membrane permeability, disrupting the metabolic functions.[119] Furthermore, the EOs are reported to easily penetrate through the bacterial membranes due to their lipophilic nature, causing ions leakage and cell death. For example, tea three oil inhibited the *E. coli* and *S. aureus* growth due to altered cell permeability and loss of K+ ions.[119,120] The ability of the EOs to pass through the cell membrane may disarrange the membrane composition of polysaccharides and fatty acids. In similar fashion, the hydrophobic carvacrol affects the fatty acids composition and permeability of the cell membranes, leading to intracellular leakage and death. Likewise, citronellal and carveol have demonstrated to disrupt the bacterial cell integrity, causing K+ ions loss.[121] Such mechanisms of action are reported to have low risk of drug resistance development.[122]

2.3.4 Nano-enabled materials to manage bacterial infections and resistance development

Nano-sized materials are considered as a potential alternative to the conventional antibiotics and could mitigate the drug failure due to their unique physico-chemical properties such as greater surface area to volume ratio, size, chemical reactivity, biological mobility.[123] Several studies of nanovehicles have reported to be more effective towards MDR pathogens and biofilms, compared to their bulk solutions.[124,125]

Overall, the NPs may act via diverse mechanisms of action, such as disrupting the membrane integrity or ROS production (**Figure 2.4**).[126] NPs are capable to interact electrostatically with the bacterial cell membranes, causing membrane perforation,

interruption of membrane transport functions, cell leakage, and cell death.[126] The oxidative burst due to the large amount of ROS release causes damage to the cell organelles, DNA and ribonucleic acid (RNA), enzymatic inhibition, and alteration of macromolecules. The low ROS concentrations provoke mutations, whereas the high ROS concentrations lead to cell death.[127]
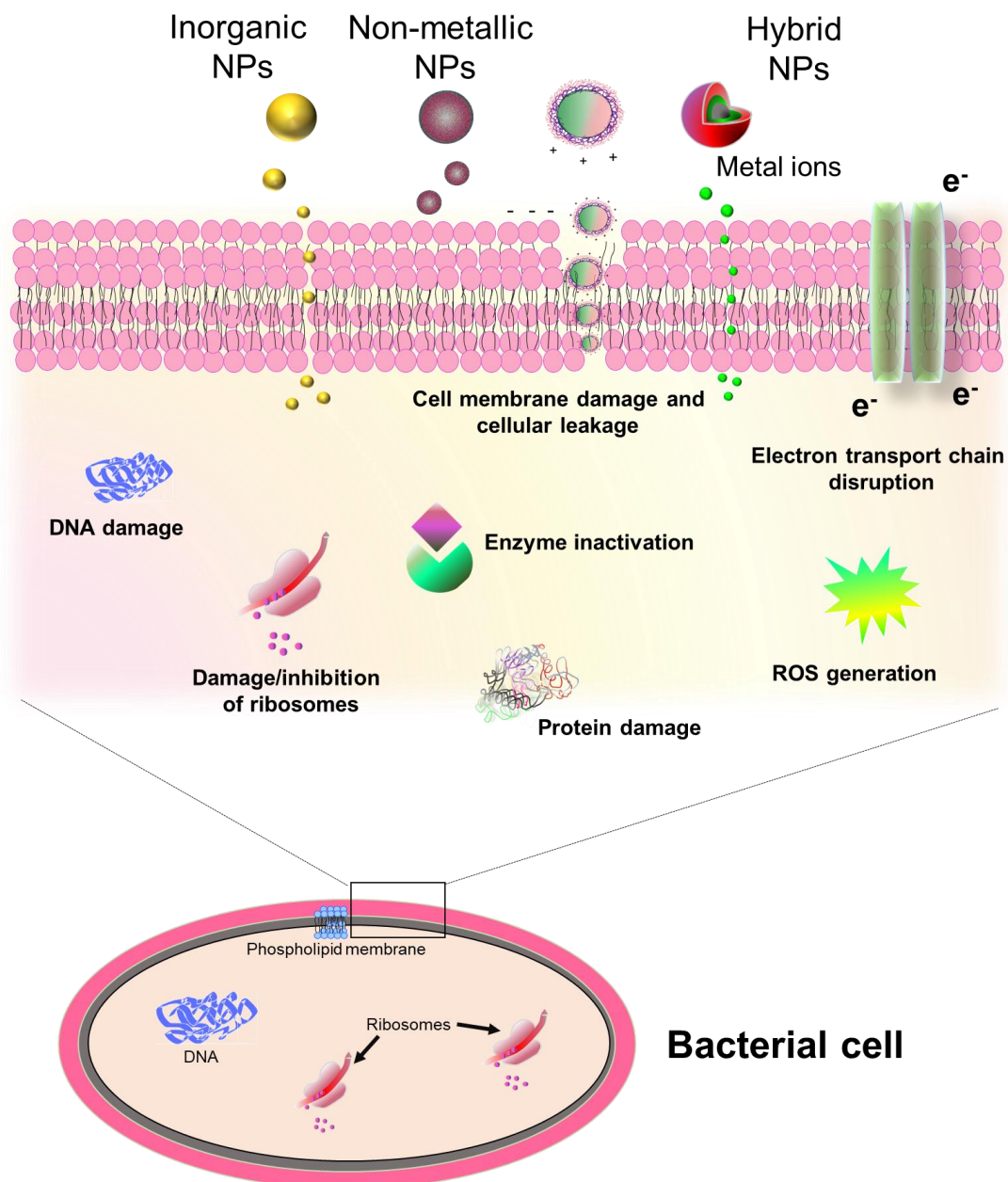
Figure 2. 4 Schematic representation of the mechanisms involved in the NPs interaction with free-floating bacterial cells.

2.3.4.1 Inorganic nanoparticles

Metal and metal oxide NPs appeared to be more effective antimicrobial agents with lower risk of resistance development, compared to many existing antibiotics.[128] The most widely investigated metal and metal oxide NPs are Ag, ZnO, copper oxide (CuO), titanium oxide (TiO$_2$), magnesium oxide (MgO), calcium oxide (CaO), and iron oxide (Fe$_3$O$_4$).[129] The antibacterial mechanisms of action of the metal NPs involve cell damage, disruption of bacterial cell wall, metal ion release, and ROS generation, associated with lower risk of resistance development.[128,129] Due to their antibacterial potential, the metal NPs have been used in food processing and packaging, textiles, surgical and medical devices.[130]

AgNPs are recognized as potent antimicrobial agent against bacterial, viruses, and fungi from ancient times. They are one of the most exploited metal NPs in medical devices, wound dressing materials, textiles, and water membranes.[131] It is known that the antibacterial properties are size-dependent and the smaller NPs demonstrate better killing activities. Moreover, the bacteria are less vulnerable to develop resistance to Ag, compared to existing antibiotics.[128] Despite that AgNPs could efficiently eradicate the free-floating cells; their bactericidal activity was significantly decreased on the sessile bacterial communities. This phenomenon is suggested to be due to the NPs aggregation onto the established biofilms, causing loss of antibacterial properties.[132] The mechanisms of action of AgNPs are not clearly understood, however, several studies have suggested that the NPs disturb the bacterial membrane, inhibit the respiratory chains, or induce the ROS production. Nevertheless, the AgNPs application is limited due to low stability and toxicity towards mammalian cells.[133] Gold (Au) NPs have been widely used for theranostic applications (e.g. cancer therapy, biosensing), gene therapy, and biological purposes. A number of reducing agents and stabilizers have been adopted to obtain stable and biocompatible AuNPs with controlled size and shapes, able to functionalize different antimicrobial peptides, capable to interact with bacterial cell membrane and disintegrate it.[134]

CuO NPs, ZnO NPs, and TiO$_2$ are considered as strong bactericidal agents towards Gram-positive and Gram-negative bacteria.[135] In general, metal oxide NPs release metal ions very slowly and can be easily up taken by the cell from the extracellular environment. Inside the cell, they can react with carboxyl, thiol, and amino functional groups from nucleic acids and proteins, causing cell structural changes and alteration of

the normal cell physiological processes. Furthermore, the metal oxide NPs can interact with the lipoproteins, phospholipids, and lipid polysaccharides from Gram-negative bacterial cell wall, and with peptidoglycans in the Gram-positive bacterial membrane, interrupting the cell functions.[136] For example, CuO NPs were widely used as anti-septic compound in agricultural systems and antibacterial agent in skin healthcare for controlling severe skin infections. The CuO NPs can induce ROS generation and harm the lipids, proteins and nucleic acids, associated with cell death.[137] Over the past years, the cytotoxicity and antibacterial properties of ZnO NPs have been substantially investigated. Several studies demonstrated the strong bactericidal potential of ZnO NPs against medically relevant pathogens.[138] Moreover, ZnO NPs have been widely used in combination with variety of polymers for functionalization of fabrics,[138,139] medical devices,[140] and contact lenses.[141] Joost *et al.* reported that TiO_2 NPs disturbed the bacterial cell membrane, associated with cell leakage and death.[142] NPs, such as MgO and CaO NPs, showed high antibacterial efficacy due to interaction with the bacterial cell membrane, ROS production and alkalinity.[143]

Recently, the integration of two different metals in the same nanostructure is of particular interest due to their enhanced synergistic antibacterial efficiencies compared to the monometallic counterparts. For instance, ZnMgO nanocomposites have demonstrated to be more antibacterial compared to the ZnO NPs and MgO NPs alone. ZnO nanocrystals were more antibacterial towards Gram-negative *E. coli* and Gram-positive *Bacillus subtilis*, in comparison to nano-MgO, however, the nano-ZnO was toxic to human HeLa cells. The integration of both metal oxides led to safe-by-design ZnMgO nanostructures with strong bactericidal activity towards *B. subtilis* and improved biocompatibility, suggesting their potential as alternative therapeutics to manage bacterial infections.[144] In another study, Zhao *et al.* described the engineering of Au/platinum (Pt) NPs as promising antibacterial agents towards sensitive and drug-resistant pathogens, compared to the pristine AuNPs and PtNPs, which did not display any antibacterial activities. The bimetallic NPs disrupted the bacterial cell membrane, leading to dissipation of the diffusion potential in bacterial cell membrane and increased the adenosine triphosphate levels. Moreover, the bimetallic Au/Pt NPs did not affect the umbilical vein endothelial cells viability, providing new promising perspectives to combat bacterial pathogens.[145]

2.3.4.2 Non-metallic nanoparticles

High interest is directed to the nanotransformation as a potential approach that may solve the failure of existing antimicrobials.[124] The engineering of nanoscaled cationic polymers, e.g. AM and chitosan resulted in stronger antibacterial activity, compared to the bulk solutions due to the improved interaction with bacterial cell membrane and enhanced membrane disturbance.[108] Phenolic compounds such as lignin in nanoform demonstrated increased antibacterial properties against Gram-positive and Gram-negative bacteria due to the stronger interaction with the bacterial species and inhibiting essential biological processes.[146] The development of penicillin G nanospheres led to elimination of penicillin-resistant Gram-negative *E. coli* and *P. aeruginosa* and suppressed the biofilms growth.[125] Moreover, the nanoformulation of vancomycin enabled the drug interaction with the bacterial cell membrane and boosted the antibacterial activity towards Gram-negative *E. coli* and *P. aeruginosa*. The nanospherisation increased the bacterial susceptibility to the vancomycin in the biofilm structure, compared to the pristine counterparts.[124] Nanotechnology, considered as a strategy to improve the drug stability and antibacterial activity, and lower the risk of resistance appearance, mostly relies on liposomes, lipid NPs, and NCs as drug carriers to the site of infection.[147] The encapsulation of antibiotics such as streptomycin, gentamicin, ciprofloxacin, and penicillin in liposomes gave them a "second life" against MDR pathogens, compared to their pristine counterparts. Gentamicin-polyehylenglycol liposomes demonstrated strong antibacterial activity against drug resistant *K. pneumonia* in *in vivo* studies.[148] Tobramycin-loaded liposomes resulted in enhanced antibacterial activity towards medically relevant *S. aureus*, *E. coli*, and *P. aeruginosa* at lower concentration of the antibiotic.[149]

2.3.4.3 Hybrid nanoentities

The engineering of hybrid nanoentities composed of at least two different compounds is appealing approach to overcome the limits of the single materials and/or to impart novel multifunctional properties not possible for the individual nano-architectures.[150] The most attractive approach is the combination of metals/metal oxides with polymers/biopolymers for generation of stable hybrid nanocomposites with high antibacterial efficiency at low non-toxic concentrations. Generally, the increased surface area and the small size of the nanomaterials acquires an overage surface energy,

compared to the pristine counterparts, making the NPs thermodynamically unstable, e.g. unprotected Au or AgNPs showed irreversible aggregation and precipitation. Reduction of the NPs' surface energy could improve their thermodynamic stability and prevent them from aggregation.[151] The reduction of the metal ions using polymers, biopolymers, surfactants or enzymes enhanced the NPs stability and biological properties.[152,153] Chitosan was employed as reducing and capping agents for the synthesis of AgNPs with long-term stability and enhanced antibacterial efficacy. The developed hybrid nanoentities resulted in stronger bactericidal properties in comparison with pristine chitosan and AgNPs due to the cationic nature of the polymer which increased the NPs interaction with bacterial cell membrane, causing membrane disturbance.[152] In another study, biocompatible lignin was used for the production of novel lignin-capped AgNPs against MDR bacteria. The lignin shell enhanced the NPs surface activity and their capability to interact with the bacterial membrane, eradicating Gram-positive and Gram-negative MDR clinical isolates.[154] Employing lignin as a reducing and capping agent, hybrid lignin-tellurium NPs were developed. These hybrid nanocomposites showed complete elimination of medically relevant Gram-negative *E. coli* and *P. aeruginosa* and inhibited the Gram-positive *S. aureus* growth due to bacterial membrane disturbance and ROS generation.[155]

On the other hand, the antimicrobial peptides have demonstrated high potential to manage MDR bacteria and inhibit biofilm formation. The engineering of hybrid polymyxin B and AgNPs increased the bacterial membrane disturbance due to interaction between positively charged NPs and the negatively charged bacterial membranes, resulting in increased bactericidal activity, compared to the individual compounds.[156] Non-specific mechanisms of action, such as membrane disturbance, decreased the possibility of resistance development.[151]

Recently, two complementary strategies have been integrated to develop novel hybrid nanocomposites of bactericidal Ag and biofilm degrading α-amylase with improved functionalities against planktonic and sessile Gram-positive and Gram-negative bacteria. The application of α-amylase could degrade the extracellular polymeric matrix and increased the bacterial susceptibility to the bactericidal agent.[153]

QQ enzymes interrupt the processes implicated in the bacterial pathogenesis without affecting the bacterial growth, possessing lower selective pressure, making the bacteria more vulnerable to the antibacterial agents.[157] Vinoj *et al*. decorated AuNPs with

lactonase against the biofilm formation of pathogenic Proteus species. The enzyme coated NPs exhibited increased antibiofilm activity and decreased exopolysaccharides production compared to the enzyme in bulk form.[76]

Engineering of targeted NPs as drug delivery nanosystems showed high potential for treatment of bacterial infections. The combination of a bactericidal nanoparticulate carrier with specific targeting element drives the drug to the specific target increasing the therapeutic index of the biocide and reducing its undesirable side effects.[123] Engineering of vancomycin-loaded NPs tagged with the cyclic 9-amino acid peptide CARGGLKSC for selective elimination of *S. aureus* in infected tissues has been reported. The developed targeted nanodevice increased the antibacterial activity specifically towards *S. aureus* and decreased the needed systemic dose, reducing the side effects *in vitro* and *in vivo*.[15] In another study, Meeker *et al*. developed daptomycin-loaded polydopamine-coated Au nanocages, conjugated to specific antibody as a hybrid photothermal and drug delivery nanocostruct targeting *S. aureus*. The conjugation of antibody on the NPs surface demonstrated increased therapeutic synergy and selective antibiotic efficacy towards both planktonic and sessile MRSA strain.[158]

2.3.4.4 Hybrid nanostructured coatings

Significant efforts are being made for managing medical devices-associated bacterial infections by engineering of hybrid nanostructured antibacterial/antibiofilm coatings on the devices that integrate different antibacterial compounds with multimodal antimicrobial mechanisms, acting synergistically to hinder the biofilm formation and growth.[159] Numerous studies of surface functionalization with hybrid nanocomposites of enzymes,[77] QS inhibitors,[79] metal/metal oxide NPs,[139,140] polymeric NPs[108] have been reported. For example, Wei *et al*. described the development of bifunctional AgNPs with the antithrombotic enzyme nattokinase and subsequently embedded them into an LbL implant coating in order to prevent bacterial infections and thrombosis. The coated material displayed high antibacterial efficacy against *E. coli* and *B. subtilis* coupled to anticoagulant activity.[160] A dual-level antibacterial coatings of Ag/chitosan or Ag/AM synergistically inhibited the bacterial growth of the Gram-positive *S. aureus* and Gram-negative *E. coli* during a 5-days course, and demonstrated long-term stability under continuous flow of water, indicating their promising application for water treatment.[161]

A stimuli-responsive hybrid multilayer coating of AM nanospheres, combined with HA onto silicone catheters has been developed. The obtained hybrid nanocoating was stable in the absence of bacteria, whereas in the presence of bacteria, the produced by the pathogen virulent factor hyaluronidase degraded the HA layer in the coating. Upon the HA degradation the layers were disassembled, subsequently the bactericidal AM spheres were released and the bacterial growth and biofilm formation on the catheters' surface were impaired.[108] Anghel *et al*. developed nano-modified prosthetic device with magnetic NPs coated with EO from *Mentha piperita* for prevention of colonization of *S. aureus*. These dual-functional nanostructures impeded the bacterial colonization on the material's surface due to the bactericidal/anti-adherence properties of the EO and its stabilization by the core/shell NPs, showing to be promising strategy to prevent prosthesis-associated infections.[162] Nanostructured coatings of bimetallic Ag/Ti NPs decreased the bacterial cell viability of sensitive *E. coli* and *P. aeruginosa*, and MDR *Acinetobacter baumannii* and *P. aeruginosa* within 3 h of contact.[163] In another study, Srisang *et al*. reported the functionalization of Foley urinary catheters with chlorhexidine-loaded NPs (in form of nanospheres and micelles) using dip and spray coating methods. The nanocoatings showed stability and impaired the encrustation and crystallization on the catheters' surface, compared to the pristine catheters in *in vivo* model, suggesting the efficacy of these functionalization to delay the occurrence of early onset of CAUTIs.[164]

2.4 Layer-by-Layer assembly as a tool for engineering of highly efficient antimicrobial nanomaterials

The LbL assembly approach is a simple and versatile technique for design and engineering of multifunctional coatings on a diversity of surfaces without the utilization of harsh chemicals and costly manufacturing processes.[165] The technique was used to coat substrates providing controlled thickness of the tailored multilayer structures for various applications. The LbL method comprises spin, spray, and immersive assembling strategies for development of innovative coatings with desirable nanofeatures, integrating for instance enzymes, biomacromolecules, NPs, dyes, or viruses, onto inert/active templates and 2D and 3D surfaces of medical devices (**Figure 2.5**).[166,167]

The main driving force implicated in spin assembly is the spin speed of the pristine substrate enabling the layers' deposition with well-defined micropatterns. The spinning

assembly technology allows for faster and more homogeneous multilayers build up on the substrate surface, compared to the immersive assembly, however, its application is limited to small planar material surfaces.[168,169] A set of forces, e.g. electrostatic interactions, which cause the materials deposition and rearrangement, and viscous, centrifugal, and air shear forces, enhancing the desorption of the weak bounds and film dehydration are involved in this coating process.[169]

The spray assembly strategy deposits aerosolizing polyelectrolyte solutions onto the substrates. The bulk movement in the spray and the random movement in the liquid layer are the main driving forces in the deposition process. The random movement in the liquid layer leads to material arrangement and increases its convection close to the substrate surface. Due to its simplicity and speediness in coating of large surfaces with different topography, the spray assembly technique is suitable for industrial-scale applications.[167]

The immersive assembly is the most common method enabling the engineering of interpenetrated multilayer compositions based on dip-and-rinse principles. Practically, due to its flexibility, the method is compatible for coating of different substrates with any charged layer material. This approach has been applied for coating of a variety of surfaces such as spherical nano/micro particles, planar surfaced or inside pores with desirable materials. After each layer deposition, an additional washing step is required for removing the excess of non-assembled material.[167]

The LbL assembly allows the formation of more homogenous coatings, compared to other non-LbL methods, based on the alternate deposition of oppositely charged polyelectrolyte layers without the necessity of any chemical modifications. In LbL the electrostatic interactions are the main driving forces between the building layers, however, other interactions can be also involved, such as Van der Waals forces, hydrogen bonds, charge transfer, covalent bonds, and hydrophobicity.[170] The LbL assembling allows to control the thickness and roughness of the multilayered structures by varying the experimental conditions, including the concentration of the polyelectrolytes, pH, and ionic strength.[171]
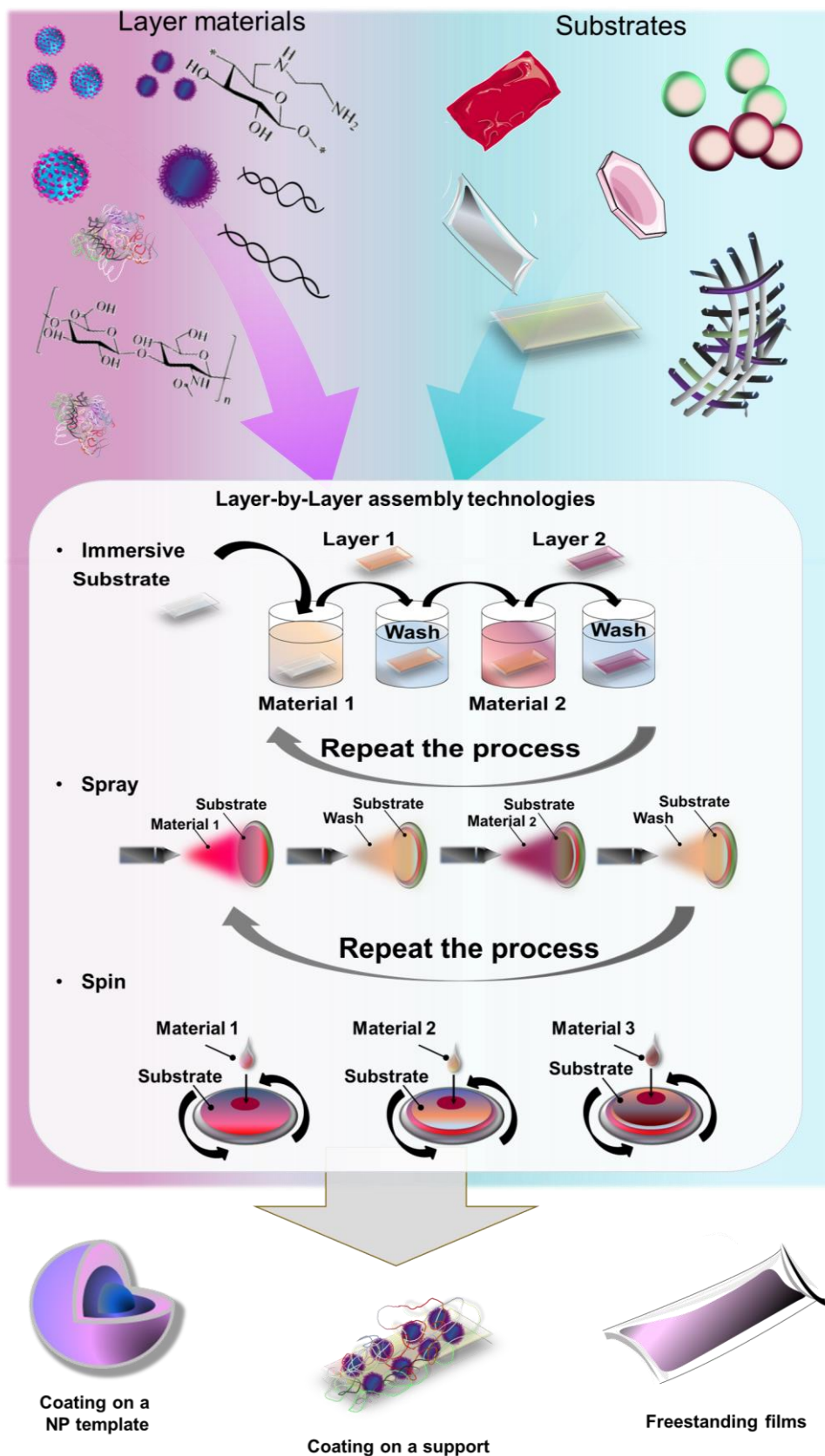
Figure 2. 5 LbL assembly technologies. Schematical representation of the three major technology categories for LbL assembly used for development of functional materials.

The versatility in the control of the nanostructured architectures makes the LbL technique an attractive approach in the biomedical field for engineering of multifunctional nanocomposites,[108] nanocoatings,[77] delivery nanoentities,[172] and membranes.[173] The coating strategy has been employed for the generation of multilayer films and stand-alone structures for biomedical applications.[174] In the past three decades, new therapeutic avenues have been developed to eliminate the bacterial pathogens and inhibit the biofilm formation based on the LbL method.

The multilayer deposition on nanoparticle templates has found application in biomedicine as drug delivery micro/nanosystems with controlled drug release and improved drug stability. The delivery of the antibacterial cargo relies upon external stimuli, such as temperature, pH, and electric field.[174,175] Metabolites secreted by the bacterial pathogens in the extracellular environment could also trigger the active agents' release. Bacterial production of lactic acid and acetic acid, lowering the environmental pH, leads to destabilization of the layers build up and elution of the bactericidals. For example, Zhuk *et al.* developed pH-responsive self-defensive films of tannic acid and positively charged tobramycin, gentamicin, and polymyxin B in an LbL fashion. The increment of acidification causes the disassembly of the layers and drug liberation from the films.[176] Despite the decrease of pH at the site of infection, the pathogens produce multiple virulence factors such as toxins and enzymes.[177] The polymer-hydrolyzing enzymes are able to degrade the layers, resulting in cargo release from the coatings. Unlike the pH- or temperature-responsive strategies, the enzymes secretion is specific for the bacterial species and could allow for a selective eradication of the targeted pathogens from the multilayer structures.[176] Thus, the stimuli responsive nanosystems could enhance the bacterial eradication and minimize the risk of drug resistance occurrence.[178] Wu *et al*. reported enzyme-responsive biohybrid nanomaterials of drug-loaded mesoporous silica NPs decorated by LbL with lysozyme, HA, and 1, 2-ethanediamine modified polyglycerol methacrylate for eradication of the Gram-positive *S. aureus*. The cationic nature of the polymers allowed the multivalent interaction with negatively charged bacterial cell membrane, and the release of encapsulated drug upon hyaluronidase production by *S. aureus*.[179] In a similar fashion, Cortese *et al*. generated biocompatible pH- and enzyme-responsive LbL NPs of drug loaded poly-caprolactone NPs, decorated with AgNPs, pH-responsive chitosan, and an enzyme-sensitive polymer for eradication of Gram-negative *E. coli* and Gram-positive *S. aureus*.[180]

Although the synthetic polyelectrolytes have been widely explored for development of delivery systems, their clinical application is limited due to their non-biodegradability and cytotoxicity. Natural polysaccharides and their derivatives have been used for preparation of LbL drug delivery nanosystems due to their excellent biodegradability, biocompatibility, and bioactivities. Multilayer building blocks made of chitosan, sodium alginate, dextran sulfate, carboxymethyl cellulose, and HA have been described for preparation of shell capsules.[181] For example, Cui et al. reported the engineering of quaternized chitosan and HA multilayer contact-killing microcapsules on sacrificial colloidal templates. The obtained capsules with upper layer of quaternized chitosan demonstrated to be more efficient towards E. coli, compared to the capsules ending with HA due to the enhanced microcapsule interaction with the bacterial cell membrane, and further were not toxic to myoblast cells.[172]

The possibility of incorporating different antibacterial compounds into the multilayer capsules is one of the most appealing advantages of the LbL technique for drug encapsulation coupled to reduced toxic side effects. Sangfai et al. described the functionalization of Ti implant surfaces with vancomycin-loaded gelatin NPs, coated with multilayers of gelatin and chitosan. The deposition of the LbL NPs onto Ti surface led to better surface roughness-controlled osteoblast cells proliferation and showed strong antibacterial activity towards S. aureus.[182] Gnanadhas et al. developed pH-responsive LbL chitosan-dextran sulphate NCs, loaded with ciprofloxacin as efficient targeted drug delivery nanosystem. The NCs targeted and eradicated intracellular Salmonella infection at reduced dosage of the ciprofloxacin in the in vitro and in vivo studies, compared to the bulk antibiotic.[183] In another study, a photosensitizer curcumin was encapsulated in zeolitic imidazolate framework-8 nanomaterials and subsequently decorated with biocompatible HA and amino-bearing chitosan using LbL technique. The developed light responsive NPs synergistically eliminated E. coli and S. aureus under blue-light irradiation due to the enhanced interaction with the bacterial cell membrane and the generation of ROS.[184]

The engineering of hybrid nanomaterials could synergistically improve the therapeutic efficacy at lower concentrations of the antibacterials, reducing their cytotoxic effect. Wang et al. have developed antibacterial and recyclable LbL AgNPs armed magnetic nanoentities coated with lysozyme and tannic acid, responsive to the application of magnetic field. The developed nanocomposites demonstrated strong efficiency against

E. coli and *S. aureus*.[185] Similarly, magnetic Fe_2O_3 NPs core were decorated with chitosan/poly (ethylene glycol) shell and loaded with gentamicin to achieve a potent antibiotic delivery. The chitosan/poly (ethylene glycol) shell was protonated under acidic conditions, improving the drug stability at low pH and promoted the interaction with negatively charged bacterial cell membrane. The developed nanocomposites resulted in better antibacterial activity against *S. aureus*, compared to the antibiotic bulk solution. Moreover, the employment of external magnetic field led to better NPs penetration within established biofilm structure, allowing the antibiotic delivery for elimination of mature biofilms.[186]

2.5 Sonochemistry for manufacturing of functional nanomaterials and nanostructured coatings

Most of the methods for engineering of durable hybrid NPs coating on medical devices, textiles, or water filter membranes are time-consuming and cost-inefficient and require chemical pre-treatment and further processing steps.[141,187] Moreover, the complexity and inability to transfer the technology from lab to large scale frequently limit their industrial applications. Recently, the International Union of Pure and Applied Chemistry (IUPAC) announced sonochemistry as a leading emerging technology in chemistry in 2021 and highlighted the potential of US in manufacturing of functional coatings.[188] US is considered as an environmentally friendly and highly efficient technique for generation of different types of antibacterial/antibiofilm nanocomposites and nanostructured coatings on medical devices[140] or textiles in a scalable one-step process.[139] This technique goes beyond the current "stepwise" approach for NPs synthesis and their inclusion in the final products. The efficiency of US irradiation in liquids induces acoustic cavitation phenomena, involving the formation, growth, and collapse of cavitation bubbles (**Figure 2.6A**). The US generates a strong cavitation that improves the homogeneity of the NPs solution, controlling the NPs aggregation.[140,189] The approach has been widely applied for the *in situ* formation and simultaneous coating of surfaces with multi-material NPs or in a "throwing stones" mode of sonochemical coating with commercial NPs without damaging the coated materials.[138,190] The collapse of the cavitation bubbles formed upon sonication, produces shock waves and microjets that drive the NPs with high velocities towards the material's surface (**Figure 2.6B**).[191] The versatility of the US method has been

demonstrated by incorporating a variety of nanomaterials such as metal/metal oxides, antimicrobial and antibiofilm polymers and enzymes on woven/nonwoven materials, water treatment membranes, and medical devices.[139,140,187,189]
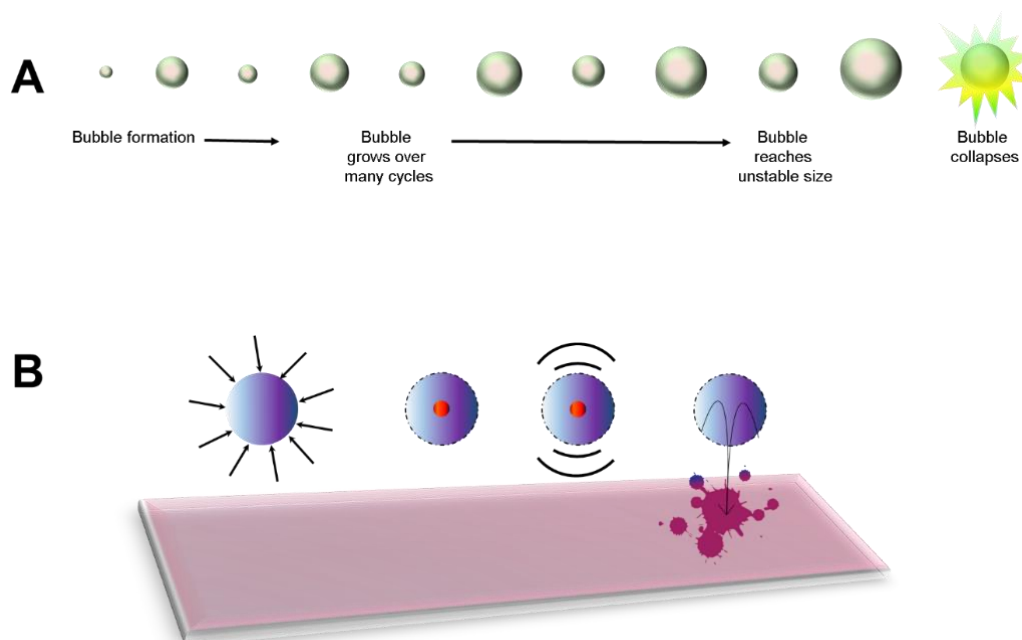
Figure 2. 6 Main steps in the US process. (A) Formation, growth and collapse of cavitation bubbles, generated upon sonication of liquids. (B) Microjets and shock waves produced upon the collapse of the acoustic bubbles project the developed NPs at high velocities towards the materials' surface.

The sonochemical technology for engineering of multifunctional nano-enabled coatings was recently widely employed due to its simplicity, fastness, and mild processing conditions. Petkova *et al*. generated hybrid coating of ZnO NPs and chitosan on cotton fabrics in a one-step sonochemical process. The combination of metal NPs and biopolymer improved the durability of the coating on textiles, maintaining strong antibacterial activity against *S. aureus* and *E. coli* after multiple washing cycles.[139] In another study, cotton medical textiles were functionalized with bactericidal ZnO NPs and gallic acid in a single step sono-enzymatic approach. The obtained hybrid coating demonstrated strong stability and antibacterial activity after 60 washing cycles at hospital laundry conditions.[138] US functionalization of urinary catheter with Zn-doped

CuO NPs exhibited antibiofilm activity and biosafety *in vitro* and *in vivo* models, showing to be a promising strategy to delay CAUTIs.[140] High intensity US has been employed for the development of AgNPs, reduced in the presence of ethylene glycol and ammonia and simultaneously deposited on nylon 6, 6 surfaces. The obtained nanocoating displayed ability to eliminate Gram-positive and Gram-negative bacteria.[192] Natal *et al*. developed ZnO and MgF$_2$ NPs coating on the cochlear implant that synergistically inhibited the bacterial growth and colonization by *S. pneumonia* and *S. aureus*.[189] Hoyo *et al.* reported the functionalization of contact lenses with antibacterial ZnO NPs, chitosan and antioxidant gallic acid in a one-step US process. The presence of gallic acid and chitosan imparted antioxidant properties, increased the wettability of the contact lenses and improved the comfort of the material. The engineered nanostructured coating resulted in stronger antibacterial performance towards *S. aureus*, without affecting the mammalian cell lines viability.[141]

3 Objectives of the Thesis

The main objective of the thesis *is to engineer nanomaterials for controlling the bacterial pathogenesis and resistance occurrence*. Novel strategies based on nanotechnology, QS, biopolymers, and targeting elements will be employed to develop antimicrobial and antibiofilm approaches with minimal risk of bacterial resistance appearance. To achieve the main goal of the thesis, the following **specific objectives** have been defined:

i) To develop multilayered coating of antibacterial amino-bearing AM and biocompatible HA on biologically inert NP templates using the LbL technique. The presence of **cationic AM layers onto the NP template will create high local positive charge density, which, synergistically with the nanoform would enhance NPs interaction with the bacterial membrane, associated with reduced risk of resistance development**.

ii) To develop LbL hybrid enzyme/biopolymer/metal nanoentities with enhanced antibacterial and antibiofilm activities against the Gram-negative *P. aeruginosa*. **The inclusion of QQ acylase on the bactericidal nano-Ag core will increase the pathogen susceptibility to lower and safe to human cells AgNPs concentrations and will inhibit the biofilm formation.** The deposition of membrane disturbing AM is expected synergistically with the nanotemplate to improve the hybrid NPs interaction with the bacterial membrane, potentiating the bactericidal activity of AgNPs.

iii) To generate targeted antibody-enabled NCs loaded with antibacterial oregano EO for selective elimination of Gram-positive *S. aureus*. **The antibiotic-free EO NCs grafted with a targeting antibody will increase the NCs bactericidal efficacy against the Gram-positive *S. aureus* at a lower dosage** and, at the same time, will reduce the resistance development and the toxic effects on non-targeted bacteria and human cells.

iv) To develop **durable hybrid nanostructured coatings on urinary catheters in a single-step high-intensity US process. The simultaneous deposition of antibacterial ZnO NPs and matrix-degrading amylase, targeting the extracellular matrix polysaccharide will inhibit the bacterial colonization on the catheters surface providing bacterial susceptibility to ZnO NPs, and further bacterial elimination.** The engineered nano-enabled coating would

impede the biofilm formation on indwelling medical devices and prevent the occurrence of CAUTIs in an *in vivo* model.

.

4 Materials and Methods

4.1 Materials and reagents

Microcrystalline cellulose (Avicel PH-101 from Fluka) was used for the preparation of the 6-deoxy-6-(ω-aminoethyl) AM (25 kDA) derivative as previously described.[193] Negatively charged NPs of monobutyl ester of poly (methyl vinyl ether/maleic acid) with hydrodynamic diameter 83.1 nm and zeta-potential –22.7 mV were produced according to the proprietary technology of Bionanoplus (Spain).[194] HA, with an average Mw~25 kDa was obtained from Lifecore Biomedical (USA). Acylase from *A. melleus* (E.C 3.5.1.14; 4.5 % (w/w) protein content and 2.49 U mg^{-1} specific activity, pI = 2.3) was purchased from Sigma Aldrich (Spain). Zein, a protein extracted from maize was obtained from Flo Chemical Corporation (MA, USA) and used for the NCs preparation. Oregano EO from *Thymbra capitata* (100 % pure) was kindly provided by the TELIC S.A. (Barcelona, Spain). AlamarBlue® cell viability reagent was purchased from Invitrogen, Life Technologies Corporation (Spain). ZnO NPs (size < 100 nm, zeta-potential = +28 mV) and α-amylase from *Bacillus amyloliquefaciens* (32 mg mL^{-1} protein content and 20 U mg^{-1} specific activity) were purchased from Sigma Aldrich (Spain). Ultrapure water (MilliQ® plus system, Millipore) with 18.2 MΩ.cm resistivity was used in most of the experiments. Nutrient broth (NB) was provided by Sharlab (Spain). L-α-phosphatidylethanolamine (PE) from *E. coli*, was purchased from Avanti Polar Lipids, Inc. (Alabama, USA). Polydimethyl/vinylmethyl siloxane urinary (Foley) catheters were provided by Degania Silcone Ltd. (Israel). All other chemical and microbiological reagents were purchased from Sigma Aldrich unless otherwise specified.

4.2 Bacteria and human cells

The bacterial strains *S. aureus* (ATCC® 25923™), *E. coli* (ATCC® 25922™), *P. aeruginosa* bacterium (ATCC® 10145™), the human foreskin fibroblast cells (ATCC® CRL-4001™, BJ-5ta), and keratinocyte (HaCaT cell line) were obtained from American Type Culture Collection (ATCC LGC Standards, Spain). *Chromobacterium violaceum* (CECT 5999), a mini-Tn5 mutant of *C. violaceum* (ATCC® 31532™) which cannot produce violacein without exogenous addition of AHLs, was purchased from Spanish Type Culture Collection (CECT, Spain).

4.3 Experimental methods

4.3.1 Layer-by-layer decorated nanoparticles with tunable antibacterial and antibiofilm properties against both Gram-positive and Gram-negative bacteria

4.3.1.1 LbL coating of NPs

Multilayer NPs were developed in an LbL fashion (**Scheme 4.1**). Negatively charged monobutyl ester of poly (methyl vinyl ether/maleic) acid NPs was used as a template for alternating deposition of polycationic AM and oppositely charged HA. For LbL assembly, 7.35 mL of NP template (in mQ water, pH 4.5) was mixed with 0.65 mL of 10 mg mL^{-1} AM solution (in mQ water, pH 4.5). The samples were agitated for 5 min and left for 1 h to allow the deposition of the first layer. Afterward, the NP$_{AM/HA}$-AM was ultracentrifuged at 18 000g for 50 min. The pellets were resuspended in 7.35 mL of water with pH 4.5 and then incubated for 1 h with the negatively charged HA (10 mg mL^{-1}, pH 4.5). The steps were repeated until five bilayers of AM/HA were formed. The concentration of the NP template was 7.72×10^{14} NPs mL^{-1}, whereas the final concentration of the LbL-coated NPs was adjusted to 8×10^{10} NPs mL^{-1}.
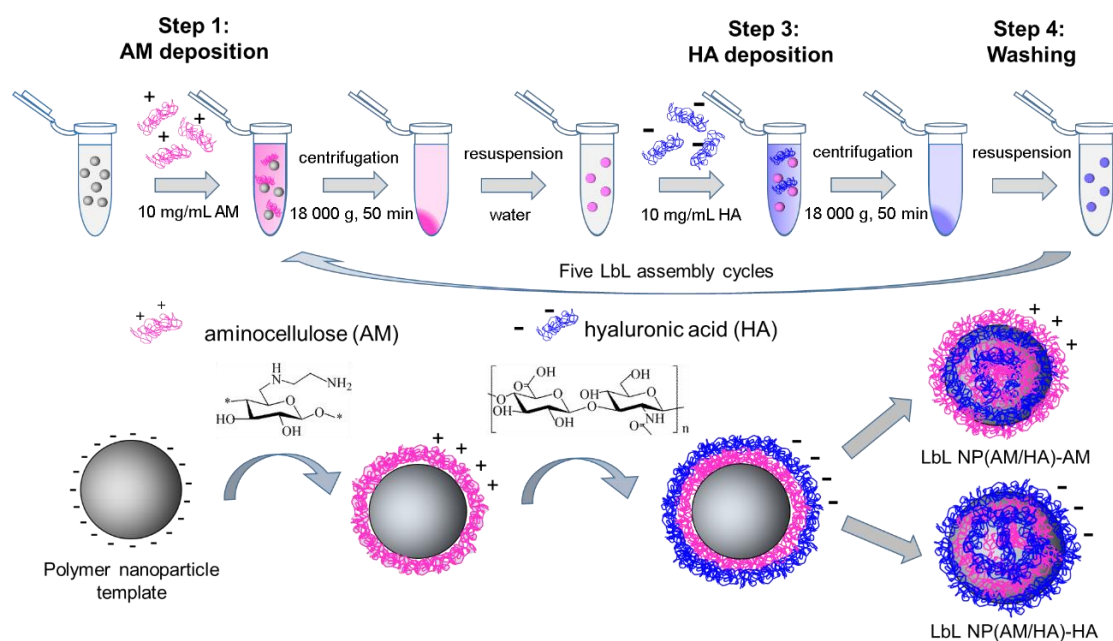
Scheme 4. 1 Schematic illustration of the polymeric NP template decoration in an LbL fashion yielding 8×10^{10} NPs mL^{-1}

4.3.1.2 LbL coating of NPs with fluorescein isothiocyanate-labeled AM

10 mg mL^{-1} solution of AM was prepared in sodium carbonate buffer pH 9. Fluorescein isothiocyanate (FITC) was dissolved in anhydrous dimethyl sulfoxide (DMSO) at 1 mg mL^{-1}. For each 1 mL of AM solution, 50 µL of FITC solution were added slowly under stirring and then the reaction was incubated in dark for 8 h at 4 °C. The unreacted FITC was removed using PD-10 desalting columns (Sigma Aldrich). The LbL assembly of FITC labeled AM and HA was performed on the polymer NPs template. The coating of colloidal particles was confirmed using fluorescence microscope. The detected fluorescence is from the successful multilayered deposition of the cationic AM on the NPs' surface.

4.3.1.3 Characterization of the NPs

The successful buildup of the LbL constructs was studied by measuring the variation of zeta-potential of the NPs after each layer of deposition. The zeta-potential of NPs in water was determined using a Zetasizer Nano Z (Malvern Instruments Inc., U.K.). After the LbL assembly, the size of the NPs was assessed by nanoparticles tracking analysis (NTA) performed in flow mode with a NanoSight LM10 instrument (Malvern Instruments Inc., U.K.) equipped with LM10 Laser 405 nm NP viewing unit and sCMOS camera. Software NTA 3.2 was used to capture several frames of the NP suspension to obtain the size of particles and their final concentration. The reported average particle size represents the mean values ± standard deviations of five measurements per sample. The size and morphology of the LbL NPs were also examined by transmission electron microscope (TEM) using a TEM JEOL 1010 equipped with a camera CCD Orius (GATAN) at an operating voltage of 80 kV. The sample was prepared by dropping the NP solution on formvar/carbon-coated grids and stained with uranyl acetate.

4.3.1.4 Determination of primary amino groups on the NP surface

Fluorescamine is a nonfluorescent dye that reacts with primary amino groups and forms highly fluorescent compounds.[195] It was used to determine the available amino groups on the AM polymer and multilayered NPs. For the assay, 75 µL of the samples was mixed with 25 µL of 3 mg mL^{-1} fluorescamine reagent (dissolved in DMSO) and incubated at room temperature (RT) for 3 min. Then, the fluorescence at 390/470 nm

was measured and the amino groups were calculated from the calibration curve built with L-methionine as a standard.

4.3.1.5 Antibacterial activity of LbL engineered NPs

The antibacterial activity of LbL decorated NPs was assessed toward Gram-positive *S. aureus* and Gram-negative *E. coli*. Briefly, bacteria were grown overnight at 37 °C in NB medium. Then, 50 µL each of the LbL $NP_{AM/HA}$-AM and LbL $NP_{AM/HA}$-HA with concentrations 8×10^{10}, 4×10^{10}, and 2×10^{10} NPs mL^{-1} were mixed with 50 µL of bacterial inoculum (optical density (OD)$_{600}$ = 0.01), $\sim 10^5 - 10^6$ colony-forming units (CFU) mL^{-1} in 96-well polystyrene plates. The samples were incubated for 24 h at 37 °C with shaking at 230 rpm. Then, bacterial growth in the presence of NPs was assessed measuring the OD at 600 nm in a microplate reader (Infinite M200, Tecan, Austria). The samples where no turbidity (no bacteria growth) was observed (OD$_{600}$ $\sim$ 0) were considered as minimum inhibitory concentrations (MIC). In addition, the number of survived bacteria during NP treatment was determined after plating 15 µL of the suspensions onto specific agar and further incubation for 24 h at 37 °C. Bacterial inoculum without NPs served as the negative control (no inhibition) and gentamicin (100 µg mL^{-1}) as a positive control (growth inhibition) in all of the experiments.

4.3.1.6 Antibacterial activity of AM against S. aureus and E. coli

The antibacterial activity of the AM was assessed against *S. aureus* and *E. coli*. The OD measurements showed that 80 µg mL^{-1} of AM (3.5 µmol mL^{-1} amino groups) is the minimal concentration needed to eradicate both bacterial strains. The amino groups functionalities on the surface of the NPs (1.09 µmol mL^{-1}) and those present in the bulk AM solution (3.5 µmol mL^{-1}) were different and confirmed the synergy between the nanoform and amino groups.

4.3.1.7 Bacteria time-killing kinetics

The minimal time necessary for the NPs to eradicate bacteria was determined using a time-killing kinetics assay. Overnight-grown bacterial suspensions were diluted in sterile 100 mM phosphate buffered saline (PBS, pH 7.4) to an OD$_{600}$ = 0.01 ($\sim 10^5 - 10^6$ CFU mL^{-1}). For the assay, 200 µL of the bacteria was mixed with 200 µL of the

samples, 4×10^{10} NPs mL^{-1} (concentration, corresponding to MIC), and incubated at 37 °C with 230 rpm shaking. At 15, 45, and 60 min, the survived bacteria were enumerated using the drop plate method. In total, 15 µL of diluted *E. coli* and *S. aureus* suspensions was plated on selective chromogenic coliform and Baird Parker agar, respectively. After 24 h incubation at 37 °C, the grown colonies were counted. Bacteria in PBS were used as a negative control (no bactericidal activity). Bacterial cell viability was further assessed with fluorescence microscopy using Live/Dead BacLight Bacterial Viability kit comprising two nucleic acid fluorescent dyes, SYTO9 and propidium iodide (PI). LbL-coated NPs ending with AM (100 µL) were incubated for 1 h with *S. aureus* and *E. coli* and then mixed with 20 µL of SYTO9 and PI in the ratio 1:1. After 15 min, the samples were visualized under fluorescence microscopy using 100 × objective lens. The live cells were stained in green and the dead ones in red.

4.3.1.8 Interaction of the NPs with cell membrane models

The mechanism of action of the developed NPs was studied under biomimetic conditions by means of the Langmuir technique. The interaction of the NPs with a cell membrane model-a monolayer composed of PE extracted from *E. coli*-was assessed in a Langmuir trough equipped with two mobile barriers (KSV NIMA Langmuir-Blodgett Deposition Troughs, model KN2002, Finland) mounted on an antivibration table and housed in an insulation box at 23 ± 1 °C. The surface pressure (π) was measured by a Wilhelmy balance connected to the trough. The PE monolayer was prepared by spreading 40 µL of 0.5 mg mL^{-1} phospholipid on PBS (pH 7.4) subphase and compressing until the pressure of natural cell membranes ($\pi = 33$ mN m^{-1}) was reached. After stabilization of the monolayer, 300 µL of the NPs at concentration 8×10^5 NPs mL^{-1} was injected beneath the monolayer and the variation of the pressure over time was recorded.

4.3.1.9 Biofilm inhibition test

The antibiofilm activity of the AM/HA decorated NPs was also evaluated using colorimetric crystal violet assay. Briefly, 50 µL of 4×10^{10} NPs mL^{-1} NP$_{AM/HA}$-AM and NP$_{AM/HA}$-HA and 50 µL of bacteria in tryptic soy broth (TSB) (OD$_{600}$ = 0.01) were placed in a 96-well microplate. The microplate was then incubated for 24 h at 37 °C under static conditions to allow bacteria to form biofilms. After the incubation, the non-

adhered bacterial cells were washed three times with 200 μL of distilled H_2O and the microplate was incubated for 60 min at 60 °C for biofilm fixation. The biofilm was stained for 5-10 min with 200 μL of 0.1 % (w/v) crystal violet solution, washed three times with distilled H_2O, and dried at 60 °C. Next, 200 μL of 30 % (v/v) acetic acid was added to dissolve the crystal violet and the plate was incubated for 15 min at RT. Then, 125 μL of each well was transferred to a new 96-well microplate, and the absorbance was measured at 595 nm. The amount of the dye is directly proportional to the total biomass on the surface, including bacteria cells and EPM. Gentamicin (100 μg mL^{-1}) was used as a positive control (biofilm inhibition).

4.3.1.10 Biocompatibility of NPs

Human fibroblast cell line BJ-5ta was used to determine the toxicity of the LbL-coated NPs toward mammalian cells. Briefly, the cells were maintained in Dulbecco's modified Eagle's medium (DMEM, ATCC) containing 10 % (v/v) fetal bovine serum, 1 % penicillin, and 200 mM glutamine, at 37 °C in a humidified atmosphere with 5 % CO_2. At preconfluence, the cells were harvested using trypsin-EDTA (ethylenediaminetetraacetic acid) (ATCC-30-2101, 0.25 % (w/v) trypsin/0.53 mM EDTA solution in Hank's BSS without Ca or Mg) and seeded at a density of 60×10^4 cells per well on a 96-well tissue culture treated polystyrene plate (Nunc). After 24 h, the cells were washed with sterile PBS (pH 7.4) and the NPs at their bactericidal concentrations were placed in the wells. The cells were incubated at 37 °C for 45 min within contact with the NPs. Then the samples were removed, the growth media withdrawn, and the cells washed with 100 mM PBS, pH 7.4, and stained for 4 h at 37 °C with 100 μL of 10 % (v/v) AlamarBlue cell viability reagent in DMEM. Thereafter, the absorbance at 570 nm was measured, using 600 nm as a reference wavelength, in a microplate reader. All results are reported as mean values ± standard deviations (n = 3).

4.3.2 Layer-by-layer coating of aminocellulose and quorum quenching acylase on silver nanoparticles synergistically eradicate bacteria and their biofilms

4.3.2.1 AgNPs synthesis

Single step citrate reduction reaction was employed for the preparation of AgNPs. The glassware used for AgNPs synthesis was thoroughly washed with aqua regia (HCl and HNO_3 in 3:1). 0.02 % Silver nitrate ($AgNO_3$ w/v) was dissolved in 100 mL mQ water

and boiled at 150 °C under continuous stirring. 2 mL of sodium citrate solution (in mQ water) were added to the AgNO₃ solution dropwise. Then, the solution was left for ≈ 30–40 min at 150 °C under continuous stirring.

4.3.2.2 LbL coating of AgNPs with AM and acylase

Negatively charged AgNPs were used as colloidal templates for LbL deposition of the positively charged AM and negatively charged acylase. AgNPs were diluted (2 x) in mQ water and the pH was adjusted to 8. The deposition of each oppositely charged layer onto the AgNPs template was carried out by mixing 7.35 mL of the diluted AgNPs with 0.65 mL of 10 mg mL^{-1} of AM (in mQ water) deposited as a first layer, and acylase (in 100 mM Tricine buffer, pH 8.0) as a second layer. The samples were agitated for 5 min and were left for 1 h at RT. After the AM deposition, the NPs were ultracentrifuged at 18 000 rpm for 50 min, while after the acylase deposition the centrifugation was carried out for 15 min at 15 000 rpm. Finally, the pellets of LbL Ag@AM_AC NPs were collected and resuspended in 1 mL mQ water. In order to outline the role of acylase in the hybrid nanoentities, further control was developed NPs decorated with noncatalytically active 10 mg mL^{-1} bovine serum albumin (BSA), instead of QQ acylase. These samples (LbL Ag@AM_BSA NPs) were used as a control in the antibacterial test.

4.3.2.3 NPs characterization

Spectrophotometric measurements were performed in a microplate reader Infinite M200, Tecan (Austria). The UV-vis spectra were collected in the range of 300-600 nm, recording absorbance at a 2 nm step. TEM and dynamic light scattering was used to determine the size and the zeta-potential of the AgNPs. The successful buildup of the LbL constructs was studied by measuring the variation in zeta-potential of the NPs after each layer deposition. The zeta-potential and the NPs concentrations were assessed using Zetasizer Nano Z (Malvern Instruments Inc., U.K.) and NTA as previously described in Section 4.3.1.3. The size and morphology of the LbL NPs were also examined by TEM using a TEM JEOL 1010 equipped with a camera CCD Orius (GATAN) at an operating voltage of 80 kV. The sample was prepared by dropping the NP solution on carbon-coated grids.

4.3.2.4 Enzymatic activity

The enzyme activity of LbL Ag@AM_AC NPs was evaluated by a colorimetric assay using N-acetyl-L-methionine (NAMET) as a substrate and in a bioassay using *C. violaceum* CECT 5999. In the colorimetric assay, 200 µL of tricine buffer (100 mM, pH 8.0) and 200 µL of 0.5 mM cobalt chloride solution were added to 200 µL samples and equilibrated at 37 °C. Then, 200 µL of 100 mM NAMET in tricine buffer (100 mM, pH 8.0) were added, and the test tubes were incubated for 30 min. The reaction was stopped by rising the temperature to 100 °C for 4 min. The product of the enzymatic reaction was determined using the ninhydrin assay as follows: 200 µL of the sample was mixed with 400 µL of 2 % w/v ninhydrin solution (prepared in 200 mM citrate buffer, pH 5 and ethylene glycol monomethyl ether (1:1)) and 20 µL 1.6 % w/v stannous chloride solution. The samples were incubated for 20 min at 100 °C and cooled down before measuring their absorbance at 570 nm. Noncoated AgNPs were used as a control in all the experiments.

4.3.2.5 Quorum quenching activity

C. violaceum CECT 5999 was used to test the QQ activity of acylase and its ability to interfere with the QS process through the degradation of C6-HSLs. *C. violaceum* CECT 5999 is a mutant bacterial strain that in the presence of AHLs produces the purple pigment violacein. Briefly, the bacterium was grown on Luria Bertani broth (LB) agar (supplemented with 25 µg mL^{-1} kanamycin), and the plates were incubated at 26 °C for 48 h. Afterward, the bacterium was inoculated in LB medium supplemented with 25 µg mL^{-1} kanamycin at 26 °C for 12-16 h. For the bioassay, *C. violaceum* was diluted to optical density 0.004 (OD$_{660}$) in fresh medium supplemented with 25 µg mL^{-1} kanamycin and 5 × 10 µM AHLs (C6-HSL). Then, 350 µL of the inoculum were mixed with 350 µL of LbL Ag@AM_AC NPs and uncoated AgNPs template at their sub-inhibitory concentrations, and the samples were left at 26 °C overnight with 550 rpm shaking. Bacterium without NPs was used as a control. After the time of incubation, 200 µL of each sample were transferred in 2 mL Eppendorf, mixed with 200 µL of 10 % sodium dodecyl sulfate and vortexed for 5 s. Following that, 500 µL of 1-butanol were added for the violacein extraction and the samples were centrifuged for 5 min at 13 000 rpm. The butanol phase containing violacein was collected and the absorbance was measured at 584 nm.

4.3.2.6 Antibacterial activity of the developed NPs

The MIC and MBC of AgNPs and LbL Ag@AM_AC NPs were assessed toward the Gram-negative *P. aeruginosa*. The bacteria were grown overnight at 37 °C in Mueller Hinton Broth (MHB) medium. The antibacterial performance of the developed NPs was assessed as previously described in Section 4.3.1.5.

4.3.2.7 Transmission electron microscopy observation of NPs interaction with bacteria

LbL Ag@AM_AC NPs were incubated with *P. aeruginosa* ($OD_{600} = 0.01$, $\approx 10^5$-10^6 CFU mL^{-1}) for 3 h at 37 °C with 130 rpm shaking. Afterward, the samples were centrifuged at 4000 g for 5 min and resuspended in fresh fixative solution containing 2.5 % glutaraldehyde and 2 % paraformaldehyde 100 mM phosphate buffer (PB), pH 7.4. The samples were incubated overnight at 4 °C, washed three times with 100 mM PB, pH 7.4 and fixed in 1 % osmium tetraoxide. Then, the cells were stained with 2 % uranyl acetate, dehydrated in an ethanol, and embedded in Spurr resin. Ultrathin sections were obtained with an Ultracut E (Reichert-Jung) ultramicrotome and counterstained with lead citrate. The slices were deposited on bare mesh copper grids and the sections were observed using JEOL 1100 transmission electron microscope at 80 kV.

4.3.2.8 Determination of ROS generation

2, 7-dichlorodihydrofluorescein diacetate (DCFDA) assay was used to quantitatively measurement of ROS produced in the bacterial cells. Briefly, the bacteria were grown overnight in MHB and was centrifuged at 4000 g for 15 min and subsequently washed in sterile 100 mM PBS, pH 7.4. Then, the bacterial cells (($OD_{600} = 0.01$), $\approx 10^5$-10^6 CFU mL^{-1}) were resuspended in sterile 100 mM PBS, pH 7.4 and were treated with different concentrations of AgNPs and LbL Ag@AM_AC for 3 h at 37 °C at 230 rpm. Then, 25 µL of 100×10 µM DCFH-DA were added to the samples and the fluorescence was measured at Ex/Em = 485/535 nm. 2, 2-azobis (2-amidino-propane) dihydrochloride (AAPH) was used as a positive control.

4.3.2.9 Biofilm inhibition test

The antibiofilm activity of the AgNPs and LbL Ag@AM_AC NPs against Gram-negative *P. aeruginosa* was evaluated using colorimetric crystal violet and Live/Dead assays. The crystal violet assay was performed as previously described in Section 4.3.1.9.

The live and dead bacteria into the biofilms were observed with fluorescence microscopy using Live/Dead™ BacLight™ kit, which is comprised of the two nucleic acid fluorescent dyes, SYTO9 and PI. After the incubation, the non-adhered bacterial cells were washed three times with 200 μL sterile 100 mM PBS, pH 7.4 and the microplate was incubated with 20 μL of SYTO9 and PI in ratio 1:1. After 15 min of incubation in a dark, the samples were visualized under fluorescence microscopy using 20 x objective lens. The live cells were stained in green and the dead ones in red.

4.3.2.10 Biofilm eradication assay

The effect of the NPs on the already established *P. aeruginosa* biofilm was studied using crystal violet and Live/Dead assays. 100 μL of bacteria in TSB (OD_{600} = 0.01) were placed in 96-well microplate and the biofilm was allowed to form for 24 h at 37 °C under static conditions and the planktonic cells were washed with sterile 100 mM PBS, pH 7.4. 60 μL of NPs and 60 μL of TSB were placed in the 96-well microplate, subsequently left for 24 h at 37 °C under static conditions. After the incubation, the non-adhered bacterial cells were washed three times with 200 μL sterile 100 mM PBS, pH 7.4. For determination of the total biofilm mass the biofilms were left for fixation for 1 h at 60 °C. Then, the formed biofilms were stained with crystal violet (0.1 % w/v) and dried at 60 °C and further dissolved using 30 % v/v acetic acid. 125 μL were transferred into 96-well microplate and the absorbance was recorded at 595 nm. The live and dead bacteria were observed using fluorescence microscopy (20 x objective lens) after incubation with 20 μL of SYTO9 and PI in ratio 1:1.

4.3.2.11 Biocompatibility

The BJ-5ta cells were maintained as previously described in Section 4.3.1.10 and the biocompatibility performance of the developed NPs is detailed below. The LbL Ag@AM_AC NPs were placed in contact with the previously seeded cells and after 24 h the number of viable cells was quantified using Alamar Blue assay (AlamarBlue,

Invitrogen) as described previously in Section 4.3.1.10. The cells' morphology was examined by Live/Dead kit assay for mammalian cells. Briefly, the cells were stained for 15 min in the dark with a mixture of both stains in a ratio calcein: ethidium homodimer (4:1) in 100 mM PBS, pH 7.4. The non-reacted stains were further washed with 100 mM PBS, pH 7.4, and the cells were observed using a fluorescence microscope.

4.3.3 Antibody-enabled antimicrobial nanocapsules for selective elimination of *Staphylococcus aureus*

4.3.3.1 Protein A antibody interaction with S. aureus

The specificity of the antibody was assessed against the targeted *S. aureus* bacterium and nontargeted *P. aeruginosa* (as a control). Briefly, bacteria were allowed to grow and adhere on the surface of a 96-well polystyrene plate overnight at 37 °C. After being washed with PBS, bacteria were incubated for 4 h at RT with 100 μL of a 1/500 dilution (in 100 mM PBS, pH 7.4) of the specific antibody against protein A of *S. aureus* cell wall. Then bacteria were incubated for 1 h at RT with a secondary antibody conjugated to the enzyme horseradish peroxidase. Bacteria binding protein A-antibody were further visualized in green upon the addition of a substrate mixture containing 6.5 mM 4-hydroxybenzoic acid, 1.8 mM 2, 2′-azino-bis (3-ethylbenzothiazoline-6-sulfonic acid), and 5.1 mM hydrogen peroxide in 100 mM PBS, pH 7.4.

4.3.3.2 Antibody-enabled NCs formulation

For the EO NCs preparation, zein was dissolved in propylene glycol under magnetic agitation. Then surfactant (Tween 20, Panreac, Madrid, Spain) and cosurfactants (propanediol, Dupont Tate & Lyle Bioproducts, TN, USA; denatured alcohol, Valencia, Spain; and oleic acid, Panreac, Madrid, Spain) were added under agitation until a clear, transparent solution was obtained. Oregano EO was then added to that mixture to achieve a homogeneous organic phase. The resultant surfactant-EO-zein mixture was added under continuous agitation into water at a ratio of 3:7 (organic phase/water) to form EO NCs. Afterward, 22.5 mL of the EO NCs (negatively charged) were mixed with 5 mL of 10 mg mL^{-1} AM aqueous solution, at pH 3.3, and incubated for 1 h at RT. After that, the sample was centrifuged at 29 500g for 50 min, resuspended in 3.75 mL of mQ water, and sonicated to disaggregate the NCs for 20 min at 20 °C. The NCs were functionalized with rabbit protein A antibody using 50/20 mM/mM of EDAC/sulfo -

NHS in 100 mM PB, pH 6.5. The reaction was performed at RT for 24 h with shaking. Then the NCs were centrifuged for 40 min at 25 000g, resuspended in 500 μL of mQ water, and subjected to further analysis.

4.3.3.2 NCs characterization

The encapsulation efficiency (EE) was determined by carvacrol quantification via high performance liquid chromatography (HPLC). The zeta-potential of the NCs was determined using a Zetasizer Nano ZS as described in Section 4.3.1.3. The NCs average size, size distribution, and number of NCs per milliliter were assessed by NTA using the NanoSight NS 300 (Malvern Instruments Inc., UK) in flow mode and software NTA 3.2 to capture several frames of the NCs suspension, obtaining the final concentration and the hydrodynamic diameter of the NCs. Results are displayed as distribution plots of concentration (NCs mL^{-1}) versus particle size. The reported average NCs size represents the mean values ± standard deviations of five measurements per sample. The size and the morphology of the NCs were examined by TEM (Tecnai G2 F20, FEI company, USA) at 80 kV acceleration voltage. Prior analysis, 10 μL of the samples was placed on an ultrathin carbon film on holey carbon grids and air-dried. The immobilization of active antibody onto the EO NCs was assessed with FITC-labeled protein A. Briefly, 200 μL of Ab@EO NCs and EO NCs (3×10^9 NCs mL^{-1}) was incubated with 2 μL of FITC-protein A in the dark for 1 h with 160 rpm shaking. The samples were centrifuged at 25 000g for 45 min to remove the excess of FITC-protein A and then were resuspended in 200 μL of 100 mM PB, pH 6.5. One hundred microliters of the NCs suspension was transferred to 96-well black plates and the fluorescence intensity of each test sample was measured at Ex/Em = 490/525 nm using TECAN Infinite M 200 (Austria). In addition, 20 μL of the samples was spread on a glass slide and NCs were observed under a fluorescence microscope (Nikon/Eclipse Ti-S, The Netherlands).

4.3.3.3 Quartz crystal microbalance with dissipation monitoring

The effect of EO and Ab@EO NCs on *S. aureus* was followed in real time with a Quartz crystal microbalance with dissipation (QCM-D) (E4 system, Q-Sense, Sweden) equipped with Teflon tubing. Gold sensors (QSX 301, QSense, Sweden) were sequentially cleaned in acetone, ethanol, and isopropanol in an ultrasonic bath for 10

min at 40 °C. The sensor was then dried with nitrogen and placed in the QCM-D flow chambers at 37 °C. The experiments were performed under flow-through conditions using a digital peristaltic pump operating in push mode for the solutions that were injected into the sensor crystal chamber. At first, a stable baseline with sterile 100 mM PBS, pH 7.4, was acquired at 20 µL min^{-1} at 37 °C. The deposition of *S. aureus* and *P. aeruginosa* cells on the sensor was achieved after 3 h of circulating the inoculum (OD$_{600}$ = 0.2) in MHB. Thereafter, PBS was flowed through for ~ 1h to remove the loosely deposited bacteria and establish a second baseline. Afterward, EO and Ab@EO NCs (3×10^9 NCs mL^{-1}) were circulated for 30 min at 20 µL min^{-1}, and 100 mM PBS, pH 7.4, was flowed to establish the third baseline. The experiments were performed in triplicate for each sample. For simplification of the data interpretation, only the normalized frequency (f) and dissipation (D) shifts as a function of time of one representative sample per experimental group (fifth harmonic) are shown.

4.3.3.4 Antibacterial activity tests

The antibacterial activity of EO NCs and antibody-functionalized EO NCs was assessed toward the targeted *S. aureus* in a single and mixed coculture with nontargeted *P. aeruginosa*. Briefly, bacteria were grown overnight at 37 °C in a MHB medium. Then 50 µL of the EO NCs and Ab@EO NCs (3×10^9 NCs mL^{-1}) were mixed with 50 µL of a single *S. aureus* or dual *S. aureus* and *P. aeruginosa* inoculum in 100 mM PBS, pH 7.4 (OD$_{600}$ = 0.01, ~ 10^5-10^6 CFU mL^{-1}). The samples were incubated for 24 h at 37 °C with shaking at 230 rpm. The number of surviving bacteria during the NCs treatment was determined after the plating of 15 µL of the suspensions onto selective agar plates and further incubation for 24 h at 37 °C. A bacterial inoculum without NCs served as the negative control (no bactericidal activity).

4.3.3.5 Nanocapsules interaction with bacteria assessed by scanning electron microscopy

The specific interaction of Ab@ EO NCs with *S. aureus* in a mixed bacterial inoculum with non-targeted *P. aeruginosa* was studied by scanning electron microscopy (SEM). Briefly, 250 µL of EO and Ab@EO NCs (3×10^9 NCs mL^{-1}) were mixed with 250 µL of a bacterial inoculum of *S. aureus* and *P. aeruginosa* (OD$_{600}$ = 0.01, ~ 10^5-10^6 CFU mL^{-1}) in 100 mM PB, pH 7.4, for 3 h at 37 °C with shaking. After that, bacteria were collected and purified with 100 mM PB, pH 7.4, by centrifugation (4000g, 15 min). The

pellet was resuspended in 2 % paraformaldehyde/2.5 % glutaraldehyde fixative solution (in PB, pH 7.4) and left overnight at 4 °C. Then 100 μL of the samples was deposited on a glass slide piece. After 30 min, the cells were dehydrated using ascending grades of ethanol (25 %, 50 %, 75 %, and 100 %, 1 h each). After the samples underwent chemical drying with hexamethyldisilazane, they were sputter-coated with carbon using Emitech K-950X and analyzed in a field emission SEM (JEOL, J-7001F), operating at 10 kV with a secondary electron detector.

4.3.3.6 Biocompatibility evaluation

AlamarBlue assay and Live/Dead kit assay were used to evaluate the toxicity of the NCs towards BJ-5ta cells as previously described in Sections 4.3.1.10 and 4.3.2.11.

4.3.3.7 Antibacterial efficacy of the NCs in vitro in a coculture model of S. aureus and human cells

The antibacterial efficacy of the NCs was evaluated *in vitro* in a coculture model of human cells and *S. aureus*. The cells were seeded at a density of 60×10^4 cells per well on a 96-well tissue culture treated polystyrene plate (Nunc) and incubated for 24 h at 37 °C. Afterward, the cells were washed with 100 mM PBS, pH 7.4, and inoculated with 100 μL of *S. aureus* (OD600 = 0.01) in DMEM (without antibiotic) for 1 h more to allow bacteria to adhere to the cells. The cells were washed with PBS, and then 100 μL of the NCs was added at their bactericidal concentrations to test their antibacterial effect on S. aureus and the toxicity on the fibroblast cells. Control samples not treated and not infected, not treated and infected, and also treated with 10 μg mL^{-1} gentamycin sulfate were also performed. After 24 h of incubation, the cells were washed with 100 mM PBS, pH 7.4, and 0.5 % Triton X-100 was added for 15 min at 37 °C to disrupt the cell membrane and obtain the intracellular bacteria. The suspensions were then diluted in 100 mM PBS, pH 7.4, and further seeded on agar plates to count the live bacterial colonies. In parallel, the cells treated with the NCs were washed and immediately subjected to cytotoxicity assessment using a Live/Dead kit assay for mammalian cells as described in Section 4.3.2.11.

4.3.4 Nano-engineered hybrid zinc oxide/amylase coatings to prevent the occurrence of catheter-associated urinary tract infections

4.3.4.1 Ultrasound-assisted coating of catheters with ZnO NPs and α-amylase

The sonochemical coating was carried out using an ultrasonic transducer Ti-horn (20 kHz, Sonics and Materials VC750, USA). At first, silicone Foley (size 16 French) catheters were immersed in the ultrasonic pot containing 400 mL aqueous solutions of ZnO NPs (1 mg mL^{-1}) and/or 3.4 % α-amylase (v/v) and the coating of the samples was carried out during 15 min at 20 °C and amplitude of 50 %. The ultrasonic horn was dipped 2 cm in the solution at a distance from the catheter of approximately 5 cm. After the coating process, the samples were thoroughly washed with distilled water and air-dried. For the *in vivo* studies, entire silicone Foley catheters (size 8 French) were US coated following the same conditions as described before.

4.3.4.2 Surface characterization of the coated catheters

The surface morphology of the coated silicone catheters was studies by high resolution SEM (HRSEM) (Quanta 200 FEG from FEI (USA)). Size histogram of the deposited ZnO@AM NPs on the catheter was build using ImageJ software. The amount of the zinc oxide in the coatings was determined after extraction with 0.5 M nitric acid by Inductively Coupled Plasma (ICP)-atomic emission spectroscopy on an ICP-spectrometer ULTIMA JY2501 (France). The content of the developed materials was also assessed using energy dispersive X-ray (EDX).

4.3.4.3 Stability of the coatings

The treated silicone samples were incubated in 5 mL of artificial urine containing 25 g L^{-1} urea, 9 g L^{-1} sodium chloride, 2.5 g L^{-1} disodium hydrogen orthophosphate, 3 g L^{-1} ammonium chloride, 2.5 g L^{-1} potassium dihydrogen orthophosphate, 2 g L^{-1} creatinine, and 3 g L^{-1} sodium sulfite, pH 6.8. Then, the test tubes were placed at 37 °C under slow shaking (20 rpm) for 7 days. The stability of the metal/enzyme coatings was further studied through the changes of the amylase activity in the coatings before and after incubation in artificial urine. ICP technique was used to determine the zinc oxide leaching from the catheter surfaces.

4.3.4.4 Amylase activity in the coatings

The enzyme activity in the coatings was determined using the 3, 5-dinitrosalicylic acid (DNS) assay. Briefly, 1 cm of coated catheter was incubated with 2 mL of 1 % starch (w/v) solution in 20 mM sodium phosphate buffer (pH 6.9) for 1 h, at 37 °C with 142 rpm shaking. Then, 1 mL of the sample was mixed with 1 mL DNS reagent for 15 min at 100 °C. The samples were left to cool down on ice and the absorbance were measured at 540 nm.

4.3.4.5 Quantification of the total biofilm formation

Biofilm formation on the modified silicone materials was assessed with *E. coli* and *S. aureus*. Briefly, 1 cm of catheter samples and 1.5 mL of bacteria in TSB, ($OD_{600} = 0.01$) were placed in a 24-well microplate. The microplate was then incubated for 24 h at 37 °C under static conditions to allow bacteria to form biofilms. After the incubation, the non-adhered bacterial cells were washed three times with 2 mL of distilled H_2O and the bacterial biofilms were fixed for 60 min at 60 °C and stained with 1 mL of 0.1 % (w/v) crystal violet solution for 15 min. After being washed with water until no dye was released, the silicone pieces were placed in vials containing 1 mL of 30 % acetic acid to redissolve the crystal violet dye fixed on the samples. The absorbance of the resulting solutions was measured at 595 nm. The same procedure was used to assessed the durability of the antibiofilm activity of the coatings after their incubation in artificial urine for 7 days.

4.3.4.6 Antibacterial activity

The antibacterial activity of the modified silicone materials was assessed against *E. coli* and *S. aureus*. Briefly, 1 cm of catheter and 2 mL of bacteria in 100 mM PBS, pH 7.4 ($CFU\ mL^{-1} \sim 10^5$) were placed in 15 mL sterile falcons. The falcons were then incubated for 24 h at 37 °C with 230 rpm shaking. After the incubation, the survived bacteria were plated on selective agars, the plates were incubated for 24 h for 37 °C, and the survived bacteria were count using drop count method.

4.3.4.7 Dynamic biofilm inhibition tests

The biofilm activity of the hybrid coating of ZnO@AM NPs was analyzed under dynamic conditions using an *in vitro* physical model of catheterized human bladder (**Scheme 4.2**) as previously described.[77] Briefly, the model was autoclaved (121 °C for 15 min), subsequently the non-treated and coated silicone Foley catheters were inserted into the system and the catheter's balloon was inflated with 5 mL sterile PBS, pH 7.4. According to UNE EN1616 (Sterile Urethral Catheters for Single Use), the bladder was filled up to the catheter's eye with sterile artificial urine, pH 6.8 (supplemented with 1 mg mL^{-1} TSB), containing Gram-negative *E. coli* or Gram-positive *S. aureus* (final OD_{600} = 0.01 for each bacterium). During the 7 days of catheterization, the model was maintained at 37 °C and supplied with sterile artificial urine at a flow rate of 1 mL min^{-1}. Then, the catheter was removed, and the biofilm formation on the surface (catheter's tip and balloon) was assessed. Non-treated silicone Foley catheter served as a control sample (no biofilm inhibition). The catheters were also subjected to Live/Dead BacLight kit assay for evaluation of live and dead bacteria into the biofilms. Briefly, the samples were stained with a mixture of Syto 9 and PI (1:1) for 15 min. Then, the biofilms were rinsed with 1 mL of 100 mM PBS pH 7.4 and analyzed by fluorescent microscope. The live cells were stained in green and the dead ones in red.
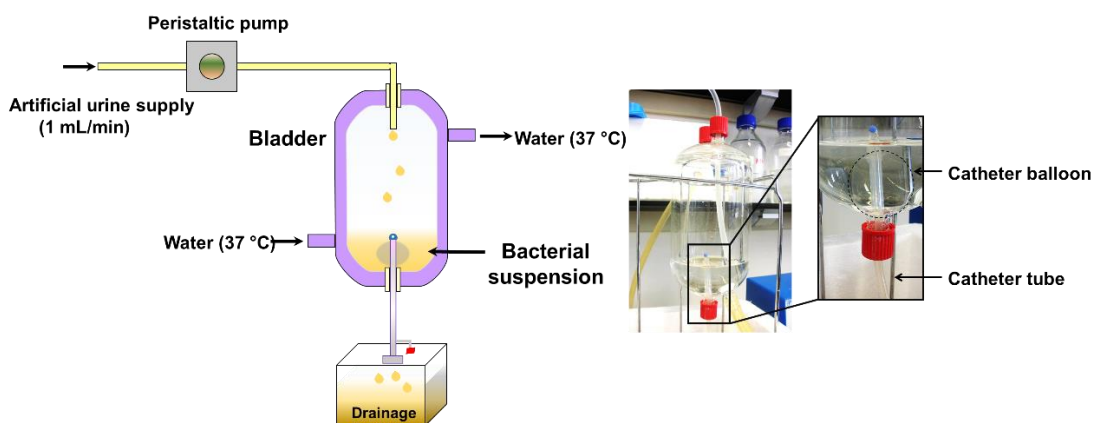
Scheme 4. 2 *In vitro* model of catheterized human bladder.

4.3.4.8 Biocompatibility assessment

The cytotoxicity of the coated catheters was evaluated using human fibroblast cells line BJ-5ta and HaCaT keratinocytes. The functionalized catheters were placed in contact with the previously cultured cells and after 24 h and 7 days of contact, the viable cells

were quantified using AlamarBlue assay kit as previously described in Section 4.3.1.10. The cells' morphology was also observed by Live/Dead kit assay for mammalian cells after exposure of the cells to the coated catheters for 24 h and 7 days as previously described in Section 4.2.11.

4.3.4.9 In vivo tests in rabbit model

The antibacterial efficacy of the hybrid NPs coatings of amylase and ZnO was assessed *in vivo*. All the experiments were carried out in animal research facility in the Institute of Experimental Morphology, Pathology and Anthropology with Museum, Bulgarian Academy of Sciences (Permit number: 11 30 127) in accordance to the national regulation № 20/01.11.2012 regarding laboratory animals and animal welfare, European legislation, International Standard ISO 10993-1:2009 for biological evaluation of medical devices and were also confirmed by the Institutional Animal Care and Use Committee. New Zealand male rabbits (n = 9), 4-5 months of age and mean body weight of 3 kg, were divided into 3 groups as follow: 1st group-is the control group of non-catheterized animals; 2nd group- is the group of animals catheterized with pristine silicone Foley catheters (size 8 French) for 7 days and the 3rd group- is composed of rabbits catheterized with hybrid ZnO@AM NPs-coated catheters for 7 days.

At the beginning of the experiment, all animals were checked clinically for their health status and were diagnosed as healthy. The catheterization procedure was carried out under general anesthesia using anesthesia mixture of tiletamine/zolazepam, xylazine and butorphanol in doses 5 mg kg^{-1}, 4 mg kg^{-1}, and 0.15 mg kg^{-1}, respectively, intramuscular administration. After application of lubricant, the sterilized under UV non-treated and treated catheters were aseptically inserted in the orificium urethrae externum and the lumen of the urethra. The insertion of the catheters was controlled and visualized using ultrasound (Ultrasound "Mindray DP-20 Vet"). After the insertion, the catheter´s balloon was inflated with air and the catheters of group 2 and 3 were secured with several dermal sutures in ventral abdominal wall to prevent their removal from the animal. Medical bandages of the pelvic zone and cervical collars were applied on the rabbits for hygienic and safety purposes, without affecting their capability to feed and drink freely. During the experiments, the heart levels, the breath rates and temperature of the animals were monitored. All animals recover smoothly and no mortality during

the anesthesia was observed. After the period of catheterization, blood and urine from each animal group were collected for further analyses.

4.3.4.9.1 Microbiological tests

The urine samples from all groups were collected aseptically and subjected to microbiological analysis. From the 1ˢᵗ-control group, 10-20 mL urine was collected after single catheterization followed by immediate removal of the device. In the microbiological studies, 0.1 mL of the collected urine were seeded on a differentiation medium (in triplicate). Additionally, the method of calibrated inoculating loops was performed to detect the presence of microorganisms. Microbiological tests were also performed for the catheters after their removal from the animals at the end of the experiment. The indwelling urinary catheters were cut and placed on ChromoBio®Urine and MH agar plates as well as in nutrient rich MHB (BUL BIO NCSPB-Sofia). The results after incubation under aerobic conditions at 37 °C for 48-96 h were reported. The quantification of microorganisms was performed by determining the arithmetic mean number of developing colonies and calculating the amount of CFU. Microscopic examinations were performed by Pfeifer method with fuchsin staining and performed under immersion with a digital microscope with a camera model B-190TV, Optika, Italy. The isolation and identification of the bacteria and fungi was carried out in accordance with the Bergey International Identifier.

4.3.4.9.2 Histopathological examination

On the seventh day of post-catheterization, the animals from each group were sacrificed and humanely euthanized for collecting materials for histology and evaluation of the local tissue reactions and inflammation indications. Tissue samples (1 cm^3 in size) from urethra, urinary bladder and kidneys were first fixed in 10 % neutral buffered formalin, then dehydrated in ethanol and embedded in paraffin. Tissue sections (3-5 μm thick) were stained in hematoxylin and eosin and examined by light microscope (Leica DM 5000B, Wetzlar, Germany). The sections were scored for the presence of epithelial desquamation or erosions, fibrosis, inflammatory reactions and foreign body responses or other pathological lesions to evaluate the morphological tissue reactions after the catheterization in both cases. Tissue samples from the control rabbits were used for comparison.

4.3.4.9.3 Biochemical analyses

Blood for complete blood count and biochemical analysis were performed by Automatic Hematology Analyzer "Mindray BC-2800 Vet" and Blood Chemistry Analyzer "MNCHIP Celercare V2". Urine test was carried out using urine analyzer with urine test strips ("Urit-50 Vet"). Additionally, whole blood and urine sediment smears were prepared for microscopic examination. Peripheral blood was obtained after puncture of the marginal dorsal vein of the ear and drops were spread on clean sterilized slides and left to air dry. Then, the dried samples were stained with DiaPath May-Grundwald Giemsa Fast Method and were examined by light microscope (Leica DM 5000B, Wetzlar, Germany).

Fresh and mixed sample of each urine was collected in a centrifuge tube and centrifuged using Centrifuge 5702R, RH Eppendorf, AG, Germany. After removing of the supernatant, the formed pellet was resuspended in 10 µL urine. The samples, were further processed for microscopic observation.

4.3.4.10 Statistical analysis

All data are presented as mean ± standard deviation. For multiple comparisons, statistical analysis by a one-way analysis of variance (ANOVA) followed by posthoc Tukey test or the unpaired two-tailed Student's t-test method, carried out using Graph Pad Prism Software 5.04 for windows (USA). P values less than 0.05 were considered statistically significant.

5 Results and Discussion
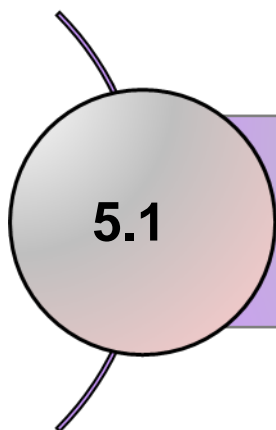
5.1

Layer-by-Layer Decorated Nanoparticles with Tunable Antibacterial and Antibiofilm Properties against both Gram-Positive and Gram-Negative Bacteria

In the current work, for the first time, inert monobutyl ester of poly (methyl vinyl ether/maleic) acid NP templates was decorated in an LbL fashion with antimicrobial AM and the biocompatible and antifouling polysaccharide HA. Using
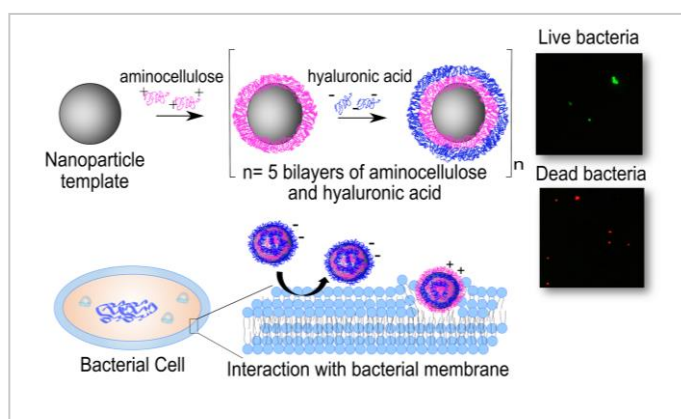
biocompatible polymer templates will avoid the need for core dissolution, which is a critical step for preserving the integrity of the multilayered composite NP. The deposition of cationic AM layers onto biologically inert NP templates was expected to create high local positive charge density, which synergistically with the nanoform of the template, would impart antibacterial efficiency to the nanoconjugates at very low concentrations. The antibacterial and antibiofilm activities of the obtained NPs were assessed against *S. aureus* and *E. coli*, in parallel to their cytotoxicity to human fibroblast cells.

5.1.1 NPs characterization

LbL technique was used to functionalize the biologically inert monobutyl ester of poly (methyl vinyl ether/maleic) acid NP template with AM and HA. The samples with outermost layer AM are designated as $NP_{AM/HA}$-AM and those ending with HA as $NP_{AM/HA}$-HA. The biopolymer multilayer buildup onto the NPs was confirmed by variations in their surface charge after each polyelectrolyte deposition step (**Figure 5.1**). The deposition of the first AM layer changed the template charge to a positive zeta-potential around +35.0 mV (**Figure 5.1**). After the adsorption of the second anionic HA layer, the surface charge reversed to approximately −38.0 mV, demonstrating the successful polyelectrolyte assembly on the NP template. After five AM/HA bilayer depositions, the zeta-potential of the NPs with AM in the outermost layer reached +40.6 mV, whereas the charge of those with HA was −26.7 mV (**Figure 5.1**). The presence of AM on the inert polymer templates was further confirmed by the green fluorescence of these NPs after five bilayer depositions of FITC-labeled AM (**Figure 5.2**).
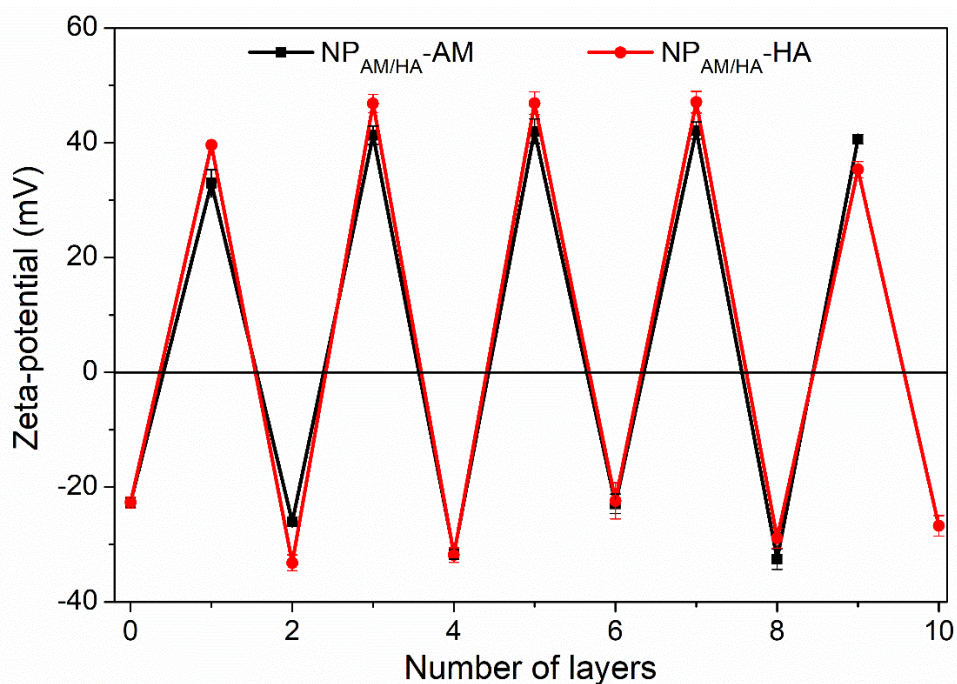
Figure 5. 1 Alternation of zeta-potential as a function of the AM and HA deposition on the NP template.
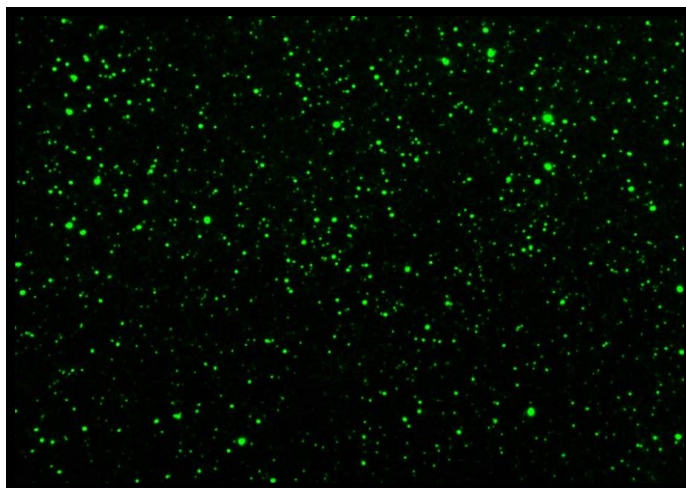
Figure 5. 2 Microscopic images of FITC-labeled AM/HA multilayers deposited on NPs surface.

The size and morphology of the NPs before and after the LbL coating with HA/AM were assessed by NTA and TEM. The template demonstrated lower hydrodynamic diameter (83.1 nm) and narrower size distribution compared to those of $NP_{AM/HA}$-AM (95.8 nm) and $NP_{AM/HA}$-HA (124.1 nm). The increase in the hydrodynamic diameter confirmed the coating of the inert NP template. Furthermore, TEM images revealed that the spherical NP templates present an average size of $\sim$ 30 nm (**Figure 5.3**), whereas the size of the coated NPs increased up to $\sim$ 40 and $\sim$ 50 nm for $NP_{AM/HA}$-AM and $NP_{AM/HA}$-HA, respectively. The difference before and after LbL evidenced the biopolymer-shell buildup on the NP template. Moreover, the original spherical shape of the polymer NPs was not altered during the LbL assembly. The differences in the NP size obtained by NTA and TEM are due to the conditions used to measure the NPs, for example, in liquid and dry states, respectively.
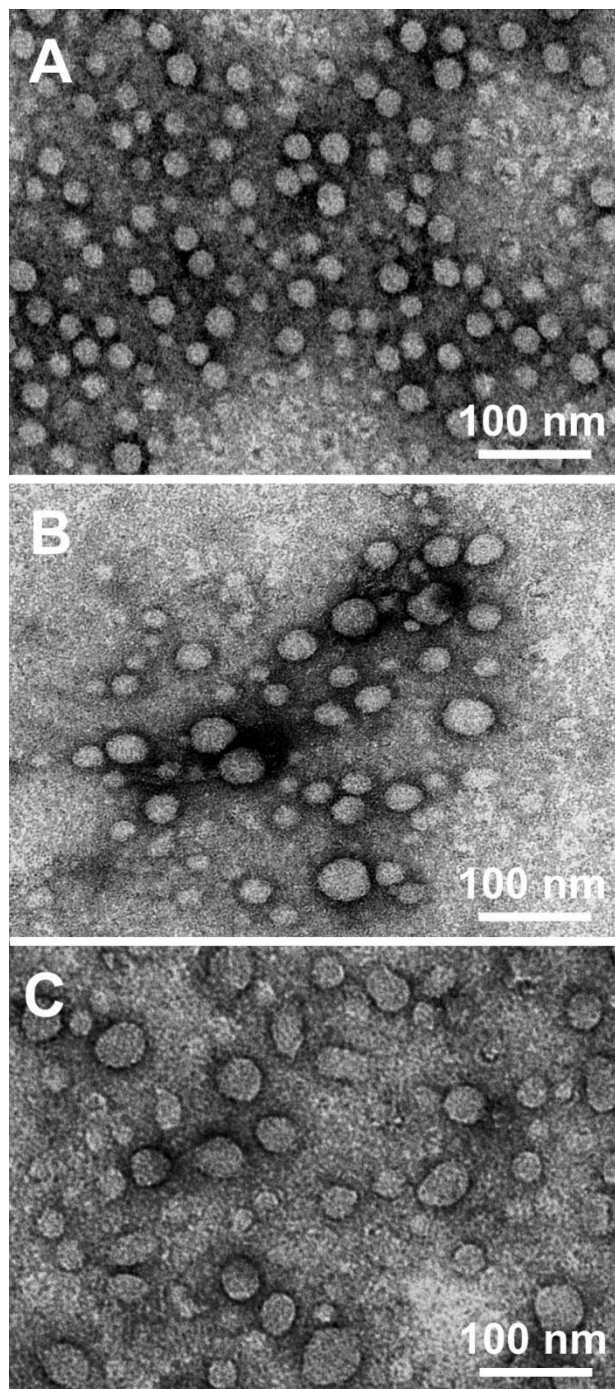
Figure 5. 3 TEM images of the NP template (A), $NP_{AM/HA}$-AM (B), $NP_{AM/HA}$-HA (C).

AM is derivative of cellulose, which is synthesized by chemo- and regioselective nucleophilic displacement reaction of p-toluenesulfonic acid ester of cellulose with ethylenediamine.[161] The cellulose modification originated an antibacterial biopolymer with free amino groups and positive charge (36.4 ± 0.75 mV). The amino groups per gram of modified polymer were determined fluorimetrically by a fluorescamine reagent (43.8 ± 0.08 μmol g^{-1} polymer). In contrast to other colorimetric and ultraviolet tests for

amino group detection, the fluorescent assay is more sensitive and allows the determination of the surface amino groups rather than their total amount.[196] The amount of available amino groups on the $NP_{AM/HA}$-AM was 1.09 ± 0.03 µmol mL^{-1}, whereas only 0.04 ± 0.011 µmol mL^{-1} was determined on the surface of the $NP_{AM/HA}$-HA. The HA adsorption onto the previously deposited AM layer resulted in the reduction of the surface available amino groups for interaction with the fluorescent dye. However, because of the interpenetrating nature of the polyelectrolyte multilayer,[197] some amino groups were still present on the $NP_{AM/HA}$-HA surface.

5.1.2 Antibacterial activity of the NPs against *S. aureus* and *E. coli.*

The growth inhibition of the Gram-positive *S. aureus* and Gram-negative *E. coli* was evaluated by measuring bacterial OD before and after 24 h treatment with $NP_{AM/HA}$-AM and $NP_{AM/HA}$-HA. Five AM bilayers was the minimum number of layers needed to obtain stable, small size LbL-coated NPs with desired antibacterial functionality, since lower number of bilayers did not demonstrate antibacterial activity (**Figure 5.4**). The $NP_{AM/HA}$-AM at concentration of 4×10^{10} NPs mL^{-1} was able to inhibit *S. aureus* and *E. coli* growth (OD $\sim$ 0), an effect not observed for the nonmodified NP templates and the NPs with HA as the outermost layer (**Figure 5.5 A, B**). The high positive charge density of $NP_{AM/HA}$-AM would facilitate their binding to the negatively charged bacterial membrane, inducing cell damage.
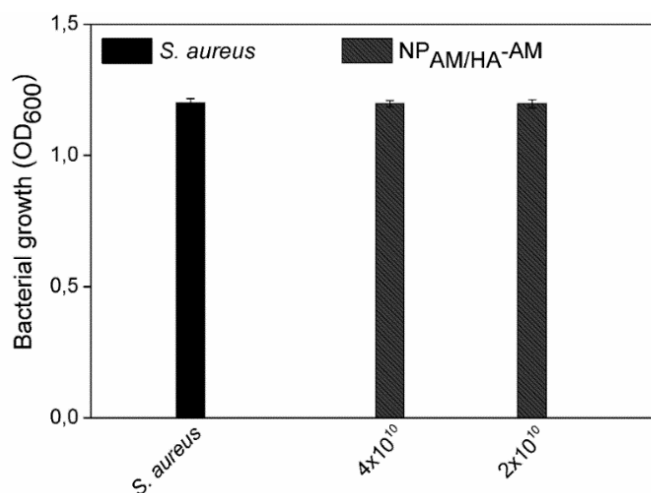
Figure 5. 4 *S. aureus* growth after 24 h incubation with NPs coated with 2.5 AM/HA bilayers.

Cationic nanostructured materials with improved membrane-disturbing capacity and antibacterial activity toward Gram-negative *E. coli* have been previously developed in our group by the sonochemical emulsification method.[104] This method utilizes high-intensity US to synthesize oil-filled nano-sized capsules of the active agents. The sonochemically-generated NCs contain surfactants in their shells that provide stability and enhance the interactions with the membrane of Gram-negative bacteria. [104,124,125] In the current work, we take advantage of the potentially enhanced interaction of the carriers with bacterial cell membranes owing to their nanosize, to engineer stable multilayered biopolymer-shell NPs without the addition of excipients and stabilizers. The antibacterial potential of the nanoconjugates was a function of the AM position in the layers. When AM was applied as an outermost layer, the NPs inhibited 100 % (OD ~ 0) *S. aureus* and *E. coli* planktonic growth (**Figure 5.5**). The bactericidal activities of these LbL NPs were then proved by culturing the samples on specific agar plates. Apparently, survived bacteria were not observed after 24 h exposure to the $NP_{AM/HA}$-AM (**Figure 5.5C, D**). Moreover, the multilayered AM-shelled NPs demonstrated improved bactericidal activity than that of the bulk AM (**Figure 5.6**). The quantity of free amino groups on the $NP_{AM/HA}$-AM was 3.5-fold lower than in the free AM, which demonstrates that the nanoform improves the AM activity, reducing the amount of the cationic agent required for complete eradication of *S. aureus* and *E. coli*. The small size and high surface-to-volume ratio of the NP template enhance the availability of the positively charged amino groups and consequently define better the interaction with bacterial cells. On the contrary, the NPs with an outermost HA layer were not able to alter the bacterial membrane and induce cell death (**Figure 5.5**). These NPs inhibited only 50 and 20 % of *E. coli* and *S. aureus* growth, respectively, acting as bacteriostatic rather than as bactericidal agents, due to the insufficient positive charge available on their surface. We reported that the specific activity of enzyme multilayer nanocoatings toward bacterial cells and biofilms is a function of the number of deposited layers as well as the position of the active agent in the assemblies.[77]
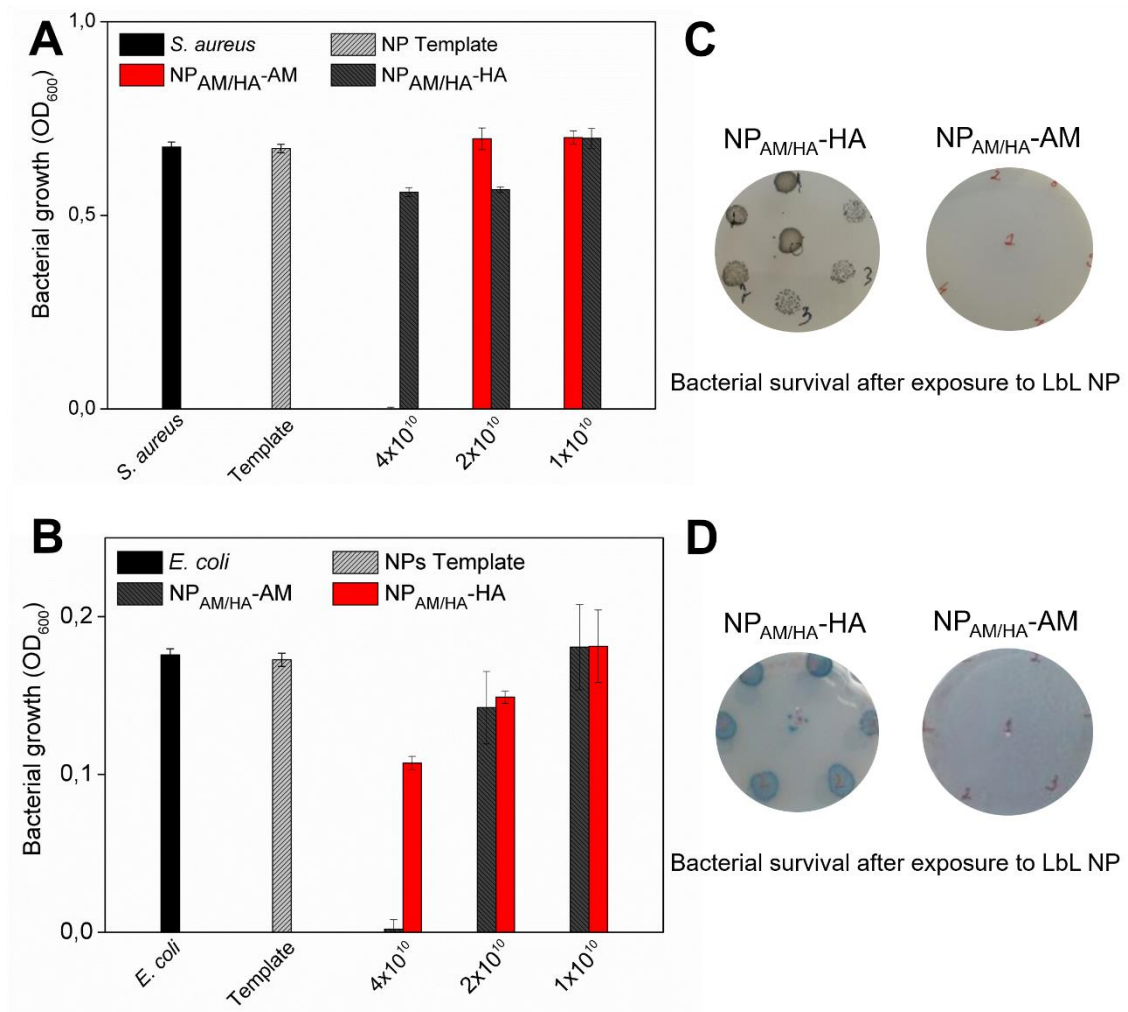
Figure 5. 5 (A) *S. aureus* and (B) *E. coli* growth after 24 h incubation with NP template and LbL coated NPs. (C) and (D) Representative images after culturing the samples on specific agar plates. (C) Black colonies of *S. aureus* and (D) blue colonies of *E. coli* were formed after 24 h incubation with NP$_{AM/HA}$-HA (left side images). No colonies were observed after incubation with NP$_{AM/HA}$-AM (right side images).
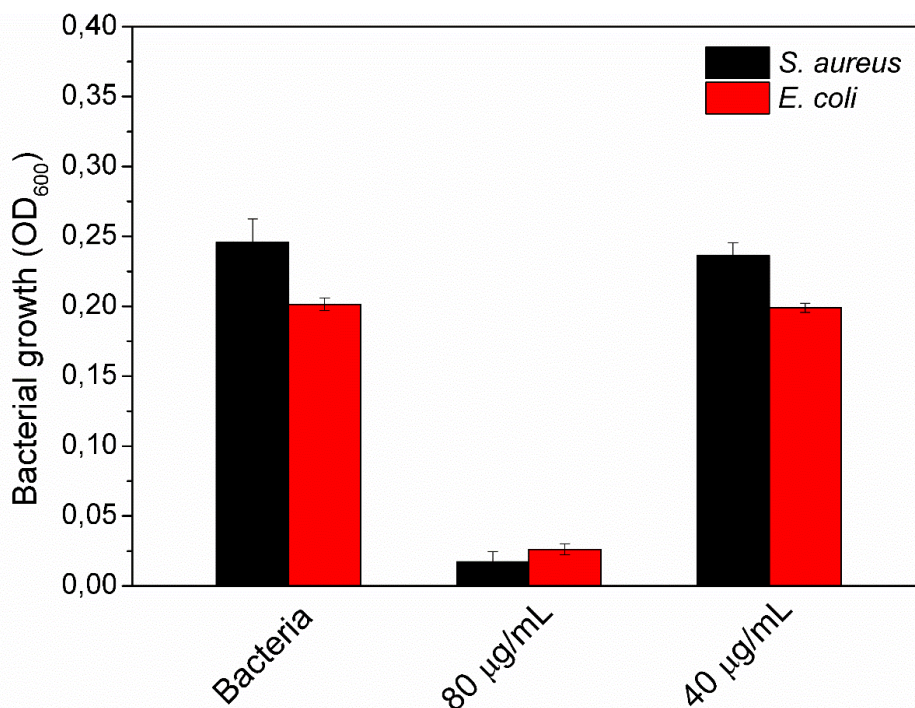
Figure 5. 6 Bacterial growth after 24 h incubation with different concentrations of AM bulk solution.

Time-killing kinetics of the LbL-coated NPs (at concentration 4×10^{10} NPs mL^{-1}) was performed to determine the viability-(CFU mL^{-1})-of the treated bacteria and define the rate at which the NPs exert their bactericidal properties.[198] The killing kinetic curves of NP$_{AM/HA}$-AM and NP$_{AM/HA}$-HA for both strains are shown in Figure 5.7. The NPs with outermost layer of AM completely eliminated *S. aureus* within 15 min (10 logs reduction). However, a longer incubation time was required in the case of *E. coli*, where 3 logs bacterial reduction was achieved within 15 min and 10 logs (full kill) after 45 min (**Figure 5.7B**). The different killing rates of the NP$_{AM/HA}$-AM against *S. aureus* and *E. coli* could be explained with the specific structure of the bacterial cell wall in Gram-positive and Gram-negative bacteria.[199] In Gram-positive bacteria, the thick outer cell wall of negatively charged polysaccharides readily interacts with the antimicrobial cationic AM, resulting in cell membrane damage. However, in Gram-negative bacteria, the cell wall is a complex double membrane structure (composed of inner and outer membranes), which is an efficient barrier to many available antimicrobials. It protects bacteria and makes the cells more resistant to numerous drugs compared to the Gram-positive bacteria.[200] From another side, NPs with HA outermost layer did not show any bactericidal activity against the studied bacterial species over the time of incubation. All

of these results demonstrated the importance of the active agent position in the NP multilayer shell as well as the synergistically enhanced killing efficiency of the combination of nanoform and high cationic surface charge density. The higher antimicrobial efficiency of the NPs with AM outermost layer in comparison to that of the NPs terminated with HA was due to the larger amount of surface available amino groups (1.09 vs 0.04 µmol mL^{-1}, respectively) able to interact with the bacterial cell wall of both tested strains.[201,202]
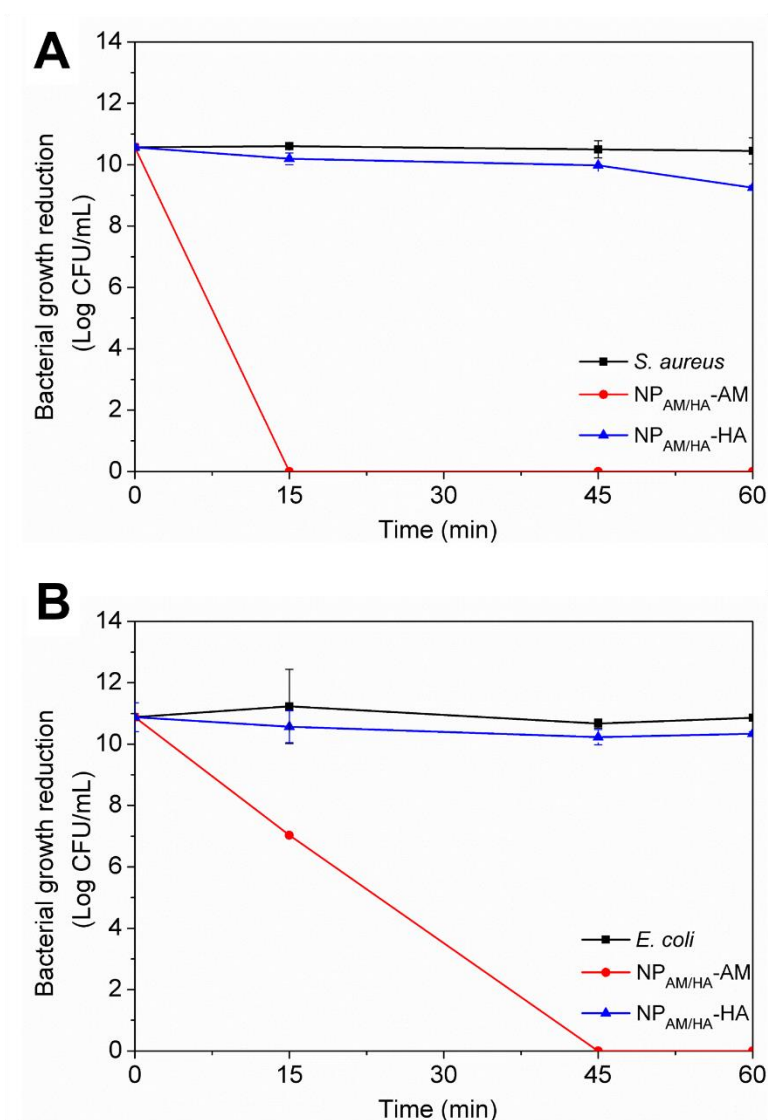
Figure 5. 7 Time-kill curves of LbL coated NPs against (A) *S. aureus* and (B) *E. coli*. *S. aureus* and *E. coli* were incubated with 4 x 10^{10} NPs mL^{-1} NP$_{AM/HA}$-HA (blue) and NP$_{AM/HA}$-AM (red) and the bacteria surviving the treatment were estimated after 15, 45, and 60 min. All data are mean values of three independent experiments.

The membrane permeability of bacterial cells treated with $NP_{AM/HA}$-AM was further evaluated using Live/Dead Kit assay. The assay contains two nucleic acid dyes- PI and SYTO9. SYTO9 stains both live and dead bacteria in green, penetrating the cell membranes, whereas the PI penetrates only the damaged membranes, displaces the SYTO9, and stains the dead cells in red. The obtained microscopic images (**Figure 5.8**) supported the viable-cell counting in the time-killing kinetic assay (**Figure 5.7**). Microscopic images of live/dead stained *S. aureus* and *E. coli* cells after incubation with the coated $NP_{AM/HA}$-AM (**Figure 5.8**) revealed the presence of only dead bacteria visualized by red fluorescence. All results taken together demonstrated that the NPs functionalized with an AM outermost layer were remarkably efficient against these bacterial species.
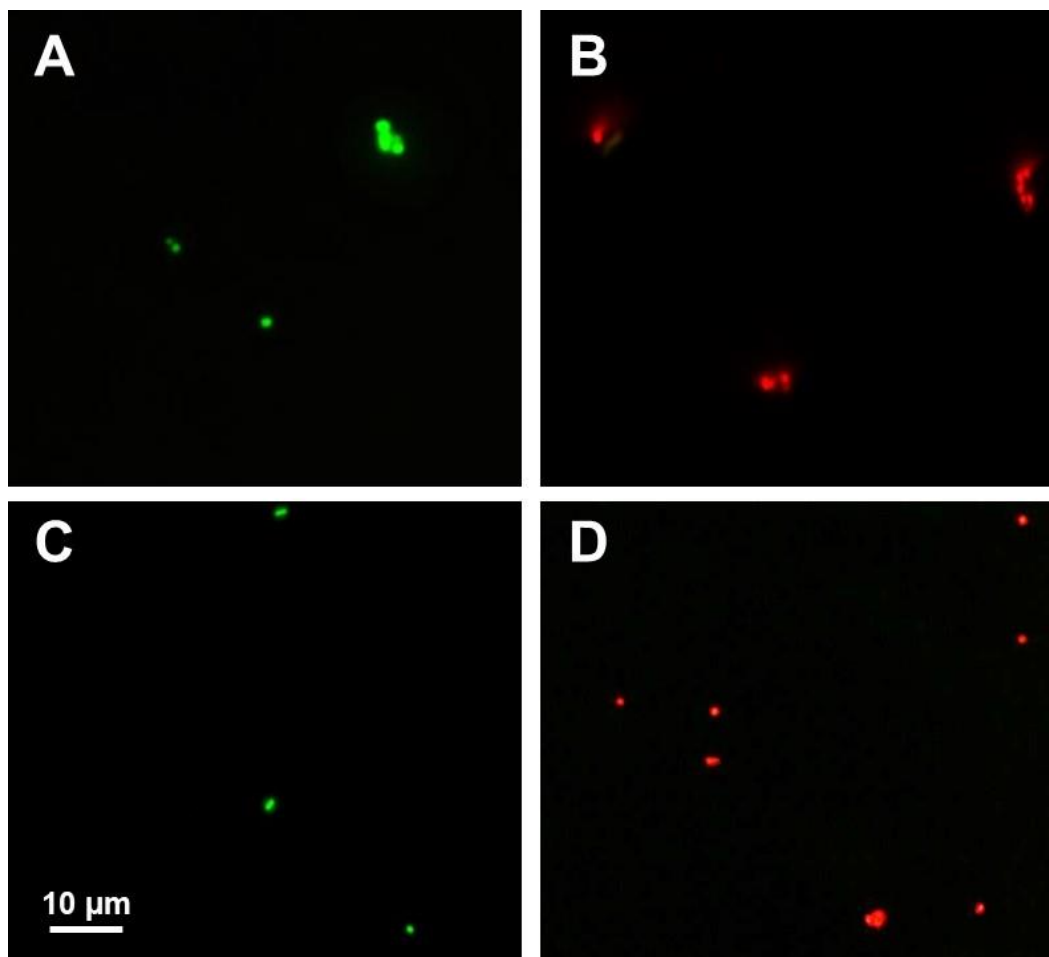
Figure 5. 8 Fluorescence images (100 x magnification) of (A) *S. aureus*, (B) *S. aureus* treated with $NP_{AM/HA}$-AM, (C) *E. coli*, (D) *E. coli* treated with $NP_{AM/HA}$-AM. The green and red fluorescence images are overlaid. Nonviable bacteria are stained in red, while the viable bacteria appear green.

5.1.3 Interaction of the coated NPs with model bacterial membranes

To corroborate the *in vitro* results and confirm the bactericidal mechanism of action of the multilayered biopolymer-shell NPs, solutions of the template and the LbL-coated NPs were injected into the subphase beneath the model PE monolayer, previously formed at 33 mN m^{-1}. The increase of the surface pressure (π) as a function of time demonstrated the membrane disrupting effect of $NP_{AM/HA}$-AM, whereas no effect or negligible effect was observed for the template and $NP_{AM/HA}$-AM, respectively (**Figure 5.9**). The disrupting effect of the AM-terminated NPs correlates well with the higher concentration of the amino groups (27-fold more) in their outermost layer, compared to that of the HA ending NPs. The latter NPs showed little or almost negligible membrane disturbance effect and were not able to kill the cells because most of their amino groups are buried under the HA layer and are not accessible for interaction with PE. Disrupting bacterial cell membrane as a result of the electrostatic interaction between the positively charged NPs and the negatively charged bacterial membrane is considered a valuable alternative to effectively reduce bacterial spread and drug resistance occurrence. Bacterial membrane is highly evolutionarily conserved, and the possibility to be modified by fast single mutation is very low.[203]
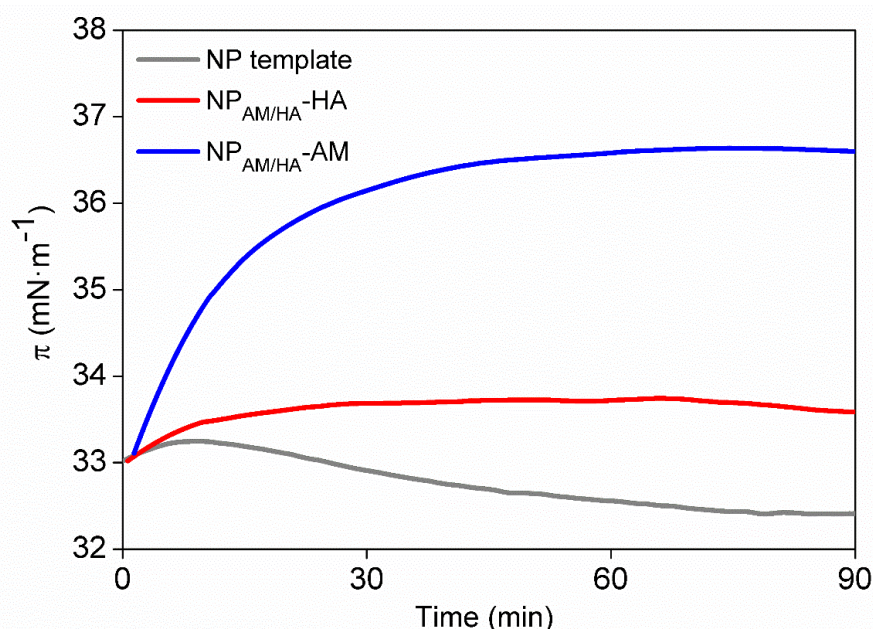
Figure 5. 9 Kinetic adsorption process after the incorporation of the NP template and LbL coated NPs into the air/water interface of the PE monolayer at $\pi = 33$ mN m^{-1}.

5.1.4 Biofilm Inhibition

The ability of the LbL-coated NPs of restricting *S. aureus* and *E. coli* biofilm growth on a model polystyrene surface was further examined. Despite the different conditions used in the biofilm inhibition tests (e.g., growth medium and static conditions), the AM-terminated NPs inhibited by 94 and 40 %, respectively, the *S. aureus* and *E. coli* cells adhesion and biofilm formation (**Figure 5.10**). At bactericidal concentration (4×10^{10} NPs mL^{-1}), the NPs were able to interact with the negatively charged *S. aureus* cell membrane, eradicate the bacteria, and consequently inhibit cell adhesion and biofilm establishment on the surface. However, the NP antibiofilm potential toward Gram-negative *E. coli* was significantly lower. The decrease in the antibiofilm activity of AM-terminated NPs toward *E. coli* could be due to the diminished antibacterial effect of the NPs on Gram-negative bacteria compared to that on Gram-positive species under the conditions tested.[199] Moreover, several studies have reported that positively charged polymers may interact with *E. coli*, increase the cell aggregation, and stimulate bacterial sedimentation on the surfaces. Zhang *et al.* found that the electrostatic interactions between the positively charged polymer and negatively charged *E. coli* cells, instead of killing the cells, increase the bacterium insusceptibility to antibiotics and induce biofilm formation. In the presence of cationic polymers, the cells aggregated and formed clusters where bacteria grew and accumulated signaling molecules inducing biofilm formation.[204] In a similar way, the NP$_{AM/HA}$-AM may bind to the outer cell membrane and agglomerate the *E. coli* cells into biofilm clusters on the surface. At nonbactericidal concentration, the NP$_{AM/HA}$-HA NPs were able also to affect planktonic cells and prevent *E. coli* and *S. aureus* biofilm establishment. The addition of the NP formulation in bacterial suspension reduced the surface colonization and the total biofilm growth of *E. coli* and *S. aureus* by 62 and 99 %, respectively. HAs have been widely used in engineering antifouling coatings on materials and surfaces to improve their stability and functionalities for the intended biomedical application.[205] Its antifouling properties appeared very promising to reduce nonspecific protein adsorption and strengthen NP stability in complex serum containing media. [206] In this study, we employed the antifouling HA to build an antibacterial multilayered shell with AM on a biocompatible NP template. We found that the HA position as an outermost layer of the NPs defines better efficacy toward *E. coli* biofilms. Nevertheless, the exact mechanism of antibiofilm action of HA-terminated NPs is unclear; we believe that its deposition

contributed to the improved colloidal stability of $NP_{AM/HA}$-HA in TSB growth medium and consequently enhanced NP efficacy toward Gram-negative strains (**Figure 5.10**).
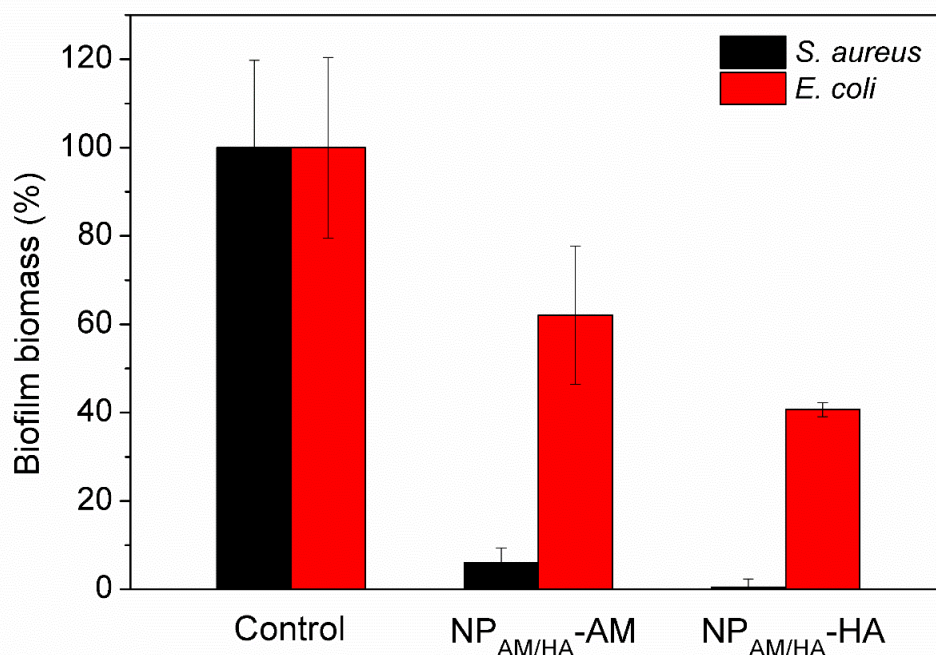
Figure 5. 10 Crystal violet assessment of biofilm formation of *S. aureus* (black bars) and *E. coli* (red bars) after incubation for 24 h with the biopolymer-coated NPs.

In general, the developed multilayer NPs of HA and AM demonstrated strong antibacterial activity and ability of restricting the biofilm formation of common Gram-negative and Gram-positive pathogens. The engineered LbL NPs could be further exploited in the development of skincare formulations for treatment of skin infections, wound dressings, or coatings on medical surfaces for controlling bacterial infections and developing drug resistance.

5.1.5 Biocompatibility of the LbL decorated NPs.

The biocompatibility of the antibacterial agents is a major issue for applications in humans. Therefore, the potential toxicity of the coated NPs toward fibroblasts cells was evaluated. A study with human fibroblast cells demonstrated that all coated NPs were biocompatible, with no difference in cell viability observed among the experimental groups (**Figure 5.11**). The morphology of the human cells treated with bactericidal concentration of LbL-coated NPs was not changed when compared to that of the

control-only fibroblast cells with growth medium (**Figure 5.12**). These results demonstrate that the developed NPs are safe for uses in contact with human cells. The mammalian and bacterial cells differ in the lipid composition of their membranes, which is the reason for the highly selective toxicity of positively charged polymers toward bacteria.[207] The LbL-engineered NPs showed high antibacterial and antibiofilm efficiencies coupled to biocompatibility, which would make possible their fast uptake in biomedical applications.
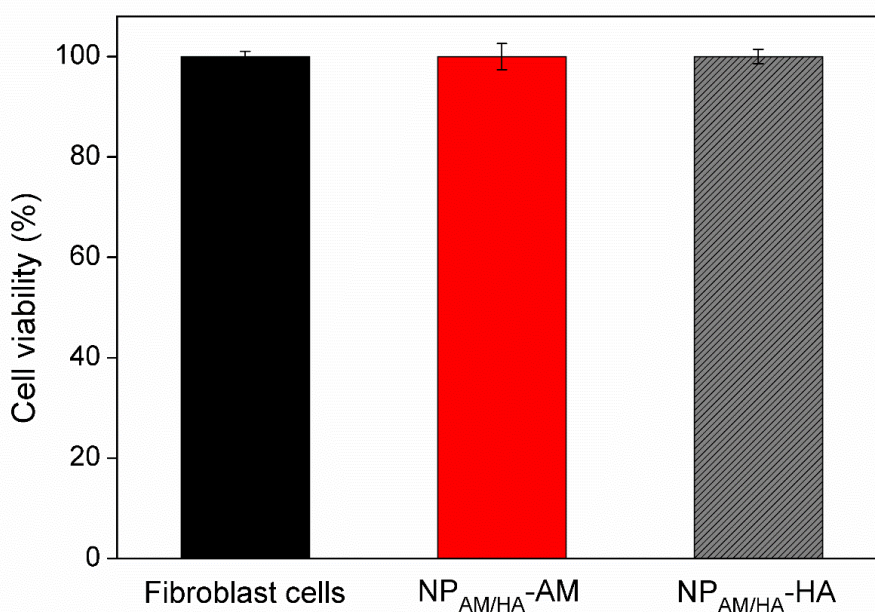
Figure 5. 11 Viability (%) of human fibroblasts exposed to LbL coated NPs.
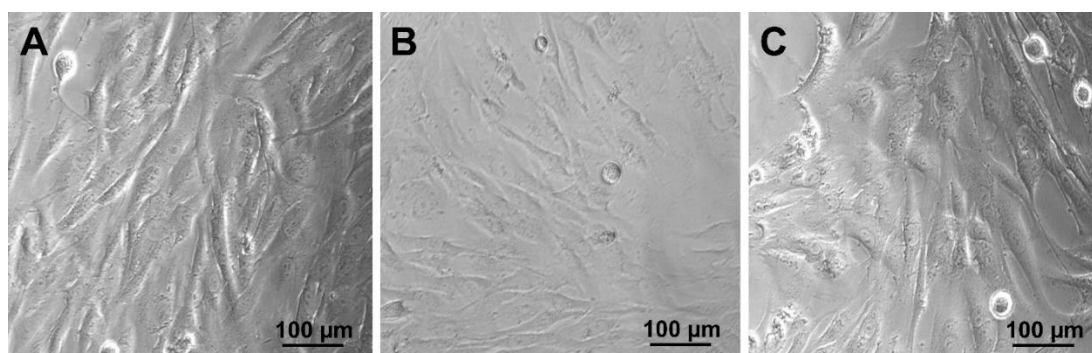
Figure 5. 12 Morphology of human fibroblasts exposed to (A) $NP_{AM/HA}$-AM; (B) $NP_{AM/HA}$-HA; (C) Control human fibroblast cells.

5.1.6 Conclusions

In an attempt to produce novel antibacterial agents, bioinert polymer NP templates were functionalized with multilayers of biocompatible HA and antimicrobial AM in an LbL coating approach. The LbL-engineered nanoassemblies were able not only to kill planktonic bacterial cells, but also to prevent biofilm formation. The NPs with AM as an outermost layer showed strong antibacterial efficiency against both Gram-positive and Gram-negative bacteria for exposure time of less than 1 h. Moreover, the functionalized NPs demonstrated enhanced capacity of the nanolayered AM to interact with and disrupt the negatively charged bacterial cell membranes at lower concentration in comparison to its bulk solution. On the contrary, the LbL functionalized NPs were able to inhibit the formation of biofilm by *S. aureus* and impede biofilm growth by *E. coli*, without affecting the morphology of human fibroblast cells. The antibacterial and antibiofilm efficiencies of the AM-ended NPs coupled to their biocompatibility suggest that this novel antibacterial agent may have a great potential in prevention of bacterial infections. Further investigations *in vivo* should be pursued to study the potential of these NPs for treatment of infectious diseases.

5.2

Layer-by-Layer Coating of Aminocellulose and Quorum Quenching Acylase on Silver Nanoparticles Synergistically Eradicate Bacteria and Their Biofilms

In the current study, the coating of antibacterial AgNPs with membrane disrupting biopolymer is expected to create high local positive charge density, which synergistically with the activity of the nano-sized template will improve the interaction of the novel hybrid NPs with bacterial membranes and potentiate the bactericidal activity
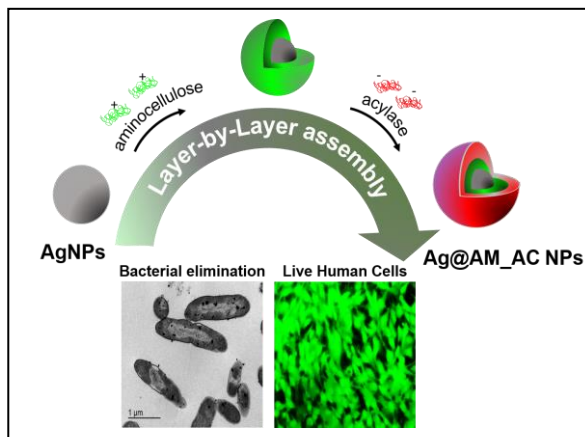
of AgNPs at lower dosage. Furthermore, the inclusion of acylase in the nano-hybrids will inhibit the establishment of *P. aeruginosa* biofilm, making the pathogen susceptible to low and safe to human cells AgNPs concentrations. The functionality of the novel NPs will be evaluated in terms of QS inhibition potential, antibacterial activity and capacity to prevent and eradicate P. aeruginosa biofilms. Finally, the cytotoxicity of the NPs will be assessed in vitro toward human fibroblasts cells.

5.2.1 NPs characterization

AgNPs were produced and used as an active antibacterial NP-template for LbL self-assembling with amino-bearing AM and anti-QS acylase (**Figure 5.14A**). The synthesis of AgNPs was carried out in an aqueous solution as previously described.[208] The change from transparent to green-grey colored suspension and the appearance of the absorbance peak at 400 nm confirmed AgNPs formation (**Figure 5.13**).
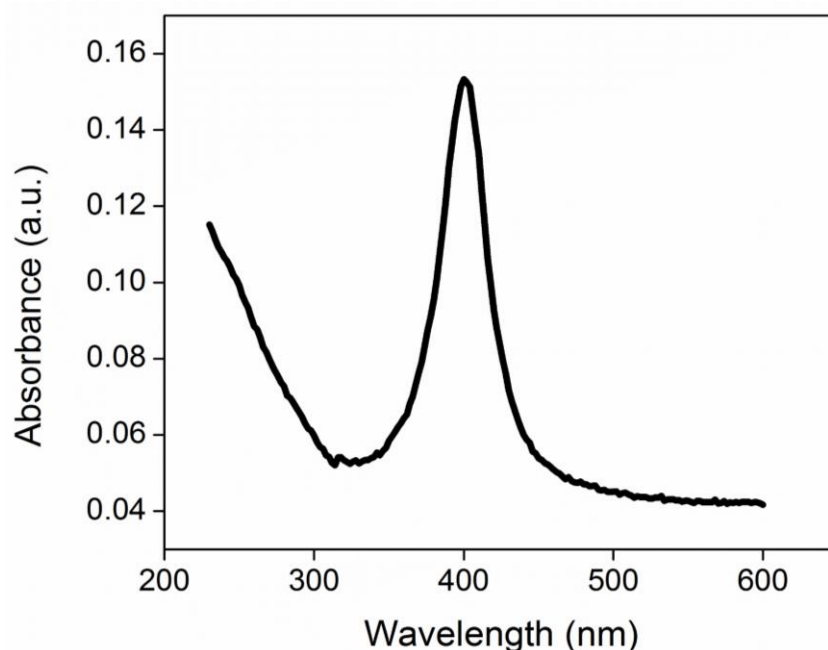
Figure 5. 13 UV-Vis scan of AgNPs.

The resulting NPs, with −56,15 mV zeta-potential and 30 nm size were then sequentially coated with oppositely charged AM and acylase in an LbL fashion. The positively charged AM was applied as a first layer, changing the AgNPs zeta potential to +30.8 mV. Subsequently, the deposition of negatively charged QQE acylase switched the NPs surface charge to −29.97 mV forming stable LbL Ag@AM_AC NPs (**Figure 5.14B**). The morphology of the LbL Ag@AM_AC NPs was further assessed using TEM. TEM images (**Figure 5.14C, D**) revealed the generation of quasi-spherical in shape NPs with an average size of 30-35 nm, which are embedded in a hybrid macromolecular shell of AM and acylase. The data revealed a small size of the NPs (**Figure 5.14E**). The scanning transmission electron microscope (STEM) mapping and EDX spectroscopy of an individual LbL Ag@AM_AC NP further confirmed the presence of elemental silver in the metal NP core (bright central region), as well as

carbon and oxygen in the AM and acylase shell (**Figure 5.14F**). The Cu ions detected by the EDX (**Figure 5.14G**) are from the grid used for the analysis.
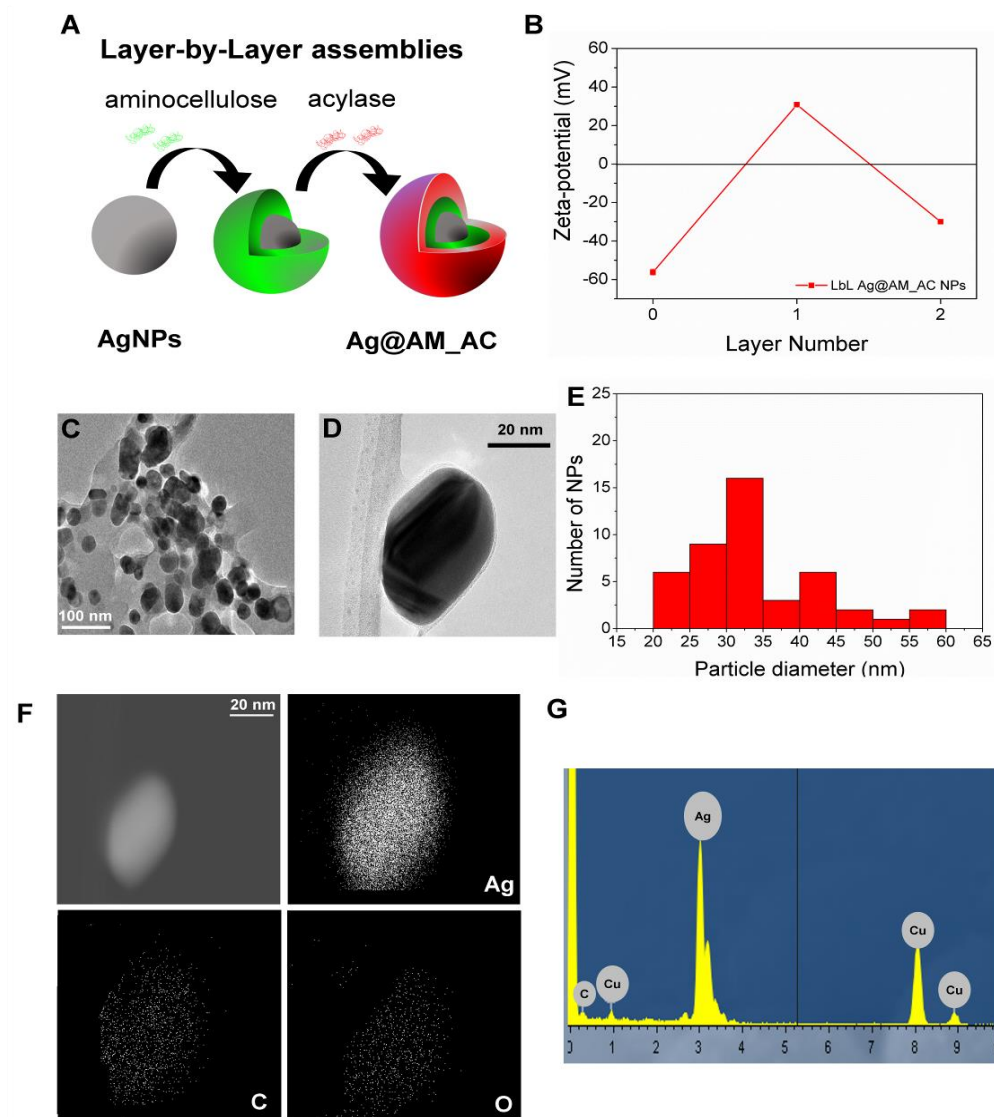
Figure 5. 14 LbL Ag@AM_AC NPs preparation and characterization. (A) Schematic representation of AgNPs template coating with AM and AC using LbL approach. (B) Zeta-potential of the NPs after each layer deposition. (C, D) TEM images of LbL Ag@AM_AC NPs at different magnifications. (E) Histogram of LbL Ag@AM_AC NPs size distribution based on the total count using ImageJ software. (F) Elemental mapping image and (G) STEM-EDX spectrum of an individual LbL Ag@AM_AC NP.

The activity of acylase in the LbL Ag@AM_AC NPs was further assessed following a colorimetric method and an *in vitro* bioassay with a reporter bacterial strain. In the colorimetric assay, the enzymatic activity of acylase was confirmed via the degradation of N-acetyl-L-methionine substrate to L-methionine and the subsequent development of purple color upon interaction with ninhydrin[90] (**Figure 5.15**).
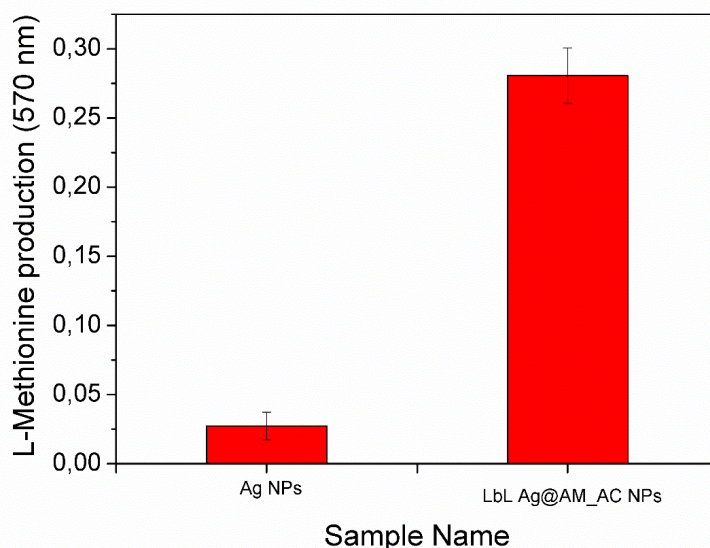
Figure 5. 15 L-Methionine production in the presence of AgNPs and LbL Ag@AM_AC NPs.

The QQ activity of the enzyme after its deposition onto the AgNPs templates was demonstrated through the degradation of the QS signals in *C. violaceum* CV026. *C. violaceum* CV026 is mini-Tn5 mutant that produces a purple pigment (violacein) upon the addition of AHL signaling molecules.[209] The QQE degrades the AHL signals, consequently inhibiting the violacein production.[210] This Gram-negative bacterium has been used in our group to demonstrate the anti-QS potential of acylase from *A. melleus*.[77,90] LbL Ag@AM_AC NPs, at sub-inhibitory concentrations (1.56×10^7 NPs mL^{-1}), degraded the AHLs and disrupted the QS process, reducing the violacein production by 45 % (**Figure 5.16B, C**), without affecting *C. violaceum* growth (**Figure 5.16D**). The same amount of pristine AgNPs, however, did not influence the production of this pigment, confirming the presence of active enzyme on the nanotemplate, which is able to quench the signals and inhibit the QS-regulated behavior in the Gram-negative pathogen *P. aeruginosa*. Interruption of QS in the extracellular environment is a new approach for attenuation of bacterial virulence and boosting the bactericidal activity of existing antimicrobials at lower dosage.[157] Moreover, the anti-QS based strategy reduces the risk of drug resistance development.
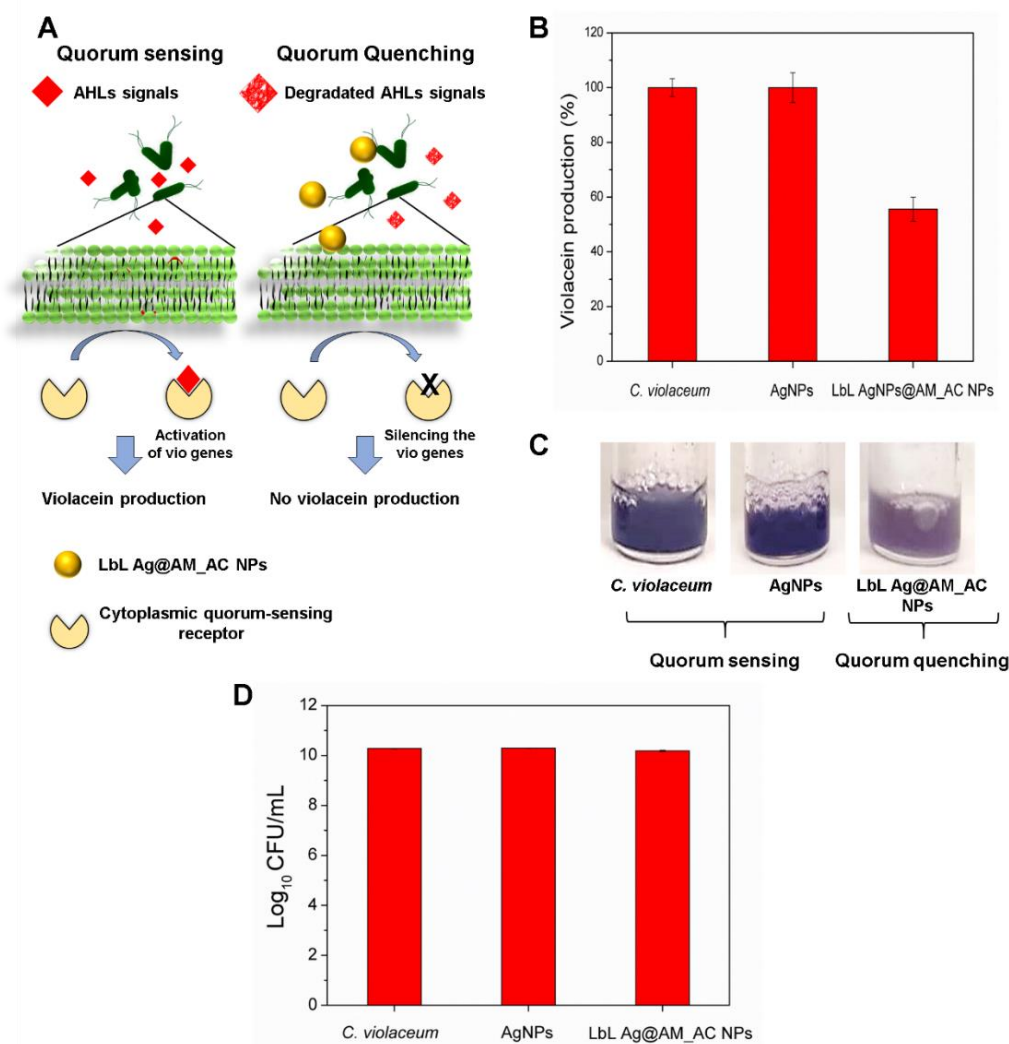
Figure 5. 16 Violacein production by *C. violaceum*. (A) The AHL signals bind to the cytoplasmic QS receptor and switches on the *vio* genes, activating the violacein production (left). The presence of QQ active NPs breaks down the AHL signals, silencing the expression of the *vio* genes, subsequently inhibiting the violacein production (right). (B) Quantification of QS regulated violacein production (%) by *C. violaceum* and (C) Representative images of violacein production in presence of AgNPs and LbL Ag@AM_AC NPs. (D) *C. violaceum* cell viability after incubation with AgNPs and LbL Ag@AM_AC NPs.

5.2.2 Antibacterial efficiency of AgNPs and LbL Ag@AM_AC NPs

The stand-alone AgNPs demonstrated antibacterial activity against *P. aeruginosa* at concentration of 1×10^9 NPs mL^{-1} (**Figure 5.17**). However, the functionalization of AgNPs with AM enhanced their bactericidal activity by 2-fold. The nanoscale transformation of amino-bearing polymers enhanced the availability of the positively charged amino groups, resulting in increased interaction with bacterial cells and stronger bactericidal effect than the pristine solution.[104] Furthermore, the inclusion of

QQ acylase improved 4-fold the NPs inhibitory efficacy against *P. aeruginosa* (**Figure 5.17**).

In order to study the physical changes of bacteria upon exposure to LbL Ag@AM_AC NPs, ultrastructural analysis using TEM was performed. A clear difference in the morphology between the non-treated (**Figure 5.17C**) and treated with NPs (**Figure 5.17D**) *P. aeruginosa* cells was observed. The LbL Ag@AM_AC NPs adsorbed onto the bacterium surface, leading to outer membrane disintegration and cytoplasmic leakage. Moreover, some of the LbL NPs were observed in the cytoplasmic space, indicating their ability to penetrate the membrane and affect essential for bacterial cells life-supporting metabolic processes as cells respiration (**Figure 5.17D**).
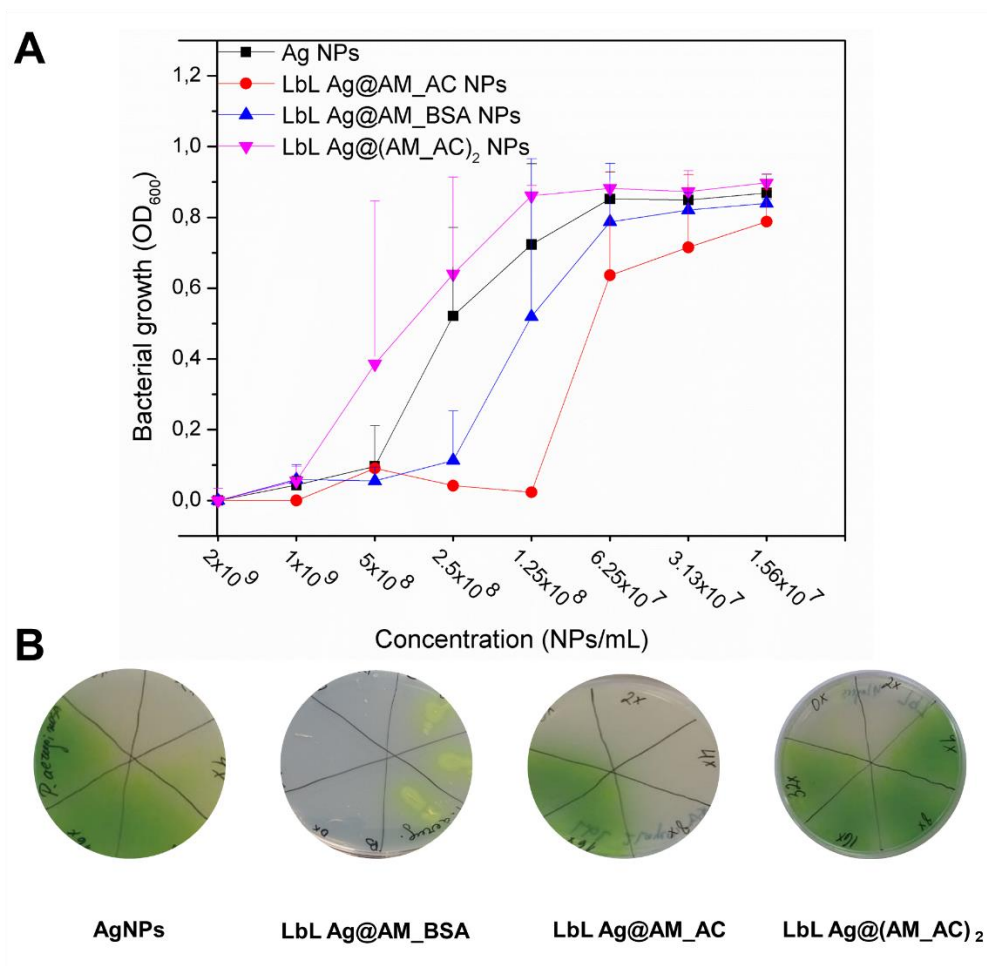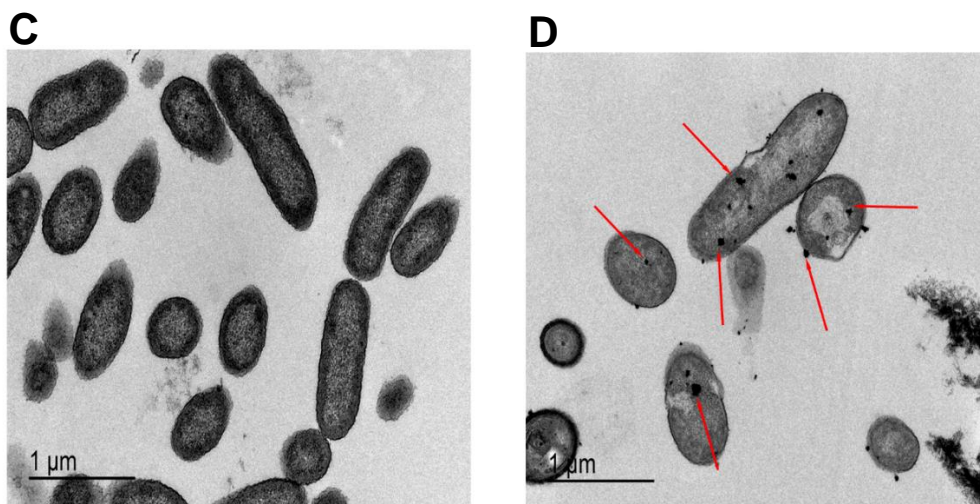
Figure 5. 17 (A) *P. aeruginosa* growth after 24 h incubation with AgNP template, LbL Ag@AM_AC NPs, LbL Ag@AM_BSA NPs, and LbL Ag@AM_AC NPs at different concentrations. (B) Representative images after culturing the samples on selective agar plates. TEM images of *P. aeruginosa* (C) before and (D) after exposure to LbL Ag@AM_AC NPs.

The ability of acylase to interfere with QS in *P. aeruginosa* and attenuate its virulence is thought to potentiate the bactericidal capacity of the actives, lowering their antibacterial effective concentrations. In order to outline the role of the enzyme, the AgNPs template were coated with antibacterial AM and a catalytically inert protein, e.g., BSA, instead of acylase (**Figure 5.17A).** The obtained control NPs possess similar physicochemical properties (i.e., size, zeta-potential and concentration) as the LbL Ag@ AM_AC NPs, but were less active toward *P. aeruginosa*, confirming the synergistic role of acylase and AM in enhancing the antibacterial properties of the AgNPs template. The bactericidal activity of LbL Ag@AM_AC was further confirmed after plating onto selective Cetrimide agar. The LbL Ag@AM_AC NPs completely eliminated the *P. aeruginosa* cells at lower concentrations when compared to the same amount of AgNPs due to the complementary action of the bactericidal nano-sized core and the anti-QS acylase (**Figure 5.17B**). Although, our pervious findings in Section 5.1 have shown that higher number of layers is needed to introduce desired antibacterial functionality on inert NP template, herein the deposition of more AM/acylase layers did not result in enhanced bactericidal activity. In contrary, more layers diminished the effect of the active AgNPs template and no synergy between the nanoform and polymeric AM acylase shell was observed (**Figure 5.17A, B**).

It could be anticipated that the novel hybrid NPs kill bacteria via a combination of mechanisms including interaction with bacterial cell wall, ROS production[211] and modulation of microbial signal transduction pathways.[212] The potential of AgNPs template and LbL Ag@AM_AC NPs to generate ROS and kill *P. aeruginosa* was further investigated. In contrast to the positive control, (ROS inducer-bacteria incubated with AAPH, the AgNPs and LbL Ag@ AM_AC NPs did not generate ROS similar to the negative control containing only bacteria (**Figure 5.18).** Thus, the bactericidal AgNPs and LbL Ag@AM_AC NPs cause cellular death without ROS-related oxidative damage.
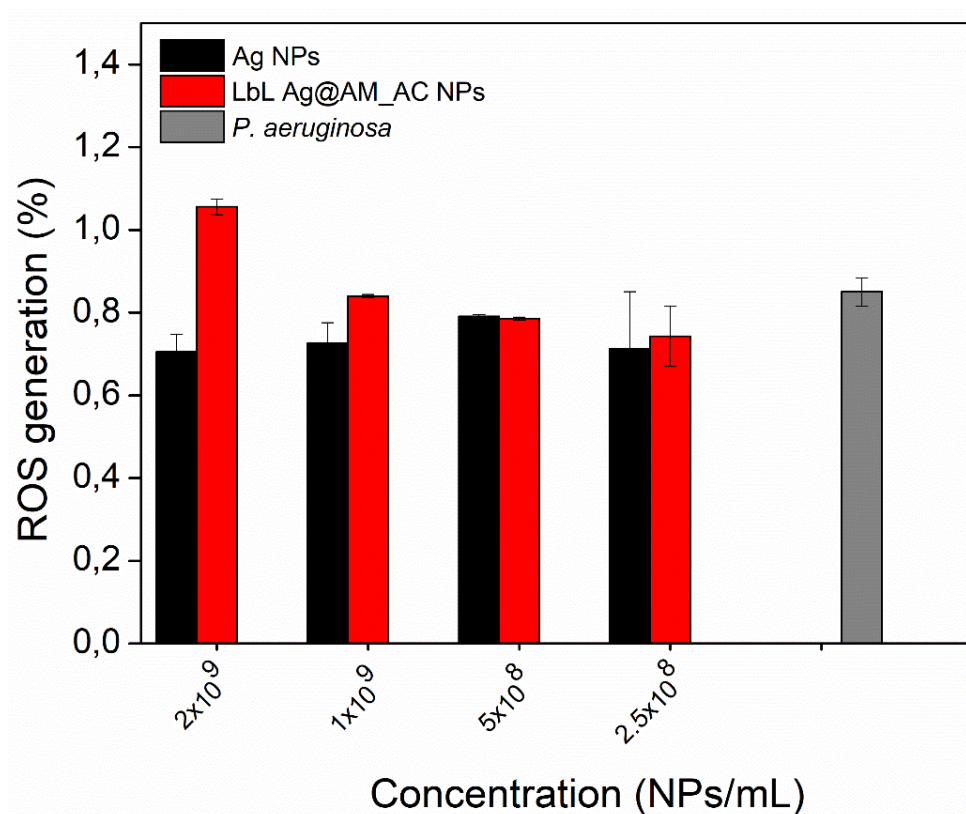
Figure 5. 18 NPs induced ROS generation in *P. aeruginosa*.

5.2.3 Antibiofilm activity

P. aeruginosa is an opportunistic Gram-negative pathogen, responsible for variety of difficult to treat infections due to its ability to attach and form robust biofilm structures on medical devices and living tissues that aggravate the host immune response and resist the antibiotic therapies. *P. aeruginosa* biofilm formation is a complex bacterial

mode of growth, which is under the control of QS.[71] In this work, we aimed to develop hybrid NPs that interrupt the QS process via degradation of the AHL signaling molecules and thus effectively inhibit and eliminate the biofilm growing *P. aeruginosa* cells at lower concentrations than the stand alone AgNPs. The antibiofilm activity (biofilm growth inhibition and elimination) of the NPs was studied by crystal violet and Live/dead BacLight assays to quantify the total biofilm mass and visualize the live and dead cells on a model polystyrene surface.

5.2.3.1 Inhibition of P. aeruginosa biofilm formation by LbL Ag@AM_AC NPs

P. aeruginosa was cultured in the presence of different concentrations of LbL Ag@AM_AC NPs and AgNPs for 24 h to determine the minimum biofilm inhibitory concentration (MBIC). The MBIC is defined as the concentration at which the total biofilm mass was inhibited by > 90 %, when compared to the control with only bacteria corresponding to 100 % biofilm formation. The MBIC of the NPs decorated with AM and anti-QS enzyme was 8-fold lower (6.25×10^7 NPs mL^{-1}) than the MBIC of the pristine AgNPs (5×10^8 NPs mL^{-1}) (**Figure 5.19A**).
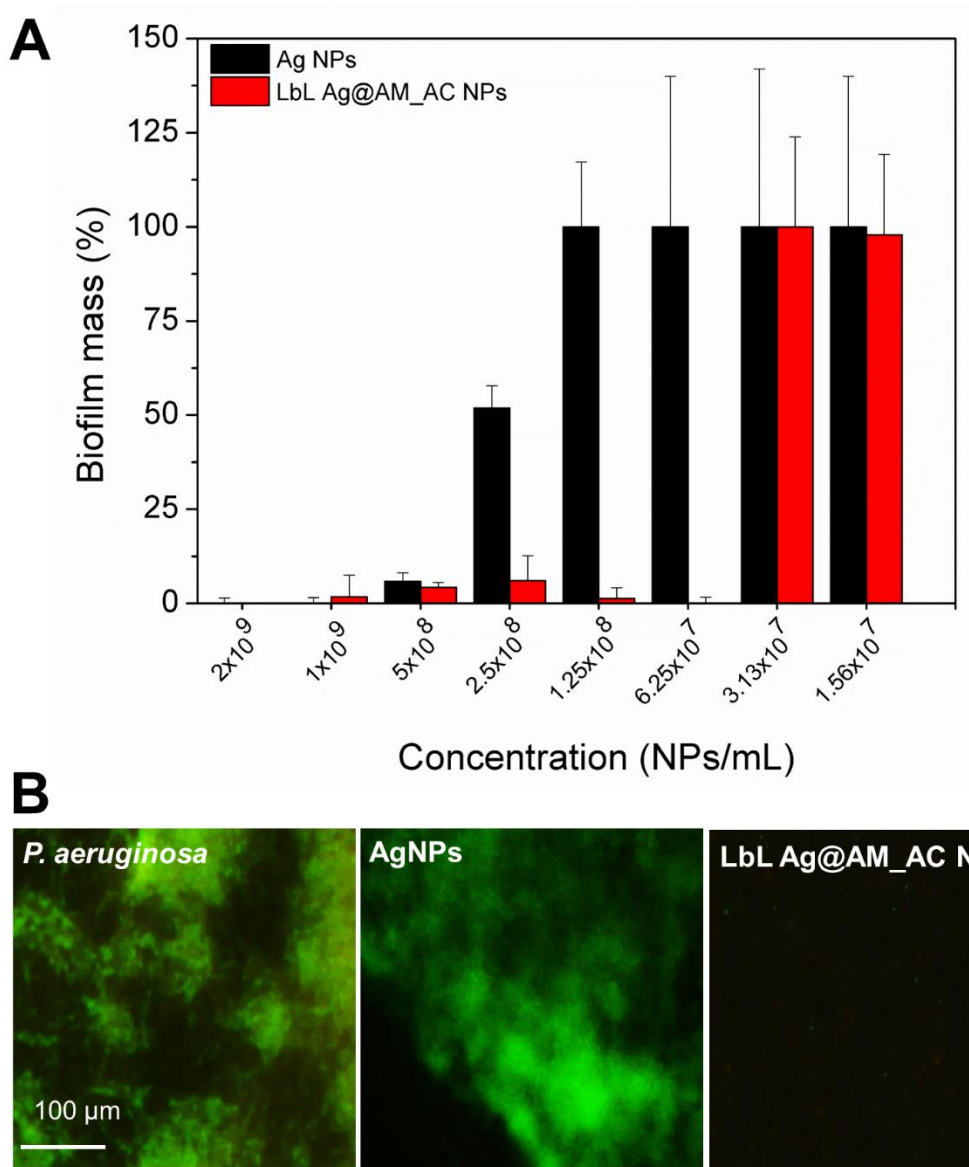
Figure 5. 19 *P. aeruginosa* biofilm inhibition. (A) MBIC determination of the NPs using crystal violet assay. (B) Live/dead™ *Bac*Light™ kit microscopic visualization. The green and red fluorescence images are overlaid. Nonviable bacteria are stained in red, while the viable bacteria appear green.

The obtained microscopic images of *P. aeruginosa* biofilms after 24 h incubation with LbL Ag@AM_AC NPs at the determined MBIC further confirmed their enhanced antibiofilm activity (**Figure 5.19B**). The LbL Ag@AM_AC NPs at their MBIC completely inhibited the biofilm growth of *P. aeruginosa* observing only few individual cells on the surface. In contrast, the AgNPs at the same concentration, showed negligible antibiofilm activity and formed typical for the mature biofilm bacterial

clusters, similar to the control (only *P. aeruginosa*) (**Figure 5.19B**). All these results indicated the synergy between the bactericidal nano-sized template and the antibiofilm acylase enzyme. Interrupting the QS process through acylase-catalyzed degradation of bacterial signals in the extracellular bacterial space have been shown very effective for inhibiting *P. aeruginosa* virulence and establishment of drug resistant biofilms, without bacteria killing.[157] Herein, the deposition of acylase on the bactericidal AgNPs yielded multifunctional nanoentities able to inhibit the QS-regulated pathological processes and at the same time completely eliminate the biofilm forming bacteria at lower dosage of the bactericidal agent, thus exerting less evolutionary pressure on bacteria for resistance development. The engineered LbL NPs demonstrated high potential for eradicating *P. aeruginosa* and therefore could be exploited in the development of coatings on medically relevant surfaces for preventing biofilm associated infections.

5.2.3.2 Elimination of P. aeruginosa biofilms with LbL Ag@AM_AC NPs

P. aeruginosa cells in already established biofilms are enclosed in EPM, which is the bacterium protective barrier against the action of the immune system and the effective penetration of the conventional drugs.[71] Therefore, the potential of the LbL Ag@AM_AC NPs to overcome the inherent biofilm resistance and penetrate through the *P. aeruginosa* biofilm was further assessed. The minimum biofilm eradication concentration (MBEC) of the LbL Ag@AM_AC NPs, i.e., the lowest NPs concentration at which bacteria fail to re-grow, was determined using crystal violet. The MBEC of the novel NPs was 8-fold lower (1.25×10^8 NPs mL^{-1}) than the MBEC determined for the stand-alone AgNPs template (2×10^9 NPs mL^{-1}) (**Figure 5.20A**).
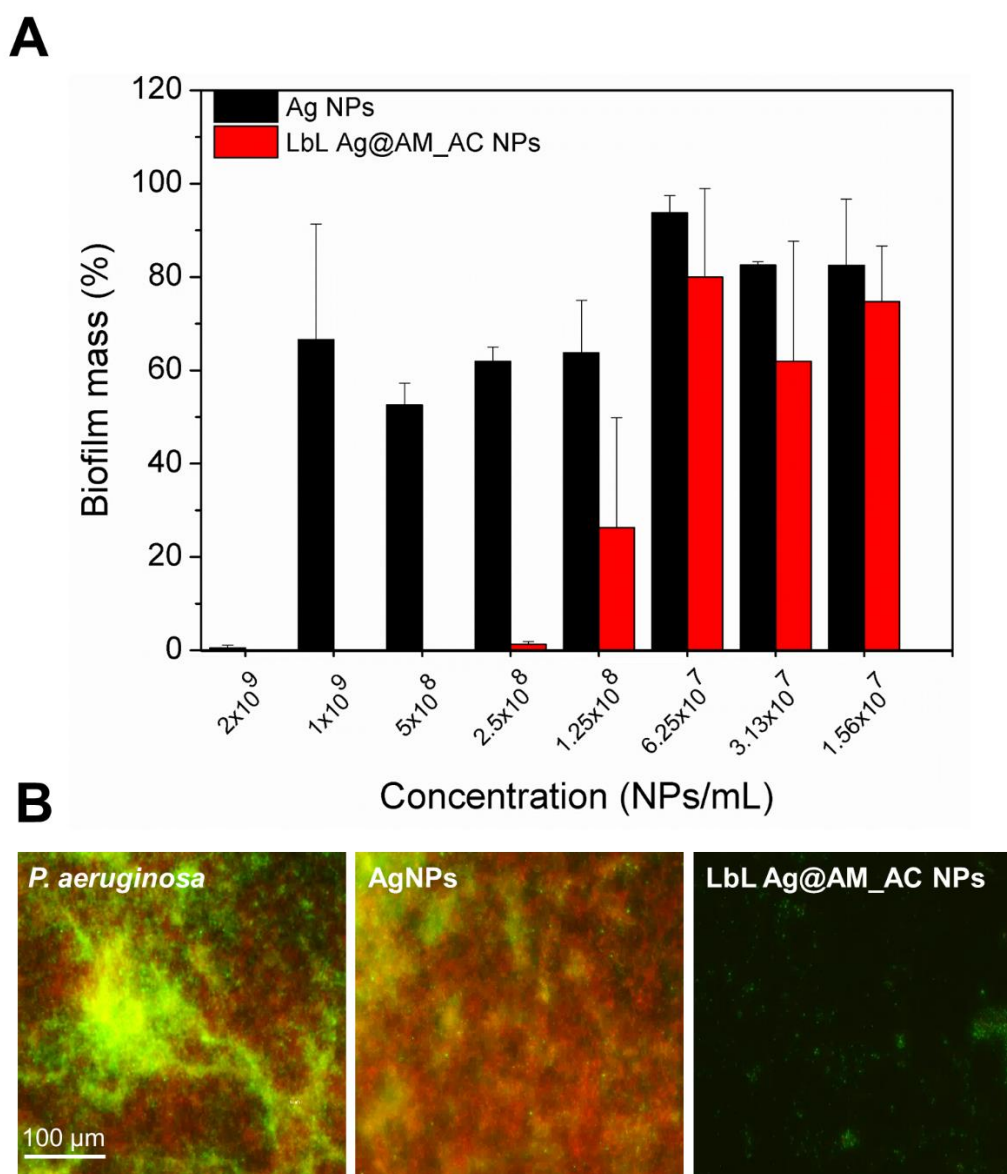
Figure 5. 20 Elimination of 24h grown *P. aeruginosa* biofilm. (A) MBEC determination of the NPs using crystal violet assay. (B) Live/dead™ *Bac*Light™ kit microscopic visualization of *P. aeruginosa* biofilm after 24 h treatment with AgNPs and LbL Ag@AM_AC NPs at the same concentration (6.25×10^7 NPs mL^{-1}). The green and red fluorescence images are overlaid. Nonviable bacteria are stained in red, while the viable bacteria appear green.

Although the anti-QS approaches are considered more relevant in inhibiting the early stage of biofilm formation, rather than acting on already established surface-attached bacterial communities, several studies have demonstrated the ability of acylase to reduce bacterial biofilms. These findings are in line with the assumption that the QS signaling has an important role for maintaining the integrity of already formed *P. aeruginosa* biofilm.[213–215] In particular, the process is part of the eDNA release and the structural stability of the biofilm.[71] We believe that the nanoformulated acylase weakens

and destabilizes the protective EPM barrier, enhancing the access of therapeutic NPs to the bacterial cells in the mature biofilm. Moreover, decorating the AgNPs with a cationic polymer adds an additional mechanism for bacteria killing, through membrane disruption, potentiating the antibacterial and antibi-ofilm activities of AgNPs at lower concentrations.[216,217] Previous results of our group, have demonstrated enhanced antibacterial and biofilm activities of nanoformulated antimicrobials (such as AM, penicillin and vancomycin) in comparison to their bulk counterparts, due to easier penetration into biofilm structures and access to the target bacteria.[218] The effect of LbL Ag@AM_AC NPs and AgNPs template (at concentration 1.25×10^8 NPs mL^{-1}) on established biofilms was assessed with fluorescence microscopy after Live/Dead staining. A significant decrease in the cell viability and biofilm density was observed when the 24 h old biofilm was treated with LbL Ag@AM_AC NPs (**Figure 5.20B**). In contrast, the application of unmodified AgNPs resulted in reduced cells viability, however, without any significant decrease/elimination of the total biofilm mass (**Figure 5.20B**). Therefore, the novel LbL Ag@AM_AC NPs possess great therapeutic potential and could be employed in the design of topical formulations for treatment of severe skin infections or for coating of medical devices and surfaces in contact with humans.

5.2.4 Biocompatibility assessment

AgNPs are known antibacterial agent widely used as disinfectant or coating of medically relevant surfaces,[219] however their biocompatibility is an important issue to be considered for biomedical application. Therefore, the viability of human cells upon exposure to AgNPs template and LbL-decorated NPs at their bactericidal concentrations was assessed after 24 h of incubation. AgNPs demonstrated high toxicity and reduced by 20 % the viability of human cell (**Figure 5.21**), while nearly 100 % of the skin cell fibroblasts were viable in the presence of functionalized with AM and acylase AgNPs (**Figure 5.21A**). Unlike the AgNPs, the LbL Ag@AM_AC NPs did not cause cell morphology changes compared to the negative control (**Figure 5.21B**). The toxicity of AgNPs greatly depends on their concentration, size, shape, surface chemistry/coating and dissolved silver ions from the NPs.[220] Here, to benefit from the outstanding performance of AgNPs in terms of microbial elimination and at the same time minimize their toxicity, we engineered in a safety approach novel biomaterial-coated AgNPs Functionalization of the AgNPs with biocompatible and antibacterial polymers and

enzymes is a promising strategy to change the AgNPs toxicity profile and boost their bactericidal properties.
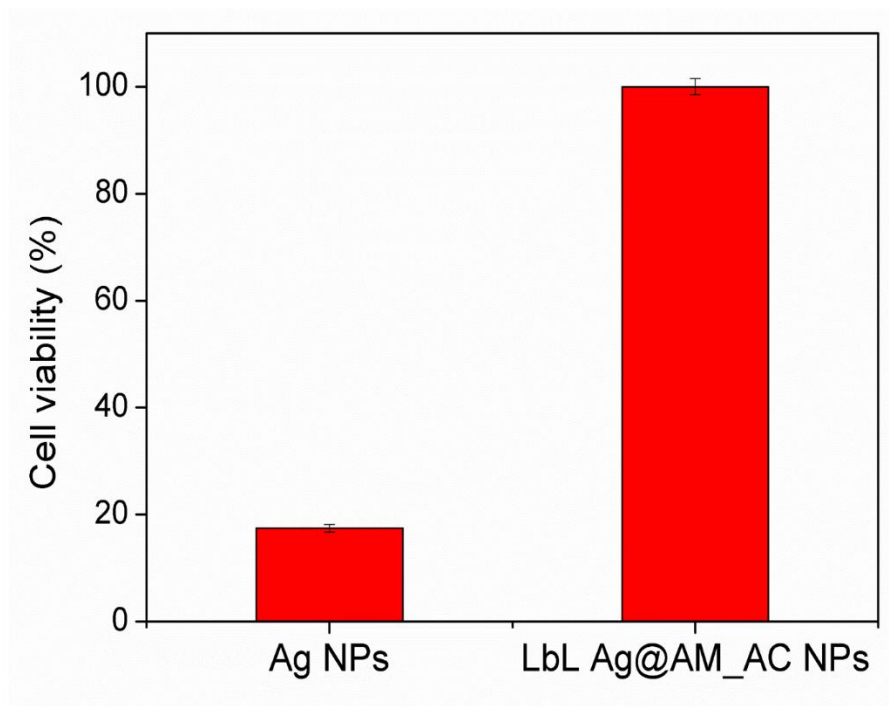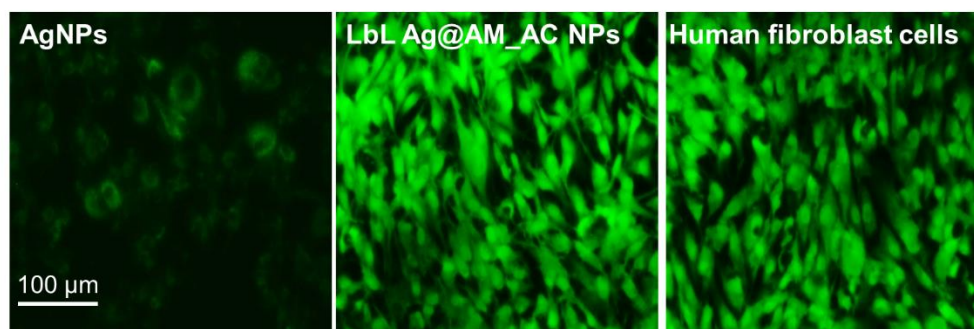
Figure 5. 21 Cytotoxicity evaluation. (A) Viability (%) of human fibroblasts exposed to AgNPs and LbL Ag@AM_AC NPs after 24 h of incubation assessed by the AlamarBlue assay. (B) Live/death assay of human fibroblasts after 24 h exposure to AgNPs and LbL Ag@AM_AC NPs. The green and red fluorescence images are overlaid.

5.2.5 Conclusions

In this work AgNPs were LbL coated with antimicrobial AM and QQ acylase in order to generate safe and highly efficient antibacterial and antibiofilm hybrid nanoentities. The bilayered decoration of AgNPs template resulted in 4-fold enhanced bactericidal activity toward the Gram-negative *P. aeruginosa* due to the synergy between the metal core and the nanoformulated antibacterial AM and antibiofilm acylase. Moreover, these hybrid NPs were able to degrade the AHL signaling molecules of Gram-negative bacteria, inhibiting the QS regulated biofilm formation by *P. aeruginosa* at lower concentrations than the pristine AgNPs. The anti-QS acylase has also affected the pathogenicity and the integrity of already established *P. aeruginosa* biofilm, increasing the bacterium susceptibility to antibacterial AgNPs. LbL building of a biocompatible shell of AM and acylase around the AgNPs is a safe-by-design approach for development of metal-based nanoantimicrobials with decreased toxicity to mammalian cells and improved efficacy. The combination of membrane-disrupting AM and QQ acylase on the AgNPs surface provides an innovative tool for treatment of bacterial infections, at minor risk for resistance development.

5.3 Antibody-enabled Antimicrobial Nanocapsules for Selective Elimination of Gram-positive *Staphylococcus aureus*

In this study, NCs, loaded with antibacterial oregano EO for effective elimination of Gram-positive *S. aureus* were generated. The EO NCs were coated with AM to provide reactive groups on the NCs surface for the grafting of an antibody that is specific against *S. aureus*. The EO NCs functionalization with a targeting antibody increased the NCs bactericidal efficacy against the Gram-positive *S. aureus* at a lower dosage and, at the same time, will reduce the toxic effects on non - targeted bacteria and human cells. The selective antibacterial activity of the antibody - functionalized EO NCs toward *S. aureus* was further evaluated in vitro in a single and mixed bacterial inoculum with non-targeted *P. aeruginosa*. Finally, the biocompatibility and the treatment efficacy were validated in an in vitro co-culture model comprising human fibroblast cells and *S. aureus* bacteria.
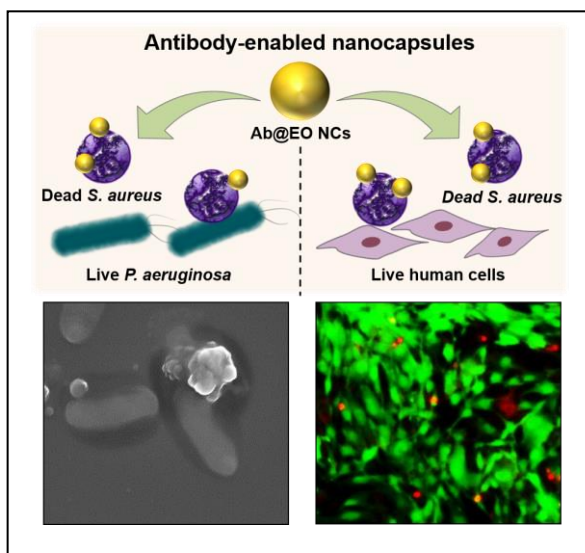
_____

This section is based on the following publication:

Ivanova K, **Ivanova A**, Ramon E, Hoyo J, Sanchez-Gomez S, Tzanov T. Antibody-Enabled Antimicrobial Nanocapsules for Selective Elimination of Staphylococcus aureus. ACS Applied Materials & Interfaces 2020, http://dx.doi.org/10.1021/acsami.0c09364.

5.3.1 Targeted NCs formulation and characterization

EO NCs were produced using a proprietary self-assembly nanoencapsulation technology[194] based on propylene glycol, a water-miscible nonvolatile organic solvent, and zein, a hydrophobic protein found in maize. The technology is simple and versatile and allowed the formation of stable and homogeneous zein NCs loaded with the hydrophobic oregano EO from *Thymbra capitata*.[194] High EO EE, of about 86 %, was determined by carvacrol quantification with HPLC. Zein NCs containing EO with an average size of 94 ± 3.7 nm, low polydispersity index < 0.2, and −33 ± 0.5 mV zeta-potential (at pH 3.3) (Figure **Figure 5.23**), indicating uniform size distribution and colloidal stability, were stored for 6 months at RT without any visible signs of aggregation and precipitation. The negative surface charge of the EO NCs could be due to the surfactant excipients employed to provide higher colloidal stability of the final formulation or modulation of the zein conformation upon nanotransformation.[221–223] As anticipated, and based on our previous experience,[104] the EO encapsulation led to enhanced antibacterial efficacy against the targeted *S. aureus* at lower dosage, when compared to the same amount of the pristine oil (**Figure 5.22**).
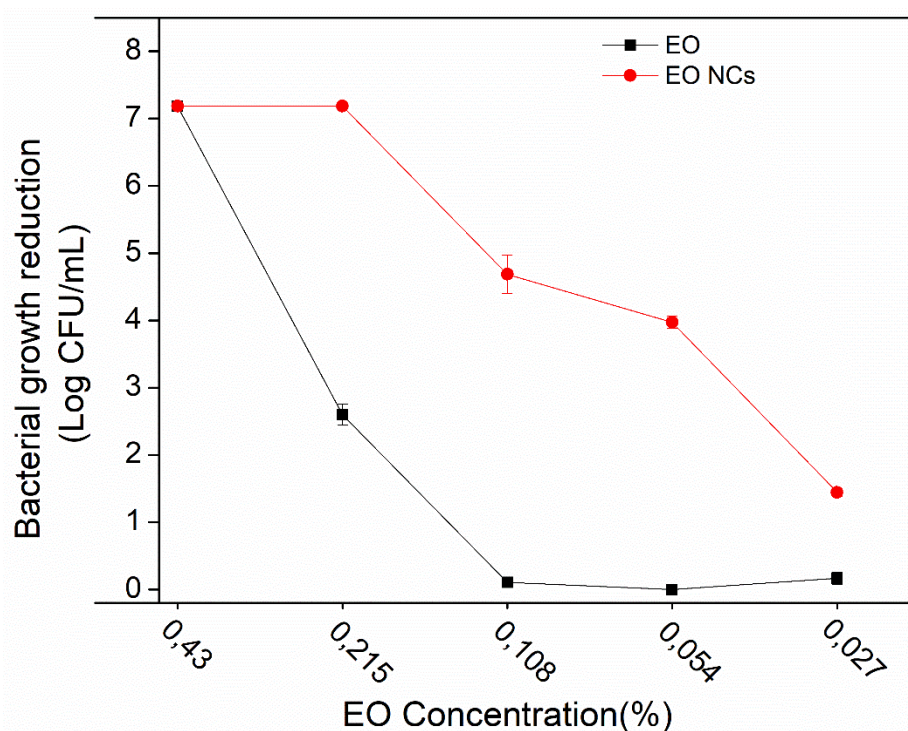
Figure 5. 22 *S. aureus* growth reduction after 24 h incubation with free (black lines) and encapsulated EO (red lines) at different concentrations. The EO encapsulation led to enhanced antibacterial efficacy against *S. aureus* at lower amounts, when compared to the amount of pristine oil.

The negatively charged EO NCs were further coated with positively charged AM (36.4 ± 0.75 mV), following the principles of electrostatic-driven self-assembly, to introduce more reactive amino groups onto the NCs surface for grafting of the *S. aureus* targeting antibody (**Figure 5.23A**). The AM deposition onto the EO NCs led to a change of the zeta-potential from −33 ± 0.5 to +33.8 ± 0.4 mV (**Figure 5.23I**), as well as an increase of the average NCs size from 94 ± 3.7 to 114 ± 3.5 nm. The presence of amino groups on the AM-decorated EO NCs (AM_EO NCs) surface was confirmed by staining with fluorescamine reagent. The amount of available primary amino groups on the NCs was 27-fold higher in the case with the AM_EO NCs than that of the pristine EO NCs, where negligible amounts (1.4 µg mL^{-1} ± 0.2), originating from the low-availability of lysine and arginine zein amino acids,[224] were determined. These AM_EO NCs demonstrated enhanced antibacterial efficacy (**Figure 5.24**) against *S. aureus* compared to the pristine EO NCs at the same concentrations (∼ 1.5 × 10^9 NCs mL^{-1}) because of the higher availability of primary amino groups, leading to improved interaction and disruption of the bacterial membrane.[104] Consequently, those groups were lost upon the immobilization of the targeting antibody. This was confirmed by the changes in the zeta-potential from positive to negative for the antibody-enabled EO NCs (Ab@NCs) (**Figure 5.23I**), suggesting that the AM would not play a role in the NCs antibacterial activity.

The AM_EO NCs were functionalized with an antibody that was specific against *S. aureus*[158] by carboxyl-to-amine cross-linking using 1-ethyl-3-(3-(dimethylamino) propyl) carbodiimide and N-hydroxysulfosuccinimide to obtain the targeted Ab@EO NCs (**Figure 5.23A**). Prior to immobilization, the specificity of the antibody toward the targeted bacterium was confirmed using a secondary antibody conjugated to the enzyme horseradish peroxidase.[225] The development of the green color was observed only in those samples where *S. aureus* bacterium was present, but was not detected in the control sample of the nontargeted *P. aeruginosa*, indicating the specific interaction with the bacterium of interest (**Figure 5.23C**).

Considering the fact that the carboxyl groups are ubiquitous throughout the antibody's structure including the antigen binding site, the binding affinity of the immobilized on EO NCs antibody with the antigen was assessed using FITC-conjugated protein A from *S. aureus* (**Figure 5.23D**).[226] The FITC-protein A binding with the Ab@EO NCs resulted in a green fluorescent light emission measured at 525 nm using a fluorescence

spectrophotometer (**Figure 5.23B**). The green light from the Ab@EO NCs was also observed by a fluorescence microscope (**Figure 5.23E**). Such behavior was not found in the EO NCs, which evidenced the successful grafting of the antibody, which was able to interact with protein A at the *S. aureus* surface.

The developed Ab@EO NCs had a mean size of about 134.9 ± 13.2 nm and −28.63 ± 1.19 mV zeta-potential (**Figure 5.23I**). This high zeta-potential (≥ 20 mv) was further reflected in the high colloidal stability, without any visible signs of precipitation, for a long period (up to 6 months) of storage at 4 °C. The Ab@EO NCs size distribution profile, obtained by NTA, showed predominantly three size subtypes at 96.4 ± 9.8, 133 ± 8.6, and 180.9 ± 23.7 nm, with a very narrow distribution profile and low polydispersity (**Figure 5.23H**). Furthermore, the morphology and the size of the Ab@EO NCs were examined by TEM. The images revealed predominantly sphere-like-shaped Ab@EO NCs with a size distribution in the range between 60 and 140 nm (**Figure 5.23F, G**), similar to the results obtained by NTA (**Figure 5.23H**). Small aggregates due to the samples drying during the preparation for TEM analysis could also be observed.
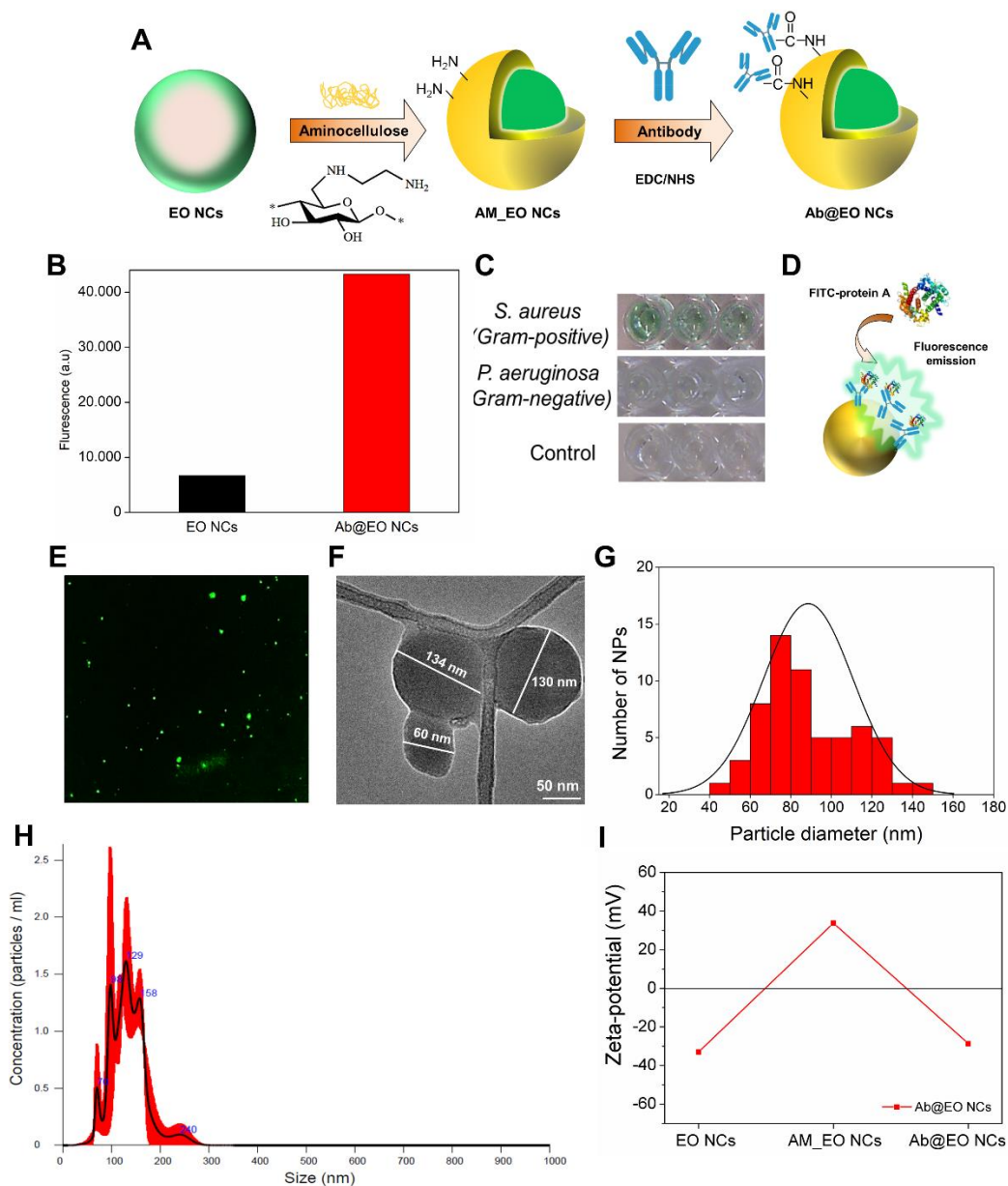
Figure 5. 23 Fabrication and characterization of Ab@EO NCs. (A) Schematic representation of Ab@EO NCs preparation. (B) Fluorescent intensity measurement at Ex/Em = 490/525 nm upon FITC-protein A binding with the Ab@EO NCs. (C) Green color development after antibody interaction with targeted *S. aureus*. (D) Interaction of antibody-enabled EO NCs with FITC-labelled protein A. (E) Florescence microscopy images of FITC-protein A bound Ab@EO NCs. (F) TEM images of Ab@EO NCs at different magnifications. (G) Histogram of the Ab@EO NCs size distribution based on the total count of 60 NPs using ImageJ software. (H) NTA analysis of Ab@EO NCs and (I) zeta-potential values for pristine EO NCs, EO_AC NCs and Ab@EO NCs.

5.3.2 Antibacterial activity towards *S. aureus*

The antibacterial efficiency of the developed nontargeted and targeted EO NCs was assessed *in vitro* against *S. aureus* by quantitative plate count method. EO NCs effectively reduced the growth of *S. aureus* at 4-fold lower concentrations than the bulk oil (**Figure 5.22**). The active principle of the NCs-oregano EO- is composed of oxygenated monoterpenes (77.5 % of the composition), the monoterpenoid carvacrol being the main antibacterial constituent (73.8 %).[157] This monoterpenoid is the component responsible for the strong antimicrobial activity of the oregano oil against both Gram-negative and Gram-positive bacteria and its higher bactericidal effect at very low concentrations than other known EOs such as clove bud and thyme.[227] It has been proved that carvacrol can affect the lipids' ordering and stability of bacterial membrane that in turn increases the membrane permeability, causing cellular lysis and death. Additionally, carvacrol may inactivate intracellular components, such as enzymes involved in energy production, which also leads to bacterial damage and elimination.[119,228]

Although the nontargeted EO NCs were active against *S. aureus*, they showed lower antibacterial activity than the developed Ab@EO NCs at the same concentrations (1.5×10^9 NCs mL^{-1}). Up to 2-fold improvement was observed for Ab@EO NCs because the antibody drives the bactericidal EO NCs directly to the *S. aureus*, increasing the local bactericide concentration on the bacterial surface for a short period of time and thus potentiating its bactericidal efficacy (**Figure 5.24**).
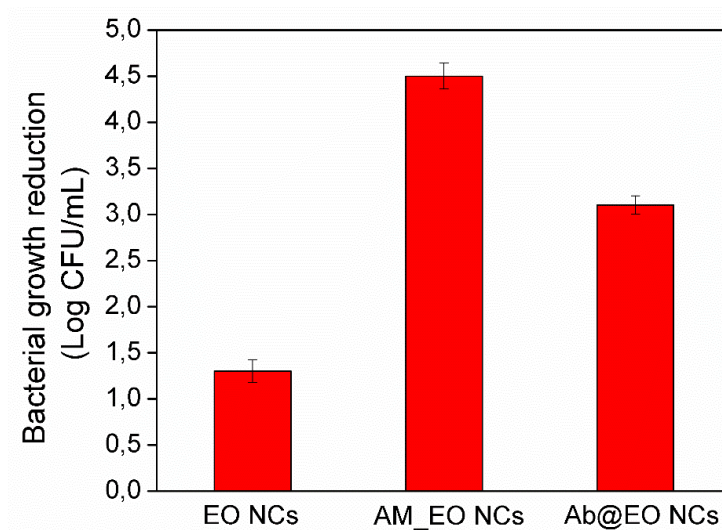
Figure 5. 24 Antibacterial activity of EO and Ab@EO NCs (concentration ≈ 1.5 x 10^9 NCs mL^{-1}) against *S. aureus*.

5.3.3 Real-time monitoring of the NCs interaction with *S. aureus*

QCM-D was used to monitor in real time the effect of the Ab@EO NCs on the targeted bacterium under dynamic conditions. QCM-D allowed us to study the NCs-cells interactions as the piezoelectric mass sensing together with the monitoring of dissipation changes provide information about the different stages of bacterial growth, for example, cells attachment, biofilm formation, cellular lysis, and dispersion.[229] This technique has been routinely used in our group to study the toxic effects of antibacterial nanomaterials on biomimetic bacterial and mammalian membranes, as well as to identify time-dependent changes in bacterial attachment and growth.[153] In this work, *S. aureus* was first deposited onto the QCM sensor, and the changes in the frequency and dissipation upon the circulation of the targeted and nontargeted EO NCs were assessed (**Figure 5.25**). At first, the addition of the bacterial inoculum caused a rapid decrease of the frequency ($\sim$ 20 Hz) (**Figure 5.25A** zone II) from the 100 mM PBS, pH 7.4 baseline (**Figure 5.25A** zone I), attributed to the combined effect of a fast "bulk shift" caused by the change from PBS to MHB, and the adsorption of MHB components and bacterial cells onto the disk.[153] After 3 h of circulation, adhesion of *S. aureus* was achieved, as confirmed by the decrease of the frequency and increase in the dissipation (**Figure 5.25A** zone II). This was supported by the results obtained following a PBS rinse of loosely adhered cells (**Figure 5.25A** zone III), leading to a slight frequency increase/dissipation decrease and ultimately the establishment of a steady-state frequency and dissipation signals at levels lower than the original baseline (**Figure 5.25A** zone I).

Following the formation of a stable *S. aureus* adlayer, the NCs were flowed through with a speed of 20 μL min^{-1} at 37 °C for 45 min. The injection of the Ab@EO NCs caused a decrease of the frequency, possibly translating into a rapid removal of the cells from the sensor (**Figure 5.25A** zone IV). Upon PBS rinsing, the frequency decrease remained stable at the level of the clean, that is, bacteria-free, crystal (**Figure 5.25A** zone I), implying a decrease of the cellular mass and almost complete *S. aureus* elimination from the surface.[229,230] Moreover, the Ab@EO NCs led to changes in the dissipation shifts, which was ascribed to increased water content, rearrangements of the cells on the crystal surface, and morphology changes.[153] A similar tendency was obtained for the control EO NCs; however, the frequency measurements reached a stable state at higher levels ($\cong$ -15 Hz) than the Ab@EO NCs ($\cong$ -5 Hz), suggesting a

lower efficacy of these NCs against the targeted cells (**Figure 5.25A** zone V). These results corroborated the improved killing efficacy of the Ab@EO NCs compared to the pristine EO NCs observed in the antimicrobial tests (**Figure 5.24**). Such behavior was not observed when the experiments were performed with the nontargeted *P. aeruginosa* cells (**Figure 5.25B**). Therefore, targeting via an antibody that is specific against *S. aureus* could be a way to ensure the rapid delivery of the nanoformulated bactericide and the effective elimination of the pathogen from the site of infection.
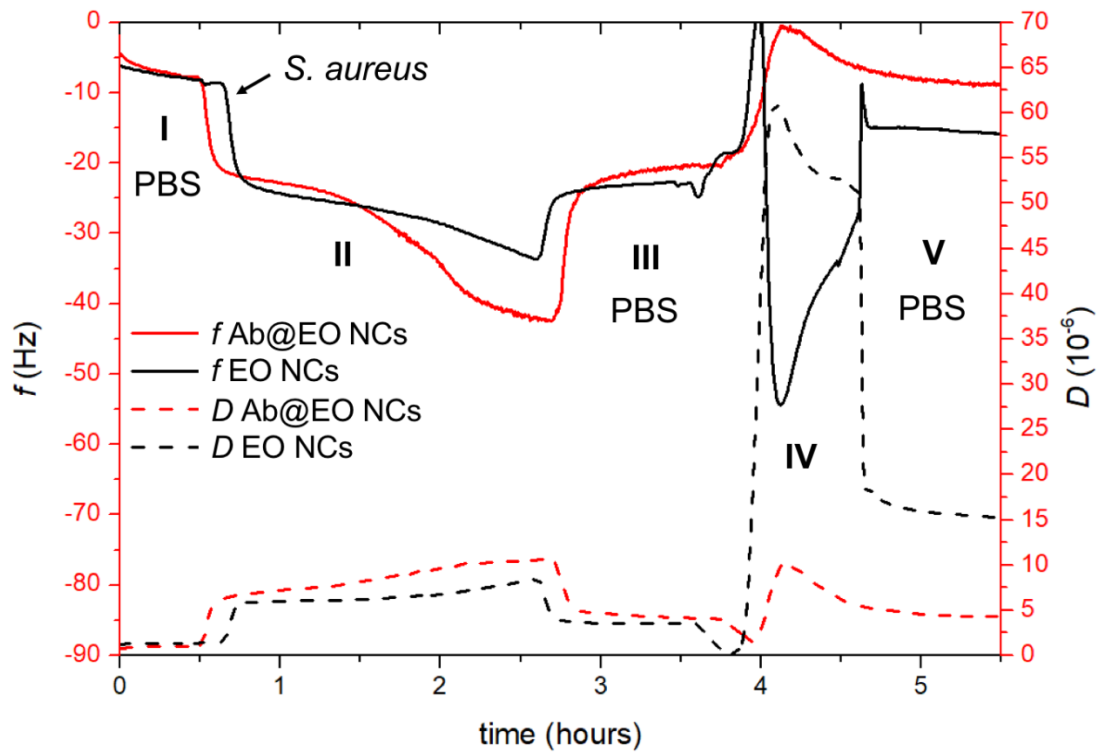
B
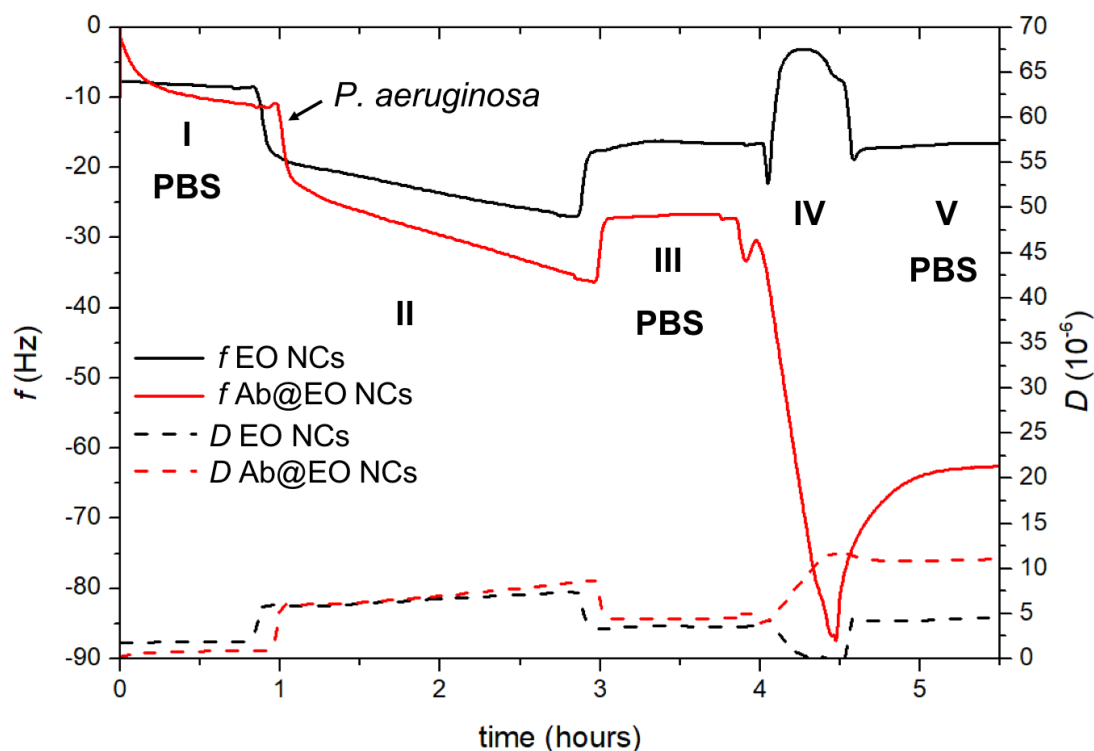
Figure 5. 25 (A) Interaction of EO NCs and Ab@EO NCs with *S. aureus* assessed by QCM-D. The shift in the frequency and dissipation are represented with solid and dashed lines, respectively. The numbers I, II, III, IV and V indicate the different zones, respectively the baseline with PBS, bacterial adhesion, baseline after washing of loosely adherent cells, NCs insertion and PBS washing. (B) Interaction of EO NCs and Ab@EO NCs with *P. aeruginosa* assessed by QCM-D. The shift in the frequency and dissipation are represented with solid and dashed lines, respectively. The numbers I, II, III, IV and V indicate the different zones, respectively the baseline with PBS, bacterial adhesion, baseline after washing of loosely adherent cells, NCs insertion and PBS washing.

5.3.4 Selective antibacterial activity of the Ab@EO NCs towards targeted *S. aureus*

S. aureus is an opportunistic human pathogen found in many skin infections.[231] Currently, control of skin infections has been obtained with antiseptics (e.g., chlorhexidine and triclosan) and antibiotics (e.g., mupirocin and fusidic acid), which affect the beneficial skin microbiota, increase the risk of the development of AMR, and at higher amounts may cause side effects.[64] In this work, we aimed to develop targeted bactericidal nanosystems to selectively eradicate the *S. aureus* pathogen, without affecting other beneficial bacterial strains. The specific action of the Ab@EO NCs on the targeted *S. aureus* was confirmed *in vitro* upon their incubation with a mixed inoculum containing *S. aureus* and nontargeted *P. aeruginosa* as model Gram-negative bacteria found in the skin flora (**Figure 5.26A**). The bacterial viability after exposure to the antibody-functionalized and nonfunctionalized EO NCs was assessed by plating on

selective-for -*S. aureus* and -*P. aeruginosa* agars. As expected, the EO NCs demonstrated antibacterial effect on both bacteria (**Figure 5.26B**). Up to 1.9 and 1.3 log reduction was obtained for *S. aureus* and *P. aeruginosa*, respectively. In contrast, the EO NCs tagged with antibody that was specific against *S. aureus* resulted in more localized delivery of the nano-sized bactericide to the target, and up to 3 log reduction of the initial bacterial load was obtained. Such effect, however, was not observed for the nontargeted *P. aeruginosa* because of the absence of the specific ligand that could drive the antibacterial EO NCs to the target cells (**Figure 5.26B**).

A
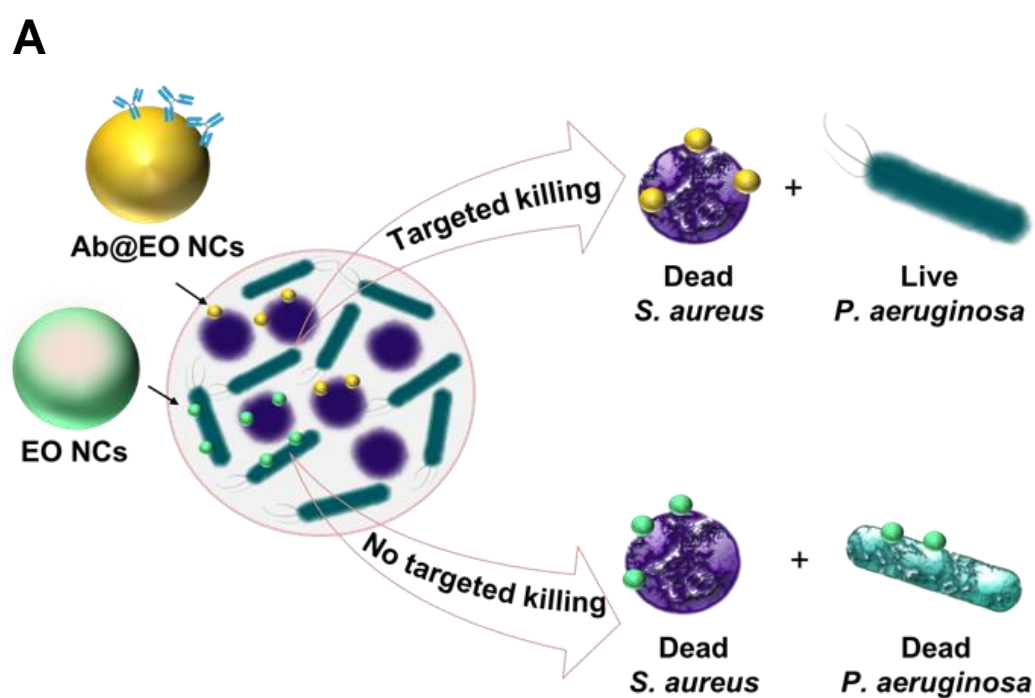
B
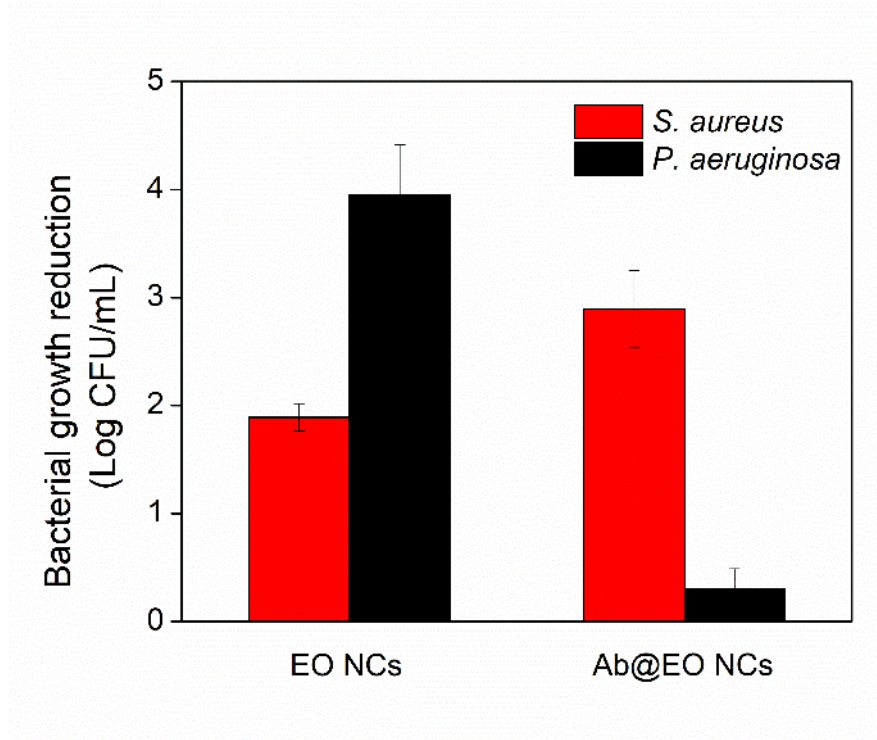
C
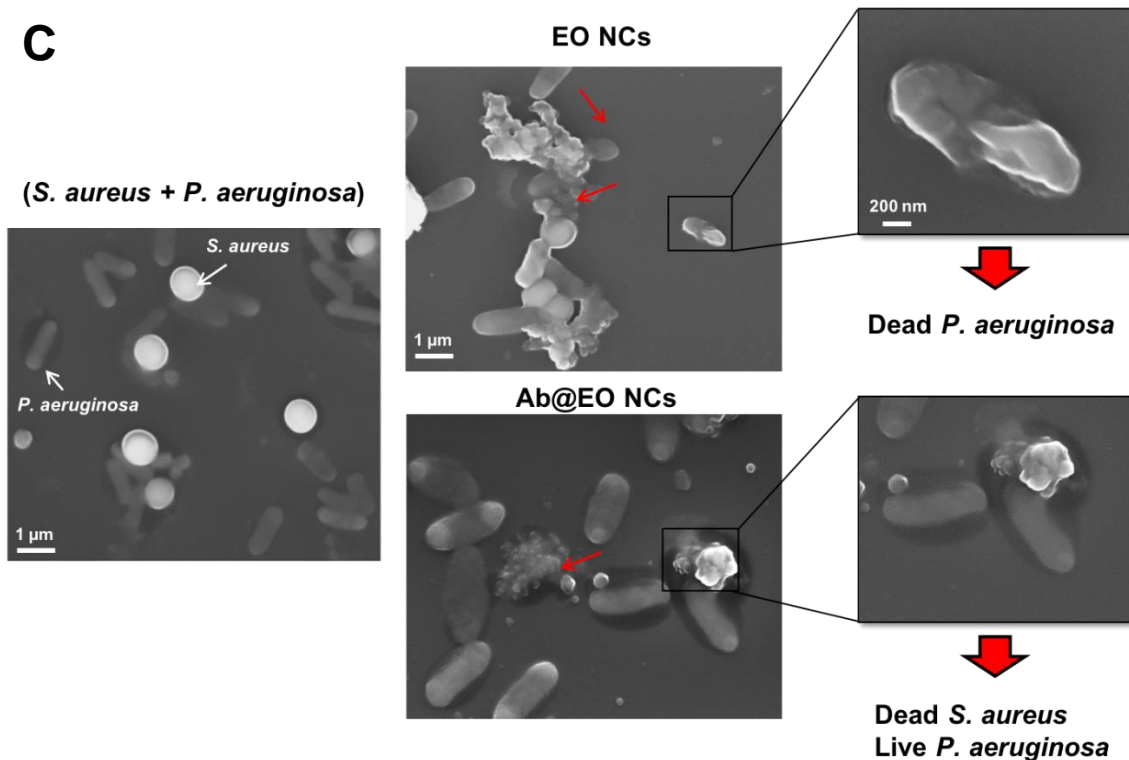
Figure 5. 26 Antibacterial activity of EO NCs and Ab@EO NCs in mixed bacterial inoculum. (A) Schematic representation of the EO NCs and Ab@EO NCs interaction with *S. aureus* and *P. aeruginosa*, when are growing together. (B) *S. aureus* and *P. aeruginosa* growth reduction (Log (CFU mL^{-1})) upon exposure to the EO NCs and Ab@EO NCs. (C) SEM images of *S. aureus* (round-shaped) and *P. aeruginosa* (rod-shaped) bacteria without any treatment and incubated with EO NCs and Ab@EO NCs. White and red arrows indicate live and damaged bacterial cells, respectively.

The selective bactericidal activity of the Ab@EO NCs was further studied using SEM. The SEM images demonstrated that the control *S. aureus* and *P. aeruginosa* cells without the NCs were intact and did not present any morphological changes (**Figure 5.26C**). *S. aureus* appeared spherical with a size of up to 1 μm in diameter, whereas *P. aeruginosa* were rod-shaped, measuring 0.2-0.4 μm in width and 1-1.5 μm in length. Clear differences between the control and the bacteria treated with EO NCs and Ab@EO NCs were observed. In the case of EO NCs, changes in the surface morphology of both *S. aureus* and *P. aeruginosa* cells associated with cellular death could be detected (**Figure 5.26C**), which is in agreement with the results from the live cells counting (**Figure 5.26B**). On the other hand, the interactions driven by the antibody functionalization do not seem to induce any antibacterial effect on the nontargeted *P. aeruginosa* because the overall microorganism morphology was not affected and appeared similar to that of the control without bactericidal treatment. This, however, was not found for *S. aureus* and significant morphological changes were observed after incubation with Ab@EO NCs (**Figure 5.26C**). The altered cell morphology indicated cell damage, which eventually led to leakage of cytoplasmic contents and cellular death. These results corroborated the selective antibacterial efficacy observed in the quantitative plate count method (**Figure 5.26B**), and therefore confirmed that in a mixed bacterial inoculum the antibody-functionalized NCs specifically interact with the *S. aureus* surface and could be used for effective elimination of this bacterium at the site of infection.

5.3.5 Cytotoxicity of the Ab@EO NCs

Nanoformulation of EO represents an effective approach to enhance their physical stability and potentiate the bactericidal activity toward both susceptible and AMR bacteria.[136] However, the potential toxicity of the nano-sized materials, associated with their unique physicochemical properties, may impede their biomedical application. The cytotoxicity of the developed Ab@EO NCs was evaluated in vitro on human fibroblast cells using AlamarBlue reagent for quantification of the metabolically active cells, and a live/dead viability/cytotoxicity assay kit for microscopic visualization of live and dead cells. The Live/Dead assay kit is based on the simultaneous determination of live and dead cells with two fluorescence probes: (i) calcein, which is well-retained within the

live cells, producing green fluorescence, and (ii) ethidium homodimer-1 that enters cells with damaged membranes, producing red fluorescence in the dead cells.

The results from both tests did not show any significant cytotoxicity and antiproliferative effect of the Ab@EO NCs on the human cells after 24 h of exposure at their bactericidal effective concentration. Up to 80 % of the skin fibroblasts were metabolically active, as calculated in comparison to the control-cells without NCs-indicating desirable innocuousness of the novel Ab@EO NCs for therapeutic antibacterial applications (**Figure 5.27A**). Additionally, fluorescence microscopic images after live/dead staining demonstrated that the NCs did not induce any changes in the cellular morphology and most of the cells were alive, thus appearing green (**Figure 5.27B**).

A
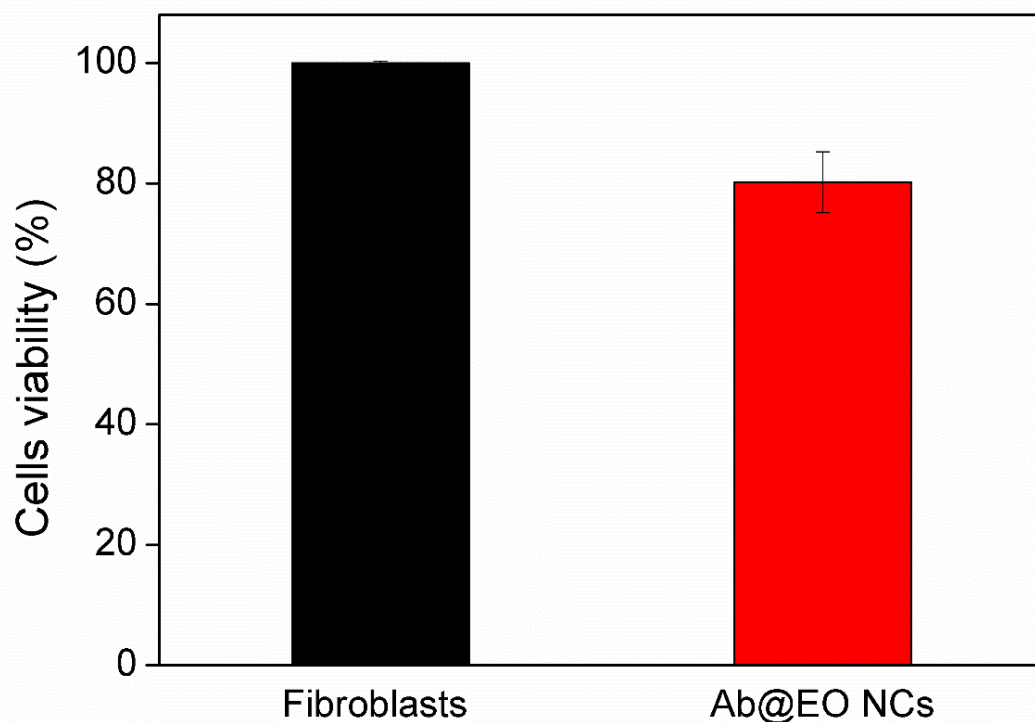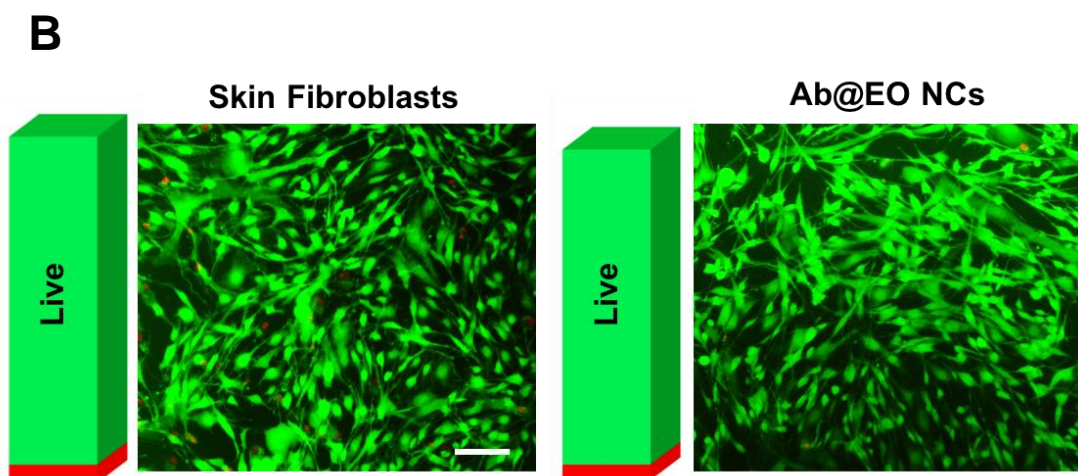
Figure 5. 27 Cytotoxicity of Ab@EO NCs. (A) Viability (%) of human fibroblasts exposed to Ab@EO NCs after 24 h of incubation, determined by AlamarBlue assay. (B) Live/Dead assay of human fibroblasts after 24 h exposure to Ab@EO NCs. Overlapped images of live (green) and dead (red) cells. The bars aside each image represent the green and fluorescence intensities obtained after measuring at λex/em = 494/517 nm and λex/em = 528/617 nm for calcein and ethidium homodimer-1, respectively. Scale bar corresponds to 100 μm.

5.3.6 Antibacterial efficacy of the Ab@EO NCs in an *in vitro* coculture model of *S. aureus* and human cells

Finally, the selective bacterial eradication and treatment efficacy of the Ab@EO NCs was evaluated in an *in vitro* coculture model composed of the target *S. aureus* bacterium and human skin fibroblasts, which are critical for skin healing and recovery.[232] Human cells were infected with *S. aureus* and then exposed to the Ab@EO NCs at their defined antibacterial dosage. Afterward, *S. aureus* bacterial growth was quantified via a plate count method, while the viability of the skin fibroblasts was determined by a live/dead viability/cytotoxicity assay kit. The fluorescence microscopy images after staining of the cocultured cells demonstrated the negative (i.e., lethal) effect of *S. aureus* on the human cells, supported by the increased number of dead fibroblasts. *S. aureus* produces a variety of toxins (e.g., hemolysins and leukotoxin) to damage biological membranes and cause cell death during the infection establishment. The bacterium has been reported to induce direct cytotoxic effect on different human cells, organs, and tissues.[231] In contrast to the nontreated sample, single supplementation of the targeted NCs protected the fibroblast cells from the *S. aureus*-induced cellular damage,

preserving the cells' viability and morphology (**Figure 5.28**). At the same time, the *S. aureus* growth was inhibited by 80 % (**Figure 5.29**). It is worth mentioning that despite the promising antibacterial activity of pristine EO NCs, these demonstrated negligible bactericidal effects on *S. aureus* in our *in vitro* infection model in comparison to the Ab@EO NCs, and at the same time did not maintain the skin fibroblasts viability (**Figure 5.29, 5.28**). Therefore, the novel Ab@EO NCs developed in this work are effective and safe antibacterial agents for selective elimination of the pathogen. Antibody-enabled targeting of the antibacterial EO is a promising strategy to boost their bactericidal activity toward *S. aureus* and lower the adverse effects on the human cells.
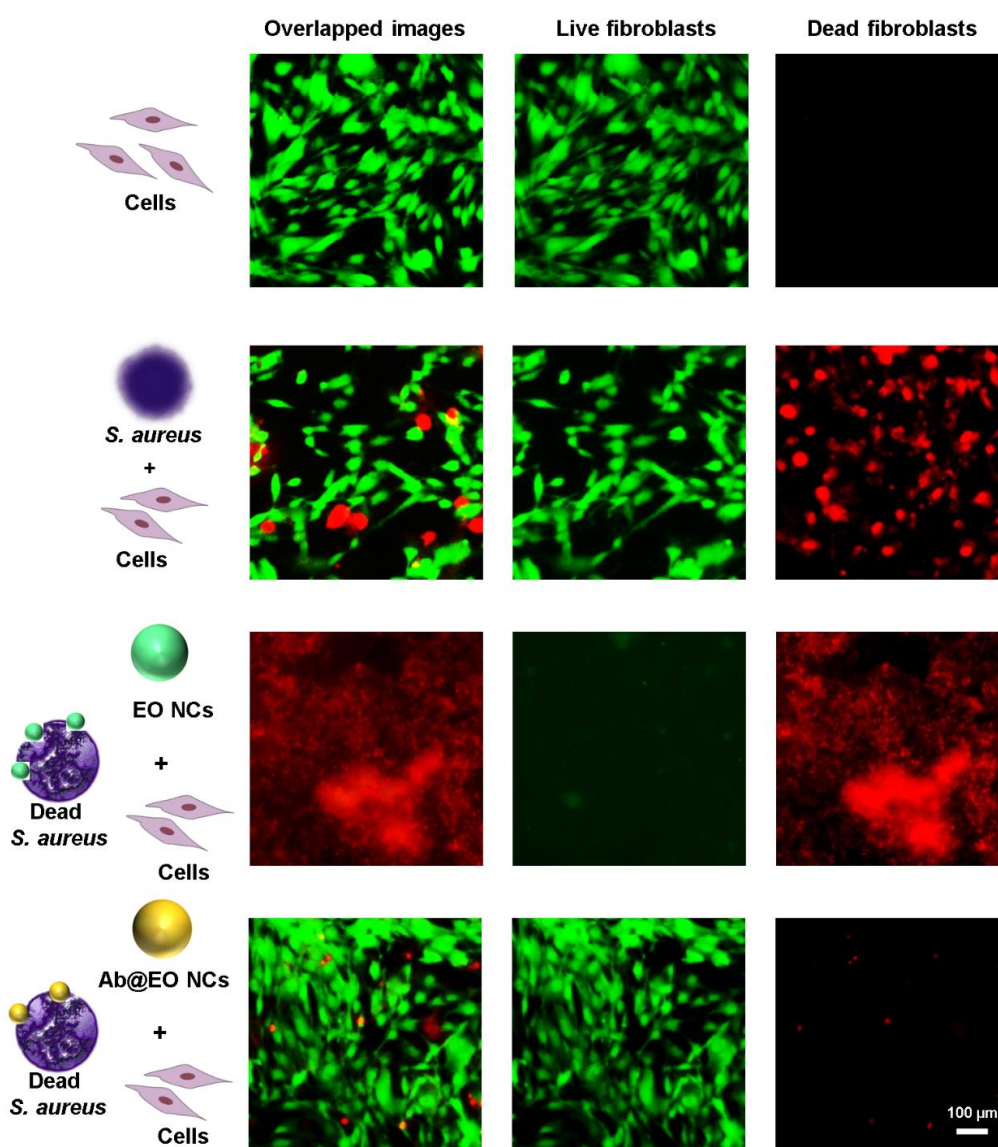
Figure 5. 28 Live/Dead kit staining of non-infected and *S. aureus* infected human cells with and without treatment with Ab@EO NCs.
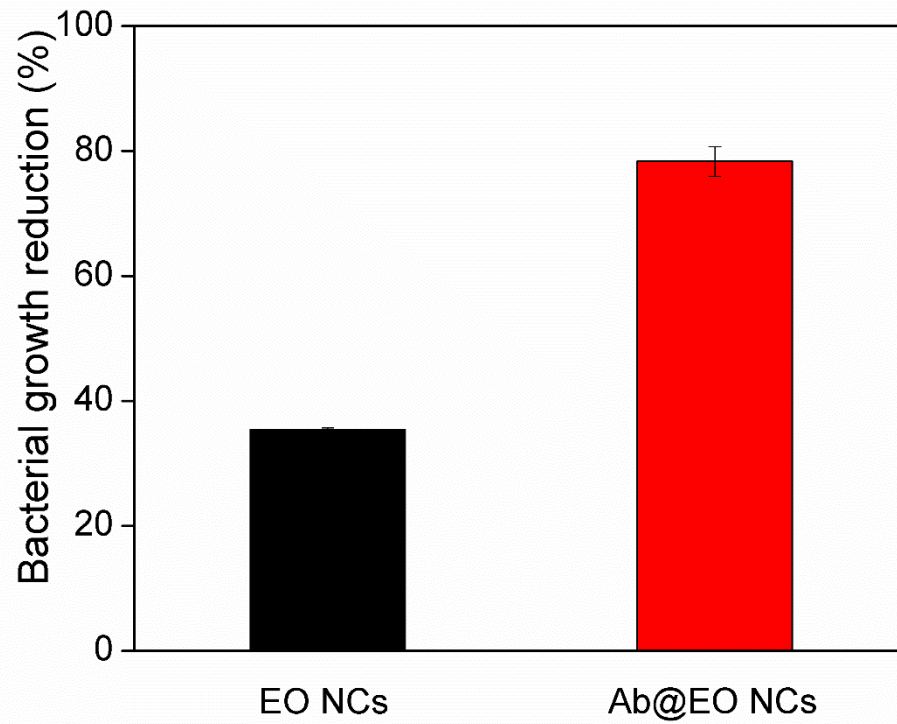
Figure 5. 29 *S. aureus* growth reduction in an in vitro coculturing model with human cells after treatment with EO and Ab@EO NCs.

5.3.7 Conclusions

AMR has raised the need for engineering novel highly effective antibacterials with reduced toxicity and lower selection for resistant bacterial strains. Herein, a novel targeted antibacterial strategy for selective elimination of Gram-positive *S. aureus* was developed on the basis of plant-derived bactericidal EO with a low potential for resistance development. At first, stable and highly antibacterial EO NCs were formulated by self-assembly nanoencapsulation technology employing the plant-derived protein zein. The EO NCs with improved bactericidal efficacy compared to the bulk oil were further coated with biocompatible and biodegradable AM to introduce more reactive groups onto the NCs surface for chemical immobilization of the *S. aureus*-targeting antibody. The Ab@EO NCs, combining the high reactivity of the nanoform with the specific driving force of the antibody, generated a novel nanosystem with enhanced antibacterial activity and the potential to selectively eradicate *S. aureus* while keeping the nontargeted *P. aeruginosa* bacterium alive. Moreover, the Ab@EO NCs inhibited the *S. aureus* growth and protected the skin fibroblast cells from this pathogen, as was confirmed in an *in vitro* infection model. These results demonstrated the capacity of the Ab@EO NCs to reach and attack only the pathogen of interest, and thus could be an efficient therapeutic approach for managing *S. aureus* infections, avoiding the use of antibiotics and preventing the development of AMR.

5.4

Sonochemically Engineered Nano-enabled Zinc oxide/amylase Coatings Prevent the Occurrence of Catheter-associated Urinary Tract Infections

In this study, for the first time, a durable hybrid nanocoating of antibiofilm enzyme amylase and antibacterial ZnO NPs has been developed onto silicone urinary catheters in a one-step sonochemical process without the need for pre-activation of the silicone material. The hydrolytic enzyme α-amylase has been assembled with antibacterial ZnO NPs templates and simultaneously deposited onto silicone Foley catheters under high-intensity ultrasonic field. The US nanoformulation of dual active ZnO@AM NPs was expected to synergistically improve the antibiofilm activity of the hybrid nanocoating at minimal, non-toxic levels of the metal oxide biocide. The antimicrobial efficacy of the engineered hybrid nano-coatings has been assessed first *in vitro* under dynamic conditions simulating the urine circulation during catheterization for up to 7 days- the time frame for catheter colonization by pathogens and occurrence of CAUTIs. The biocompatibility of the coatings has been further evaluated upon exposure to mammalian cell lines for the same time period. In addition to the *in vitro* evaluation, the antibiofilm efficacy of the novel coatings for reducing the occurrence of early CAUTIs and possible side effects, such as toxicity and inflammation, has been validated *in vivo* in a rabbit model.
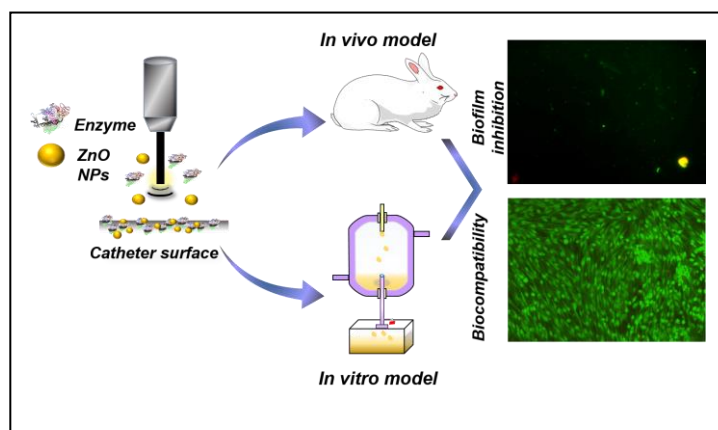
_____

5.4.1 Characterization of the coated urinary catheters

High intensity US induced mass transfer, supported by electrostatically driven self-assembling, was applied to decorate the ZnO NP core with an enzyme shell in order to develop *in situ* dual active bio-nanohybrids. The NPs surface charge in the solution was measured after the coating process. The zeta-potential of the pristine ZnO NPs changed from 17.1 ± 0.8mV to -22.7 ± 0.5 mV, due to the formation of an amylase layer onto the nano-template. Simultaneously, the obtained hybrid ZnO@AM NPs were deposited onto silicone urinary catheters in a "throwing stone" mode upon the application of US and taking advantage of the non-specific protein adsorption on silicones (**Figure 5.30A**). The surface morphology of the catheters coated with ZnO@AM NPs was observed using HRSEM (**Figure 5.30C**). The HRSEM analysis of the coated sample showed a dense layer of ZnO@AM NPs with an average size of 192 nm and a narrow NPs size distribution (**Figure 5.30B**).

Previous studies have reported that proteins may adsorb onto colloid particles through a combination of hydrogen bonding, electrostatic, van der Waals, and hydrophobic interactions.[166] In our work, the electrostatic attraction between the positively charged ZnO NPs and negatively charged amylase led to the formation of NP composites that were simultaneously deposited in a uniform layer onto the catheter's surface applying high-intensity US. The formation, growth and collapse of cavitation bubbles, generated upon sonication of liquids, determine the rationale of the deposition process. Microjets and shock waves formed upon the collapse of the acoustic bubbles [189] project the synthesized ZnO@AM NPs at high velocities towards the catheter's surface where the NPs attach by physical interactions between the highly hydrophobic polydimethyl/vinylmethyl siloxane and hydrophobic protein domains. Hydrophobic clusters of a large number of aromatic amino acid residues, e.g. tryptophan, tyrosine and phenylalanine, exposed in α-amylase structure promote the protein adsorption. [233]

ICP analysis, carried out to determine the amount of ZnO onto the catheters treated with ZnO NPs in presence and absence of amylase, showed up to 10-fold lower amount of ZnO (ca. 0.002 wt %) in the hybrid ZnO@AM NPs coating when compared to the coating prepared with only ZnO NPs (ca. 0.038 wt %) (**Table 5.1**).
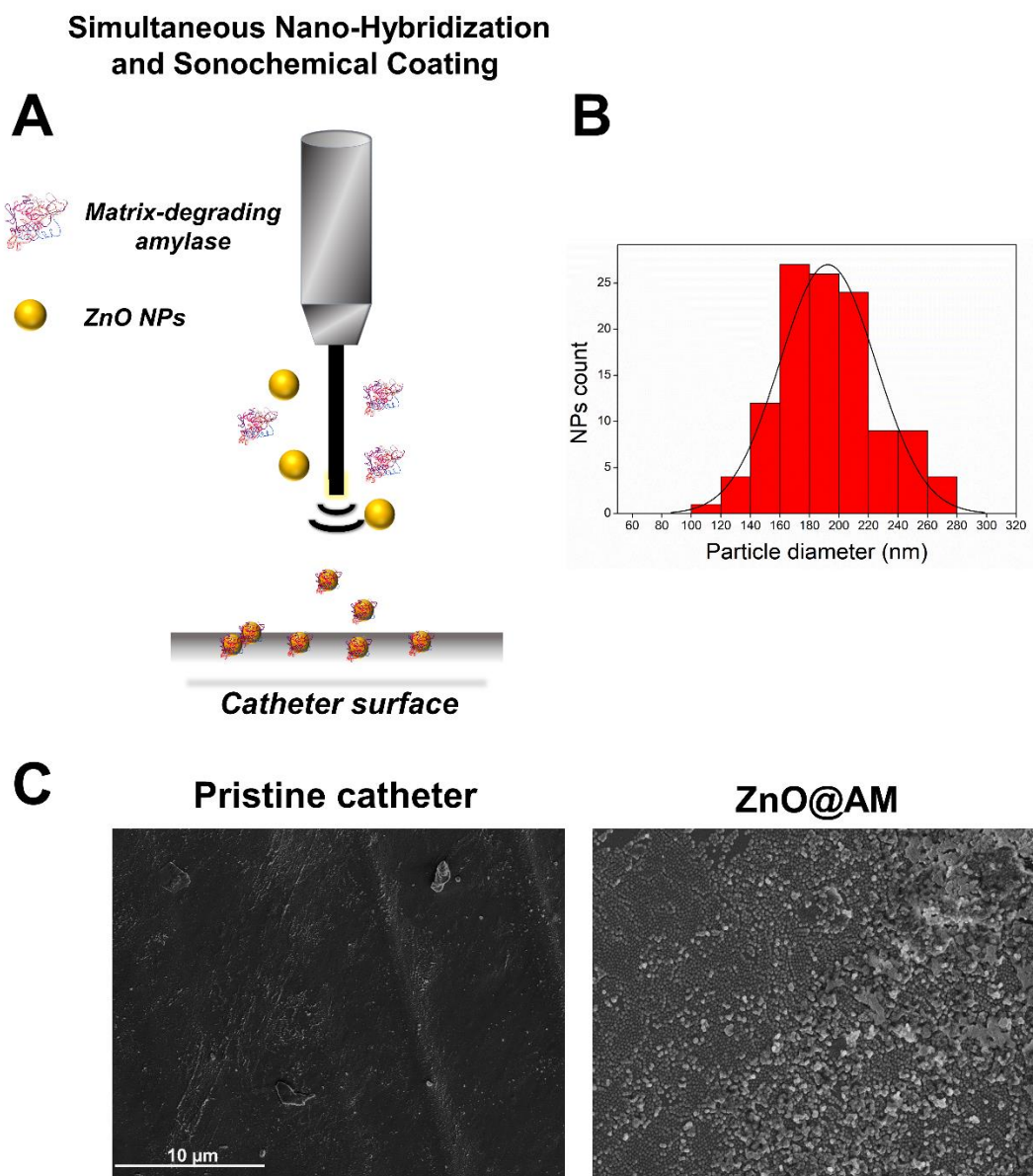
Figure 5. 30 Surface characterization of sonochemically coated with ZnO@AM NPs silicone catheter. (A) Schematic representation of the US assisted ZnO@AM NPs generation and their deposition on the silicone catheter. (B) Histogram of ZnO@AM NPs size distribution based on the total count of up to 100 NPs using ImageJ software. (C) HRSEM images of pristine and ZnO@AM NPs-coated silicone catheter.

Table 5. 1 Amount of ZnO (wt %) on ZnO NPs and ZnO@AM NPs-coated catheters before and after incubation in artificial urine.

Coated catheter	ZnO (wt %)	
	0 days (initial)	7 days (remaining)
ZnO NPs	0.038	0.011
ZnO@AM	0.0023	0.0019

5.4.2 Stability of the coatings in artificial urine

The stability of the coatings in urine is an important parameter to be considered for their practical use. Urine has a complex chemical composition, containing inorganic salts that can affect the catalytic activity of amylase and reduce the antibiofilm potential of the coatings. [234,77] Therefore, the activity of the enzyme on both amylase- and ZnO@AM NPs-coated catheters was assessed after 7 days of incubation in artificial urine (prepared according to DIN EN 1616:1999). The silicone devices coated with amylase alone lost almost 100 % of their enzymatic activity after 7 days in contact with urine under continuous agitation. However, the amylase-containing hybrid NPs coating was still active, retaining up to 80 % of its initial activity, as confirmed by the production of maltose upon the enzymatic degradation of starch (**Figure 5.31**). α-amylase is a rather robust, industrially relevant enzyme, which activity reflects the changes in the protein conformation under the effect of the application environment. The conformational stability of the enzyme is a function of external variables, such as ionic strength and composition of this environment. Prolonged exposure (7 days) to chemical denaturants, such as urea[233] and salts (NH_4^+ is a strong deactivating cation) in the artificial urine, although not in denaturing concentrations, apparently deactivated the amylase alone, while the assembling of the enzyme onto the metal oxide NP-templates and their subsequent deposition on the catheter ensured the conformational stability of the enzyme protein and its hydrolytic activity in the nano-enabled coating.
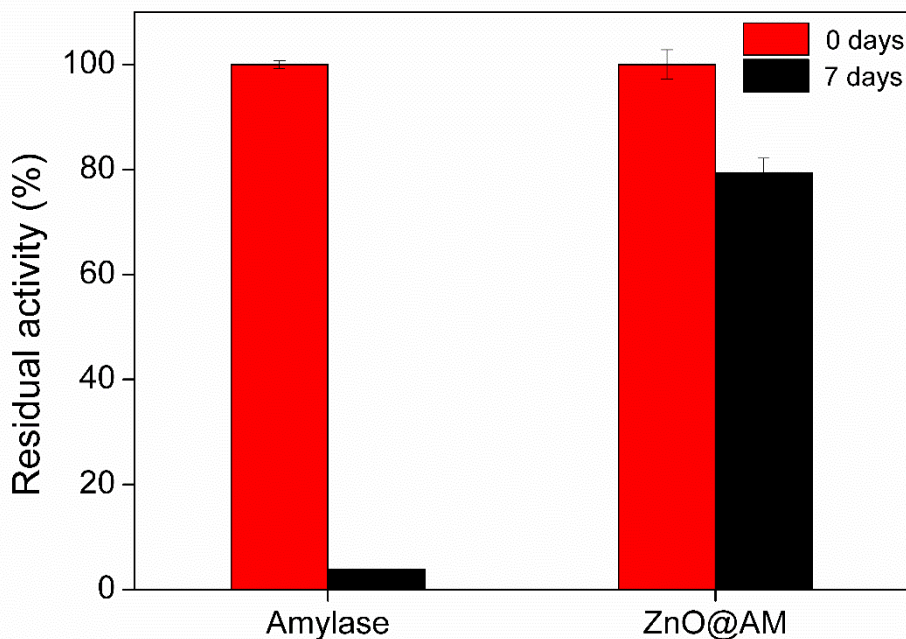
Figure 5. 31 Enzymatic activity of amylase-containing coating before and after incubation in artificial urine for 7 days with shaking. The results are expressed as the percentage of amylase activity compared to the enzyme before incubation in artificial urine.

Additionally, the leaching of ZnO NPs from the catheters over the same period of incubation in artificial urine was evaluated. ICP measurement quantified the total amount of ZnO in the ZnO and ZnO@AM NPs coatings before and after incubation in artificial urine (**Table 5.1**). Considerably lower amount of ZnO was detected on the catheters treated in the presence of amylase in comparison to the catheters treated only with ZnO NPs. On the other hand, the ICP data revealed higher stability of the hybrid ZnO@AM coatings than the individual ZnO NPs materials. High amount (83 %) of ZnO initially present on the ZnO@AM NPs-coated catheter remained on its surface after incubation in urine, while only 25 % of ZnO was detected in the case of ZnO NPs-coated catheter. The release of ZnO from these coatings is explained with the ZnO NPs dissolution induced by the phosphates in the artificial urine.[235,236] Apparently, the complexation of ZnO NPs with amylase in the hybrid coatings led to improved stability as confirmed by ICP and HRSEM data. HRSEM images of the coated catheters following their immersion in artificial urine for 7 days (**Figure 5.32**) showed a removal of the ZnO NPs, whereas no significant difference was observed for the hybrid ZnO@AM NPs coating before and after incubation. The sonochemically deposited metal oxides are not stable, and in most cases the substrate requires a pretreatment to improve the coating stability.[139,237] Here, the coating stability was provided by the

116

amylase acting as an adhesive between the hybrid metal oxide/enzyme nanocomplexes and the hydrophobic polydimethyl/vinylmethyl siloxane catheter.
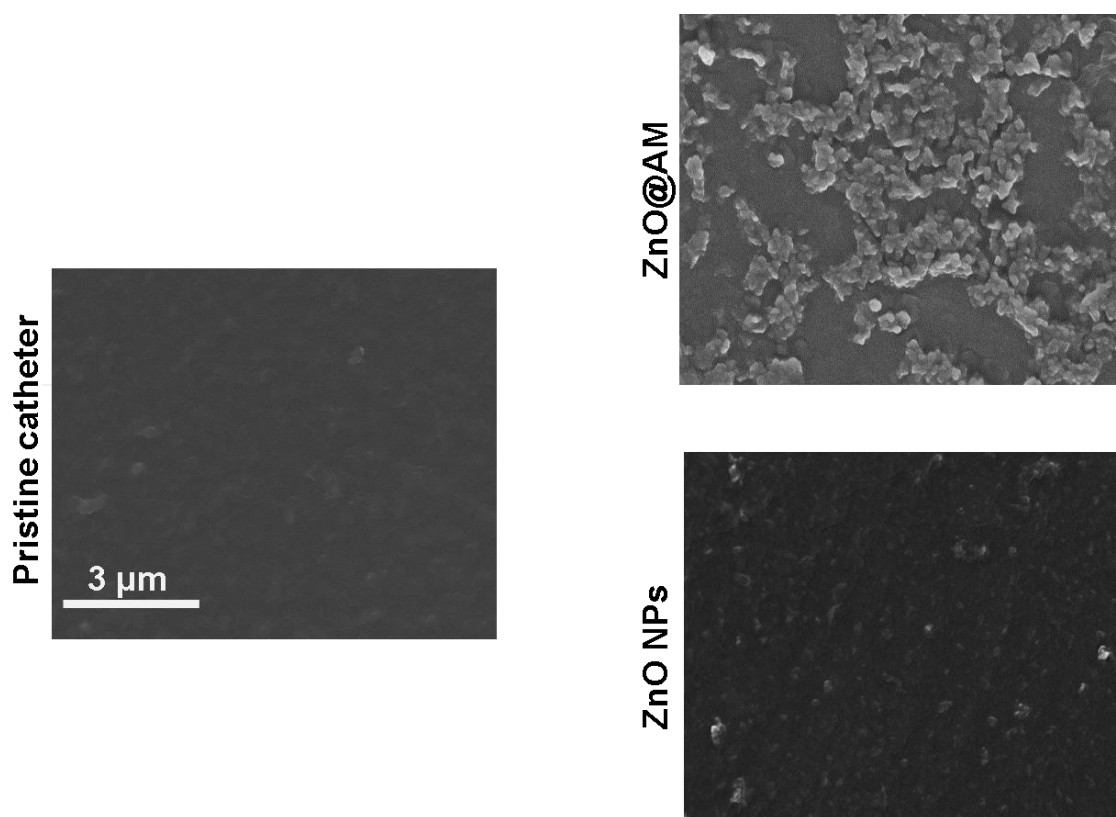
Figure 5. 32 HRSEM images of pristine, ZnO and ZnO@AM NPs-coated silicone catheter after 7 days of incubation in artificial urine.

5.4.3 Antibiofilm activity and functional stability of the coated urinary catheters

The biofilm formation by Gram-positive *S. aureus* and Gram-negative *E. coli*, the most common pathogens found in CAUTIs, was assessed on treated and non-treated catheters under static conditions using crystal violet assay.[238] Catheters, coated either with amylase or ZnO NPs alone inhibited the *S. aureus* biofilm formation by approximately 20 % and 70 %, respectively (**Figure 5.33A**). In the case of *E. coli*, both amylase and ZnO NPs coatings inhibited the biofilm formation on the catheter by around 70 % when compared to non-treated silicone (**Figure 5.33B**). Unlike *E. coli* which produces several types of potential substrates for amylase, *S. aureus* only secretes one dominant EPS involved mainly in the intercellular aggregation of the cells at the surface.[239,240] The amylase-induced degradation of several biofilm adhesives simultaneously is probably the reason for the higher efficacy of amylase-coated catheters on *E. coli* when compare to *S. aureus*.

However, the simultaneous coating with both actives led to inhibition of the total biofilm formation by 81 % for *S. aureus* and 75 % for *E. coli* (**Figure 5.33A, B**). In the hybrid ZnO@AM NPs the amylase degraded essential for biofilm adhesion and growth polysaccharides,[77] inhibiting the biofilm formation by both bacterial strains, and at the same time, increasing the susceptibility of the individual bacterial cells to the bactericidal ZnO NPs at lower concentration. Amylase has been employed in our group both individually and in combination with other enzymes (e.g. acylase)[77] or antibacterial agents (e.g. Ag)[153] to inhibit biofilm maturation, detach pre-formed biofilms, and synergistically increase the susceptibility of the biofilm forming bacteria to biocides. In contrast to commonly used antimicrobials, these hybrid antibacterial/antibiofilm agents eradicate pathogens via non-specific mechanisms of action, such as membrane damage, oxidative stress and virulence attenuation, unlikely to induce AMR development.[241]
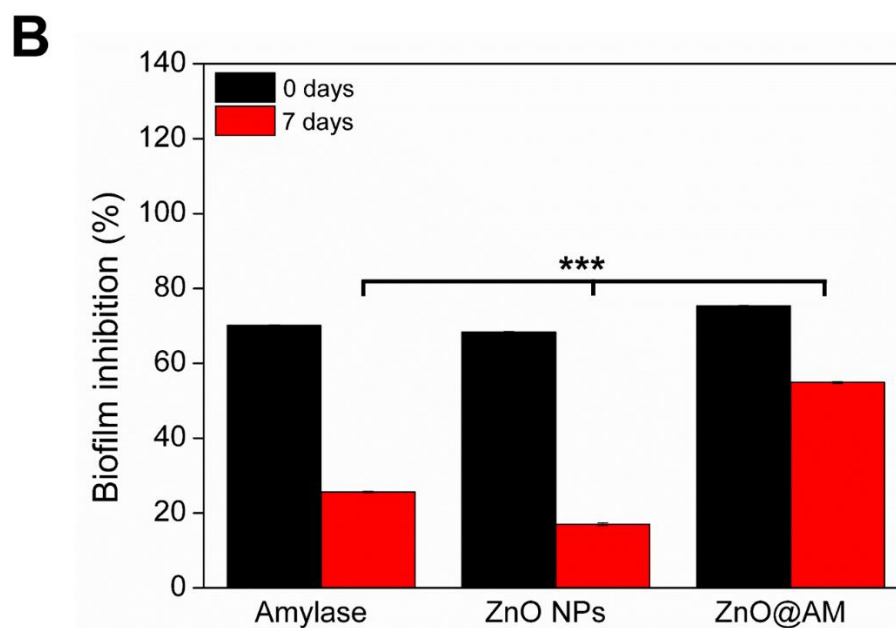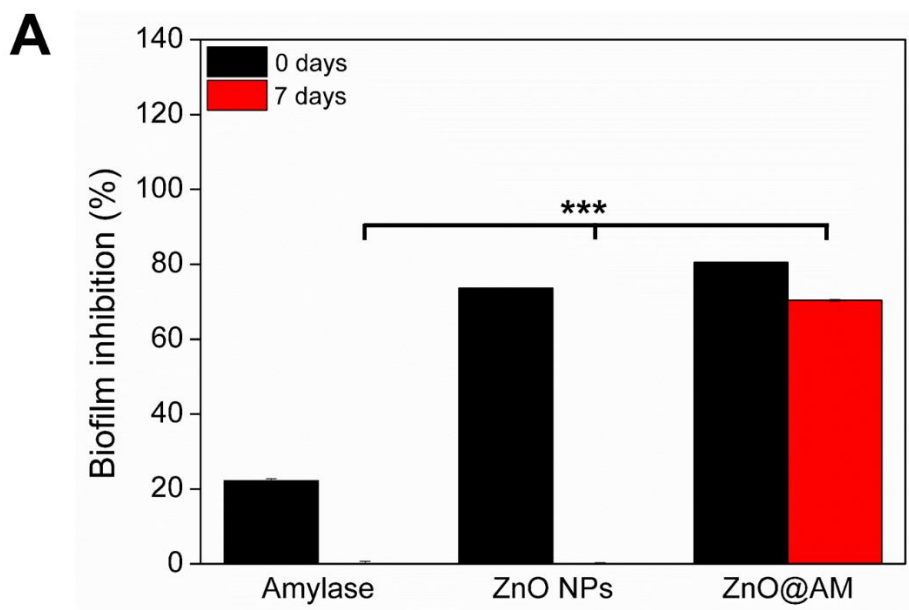
Figure 5. 33 Biofilm inhibition (%) at static condition of the coated catheters towards (A) *S. aureus* and (B) *E. coli* assessed before and after incubation in artificial urine for 7 days under continuous agitation. The results are represented in %, compared with the biofilm inhibition of pristine catheter (non-inhibition). Stars represent the statistical differences between the different groups of samples; $p < 0.05$.

In order to highlight the role of the enzyme and confirm the synergism between ZnO NPs and amylase, sonochemical coatings containing ZnO NPs and non-active protein (BSA) instead of amylase, were developed. The coatings did not show any ability to reduce the bacterial attachment and biofilm formation (**Figure 5.34**), which

demonstrates the relevance of the amylase-assisted EPS degradation for inhibition of the total biofilm formation by the hybrid ZnO@AM NPs coating. Furthermore, catheters coated with amylase did not affect the growth of free-floating bacterial cells, while the ZnO NPs functionalized devices inhibited both *S. aureus* and *E. coli* growth by 100 % and 90 %, respectively (**Figure 5.35**). These results clearly emphasize the synergy between the amylase and ZnO NPs, which is further reflected in a higher antibiofilm activity at lower concentration of the bactericidal ZnO NPs.
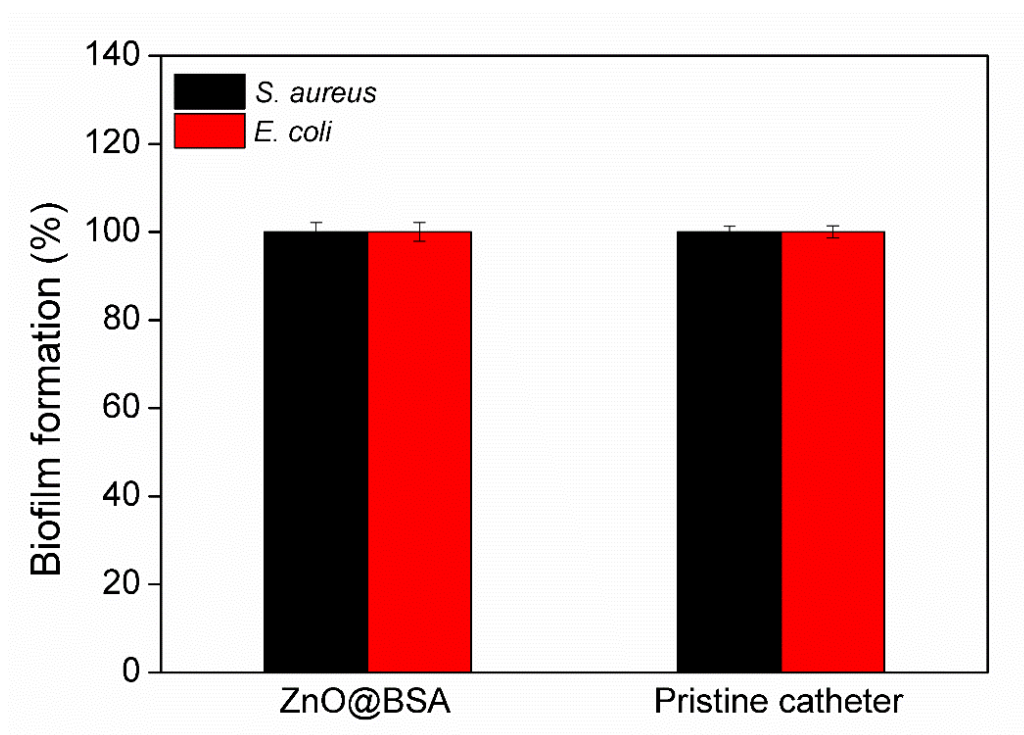
Figure 5. 34 Biofilm inhibition activity of the ZnO@BSA NPs-coated catheters.
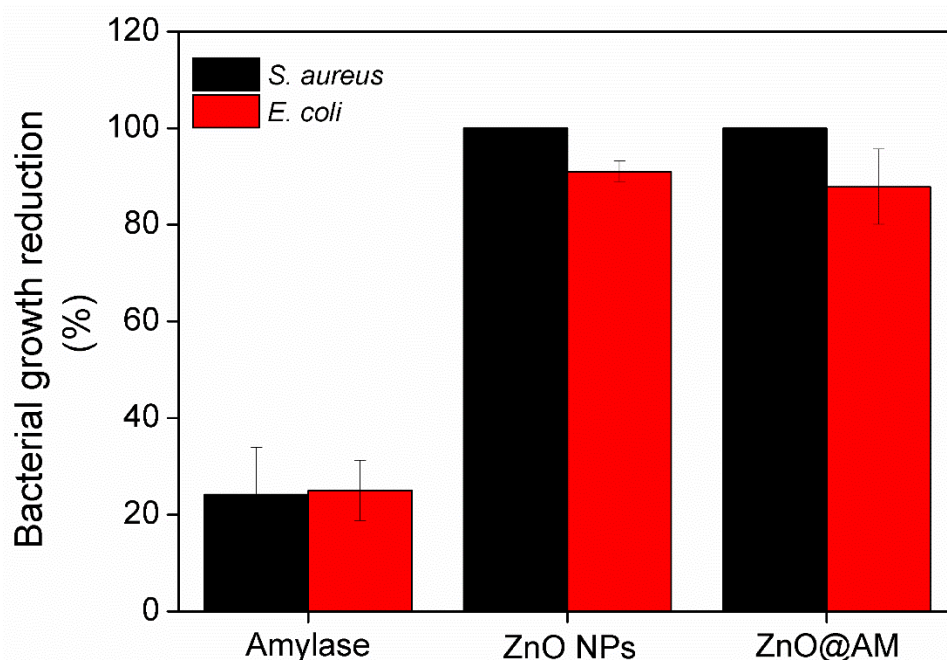
Figure 5. 35 Antibacterial activity of ZnO NPs and ZnO@AM NPs-coated catheters.

Engineering of stable at use antibiofilm coatings on indwelling urinary catheters is crucial for the effective prevention of CAUTIs. Therefore, the functional stability of the coated catheters, i.e. their ability to impair the bacterial attachment and colonization, was assessed after 7 days of incubation in artificial urine under continuous agitation.[77] Catheters functionalized with amylase or ZnO NPs alone, practically lost their ability to inhibit the static biofilm formation of both *S. aureus* and *E. coli* after incubation in urine. However, when amylase and ZnO were simultaneously deposited onto the silicone surface, a negligible decrease of their biofilm inhibition properties was observed in comparison to the non-incubated in urine samples. ZnO@AM NPs coatings lost only 10 % and 20 % of their antibiofilm activity against *S. aureus* and *E. coli*, respectively (**Figure 5.35**). These results indicate that the hybridization of ZnO NPs and amylase into a nanostructured coating on catheters is an effective antibiofilm approach against both Gram-positive and Gram-negative bacterial strains even after 7 days of exposure to artificial urine.

5.4.4 Biofilm inhibition tests under dynamic conditions in a model of catheterized human bladder

Despite of the high stability and efficiency of ZnO@AM NPs coatings in controlling the biofilm formation of both Gram-positive and Gram-negative bacteria at static

conditions, these conditions do not simulate the real scenario during catheterization. For that reason, the novel hybrid nano-enabled coatings were further challenged in dynamic biofilm inhibition tests in a model of catheterized human bladder (**Figure 5.36**), where the dynamically varying shear stress associated with urine flow may affect the bacteria adhesion on the surface or provoke coating removal.[242] This model has been widely used in our group for assessing *in vitro* the antibiofilm functionality of catheter coatings[77,234]

Since 80 % of bacterial adhesion onto medical devices and the buildup of drug-resistant biofilms occur during the first days after the device insertion,[243,244] strategies for prevention of biofilm formation within the first days of catheterization are needed. The total biofilm mass formed on the pristine and ZnO@AM NPs-coated Foley urinary devices after 7 days of catheterization was evaluated using crystal violet and Live/Dead kit assays. The sonochemical coating with ZnO@AM NPs led to reduction of both *S. aureus* and *E. coli* total biofilm formation on the catheter's balloon by 60 % and 80 %, respectively (**Figure 5.36**). The balloon of the catheter inflated inside the bladder is entirely immersed in urine during catheterization. This part of the indwelling urinary device is the most susceptible to colonization and consequent establishment of antibiotic resistant biofilms by urinary tract pathogens. Considering previous works on the biofilm growth in artificial urine,[77] we presume that the enzyme in the hybrid coatings affects the *S. aureus* and *E. coli* initial colonization on the catheter surface degrading the polysaccharide adhesives essential for bacterial attachment and growth of biofilms. The degradation of the EPS by amylase inhibits the formation of mature biofilm, further enhancing the bacterial susceptibility to bactericidal ZnO NPs in the coatings. Although, the extent of biofilm reduction was different between the different bacteria the proposed mechanism of antibiofilm action of the hybrid ZnO@AM NPs coatings is valid for both species. The variation in the antibiofilm activity is explained by the different EPS [245] and their functional role in the biofilm establishment as well as different structure of Gram-positive and Gram-negative bacterial membrane.[187]

Microscopic observations revealed less *S. aureus* than *E. coli* biofilm formation on the non-treated catheter balloon, explained with the difference between the Gram-positive and Gram-negative bacterial species and their ability to establish *in vitro* biofilms under dynamic conditions.[246] Noteworthy, the biofilm formation by *S. aureus* and *E. coli* on ZnO@AM NPs-coated catheters was completely inhibited and only few individual cells were observed. The appearance of dead bacterial cells (red cells) in the microscopic

images was due to the bactericide effect of ZnO NPs. The consistency of the results for the antibiofilm efficiency of ZnO@AM NPs coatings in both static and dynamic conditions clearly demonstrate the potential of these hybrid coatings to prevent the biofilm formation on silicone urinary catheters and therefore decrease the incidence of CAUTIs.
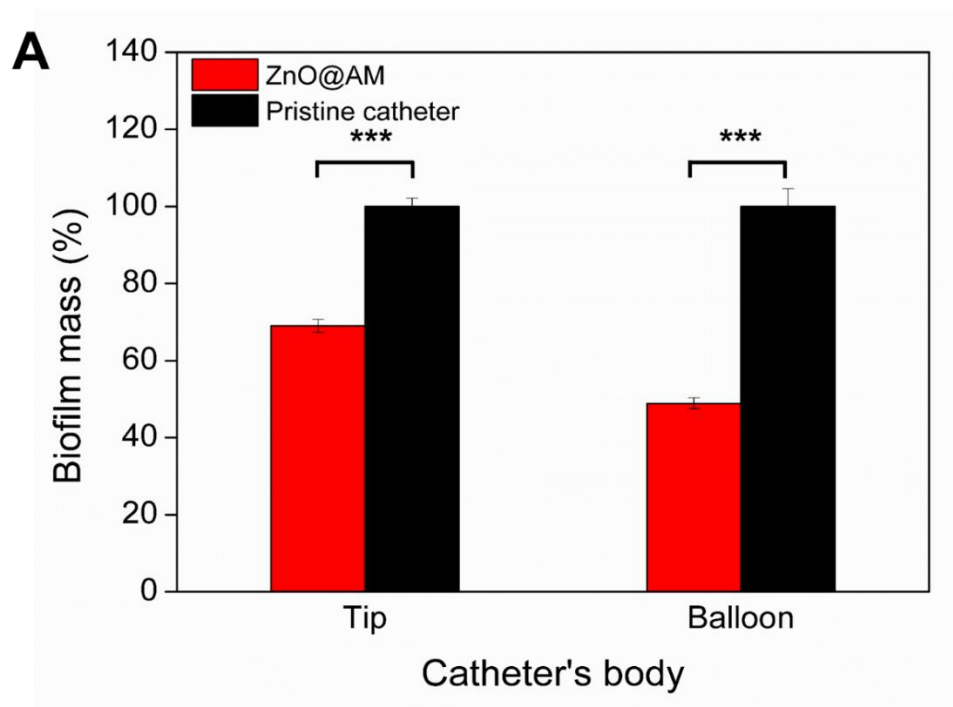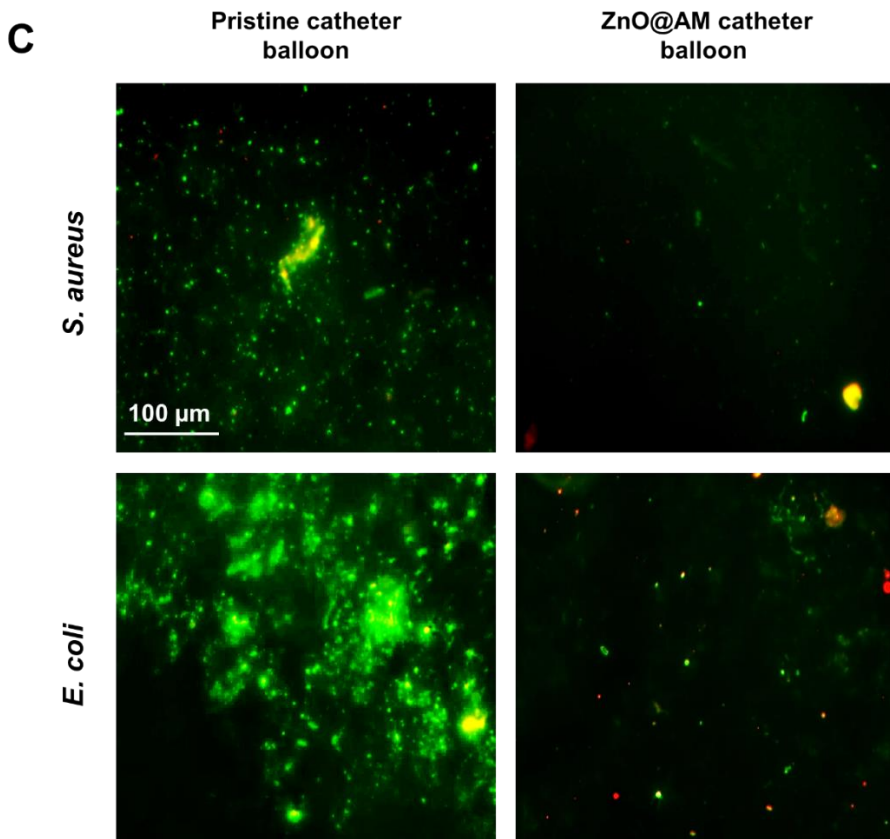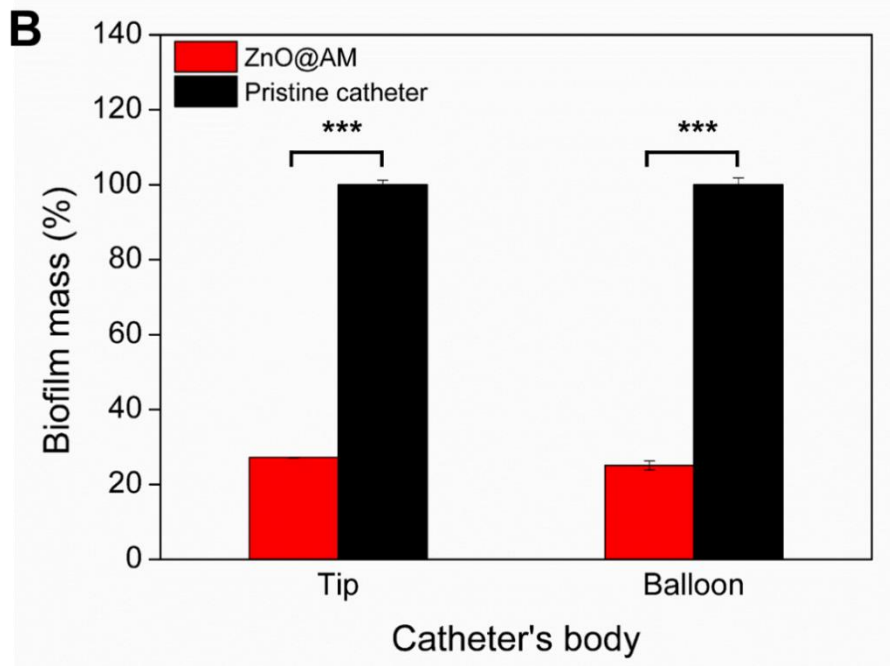
Figure 5. 36 *In vitro* biofilm inhibition in catheterized bladder model with urine recirculation. (A) In vitro model of catheterized human bladder. Total biofilm quantification of (B) *S. aureus* and (C) *E. coli* biofilm mass on ZnO@AM coated urinary catheters. Stars represent the statistical differences between the treated and pristine catheters; $p < 0.05$. (D) Fluorescence microscopy images of live (green) and dead (red) bacteria in the biofilms grown on ZnO@AM-

coated and pristine silicone Foley catheter balloon. The green and red fluorescence images are overlaid.

5.4.5 Cytotoxicity of the coatings

Since ZnO NPs at high concentrations induce cytotoxicity towards mammalian cells,[247] the biocompatibility of the developed coatings is an important parameter to be assessed for their clinical application. Cell viability assay was performed to examine the biocompatibility of the coated catheters with two lines of mammalian cells, namely human fibroblast cells and HaCaT keratinocytes. The cells' viability and morphology were observed after 24 h and 7 days of exposure to ZnO@AM NPs-coated catheters (**Figure 5.37A**). The pristine and ZnO@AM NPs-coated catheters did not affect the viability of both fibroblast cells and HaCaT keratinocytes, demonstrating 100 % biocompatibility (**Figure 5.37A**). Furthermore, the morphology of the mammalian cells in contact with the catheters was not altered (**Figure 5.37B**), suggesting that the *in vivo* use would not imply any biocompatibility concerns.
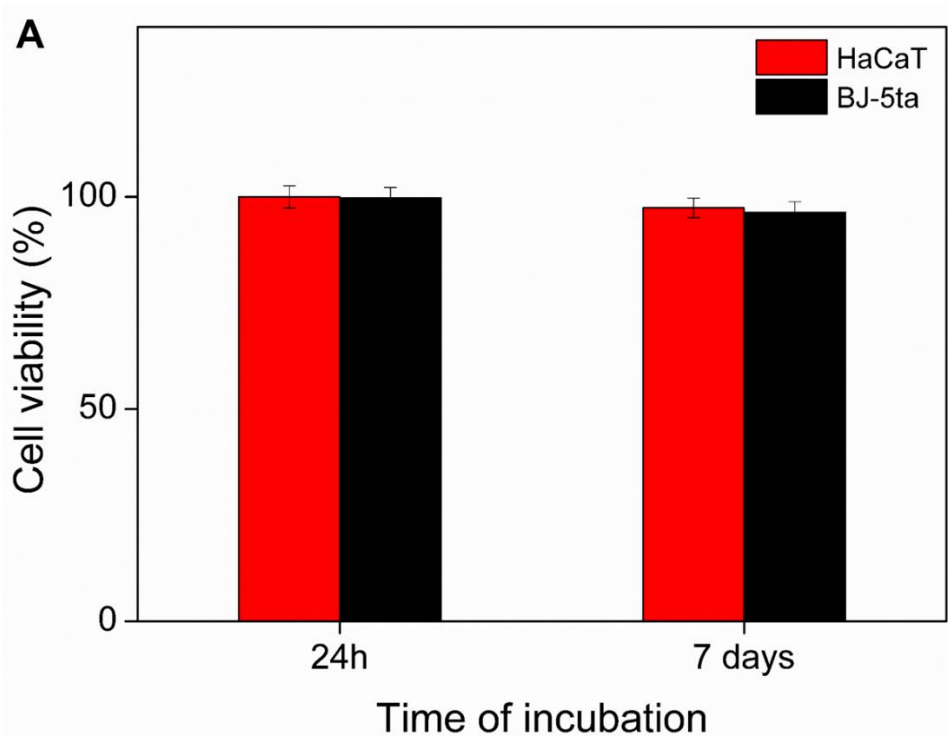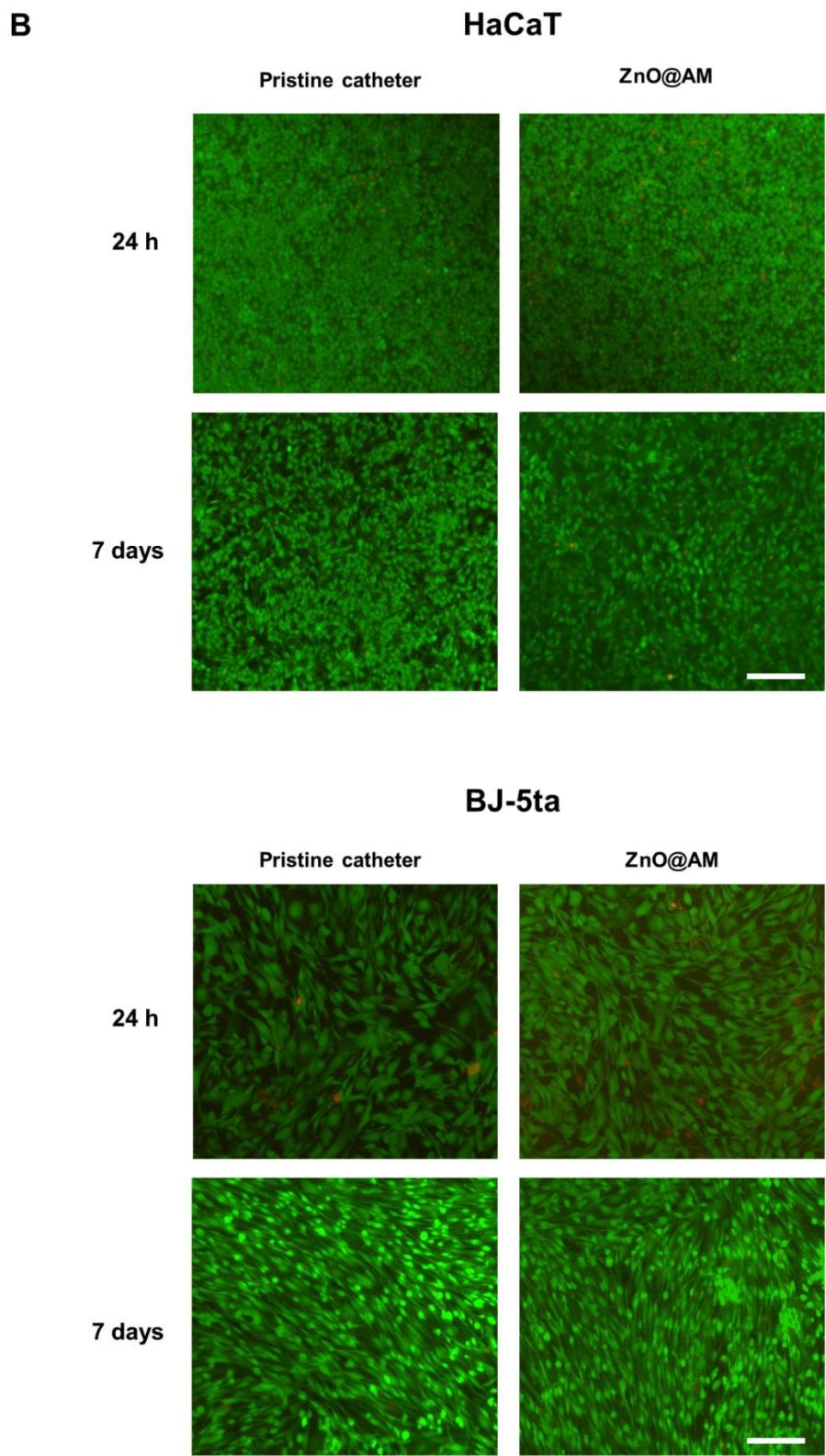
Figure 5. 37 Viability of HaCaT and BJ-5ta cell lines after exposure to the ZnO@AM NPs-coated catheters assessed by (A) AlamarBlue and (B) Live/Dead kit assays. The green and red fluorescence images are overlaid. Scale bar corresponds to 100 μm.

5.4.6 *In vivo* efficacy assessment of ZnO@AM NPs-coated catheters in a rabbit model

The ability of the coatings to reduce bacterial biofilm growth and respectively the CAUTIs occurrence was assessed *in vivo* in an established rabbit model (**Scheme 5.1**). This model does not use specific pathogen inoculum, but rather mimics the natural process by which microorganisms from the surrounding environment colonize the device surface and induce CAUTIs.[140] Additionally, the model allows to assess *in vivo* the biological safety of the coated catheters.

In the *in vivo* tests, animal groups 2 and 3 (n = 3), were subjected to catheterization, respectively with pristine and ZnO@AM NPs-coated indwelling urinary catheters, under identical experimental conditions for 7 days (this is the usual time frame for catheter colonization by pathogens and subsequent appearance of CAUTIs). Non-catheterized rabbits (group 1) were used as a control (healthy animals) in all experiments.
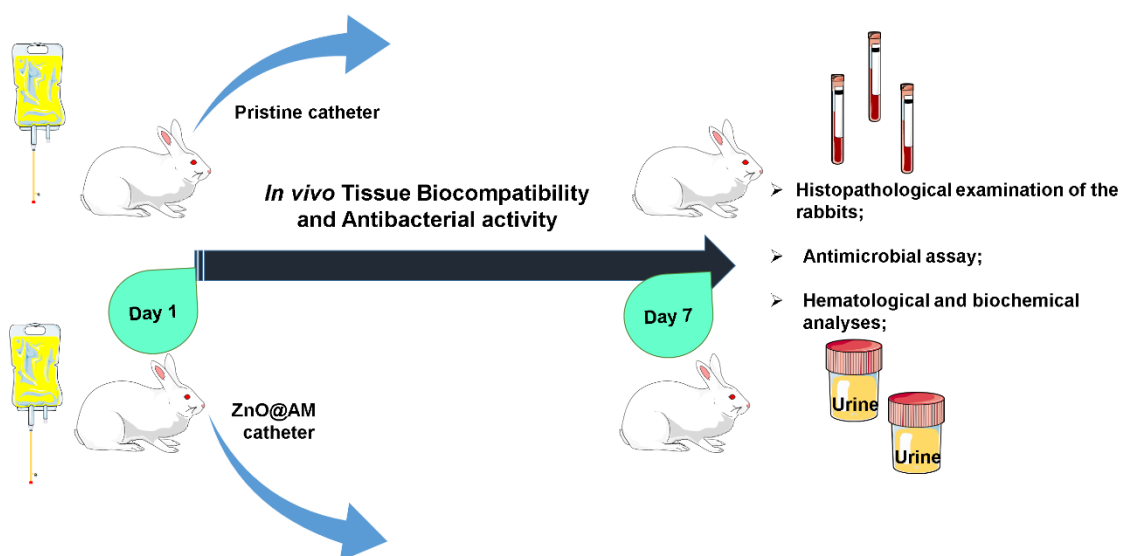
Scheme 5. 1 Schematic representation of the assays performed *in vivo* in a rabbit model.

5.4.6.1 Microbiological analysis of urine and catheters´ surfaces for UTIs detection

At the end of the catheterization period, urine samples and catheters from each group were collected and examined for bacterial contamination. However, the samples from the urine of the rabbits and the surface of the pristine catheters from group 2 were both

colonized with bacteria, mainly from genus *Enterococcus* (**Figure 5.38**). The *Enterococcus* concentration in the urine was $3.65 \times 10^3 \pm 0.54$ CFU ml^{-1} and was sufficient to cause UTI, as confirmed by the appearance of concomitant clinical symptoms such as kidney lesions and signs of developing glomerulonephritis (**Figure 5.39A**).[248] Bacteria were also detected on the catheter´s surface (17.9 ± 1.33 CFU cm^{-2}) and their organization into stable biofilms could further lead to difficult to treat UTIs.[249] In contrast to the animal group catheterized with pristine catheters, the urine samples collected from the animals treated with ZnO@AM NPs-coated catheters (group 3) were practically sterile. Less than 10^3 CFU ml^{-1} (ca. $6.5 \times 10^2 \pm 1.68$ CFU ml^{-1}) bacteria from the genus *Enterococcus* were found in the urine samples, which is not indicative for infection.[250] Although the urine had some bacterial load, the surface of the ZnO@AM NPs-coated catheters remained bacteria–free over the time of catheterization (**Figure 5.38**). These *in vivo* results are in agreement with the *in vitro* observations and confirmed the potential of the hybrid ZnO@AM NPs coating for clinical uses.
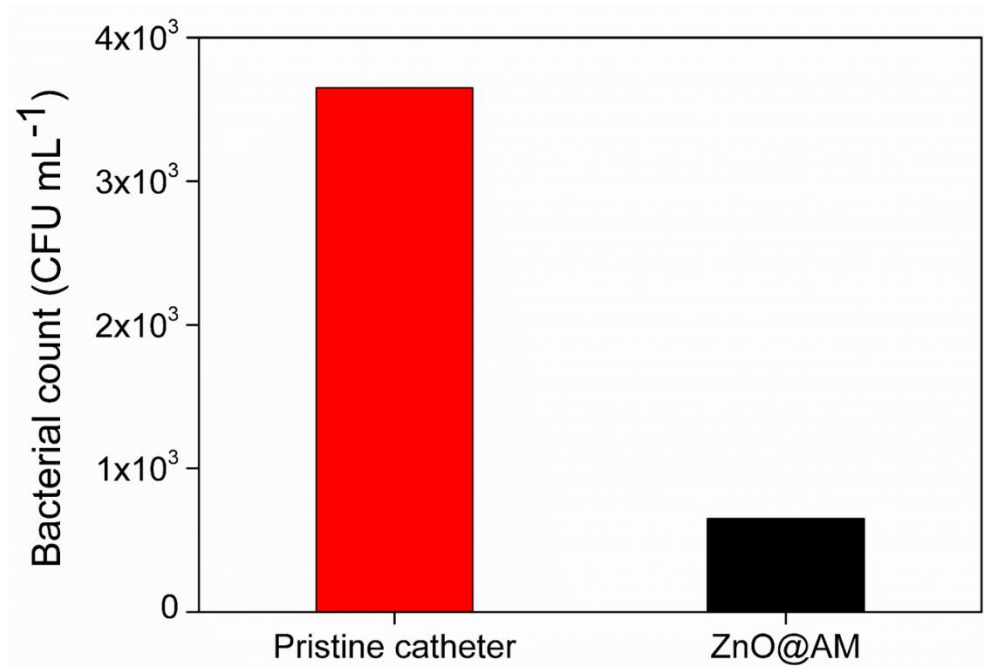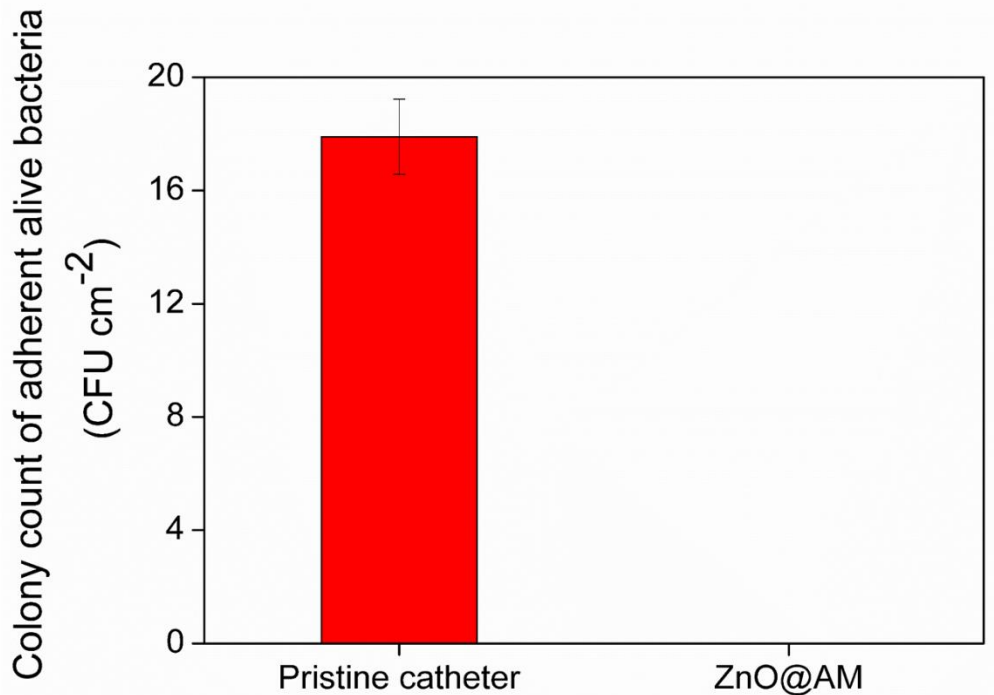
Figure 5. 38 Antibacterial properties of pristine and ZnO@AM NPs-coated catheters. (A) Colony count of bacteria from the urine samples collected from animals catheterized with pristine and ZnO@AM NPs-coated catheters. (B) Colony count of live bacteria adherent on the non-treated and ZnO@AM NPs functionalized catheters after 7 days of catheterization in the rabbit model.

5.4.6.2 Histopathology after catheterization

The urethra of the control animals from group 1 did not show any abnormalities (**Figure 5.39A**). Typical features of the epithelial lining, starting with transitional cells near the bladder, followed by pseudostratified, stratified columnar epithelium and stratified squamous approaching the *orificium* (**Figure 5.39A**, black arrow), were observed. In contrast, very mild erosions of the mucosal columnar epithelium, due to the mechanical pressure of the catheters on parts of the penile urethra during catheterization, were detected in the catheterized rabbits from groups 2 and 3 (**Figure 5.39B**, black arrows), while the urothelium in the prostatic urethra was not affected (**Figure 5.39B**). The anatomical position of the penile part of the urethra and the size of the catheters explain these findings.

Significant histopathological alterations due to catheterization were not detected in the bladders of the animals from all groups (**Figure 5.39C**). Groups 1 and 3 had normal morphology of the bladder mucosa with transitional epithelial cell lining (red arrow). Some of the animals in group 2 (non-coated catheters) appeared with mucosal lesion expressed in focal damage of epithelial linings forming microerosions of the cell barrier (**Figure 5.39C**, black arrows) and showed bladder inflammation when compare to group 3, catheterized with ZnO@AM NPs-coated devices.

The kidneys of the rabbits from group 1 (without catheterization) and group 3 (using ZnO@AM NPs-coated catheter) did not show any pathological lesions (**Figure 5.39D**). Their glomeruli and Bowman's capsules as well as the urinary tubular system were found to be with normal morphology. However, in rabbits from group 2 (pristine catheters) the pathohistological observations showed localized clusters of crescentic glomerulonephritis and vasculitis (extravasation and tissue infiltration from the bloodstream with inflammatory cells) (**Figure 5.39D**, black arrows) and preserved morphology of glomeruli (**Figure 5.39D**, red arrow heads). Zonal infiltration of renal perivascular tissues and circumferential periglomerular renal parenchyma was observed, where the pathology involved abundant local concentration of inflammatory cells. We suggest that this is related to a disorder in the lower urinary tract as the microbiological results revealed bacteria in the urine and on the surface of the pristine catheters.

Morphological observations of all blood smears from non-catheterized rabbits (group 1) and catheterized with ZnO@AM NPs-coated devices (group 3) showed normal cell ratio, unlike the group 2 (pristine catheters), which showed increased number of neutrophil granulocytes (**Figure 5.39E**, black arrow) associated with leukocyturia and

indicating the appearance of urothelial infection.[251] In the urine, sediments (many colorless to yellow-brown calcium carbonate crystals in the form of large or smaller spheroids with radial striations) of the animals from groups 1 and 3 were found (**Figure 5.39F**). Cellular constituents from urothelial linings of bladder, renal pelvis of kidneys or urethra were not seen in these groups. Microscopic aspects of the urine sediments of the animals catheterized with pristine catheters (group 2) revealed leukocytes and erythrocytes, associated with inflammation,[252] transitional epithelial cells from the mucosal linings (including umbrella cells) and sperm (**Figure 5.39F**) supporting the pathological processes.
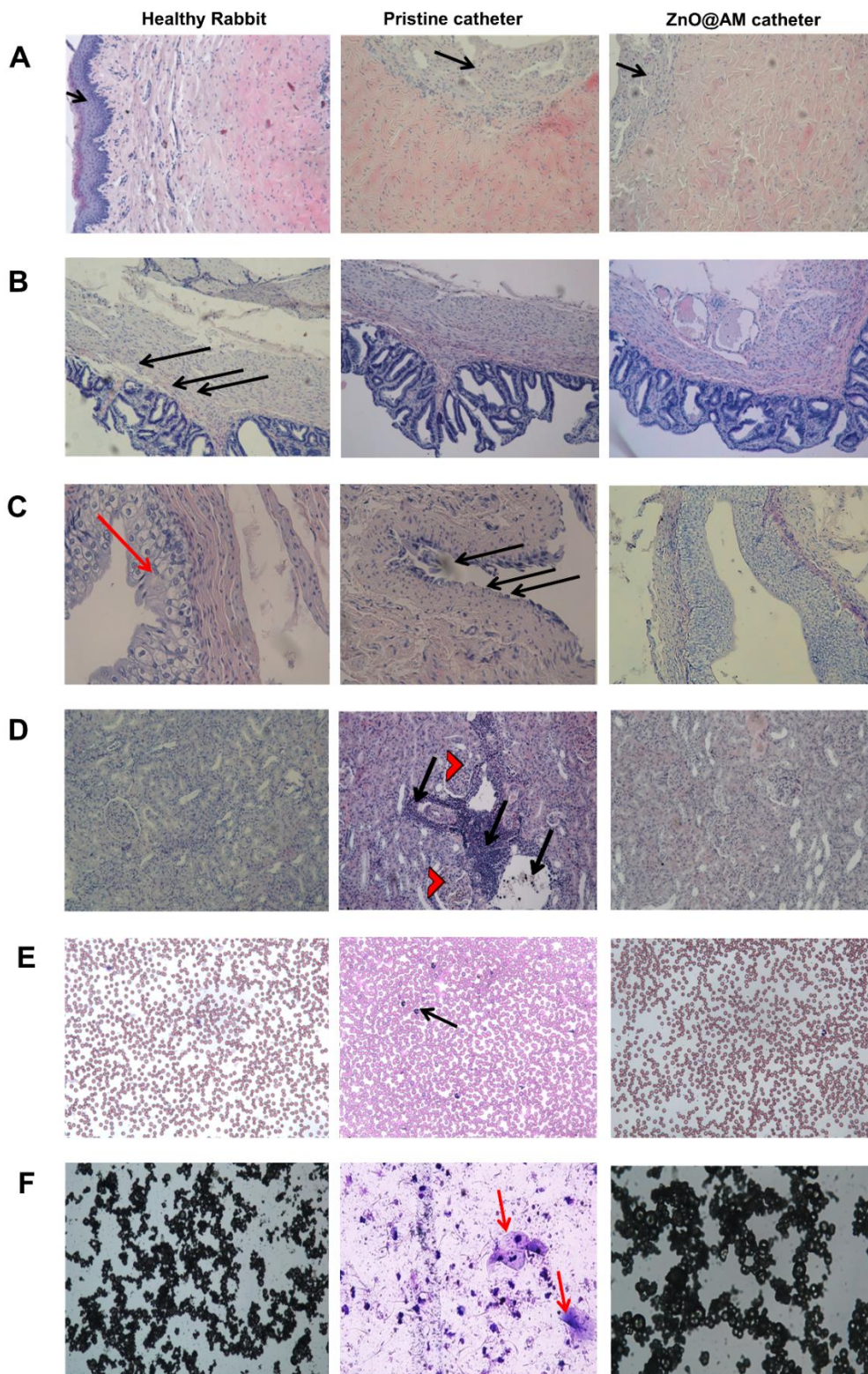
Figure 5. 39 Histopathology of (A) rabbit penile, (B) prostatic urethra, (C) bladder and (D) rabbit kidney of non-catheterized (group 1) and catheterized with pristine (group 2) and ZnO@AM NPs (group 3) catheters. Black arrows indicate epithelial lining; red arrow displays urinary bladder mucosa with transitional epithelial cell lining; red arrowheads show glomeruli. (E) Blood smears of rabbits. Black arrow indicates the neutrophil granulocytes. (F) Urine sediments of non-catheterized (group 1) and catheterized rabbits (group 2 and 3). Red arrows indicate the umbrella cells from the urinary system mucosal linings.

5.4.6.3 Hematological and biochemical analyses

Hematological and biochemical parameters[253,254] from randomly chosen animals that inform about pathological processes were further analyzed (**Table 5.2** and **Table 5.3**). Generally, the blood counts and biochemistry did not show any serious deviations with the exception of the animals treated with pristine catheters (group 2) developing glomerulonephritis, which white blood cells and monocytes count was higher than the normal levels. The granulocytes count were slightly elevated in rabbits with ZnO@AM NPs-coated catheters, whereas in group 2 the granulocytes increased significantly (**Table 5.2**), which is indicative of bacterial infection.[255]

Urine samples collected from all animal groups showed slight deviations of some parameters (**Table 5.3**). Glucose and ketone values in all studied groups were negative, which means that the rabbits did not present any severe disease. Creatinine was elevated in animals from group 1 and group 2. The histology results from the rabbits treated with the pristine catheter revealed elevated numbers of leukocytes and red blood cells, associated with UTIs. Furthermore, the urine of the animals from this group had pH 6, which is lower compared to pH measured for the healthy non-catheterized animals (group 1) and those treated with ZnO@AM NPs-coated catheters (group 3). Slightly increased levels of blood cells were found in the urine of the catheterized animals (group 2 and 3) due to the movement of the indwelling devices in the bladder lumen causing eventually microtraumas. In a summary, the conducted *in vivo* studies validated: i) the antibiofilm efficiency, ii) capacity to reduce the incidence of CAUTIs, iii) the enhanced life span and iv) safety of the novel ZnO@AM NPs-coated catheters.

Table 5. 2 Hematological blood results of non-catheterized and catheterized rabbits.

Parameter	Rabbit (Group 1)	Pristine catheter (Group 2)	ZnO@AM coated catheter (Group 3)	Standards
White Blood Count (L^{-1})	9.5×10^9	15.4×10^9	12.9×10^9	5.2-13.5
Lymphocytes (L^{-1})	2.5×10^9	2.4×10^9	3.5×10^9	3.2-9.0
Monocytes (L^{-1})	0.5×10^9	0.7×10^9	0.6×10^9	0.1-0.6
Granulocytes (L^{-1})	6.5×10^9	12.3×10^9	8.8×10^9	2.0-7.5
Lymphocytes (%)	26.1	15.8	27.13	35.2-75.6
Monocytes (%)	5.7	4.6	4.65	2.5-6.0
Granulocytes (%)	68.2	79.6	68.22	20.2-59.3
Red Blood Cells (L^{-1})	6.82×10^{12}	6.92×10^{12}	6.42×10^{12}	5.00-7.60
Hemoglobin ($g\ L^{-1}$)	152	158	158	105-170
Mean Corpuscular Hemoglobin (pg)	22.2	23.8	24.6	20.1-25.1
Mean Corpuscular Hemoglobin Concentration ($g\ L^{-1}$)	320	348	361	320-370
Albumin ($g\ L^{-1}$)	39.5	42.1	41.0	27-45
Globulin ($g\ L^{-1}$)	23.2	19.4	36.0	15-57
Albumin/Globulin	1.7	2.2	1.1	
Blood urea nitrogen ($mmol\ L^{-1}$)	6.68	5.26	8.58	3.6-10.7
Phosphate ($mmol\ L^{-1}$)	1.66	1.24	1.75	1.1-2.74
Total Bilirubin ($\mu mol\ L^{-1}$)	4.10	2.56	2.85	0-10.3
Creatinine ($\mu mol\ L^{-1}$)	72	83	87	27-141
Blood urea nitrogen /Creatinine	23	16	24	

Table 5. 3 Biochemical results of urine collected from non-catheterized and catheterized rabbits.

Parameter	Rabbit (Group 1)	Pristine catheter (Group 2)	ZnO@AM coated catheter (Group 3)
Leukocytes (cell μL^{-1})	15	125	15
Ketones (mmol L^{-1})	0	0	0
Nitrites	-	-	-
Urobilinoge	Normal	Normal	Normal
Bilirubin (μmol μL^{-1})	8.6	8.6	8.6
Gluose (mmol L^{-1})	0	0	0
Specific gravity	1.010	1.020	1.030
Red blood cells (cell μL^{-1})	0	200	25
MA (mg L^{-1})	≥ 150	≥ 150	≥ 150
Calcium (mmol L^{-1})	≥ 10	5.0	2.5
Creatinine (mmol L^{-1})	≥ 26.4	26.4	8.8

5.4.7 Conclusions

Silicone urinary catheters were simultaneously coated with matrix-degrading amylase and antibacterial ZnO NPs in a one-step US process. *In vitro*, the engineered nanohybrid coatings demonstrated significant biofilm inhibition against the most common Gram-positive and Gram-negative bacterial representatives found in CAUITs as well as high functional stability upon 7 days of incubation in artificial urine. The ZnO@AM NPs-coated catheters were also able to inhibit the *S. aureus* and *E. coli* biofilm formation by up to 60 % and 80 %, respectively, under dynamic conditions *in vitro* in a model of catheterized human bladder. The novel antibiofilm coatings were 100 % biocompatible with HaCaT and fibroblast cells and subsequently their efficacy was validated *in vivo* in a rabbit model. *In vivo*, the ZnO@AM NPs-coated catheters reduced significantly the growth of *Enterococcus* uropathogens, delaying the early onset of CAUTIs, and at the same time did not induce toxicity to the rabbit's kidney, bladder and urethra after 7 days of catheterization. Overall, the urinary catheters coated with the synergistic combination of biofilm matrix-degrading amylase and antibacterial ZnO NPs appear as a viable solution with high clinical potential for preventing CAUTIs.

6 Conclusions and Future Plans

6.1 Final conclusions

The spread of bacterial infections and antimicrobial resistance have called for development of highly efficiently therapeutic strategies with lower risk of resistance occurrence. In addition, the ability of bacteria to colonize the surfaces of medical devices and form persistence biofilms, associated with difficult-to-treat infections rises the demand for novel nano-enabled antibacterial and antibiofilm coatings. To answer these needs, the current thesis designed a platform of innovative engineered nanoentities and nanostructured coatings for control and prevention of bacterial infections with reduced risk of resistance development:

• *Nanomaterials aimed at controlling planktonic bacterial growth and biofilm establishment:*

Multilayered coating of antibacterial AM and biocompatible HA on biologically inert nanotemplate

- Polymeric NPs decorated with antibacterial AM and biocompatible HA in an LbL approach were able to eliminate Gram-positive and Gram-negative planktonic bacteria upon contact within less than 1 h.

- The LbL NPs impeded the *S. aureus* and *E. coli* biofilm formation by 94 and 40 % without affecting the cell viability and morphology of human fibroblast cells.

Biosafety nanocoating of AM and QQ acylase onto active AgNPs template

- Antibacterial AM and QQ enzyme acylase, assembled by LbL on AgNPs template, were able to interfere with QS system and increase the susceptibility of Gram-negative *P. aeruginosa* to the bactericidal AgNPs.

- The developed LbL NPs demonstrated stronger ability to counteract planktonic cells and the formation of biofilm structures, compared to the pristine AgNPs alone.

- The inclusion of AM/AC shell on the AgNPs core led to elimination of already established biofilms and improvement of the biocompatibility of the bactericidal AgNPs.

<u>Targeting of antimicrobial drug delivery nanosystem for selective bacterial elimination</u>

- Highly antibacterial and biocompatible EO NCs were formulated by self-assembly nanoencapsulation technology, based on hydrophobic protein zein, and tagged with a *S. aureus*-targeting antibody.

- The immobilized on the NCs surface antibody provided selective elimination of the targeted *S. aureus* without reducing the non-targeted *P. aeruginosa* bacterium.

- The targeted NCs demonstrated ability to protect the skin fibroblast cells from *S. aureus* in an *in vitro* infection model.

• ***Hybrid enzyme-metal nanocomposites for prevention of CAUTIs:***

<u>Simultaneous sonochemical coating of urinary catheters with antibacterial ZnO/amylase hybrid NPs</u>

- Durable nanocomposite coatings of antibacterial ZnO NPs and biofilm matrix degrading amylase were developed on urinary catheters in a one-step high intensity US process.

- The combination of both enzyme and metal oxide NPs resulted in improved stability and stronger antibiofilm activity against medically relevant pathogens, compared to the coatings with the individual ZnO NPs or amylase.

- The developed hybrid nanocoatings delayed the early onset of CAUTIs and demonstrated biosafety *in vivo* in an animal model, showing potential to prevent device-associated infections.

- A pilot line within the European project framework of PROTECT- Pre-commercial lines for the production of surface nanostructured antimicrobial and antibiofilm textiles, medical devices, and water treatment membranes, H2020-720851 based on scale-up of innovative US-assisted coated urinary catheters was developed and optimized at the new US batch machine installed at Degania, Israel. The functional activities of the produced coated silicone catheters were proven *in vitro* at BIU, Israel and at UPC, Spain.

6.2 Future perspectives

The engineering of highly efficient antibacterial/antibiofilm materials and coatings with lower risk of resistance development is a key for the control and prevention of bacterial infections and spread of drug-resistant bacterial species. The results obtained in this thesis validated the efficiency of a wide range of innovative hybrid nanoentities and nanostructured coatings to control bacterial infections being at the same time safe to human cells.

The obtained during the thesis nanoentities could be incorporated into wound dressing materials or skin care products to manage bacterial infections. Moreover, these hybrid nanomaterials will be employed as functional elements for development of nano-enabled stimuli-responsive hydrogel coatings on medical devices in the ongoing project CoatToSave-Nano-enabled hydrogel coatings against antimicrobial resistant catheter-related infections, PID2019-104111RB-I00. These nanostructured coatings will be endowed with bacteria-triggered responsiveness to virulence factors (e.g. enzymes) and changes in the local environment (e.g. pH) due to bacterial infection, to release the nanoformulated antibacterial cargo. The nanocoating approach could be extended to a broad range of material surfaces, such as textiles, contact lenses, or personal protective equipment.

The realization of this thesis has open new research directions that will be followed under running and new European and national projects at the Group of Molecular and Industrial Biotechnology (GBMI) of Universitat Politècnica de Catalunya. Versatile nano-enabling techniques, such as self-assembling, enzymatic crosslinking, sonochemistry, LbL and combinations thereof, will be used to engineer alternative to the conventional antibiotics antimicrobial nanomaterials and composites. The platform of novel antibiotic-free nano-sized materials obtained under the PhD thesis, combining QQE, natural compounds, polymers, and inorganic NPs will be employed in innovative approaches for controlling infectious diseases and resistance occurrence, including:

> ➢ Combination and nanoformulation of QQEs that interfere with the communication of Gram-negative bacteria and phage lytic enzymes targeting Gram-positive pathogens into the same nanoentities with improved antimicrobial activity, allowing to simultaneously address multiple target pathogens.

- Targeted to specific bacteria nanoactives, using human-derived antibodies and QQ signaling molecules as targeting elements, which will allow maintaining a balanced human microbiome, strengthening the host immune system against bacterial and viral pathogens.

- Novel transportation systems based on non-pathogenic bacteria (e.g. *B. subtilis* or human microbiome constituents) acting as biological carriers to deliver nanoantimicrobials to the infection site. Bimetallic NPs templates with magnetic properties coated with QQE and zwitterionic polymers in a LbL fashion for controlled delivery upon external magnetic field.

- Bacterial cell membrane camouflaged bactericidal nano-modalities to make the bioactives "invisible" to the defense mechanisms of the pathogens.

- Stimuli-responsive mesoporous silica NPs as carriers for bactericidal agents loaded using US. The bioactive-loaded NPs will be coated with an antimicrobial but biocompatible cationic polymer and biofilm matrix-degrading, QQE or phage enzymes using LbL.

- Self-Assembled 3D nano-enabled hydrogel for pH-triggered delivery of multiple nanoactives. The hydrogel will be designed using two complementary nanoparticle building blocks: i) cationic nanogels loaded with antioxidants or anti-inflamatory acteives and (ii) anionic antibacterial NPs. These oppositely charged unitary building blocks will *in situ* self-assemble via interparticle electrostatic interactions, producing multifunctional hydrogel constructs for managing bacterial infections.

142

Appendix: Scientific Contribution

Peer reviewed publications

Ivanova A, Ivanova K, and Tzanov T. "Simultaneous ultrasound-assisted hybrid polyzwitterion/antimicrobial peptide nanoparticles synthesis and deposition on silicone urinary catheters for prevention of biofilm-associated infections". *Nanomaterials*, 2021, http://doi.org/10.3390/nano11113143 (**Q1, IF: 5.076**)

Ivanova A, Ivanova K, Perelshtein I, Gedanken A, Todorova K, Milcheva R, Dimitrov P, Popova T, Tzanko T. "Sonochemically engineered nano-enabled zinc oxide/amylase coatings prevent the occurrence of catheter-associated urinary tract infections". *Materials Science & Engineering C*, 2021, doi: 10.1016/j.msec.2021.112518 (**Q1, IF: 7.328**)

Ivanova K, **Ivanova A**, Ramon E, Hoyo J, Sanchez-Gomez S, Tzanov T. "Antibody-enabled antimicrobial nanocapsules for selective elimination of *Staphylococcus aureus*". *ACS Applied Materials & Interfaces*, 2020, http://dx.doi.org/10.1021/acsami.0c09364. (**Q1, IF: 9.229**)

Ivanova A, Ivanova K, Tied A, Heinze T, and Tzanov T. "Layer-by-layer coating of aminocellulose and quorum quenching acylase on silver nanoparticles synergistically eradicate bacteria and their biofilms". *Advanced Functional Materials*, 2020, https://doi.org/10.1002/adfm.202001284 (**Q1, IF: 18.808**)

Ivanova A, Ivanova K, Hoyo J, Heinze T, Sanchez-Gomez S, Tzanov T. "Layer-by-layer decorated nanoparticles with tunable antibacterial and antibiofilm properties against both Gram-positive and Gram-negative bacteria". *ACS Applied Materials & Interfaces*, 2018, doi: 10.1021/acsami.7b16508 (**Q1, IF: 8.456**)

Book chapters

Ivanova A, Ivanova K, Tzanov T. "Inhibition of Quorum-Sensing: A new paradigm in controlling bacterial virulence and biofilm formation." In "Biotechnological Applications of Quorum Sensing Inhibitors", edited by Kalia, VC, ISBN: 978-981-10-9026-43-21, Springer, Singapore, 2018, 3-21.

Communications to meetings

Ivanova A, Ivanova K, Ramon E, Tzanov T." Engineering of nano-enabled therapeutic nanoparticles to manage bacterial infections and resistance development" (oral), Pacifichem, December 2021, Honolulu, Hawaii (USA), virtual.

Ivanova A, Ivanova K, Tzanov T. "Novel nano-enabled antibacterial strategies to prevent medical devices- associated bacterial infections and resistance occurrence" (poster), 7th Nano Today, November 2021, Guangzhou, China, virtual.

Ramon E, Ivanova K, **Ivanova A**, Tzanov T. "Nano-enabled cosmetic products with enhanced anti-ageing efficacy" (poster), 7th Nano Today, November 2021, Guangzhou, China, virtual.

Bastos-Arrieta J, Puertas-Segura A, **Ivanova A,** Ivanova K, Tzanov T. "Bacteriabots: rod – shape biological active colloid systems as potential (nano) delivery systems" (poster), 7th Nano Today, November 2021, Guangzhou, China, virtual.

Ivanova K, **Ivanova A**, Natan M, Banin E, Mantecca P, Tzanov T. "Metal/bio-based nano-hybrids for managing microbial infections and resistance occurrence" (poster), 7th Nano Today, November 2021, Guangzhou, China, virtual.

Ivanova A, Ivanova K, Tzanov T. "Ultrasound-assisted nanostructured coating of silicone with AgAu NPs and gelatin-dopamine for prevention of bacterial infections" (oral), Designer Biology, September 2021, virtual.

Bastos-Arrieta J, Puertas-Segura A, **Ivanova A**, Ivanova K, Tzanov T. "Bacteriabots as motile "stealth" biological carriers: characterization and perspectives" (poster), Designer Biology, September 2021, virtual.

Ivanova K, **Ivanova A**, Ramon E, Hoyo J, Tzanov T. "Antibody-enabled antimicrobial nanocapsules for selective elimination of Staphylococcus aureus" (poster), Designer Biology, September 2021, virtual.

Ivanova A, Ivanova K, Tzanov T. "Enzyme-decorated mesoporous silica nanoparticles for elimination of antibiotic resistant Pseudomonas aeruginosa biofilms" (oral), 3rd International Conference on Advances in Functional Materials, University of California, Los Angeles, August 2021, (USA)

Ivanova K, **Ivanova A**, Hoyo J, Tzanov T. "Nano-enabled multilayer coatings with switchable bacteria-killing activities for prevention of catheter-related infections" (oral), 3rd International Conference on Advances in Functional Materials, University of California, Los Angeles, August 2021, (USA)

Bastos-Arrieta J, **Ivanova A**, Ivanova K, Ramon E, Tzanov T. "Bacteriabots - motile "stealth" biological carriers of novel nano-antimicrobial actives" (oral), 3rd International Conference on Advances in Functional Materials, University of California, Los Angeles, August 2021, (USA)

Ivanova A, Ivanova K, Perelshtein I, Gedanken A, Tzanov T. "Simultaneous sonochemical functionalization of urinary catheters with biofilm matrix degrading amylase and antibacterial zinc oxide nanoparticles for prevention of bacterial infections" (oral), ACS National Meeting & Exposition, April 2021, virtual

Ivanova A, Ivanova K, Heinze T, Tzanov T. "Layer-by-Layer decoration of AgNPs with aminocellulose and quorum quenching acylase for controlling bacterial pathogens and their biofilms" (oral), NanoBio&Med Conference, November 2019, Barcelona (Spain)

Ivanova K, Ramon E, **Ivanova A**, Tzanov T. "Nanoengineering strategies for safe by design antimicrobial materials" (oral), 257th ACS National Meeting and Exposition, March 2019, Orlando, Florida (USA)

Ivanova A, Ivanova K, Heinze T, Tzanov T. "Safe-by-Design hybrid nanoparticles of antimicrobial silver, aminocellulose, and quorum quenching acylase eradicate bacteria and their biofilms" (oral), 257th ACS National Meeting and Exposition, March 2019, Orlando, Florida (USA)

Ivanova K, **Ivanova A**, Hoyo J, Perez S, Tzanov T. "Nanoenabled therapeutic agents against bacterial pathogens" (oral), ETPN2018 - 13th Annual event of the Europen Technology Platform on Nanomedicine, May 2018, Berlin (Germany)

Ivanova A, Ivanova K, Hoyo J, Heinze T, Tzanov T. "Antibacterial and antibiofilm layer-by-layer decorated nanoparticles" (oral), 255th ACS National Meeting & Exposition, March 2018, New Orleans, Louisiana (USA)

Ivanova K, Hoyo J, **Ivanova A**, Perez S, Tzanov T. "Hybrid nanoantibacterials for controlling bacterial infections and spread of drug resistance" (oral), 255th ACS National Meeting & Exposition, March 2018, New Orleans, Louisiana (USA)

Ivanova K, **Ivanova A**, Hoyo J, Tzanov T. "Hybrid nanocoatings of quorum quenching enzyme and antibiotic for prevention of bacterial biofilms" (oral), 2nd International Caparica Conference in Antibiotic Resistance, June 12-15, Caparica (Portugal)

Ivanova A, Ivanova K, Hoyo J, Heinze T, and Tzanov T. "Layer-by-Layer decorated nanoparticles: an efficient antibacterial and antibiofilm agent" (oral), Designer Biology: from proteins and cells to scaffolds and materials, June 7-9, 2017, Vienna (Austria)

Ivanova K, **Ivanova A**, Heinze T, Tzanov T. "Antibacterial Layer-by-Layer coating of nanoparticles" (poster), 253rd American Chemical Society National Meeting & Exposition, April 2017, San Francisco (USA)

References:

(1)   Lewis, K. The Science of Antibiotic Discovery. *Cell* **2020**, *181*, 29–45.

(2)   Annunziato, G. Strategies to Overcome Antimicrobial Resistance (AMR) Making Use of Non-Essential Target Inhibitors: A Review. *Int. J. Mol. Sci.* **2019**, *20*, 5844.

(3)   Mahoney, A. R.; Safaee, M. M.; Wuest, W. M.; Furst, A. L. The Silent Pandemic: Emergent Antibiotic Resistances Following the Global Response to SARS-CoV-2. *iScience* **2021**, *24*, 102304.

(4)   Ventola, C. L. The Antibiotic Resistance Crisis: Part 1: Causes and Threats. *Pharm. Ther.* **2015**, *40*, 277–283.

(5)   O'Neill, J. Tackling Drug-Resistant Infections Globally: Final Report and Recommendations. *Rev. Antimicrob. Resist.* **2016**, 1–84.

(6)   AMR Indistry Alliance: *AMR Industry Alliance. 2020 Progress Report*; **2020**.

(7)   Divakar, S.; Lama, M.; Asad U., K. Antibiotics versus Biofilm: An Emerging Battleground in Microbial Communities. *Antimicrob. Resist. Infect. Control* **2019**, *8*, 76.

(8)   Yin, W.; Wang, Y.; Liu, L.; He, J. Biofilms: The Microbial "protective Clothing" in Extreme Environments. *Int. J. Mol. Sci.* **2019**, *20*, 3423.

(9)   Khatoon, Z.; McTiernan, C. D.; Suuronen, E. J.; Mah, T. F.; Alarcon, E. I. Bacterial Biofilm Formation on Implantable Devices and Approaches to Its Treatment and Prevention. *Heliyon* **2018**, *4*, e01067.

(10)   Lee, N. Y.; Ko, W. C.; Hsueh, P. R. Nanoparticles in the Treatment of Infections Caused by Multidrug-Resistant Organisms. *Front. Pharmacol.* **2019**, *10*, 1153.

(11)   Shahidi, F.; Ambigaipalan, P. Phenolics and Polyphenolics in Foods, Beverages and Spices: Antioxidant Activity and Health Effects - A Review. *J. Funct. Foods* **2015**, *18*, 820–897.

(12)   Martau, G. A.; Mihai, M.; Vodnar, D. C. The Use of Chitosan, Alginate, and Pectin in the Biomedical and Food Sector-Biocompatibility, Bioadhesiveness, and Biodegradability. *Polymers (Basel).* **2019**, *11*, 1837.

(13)   Zhao, X.; Yu, Z.; Ding, T. Quorum-Sensing Regulation of Antimicrobial Resistance in Bacteria. *Microorganisms* **2020**, *8*, 425.

(14)   Vallet-Regí, M.; González, B.; Izquierdo-Barba, I. Nanomaterials as Promising Alternative in the Infection Treatment. *Int. J. Mol. Sci.* **2019**, *20*, 3806.

(15)   Hussain, S.; Joo, J.; Kang, J.; Kim, B.; Braun, G. B.; She, Z.; Kim, D.; Mann, A. P.; Mölder, T.; Teesalu, T.; Carnazza, S.; Guglielmino, S.; Sailor, M. J.; Ruoslahti, E. Antibiotic-Loaded Nanoparticles Targeted to the Site of Infection Enhance Antibacterial Efficacy. *Nat. Biomed. Eng.* **2018**, *2*, 95–103.

(16)   Prestinaci, F.; Pezzotti, P.; Pantosti, A. Antimicrobial Resistance: A Global Multifaceted Phenomenon. *Pathog. Glob. Health* **2015**, *109*, 309–318.

(17)   Dadgostar, P. Antimicrobial Resistance: Implications and Costs. *Infect. Drug Resist.* **2019**, *12*, 3903–3910.

(18) Aslam, B.; Wang, W.; Arshad, M. I.; Khurshid, M.; Muzammil, S.; Rasool, M. H.; Nisar, M. A.; Aslam, M. A.; Qamar, M. U.; Salamat, M. K. F.; Baloch, Z. Antibiotic Resistance : A Rundown of a Global Crisis. *Infect. Drug Resist.* **2018**, *11*, 1645–1658.

(19) Boev, C.; Kiss, E. Hospital-Acquired Infections: Current Trends and Prevention. *Crit. Care Nurs. Clin. North Am.* **2017**, *29*, 51–65.

(20) Revelas, A. Healthcare - Associated Infections: A Public Health Problem. *Niger. Med. J.* **2012**, *53*, 59–64.

(21) Young, P. Y.; Khadaroo, R. G. Surgical Site Infections. *Surg. Clin. North Am.* **2014**, *94*, 1245–1264.

(22) C Reygaert, W. An Overview of the Antimicrobial Resistance Mechanisms of Bacteria. *AIMS Microbiol.* **2018**, *4*, 482–501.

(23) Cantas, L.; Shah, S. Q. A.; Cavaco, L. M.; Manaia, C. M.; Walsh, F.; Popowska, M.; Garelick, H.; Bürgmann, H.; Sørum, H. A Brief Multi-Disciplinary Review on Antimicrobial Resistance in Medicine and Its Linkage to the Global Environmental Microbiota. *Front. Microbiol.* **2013**, *4*, 1–14.

(24) Mi, G.; Shi, D.; Wang, M.; Webster, T. J. Reducing Bacterial Infections and Biofilm Formation Using Nanoparticles and Nanostructured Antibacterial Surfaces. *Adv. Healthc. Mater.* **2018**, *7*, 1–23.

(25) Kohanski, M. A.; Dwyer, D. J.; Collins, J. J. How Antibiotics Kill Bacteria: From Targets to Networks. *Nat. Rev. Microbiol.* **2010**, *8*, 423–435.

(26) Arora, G.; Sajid, A.; Kalia, V. C. *Drug Resistance in Bacteria, Fungi, Malaria, and Cancer*; Cham: Springer International Publishing; **2017**. pp. 609-292017.

(27) Solís-Salas, L. M.; Sierra-Rivera, C. A.; Cobos-Puc, L. E.; Ascacio-Valdés, J. A.; Silva-Belmares, S. Y. Antibacterial Potential by Rupture Membrane and Antioxidant Capacity of Purified Phenolic Fractions of Persea Americana Leaf Extract. *Antibiotics* **2021**, *10*, 508.

(28) Tong, S. Y. C.; Chen, L. F.; Jr, V. G. F. Colonization, Pathogenicity, Host Susceptibility and Therapeutics for Staphylococcus Aureus: What Is the Clinical Relevance? *Semin Immunopathol* **2013**, *34*, 185–200.

(29) Mulvey, M. R.; Simor, A. E. Antimicrobial Resistance in Hospitals: How Concerned Should We Be? *Can. Med. Assoc. J.* **2009**, *180*, 408–415.

(30) Nikaido, H. Multidrug Resistance in Bacteria. *Annu Rev Biochem* **2009**, *78*, 119–146.

(31) World Health Organization. *Prevention of Hospital-Acquired Infections: A Practical Guide*; **2002**.

(32) Jamal, M.; Tasneem, U.; Hussain, T.; Andleeb, and S. Bacterial Biofilm: Its Composition, Formation and Role in Human Infections. *Res. Rev. J. Microbiol. Biotechnol.* **2015**, *4*, 1–14.

(33) Taraszkiewicz, A.; Fila, G.; Grinholc, M.; Nakonieczna, J. Innovative Strategies to Overcome Biofilm Resistance. *Biomed Res. Int.* **2013**, *2013*, 150653.

(34) Han, C.; Romero, N.; Fischer, S.; Dookran, J.; Berger, A.; Doiron, A. L. Recent Developments in the Use of Nanoparticles for Treatment of Biofilms. *Nanotechnol. Rev.* **2017**, *6*, 383–404.

(35) Ciofu, O.; Rojo-Molinero, E.; Macià, M. D.; Oliver, A. Antibiotic Treatment of Biofilm Infections. *Acta Pathol. Microbiol. Immunol. Scand.* **2017**, *125*, 304–319.

(36) Percival, S. L.; Suleman, L.; Donelli, G. Healthcare-Associated Infections, Medical Devices and Biofilms: Risk, Tolerance and Control. *J. Med. Microbiol.* **2015**, *64*, 323–334.

(37) Zhao, G.; Usui, M. L.; Lippman, S. I.; James, G. A.; Stewart, P. S.; Fleckman, P.; Olerud, J. E. Biofilms and Inflammation in Chronic Wounds. *Adv. wound care* **2013**, *2*, 389–399.

(38) McCaslin, C. A.; Petrusca, D. N.; Poirier, C.; Serban, K. A.; Anderson, G. G.; Petrache, I. Impact of Alginate-Producing Pseudomonas Aeruginosa on Alveolar Macrophage Apoptotic Cell Clearance. *J. Cyst. Fibros.* **2015**, *14*, 70–77.

(39) Jefferson, K. K.; Goldmann, D. A.; Pier, G. B. Use of Confocal Microscopy to Analyze the Rate of Vancomycin Penetration through Staphylococcus Aureus Biofilms. *Antimicrob. Agents Chemother.* **2005**, *49*, 2467–2473.

(40) Lima, M.; Teixeira-Santos, R.; Gomes, L. C.; Faria, S. I.; Valcarcel, J.; Vázquez, J. A.; Cerqueira, M. A.; Pastrana, L.; Bourbon, A. I.; Mergulhão, F. J. Development of Chitosan-Based Surfaces to Prevent Singleand Dual-Species Biofilms of Staphylococcus Aureus and Pseudomonas Aeruginosa. *Molecules* **2021**, *26*, 4378.

(41) Haque, M.; Sartelli, M.; Mckimm, J.; Abu Bakar, M. Health Care-Associated Infections-an Overview. *Infect. Drug Resist.* **2018**, *11*, 2321–2333.

(42) Putensen, C.; Ellger, B.; Sakka, S. G.; Weyland, A.; Schmidt, K.; Zoller, M.; Weiler, N.; Kindgen-Milles, D.; Jaschinski, U.; Weile, J.; Lindau, S.; Kieninger, M.; Faltlhauser, A.; Jung, N.; Teschendorf, P.; Adamzik, M.; Gründling, M.; Wahlers, T.; Gerlach, H.; Litty, F. A. Current Clinical Use of Intravenous Fosfomycin in ICU Patients in Two European Countries. *Infection* **2019**, *47*, 827–836.

(43) Anaissie, E.; Samonis, G.; Kontoyiannis, D.; Costerton, J.; Sabharwal, U.; Bodey, G.; Raad, I. Role of Catheter Colonization and Infrequent Hematogenous Seeding in Catheter-Related Infections. *Eur. J. Clin. Microbiol. Infect. Dis.* **1995**, *14*, 134–137.

(44) Badia, J. M.; Casey, A. L.; Petrosillo, N.; Hudson, P. M.; Mitchell, S. A.; Crosby, C. Impact of Surgical Site Infection on Healthcare Costs and Patient Outcomes: A Systematic Review in Six European Countries. *J. Hosp. Infect.* **2017**, *96*, 1–15.

(45) Jacobsen, S. M.; Stickler, D. J.; Mobley, H. L. T.; Shirtliff, M. E. Complicated Catheter-Associated Urinary Tract Infections due to Escherichia Coli and Proteus Mirabilis. *Clin. Microbiol. Rev.* **2008**, *21*, 26–59.

(46) Donlan, R. M. Biofilms and Device-Associated Infections. *Emerg. Infect. Dis.* **2001**, *7*, 277–281.

(47) Hawver, L. A.; Jung, S. A.; Ng, W. Specificity and Complexity in Bacterial Quorum-Sensing Systems. *FEMS Microbiol. Rev.* **2016**, *40*, 738–752.

(48) Lee, J.; Zhang, L. The Hierarchy Quorum Sensing Network in Pseudomonas Aeruginosa. *Protein Cell* **2014**, *6*, 26–41.

(49) Bortolotti, D.; LeMaoult, J.; Trapella, C.; Luca, D. Di; Carosella, E. D.; Rizzo, R. Pseudomonas Aeruginosa Quorum Sensing Molecule N-(3-Oxododecanoyl)-L-Homoserine-Lactone Induces HLA-G Expression in Human Immune Cells. *Infect. Immun.* **2015**, *83*, 3918–3925.

(50) Monnet, V.; Juillard, V.; Gardan, R. Peptide Conversations in Gram-Positive Bacteria. *Crit. Rev. Microbiol.* **2016**, *42*, 339-351.

(51) Scott, S. R.; Hasty, J. Quorum Sensing Communication Modules for Microbial Consortia. *ACS Synth. Biol.* **2016**, *5*, 969–977.

(52) Montebello, A. N.; Brecht, R. M.; Turner, R. D.; Ghali, M.; Pu, X.; Nagarajan, R. Acyl-ACP Substrate Recognition in Burkholderia Mallei bmaI1 Acyl-Homoserine Lactone Synthase. *Biochemistry* **2014**, *53*, 6231–6242.

(53) Papenfort, K.; Bassler, B. Quorum-Sensing Signal-Response Systems in Gram-Negative Bacteria. *Nat. Rev. Microbiol.* **2016**, *14*, 576-88.

(54) Yerushalmi, S. M.; Buck, M. E.; Lynn, D. M.; Gabriel, N.; Meijler, M. M. Multivalent Alteration of Quorum Sensing in Staphylococcus Aureus. *Chem. Commun* **2013**, *49*, 5177–5179.

(55) Pollitt, E. J. G.; West, S. A.; Crusz, S. A.; Burton-Chellew, M. N.; Diggle, S. P. Cooperation, Quorum Sensing, and Evolution of Virulence in Staphylococcus Aureus. *Infect. Immun.* **2014**, *82*, 1045–1051.

(56) Le, K. Y.; Otto, M. Quorum-Sensing Regulation in Staphylococci-an Overview. *Front. Microbiol.* **2015**, *6*, 1174.

(57) Tay, S. B.; Yew, W. S. Development of Quorum-Based Anti-Virulence Therapeutics Targeting Gram-Negative Bacterial Pathogens. *Int. J. Mol. Sci.* **2013**, *14*, 16570–16599.

(58) Cheung, G. Y. C.; Joo, H. S.; Chatterjee, S. S.; Otto, M. Phenol-Soluble Modulins - Critical Determinants of Staphylococcal Virulence. *FEMS Microbiol. Rev.* **2014**, *38*, 698–719.

(59) Xue, T.; Zhao, L.; Sun, B. LuxS/AI-2 System Is Involved in Antibiotic Susceptibility and Autolysis in Staphylococcus Aureus NCTC 8325. *Int. J. Antimicrob. Agents* **2013**, *41*, 85–89.

(60) Rezzonico, F.; Smits, T. H. M.; Duffy, B. Detection of AI-2 Receptors in Genomes of Enterobacteriaceae Suggests a Role of Type-2 Quorum Sensing in Closed Ecosystems. *Sensors (Switzerland)* **2012**, *12*, 6645–6665.

(61) Antunes, L. C. M.; Ferreira, R. B. R.; Buckner, M. M. C.; Finlay, B. B. Quorum Sensing in Bacterial Virulence. *Microbiology* **2010**, *156*, 2271–2282.

(62) Llor, C.; Bjerrum, L. Antimicrobial Resistance: Risk Associated with Antibiotic Overuse and Initiatives to Reduce the Problem. *Ther. Adv. Drug Saf.* **2014**, *5*, 229–241.

(63) Gilbert, P.; McBain, A. J. Biofilms: Their Impact on Health and Their Recalcitrance toward Biocides. *Am. J. Infect. Control* **2001**, *29*, 252–255.

(64) Williamson, D. A.; Carter, G. P.; Howden, B. P. Current and Emerging Topical Antibacterials and Antiseptics: Agents, Action, and Resistance Patterns. *Clin. Microbiol. Rev* **2017**, *30*, 827−860.

(65) Clatworthy, A. E.; Pierson, E.; Hung, D. T. Targeting Virulence: A New Paradigm for Antimicrobial Therapy. *Nat. Chem. Biol.* **2007**, *3*, 541–548.

(66) Wu, H.; Moser, C.; Wang, H. Z.; Høiby, N.; Song, Z. J. Strategies for Combating Bacterial Biofilm Infections. *Int. J. Oral Sci.* **2015**, *7*, 1–7.

(67) Bi, Y.; Xia, G.; Shi, C.; Wan, J.; Liu, L.; Chen, Y.; Wu, Y.; Zhang, W.; Zhou, M.; He, H.; Liu, R. Therapeutic Strategies against Bacterial Biofilms. *Fundam. Res.* **2021**, *1*, 193–212.

(68) Blaser, M. Antibiotic Overuse: Stop the Killing of Beneficial Bacteria. *Nature* **2011**, *476*, 393–394.

(69) Rigo, S.; Cai, C.; Gunkel-Grabole, G.; Maurizi, L.; Zhang, X.; Xu, J.; Palivan, C. G. Nanoscience-Based Strategies to Engineer Antimicrobial Surfaces. *Adv. Sci.* **2018**, *5*, 1700892.

(70) Kalia, V. C. Biotechnological Applications of Quorum Sensing Inhibitors; Kalia, V. C., Ed.

(71) Rasamiravaka, T.; Labtani, Q.; Duez, P.; El Jaziri, M. The Formation of Biofilms by Pseudomonas Aeruginosa : A Review of the Natural and Synthetic Compounds Interfering with Control Mechanisms. *Biomed Res. Int.* **2015**, *2015*, 759348.

(72) Nguyen, K. T.; Zhao, Y. Engineered Hybrid Nanoparticles for On-Demand Diagnostics and Therapeutics. *Acc. Chem. Res.* **2015**, *48*, 3016–3025.

(73) Beceiro, A.; Tomás, M.; Bou, G. Antimicrobial Resistance and Virulence: A Successful or Deleterious Association in the Bacterial World? *Clin. Microbiol. Rev.* **2013**, *26*, 185–230.

(74) Munita, J. M.; Arias, C. A.; Unit, A. R.; Santiago, A. De. Mechanism of Antibiotic Resistance. *Microbiol Spectr* **2016**, *4*, 10.1128/microbiolspec.VMBF-0016-2015.

(75) Hentzer, M.; Givskov, M. Pharmacological Inhibition of Quorum Sensing for the Treatment of Chronic Bacterial Infections. *J. Clin. Invest.* **2003**, *112*, 1300–1307.

(76) Vinoj, G.; Vaseeharan, B.; Thomas, S.; Spiers, A. J.; Shanthi, S. Quorum-Quenching Activity of the AHL-Lactonase from Bacillus Licheniformis DAHB1 Inhibits Vibrio Biofilm Formation In Vitro and Reduces Shrimp Intestinal Colonisation and Mortality. *Mar. Biotechnol.* **2014**, *16*, 707–715.

(77) Ivanova, K.; Fernandes, M. M.; Francesko, A.; Mendoza, E.; Guezguez, J.; Burnet, M.; Tzanov, T. Quorum-Quenching and Matrix-Degrading Enzymes in Multilayer Coatings Synergistically Prevent Bacterial Biofilm Formation on Urinary Catheters. *ACS Appl. Mater. Interfaces* **2015**, *7*, 27066–27077.

(78) Yang, Y. X.; Xu, Z. H.; Zhang, Y. Q.; Tian, J.; Weng, L. X.; Wang, L. H. A New

Quorum-Sensing Inhibitor Attenuates Virulence and Decreases Antibiotic Resistance in Pseudomonas Aeruginosa. *J. Microbiol.* **2012**, *50*, 987–993.

(79)   Cirioni, O.; Ghiselli, R.; Minardi, D.; Orlando, F.; Mocchegiani, F.; Silvestri, C.; Muzzonigro, G.; Saba, V.; Scalise, G.; Balaban, N.; Giacometti, A. RNAIII-Inhibiting Peptide Affects Biofilm Formation in a Rat Model of Staphylococcal Ureteral Stent Infection. *Antimicrob. Agents Chemother.* **2007**, *51*, 4518–4520.

(80)   Bahari, S.; Zeighami, H.; Mirshahabi, H.; Roudashti, S.; Haghi, F. Inhibition of Pseudomonas Aeruginosa Quorum Sensing by Subinhibitory Concentrations of Curcumin with Gentamicin and Azithromycin. *J. Glob. Antimicrob. Resist.* **2017**, *10*, 21–28.

(81)   Li, Z.; Nair, S. K. Quorum Sensing: How Bacteria Can Coordinate Activity and Synchronize Their Response to External Signals? *Protein Sci.* **2012**, *21*, 1403–1417.

(82)   Chang, C.; Krishnan, T.; Wang, H.; Chen, Y.; Yin, W.; Chong, Y. Non-Antibiotic Quorum Sensing Inhibitors Acting against N -Acyl Homoserine Lactone Synthase as Druggable Target. *PLOS Sci. Reports* **2014**, *4*, 7245.

(83)   Lade, H.; Paul, D.; Kweon, J. H. yang. Quorum Quenching Mediated Approaches for Control of Membrane Biofouling. *Int. J. Biol. Sci.* **2014**, *10*, 550–565.

(84)   Cheng, G.; Hao, H.; Xie, S.; Wang, X.; Dai, M.; Huang, L.; Yuan, Z. Antibiotic Alternatives: The Substitution of Antibiotics in Animal Husbandry? *Front. Microbiol.* **2014**, *5*, 217.

(85)   Tang, K.; Su, Y.; Brackman, G.; Cui, F.; Zhang, Y.; Shi, X.; Coenye, T.; Zhang, X. H. MomL, a Novel Marine-Derived N-Acyl Homoserine Lactonase from Muricauda Olearia. *Appl. Environ. Microbiol.* **2015**, *81*, 774–782.

(86)   Zhang, Y.; Brackman, G.; Coenye, T. Pitfalls Associated with Evaluating Enzymatic Quorum Quenching Activity: The Case of MomL and Its Effect on Pseudomonas Aeruginosa and Acinetobacter Baumannii Biofilms. *PeerJ* **2017**, *5*, e3251.

(87)   Kiran, S.; Sharma, P.; Harjai, K.; Capalash, N. Enzymatic Quorum Quenching Increases Antibiotic Susceptibility of Multidrug Resistant Pseudomonas Aeruginosa. *Iran. J. Microbiol.* **2011**, *3*, 1–12.

(88)   Gupta, P.; Chhibber, S.; Harjai, K. Efficacy of Purified Lactonase and Ciprofloxacin in Preventing Systemic Spread of Pseudomonas Aeruginosa in Murine Burn Wound Model. *Burns* **2015**, *41*, 153–162.

(89)   Lin, Y. H.; Xu, J. L.; Hu, J.; Wang, L. H.; Leong Ong, S.; Renton Leadbetter, J.; Zhang, L. H. Acyl-Homoserine Lactone Acylase from Ralstonia Strain XJ12B Represents a Novel and Potent Class of Quorum-Quenching Enzymes. *Mol. Microbiol.* **2003**, *47*, 849–860.

(90)   Ivanova, K.; Fernandes, M. M.; Mendoza, E.; Tzanov, T. Enzyme Multilayer Coatings Inhibit Pseudomonas Aeruginosa Biofilm Formation on Urinary Catheters. *Appl. Microbiol. Biotechnol.* **2015**, *99*, 4373–4385.

(91)   Jon E. Paczkowskia, Sampriti Mukherjeea, Amelia R. McCreadya, Jian-Ping Conga, Christopher J. Aquinob, Hahn Kimc, Brad R. Henked, Chari D. Smitha,

B. L. B. Flavonoids Suppress Pseudomonas Aeruginosa Virulence through Allosteric Inhibition of Quorum-Sensing Receptors. *Am. Soc. Biochem. Mol. Biol.* **2017**, 10, 4064–4076.

(92) Loughlin, C. T. O.; Miller, L. C.; Siryaporn, A.; Drescher, K.; Semmelhack, M. F. A Quorum-Sensing Inhibitor Blocks Pseudomonas Aeruginosa Virulence and Biofilm Formation. *Proc. Natl. Acad. Sci.* **2013**, *110*, 17981–17986.

(93) Geske, G. D.; Mattmann, M. E.; Blackwell, H. E. Evaluation of a Focused Library of N-Aryl L-Homoserine Lactones Reveals a New Set of Potent Quorum Sensing Modulators. *Bioorganic Med. Chem. Lett.* **2008**, *18*, 5978–5981.

(94) Kim, H.; Lee, S.; Byun, Y.; Park, H. 6-Gingerol Reduces Pseudomonas Aeruginosa Biofilm Formation and Virulence via Quorum Sensing Inhibition. *Sci. Rep.* **2015**, *5*, 8656.

(95) LaSarre, B.; Federle, M. J. Exploiting Quorum Sensing To Confuse Bacterial Pathogens. *Microbiol. Mol. Biol. Rev.* **2013**, *77*, 73–111.

(96) Pavlukhina, S. V.; Kaplan, J. B.; Xu, L.; Chang, W.; Yu, X.; Madhyastha, S.; Yakandawala, N.; Mentbayeva, A.; Khan, B.; Sukhishvili, S. A. Noneluting Enzymatic Antibiofilm Coatings. *ACS Appl. Mater. Interfaces* **2012**, *4*, 4708−4716.

(97) Darouiche, R. O.; Mansouri, M. D.; Gawande, P. V.; Madhyastha, S. Antimicrobial and Antibiofilm Efficacy of Triclosan and DispersinB Combination. *J. Antimicrob. Chemother.* **2009**, *64*, 88–93.

(98) Tetz, G. V.; Artemenko, N. K.; Tetz, V. V. Effect of DNase and Antibiotics on Biofilm Characteristics. *Antimicrob. Agents Chemother.* **2009**, *53*, 1204–1209.

(99) Alkawash, M. A.; Soothill, J. S.; Schiller, N. L. Alginate Lyase Enhances Antibiotic Killing of Mucoid Pseudomonas Aeruginosa in Biofilms. *Apmis* **2006**, *114*, 131–138.

(100) Bradford, C.; Dashiff, A.; Kadouri, D. E. The Use of Commercially Available Alpha-Amylase Compounds to Inhibit and Remove Staphylococcus Aureus Biofilms. *Open Microbiol. J.* **2011**, *5*, 21–31.

(101) Huang, K.; Yang, C.; Huang, S.; Chen, C.; Lu, Y. Recent Advances in Antimicrobial Polymers :A Mini-Review. *Int. J. Mol. Sci.* **2016,** *17*, 1578.

(102) Sendamangalam, V.; Choi, O. K.; Seo, Y.; Kim, D.-S. Antimicrobial and Antioxidant Activities of Polyphenols against Streptococcus Mutans. *Free Radicals Antioxidants* **2011**, *1*, 48–55.

(103) Shahzad, M.; Millhouse, E.; Culshaw, S.; Edwards, C. A.; Ramage, G.; Combet, E. Selected Dietary (Poly)phenols Inhibit Periodontal Pathogen Growth and Biofilm Formation. *Food Funct.* **2015**, *6*, 719–729.

(104) Fernandes, M. M.; Francesko, A.; Torrent-Burgués, J.; Carrión-Fité, F. J.; Heinze, T.; Tzanov, T. Sonochemically Processed Cationic Nanocapsules: Efficient Antimicrobials with Membrane Disturbing Capacity. *Biomacromolecules* **2014**, *15*, 1365–1374.

(105) Santos, M. R. E.; Fonseca, A. C.; Mendonça, P. V.; Branco, R.; Serra, A. C.;

Morais, P. V.; Coelho, J. F. J. Recent Developments in Antimicrobial Polymers: A Review. *Materials (Basel).* **2016**, *9*, 599.

(106) Carmona-Ribeiro, A. M.; de Melo Carrasco, L. D. Cationic Antimicrobial Polymers and Their Assemblies. *Int. J. Mol. Sci.* **2013**, *14*, 9906–9946.

(107) Matica, M. A.; Aachmann, F. L.; Tøndervik, A.; Sletta, H.; Ostafe, V. Chitosan as a Wound Dressing Starting Material: Antimicrobial Properties and Mode of Action. *Int. J. Mol. Sci.* **2019**, *20*, 1–33.

(108) Francesko, A.; Fernandes, M. M.; Ivanova, K.; Amorim, S.; Reis, R. L.; Pashkuleva, I.; Mendoza, E.; Pfeifer, A.; Heinze, T.; Tzanov, T. Bacteria-Responsive Multilayer Coatings Comprising Polycationic Nanospheres for Bacteria Biofilm Prevention on Urinary Catheters. *Acta Biomater.* **2016**, *33*, 203–212.

(109) Nederberg, F.; Zhang, Y.; Tan, J. P. K.; Xu, K.; Wang, H.; Yang, C.; Gao, S.; Guo, X. D.; Fukushima, K.; Li, L.; Hedrick, J. L.; Yang, Y. Biodegradable Nanostructures with Selective Lysis of Microbial Membranes. *Nat. Chem.* **2011**, *3*, 409–414.

(110) Waschinski, C. J.; Barnert, S.; Theobald, A.; Schubert, R.; Kleinschmidt, F.; Hoffmann, A.; Saalwächter, K.; Tiller, J. C. Insights in the Antibacterial Action of Poly(methyloxazoline)s with a Biocidal End Group and Varying Satellite Groups. *Biomacromolecules* **2008**, *9*, 1764–1771.

(111) Broxton, P.; Woodcock, P. M.; Heatley, F.; Gilbert, P. Interaction of Some Polyhexamethylene Biguanides and Membrane Phospholipids in Escherichia Coli. *J. Appl. Bacteriol.* **1984**, *57*, 115–124.

(112) Yañez-Macías, R.; Muñoz-Bonilla, A.; De Jesús-Tellez, M. A.; Maldonado-Textle, H.; Guerrero-Sánchez, C.; Schubert, U. S.; Guerrero-Santos, R. Combinations of Antimicrobial Polymers with Nanomaterials and Bioactives to Improve Biocidal Therapies. *Polymers (Basel).* **2019**, *11*, 1789.

(113) Zeng, Q.; Zhu, Y.; Yu, B.; Sun, Y.; Ding, X.; Xu, C.; Wu, Y. W.; Tang, Z.; Xu, F. J. Antimicrobial and Antifouling Polymeric Agents for Surface Functionalization of Medical Implants. *Biomacromolecules* **2018**, *19*, 2805–2811.

(114) Chen, Y.; Worley, S. D.; Kim, J.; Wei, C. I.; Chen, T. Y.; Santiago, J. I.; Williams, J. F.; Sun, G. Biocidal Poly(styrenehydantoin) Beads for Disinfection of Water. *Ind. Eng. Chem. Res.* **2003**, *42*, 280–284.

(115) Kamaruzzaman, N. F.; Tan, L. P.; Hamdan, R. H.; Choong, S. S.; Wong, W. K.; Gibson, A. J.; Chivu, A.; De Fatima Pina, M. Antimicrobial Polymers: The Potential Replacement of Existing Antibiotics? *Int. J. Mol. Sci.* **2019**, *20*, 2747.

(116) Abers, M.; Schroeder, S.; Goelz, L.; Sulser, A.; St. Rose, T.; Puchalski, K.; Langland, J. Antimicrobial Activity of the Volatile Substances from Essential Oils. *BMC Complement. Med. Ther.* **2021**, *21*, 21–124.

(117) Kim, J.; Marshall, M. R.; Wei, C. i. Antibacterial Activity of Some Essential Oil Components against Five Foodborne Pathogens. *J. Agric. Food Chem.* **1995**, *43*, 2839–2845.

(118) Skandamis, P.; Tsigarida, E.; Nychas, G. J. E. The Effect of Oregano Essential Oil on Survival/death of Salmonella Typhimurium in Meat Stored at 5°C under Aerobic, VP/MAP Conditions. *Food Microbiol.* **2002**, *19*, 97–103.

(119) Lv, F.; Liang, H.; Yuan, Q.; Li, C. In Vitro Antimicrobial Effects and Mechanism of Action of Selected Plant Essential Oil Combinations against Four Food-Related Microorganisms. *Food Res. Int.* **2011**, *44*, 3057–3064.

(120) Cox, S. D.; Gustafson, J. E.; Mann, C. M.; Markham, J. L.; Liew, Y. C.; Hartland, R. P.; Bell, H. C.; Warmington, J. R.; Wyllie, S. G. Tea Tree Oil Causes K+ Leakage and Inhibits Respiration in Escherichia Coli. *Lett. Appl. Microbiol.* **1998**, *26*, 355–358.

(121) Lopez-Romero, J. C.; González-Ríos, H.; Borges, A.; Simões, M. Antibacterial Effects and Mode of Action of Selected Essential Oils Components against Escherichia Coli and Staphylococcus Aureus. *Evidence-based Complement. Altern. Med.* **2015**, *2015*.

(122) Swamy, M. K.; Akhtar, M. S.; Sinniah, U. R. Antimicrobial Properties of Plant Essential Oils against Human Pathogens and Their Mode of Action: An Updated Review. *Evidence-based Complement. Altern. Med.* **2016**, *2016*, 21.

(123) Patra, J. K.; Das, G.; Fraceto, L. F.; Campos, E. V. R.; Rodriguez-Torres, M. D. P.; Acosta-Torres, L. S.; Diaz-Torres, L. A.; Grillo, R.; Swamy, M. K.; Sharma, S.; Habtemariam, S.; Shin, H. S. Nano Based Drug Delivery Systems: Recent Developments and Future Prospects. *J. Nanobiotechnology* **2018**, *16*, 71.

(124) Fernandes, M. M.; Ivanova, K.; Hoyo, J.; Pérez-Rafael, S.; Francesko, A.; Tzanov, T. Nanotransformation of Vancomycin Overcomes the Intrinsic Resistance of Gram-Negative Bacteria. *ACS Appl. Mater. Interfaces* **2017**, *9*, 15022−15030.

(125) Fernandes, M. M.; Ivanova, K.; Francesko, A.; Rivera, D.; Torrent-Burgu??s, J.; Gedanken, A.; Mendonza, E.; Tzanov, T. Escherichia Coli and Pseudomonas Aeruginosa Eradication by Nano-Penicillin G. *Nanomedicine Nanotechnology, Biol. Med.* **2016**, *12*, 2061–2069.

(126) Wang, L.; Hu, C.; Shao, L. The Antimicrobial Activity of Nanoparticles: Present Situation and Prospects for the Future. *Int. J. Nanomedicine* **2017**, *12*, 1227–1249.

(127) Schieber, M.; Chandel, N. S. ROS Function in Redox Signaling. *Curr. Biol.* **2014**, *24*, 453–462.

(128) Raghunath, A.; Perumal, E. Metal Oxide Nanoparticles as Antimicrobial Agents: A Promise for the Future. *Int. J. Antimicrob. Agents* **2017**, *49*, 137–152.

(129) Attarilar, S.; Yang, J.; Ebrahimi, M.; Wang, Q.; Liu, J.; Tang, Y.; Yang, J. The Toxicity Phenomenon and the Related Occurrence in Metal and Metal Oxide Nanoparticles: A Brief Review From the Biomedical Perspective. *Front. Bioeng. Biotechnol.* **2020**, *8*, 822.

(130) Martinez-Gutierrez, F.; Olive, P. L.; Banuelos, A.; Orrantia, E.; Nino, N.; Sanchez, E. M.; Ruiz, F.; Bach, H.; Av-Gay, Y. Synthesis, Characterization, and Evaluation of Antimicrobial and Cytotoxic Effect of Silver and Titanium

Nanoparticles. *Nanomedicine Nanotechnology, Biol. Med.* **2010**, *6*, 681–688.

(131) Richter, A. P.; Brown, J. S.; Bharti, B.; Wang, A.; Gangwal, S.; Houck, K.; Hubal, E. A. C.; Paunov, V. N.; Stoyanov, S. D.; Velev, O. D. An Environmentally Benign Antimicrobial Nanoparticle Based on a Silver-Infused Lignin Core. *Nat. Nanotechnol.* **2015**, *10* (9), 817–823.

(132) Wirth, S. M.; Lowry, G. V.; Tilton, R. D. Natural Organic Matter Alters Biofilm Tolerance to Silver Nanoparticles and Dissolved Silver. *Environ. Sci. Technol.* **2012**, *46*, 12687–12696.

(133) Panáček, A.; Kvítek, L.; Smékalová, M.; Večeřová, R.; Kolář, M.; Röderová, M.; Dyčka, F.; Šebela, M.; Prucek, R.; Tomanec, O.; Zbořil, R. Bacterial Resistance to Silver Nanoparticles and How to Overcome It. *Nat. Nanotechnol.* **2018**, *13*, 65–71.

(134) Sánchez-López, E.; Gomes, D.; Esteruelas, G.; Bonilla, L.; Lopez-Machado, A. L.; Galindo, R.; Cano, A.; Espina, M.; Ettcheto, M.; Camins, A.; Silva, A. M.; Durazzo, A.; Santini, A.; Garcia, M. L.; Souto, E. B. Metal-Based Nanoparticles as Antimicrobial Agents: An Overview. *Nanomaterials* **2020**, *10*, 1–39.

(135) Eshed, M.; Lellouche, J.; Matalon, S.; Gedanken, A.; Banin, E. Sonochemical Coatings of ZnO and CuO Nanoparticles Inhibit Streptococcus Mutans Biofilm Formation on Teeth Model. *Langmuir* **2012**, *28*, 12288–12295.

(136) Baptista, P. V; Mccusker, M. P.; Carvalho, A.; Ferreira, D. A.; Mohan, N. M.; Martins, M.; Fernandes, A. R. Nano-Strategies to Fight Multidrug Resistant Bacteria —" A Battle of the Titans ." *Front. Microbiol.* **2018**, *9*, 1441.

(137) Zhao, S.; Su, X.; Wang, Y.; Yang, X.; Bi, M.; He, Q.; Chen, Y. Copper Oxide Nanoparticles Inhibited Denitrifying Enzymes and Electron Transport System Activities to Influence Soil Denitrification and N2O Emission. *Chemosphere* **2020**, *245*, 125394.

(138) Salat, M.; Petkova, P.; Hoyo, J.; Perelshtein, I.; Gedanken, A.; Tzanov, T. Durable Antimicrobial Cotton Textiles Coated Sonochemically with ZnO Nanoparticles Embedded in an in-Situ Enzymatically Generated Bioadhesive. *Carbohydr. Polym.* **2018**, *189*, 198–203.

(139) Petkova, P.; Francesko, A.; Fernandes, M. M.; Mendoza, E.; Perelshtein, I.; Gedanken, A.; Tzanov, T. Sonochemical Coating of Textiles with Hybrid ZnO/chitosan Antimicrobial Nanoparticles. *ACS Appl. Mater. Interfaces* **2014**, *6*, 1164–1172.

(140) Shalom, Y.; Perelshtein, I.; Perkas, N.; Gedanken, A.; Banin, E. Catheters Coated with Zn-Doped CuO Nanoparticles Delay the Onset of Catheter-Associated Urinary Tract Infections. *Nano Res.* **2017**, *10*, 520–533.

(141) Hoyo, J.; Ivanova, K.; Guaus, E.; Tzanov, T. Multifunctional ZnO NPs-Chitosan-Gallic Acid Hybrid Nanocoating to Overcome Contact Lenses Associated Conditions and Discomfort. *J. Colloid Interface Sci.* **2019**, *543*, 114–121.

(142) Joost, U.; Juganson, K.; Visnapuu, M.; Mortimer, M.; Kahru, A.; Nõmmiste, E.; Joost, U.; Kisand, V.; Ivask, A. Photocatalytic Antibacterial Activity of Nano-TiO2 (Anatase)-Based Thin Films: Effects on Escherichia Coli Cells and Fatty

Acids. *J. Photochem. Photobiol. B Biol.* **2015**, *142*, 178–185.

(143) Sawai, J.; Himizu, K.; Yamamoto, O. Kinetics of Bacterial Death by Heated Dolomite Powder Slurry. *Soil Biol. Biochem.* **2005**, *37*, 1484–1489.

(144) Vidic, J.; Stankic, S.; Haque, F.; Ciric, D.; Le Goffic, R.; Vidy, A.; Jupille, J.; Delmas, B. Selective Antibacterial Effects of Mixed ZnMgO Nanoparticles. *J. Nanoparticle Res.* **2013**, *15*, 1595.

(145) Zhao, Y.; Ye, C.; Liu, W.; Chen, R.; Jiang, X. Tuning the Composition of AuPt Bimetallic Nanoparticles for Antibacterial Application. *Angew. Chemie - Int. Ed.* **2014**, *53*, 8127–8131.

(146) Yang, W.; Fortunati, E.; Gao, D.; Balestra, G. M.; Giovanale, G.; He, X.; Torre, L.; Kenny, J. M.; Puglia, D. Valorization of Acid Isolated High Yield Lignin Nanoparticles as Innovative Antioxidant/Antimicrobial Organic Materials. *ACS Sustain. Chem. Eng.* **2018**, *6*, 3502–3514.

(147) Singh, B. N.; Prateeksha; Upreti, D. K.; Singh, B. R.; Defoirdt, T.; Gupta, V. K.; De Souza, A. O.; Singh, H. B.; Barreira, J. C. M.; Ferreira, I. C. F. R.; Vahabi, K. Bactericidal, Quorum Quenching and Anti-Biofilm Nanofactories: A New Niche for Nanotechnologists. *Crit. Rev. Biotechnol.* **2017**, *37*, 525–540.

(148) Schiffelers, R. M.; Storm, G.; Bakker-Woudenberg, I. A. J. M. Therapeutic Efficacy of Liposomal Gentamicin in Clinically Relevant Rat Models. *Int. J. Pharm.* **2001**, *214*, 103–105.

(149) Sachetelli, S.; Beaulac, C.; Riffon, R.; Lagacé, J. Evaluation of the Pulmonary and Systemic Immunogenicity of Fluidosomes, a Fluid Liposomal-Tobramycin Formulation for the Treatment of Chronic Infections in Lungs. *Biochim. Biophys. Acta* **1999**, *1428*, 334–340.

(150) Ma, D. Hybrid Nanoparticles: An Introduction. In *Noble Metal-Metal Oxide Hybrid Nanoparticles: Fundamentals and Applications*; Mohapatra, S., Nguyen, T. A., Nguyen-Tr, P., Eds.; 2019; pp 3–6.

(151) Karakocak, B. B.; Liang, J.; Biswas, P.; Ravi, N. Hyaluronate Coating Enhances the Delivery and Biocompatibility of Gold Nanoparticles. *Carbohydr. Polym.* **2018**, *186*, 243–251.

(152) Francesko, A.; Cano Fossas, M.; Petkova, P.; Fernandes, M. M.; Mendoza, E.; Tzanov, T. Sonochemical Synthesis and Stabilization of Concentrated Antimicrobial Silver-Chitosan Nanoparticle Dispersions. *J. Appl. Polym. Sci.* **2017**, *134*, 1–8.

(153) Ferreres, G.; Bassegoda, A.; Hoyo, J.; Torrent-burgue, J.; Tzanov, T. Metal − Enzyme Nanoaggregates Eradicate Both Gram-Positive and Gram-Negative Bacteria and Their Bio Fi Lms ́,. *ACS Appl. Mater. Interfaces* **2018**.

(154) Slavin, Y. N.; Ivanova, K.; Hoyo, J.; Perelshtein, I.; Owen, G.; Haegert, A.; Lin, Y. Y.; Lebihan, S.; Gedanken, A.; Häfeli, U. O.; Tzanov, T.; Bach, H. Novel Lignin-Capped Silver Nanoparticles against Multidrug-Resistant Bacteria. *ACS Appl. Mater. Interfaces* **2021**, *13*, 22098–22109.

(155) Morena, A. G.; Bassegoda, A.; Hoyo, J.; Tzanov, T. Hybrid Tellurium-Lignin Nanoparticles with Enhanced Antibacterial Properties. *ACS Appl. Mater.*

Interfaces **2021**, *13*, 14885–14893.

(156) Ruden, S.; Hilpert, K.; Berditsch, M.; Wadhwani, P.; Ulrich, A. S. Synergistic Interaction between Silver Nanoparticles and Membrane-Permeabilizing Antimicrobial Peptides. *Antimicrob. Agents Chemother.* **2009**, *53*, 3538–3540.

(157) Ivanova, A.; Ivanova, K.; Tzanov, T. Inhibition of Quorum-Sensing: A New Paradigm in Controlling Bacterial Virulence and Biofilm Formation. In *Biotechnological Applications of Quorum Sensing Inhibitors*; Kalia, V. C., Ed.; Springer Singapore: Singapore, **2018**; pp 3–21.

(158) Meeker, D. G.; Jenkins, S. V.; Miller, E. K.; Beenken, K. E.; Loughran, A. J.; Powless, A.; Muldoon, T. J.; Galanzha, E. I.; Zharov, V. P.; Smeltzer, M. S.; Chen, J. Synergistic Photothermal and Antibiotic Killing of Biofilm-Associated Staphylococcus Aureus Using Targeted Antibiotic-Loaded Gold Nanoconstructs. *ACS Infect. Dis.* **2016**, *2*, 241–250.

(159) Li, X.; Sun, L.; Zhang, P.; Wang, Y. Novel Approaches to Combat Medical Device-Associated Biofilms. *Coatings* **2021**, *11*, 1–31.

(160) Wei, X.; Luo, M.; Liu, H. Preparation of the Antithrombotic and Antimicrobial Coating through Layer-by-Layer Self-Assembly of Nattokinase-Nanosilver Complex and Polyethylenimine. *Colloids Surfaces B Biointerfaces* **2014**, *116*, 418–423.

(161) Francesko, A.; Blandón, L.; Vázquez, M.; Petkova, P.; Morató, J.; Pfeifer, A.; Heinze, T.; Mendoza, E.; Tzanov, T. Enzymatic Functionalization of Cork Surface with Antimicrobial Hybrid Biopolymer/silver Nanoparticles. *ACS Appl. Mater. Interfaces* **2015**, *7*, 9792–9799.

(162) Anghel, I.; Grumezescu, A. M. Hybrid Nanostructured Coating for Increased Resistance of Prosthetic Devices to Staphylococcal Colonization. *Nanoscale Res. Lett.* **2013**, *8*, 6.

(163) Benetti, G.; Cavaliere, E.; Canteri, A.; Landini, G.; Rossolini, G. M.; Pallecchi, L.; Chiodi, M.; Van Bael, M. J.; Winckelmans, N.; Bals, S.; Gavioli, L. Direct Synthesis of Antimicrobial Coatings Based on Tailored Bi-Elemental Nanoparticles. *APL Mater.* **2017**, *5*, 36105.

(164) Srisang, S.; Boongird, A.; Ungsurungsie, M.; Wanasawas, P.; Nasongkla, N. In Vivo Catheterization Study of Chlorhexidine-Loaded Nanoparticle Coated Foley Urinary Catheters in Male New Zealand White Rabbits. *J. Biomed. Mater. Res. - Part B Appl. Biomater.* **2021**, *109*, 1836–1843.

(165) Lichter, J. A.; Van Vlietpa, K. J.; Rubner, M. F. Design of Antibacterial Surfaces and Interfaces: Polyelectrolyte Multilayers as a Multifunctional Platform. *Macromolecules* **2009**, *42*, 8573–8586.

(166) Caruso, F.; Schüler, C. Enzyme Multilayers on Colloid Particles: Assembly, Stability, and Enzymatic Activity. *Langmuir* **2000**, *16*, 9595–9603.

(167) Richardson, J. J.; Bjornmalm, M.; Caruso, F. Technology-Driven Layer-by-Layer Assembly of Nanofilms. *Science.* **2015**, *348*, aaa2491.

(168) Zhang, S.; Xing, M.; Li, B. Biomimetic Layer-by-Layer Self-Assembly of Nanofilms, Nanocoatings, and 3D Scaffolds for Tissue Engineering. *Int. J. Mol.*

Sci. **2018**, *19*, 1641.

(169) Cho, J.; Char, K.; Hong, J.-D.; Lee, K.-B. Fabrication of Highly Ordered Multilayer Films Using a Spin Self-assembly Method. *Adv. Mater.* **2001**, *13*, 1076–1078.

(170) Boudou, T.; Crouzier, T.; Ren, K.; Blin, G.; Picart, C. Multiple Functionalities of Polyelectrolyte Multilayer Films: New Biomedical Applications. *Adv. Mater.* **2010**, *22*, 441–467.

(171) Séon, L.; Lavalle, P.; Schaaf, P.; Boulmedais, F. Polyelectrolyte Multilayers: A Versatile Tool for Preparing Antimicrobial Coatings. *Langmuir* **2015**, *31*, 12856–12872.

(172) Cui, D.; Szarpak, A.; Pignot-Paintrand, I.; Varrot, A.; Boudou, T.; Detrembleur, C.; Jérôme, C.; Picart, C.; Auzély-Velty, R. Contact-Killing Polyelectrolyte Microcapsules Based on Chitosan Derivatives. *Adv. Funct. Mater.* **2010**, *20*, 3303–3312.

(173) Francesko, A.; Ivanova, K.; Hoyo, J.; Pérez-Rafael, S.; Petkova, P.; Fernandes, M. M.; Heinze, T.; Mendoza, E.; Tzanov, T. Bottom-up Layer-by-Layer Assembling of Antibacterial Freestanding Nanobiocomposite Films. *Biomacromolecules* **2018**, *19*, 3628–3636.

(174) Zhao, S.; Caruso, F.; Dähne, L.; Decher, G.; De Geest, B. G.; Fan, J.; Feliu, N.; Gogotsi, Y.; Hammond, P. T.; Hersam, M. C.; Khademhosseini, A.; Kotov, N.; Leporatti, S.; Li, Y.; Lisdat, F.; Liz-Marzán, L. M.; Moya, S.; Mulvaney, P.; Rogach, A. L.; Roy, S.; Shchukin, D. G.; Skirtach, A. G.; Stevens, M. M.; Sukhorukov, G. B.; Weiss, P. S.; Yue, Z.; Zhu, D.; Parak, W. J. The Future of Layer-by-Layer Assembly: A Tribute to ACS Nano Associate Editor Helmuth Möhwald. *ACS Nano* **2019**, *13*, 6151–6169.

(175) Johnston, A. P. R.; Cortez, C.; Angelatos, A. S.; Caruso, F. Layer-by-Layer Engineered Capsules and Their Applications. *Curr. Opin. Colloid Interface Sci.* **2006**, *11* (4), 203–209.

(176) Zhuk, I.; Jariwala, F.; Attygalle, A. B.; Wu, Y.; Libera, M. R.; Sukhishvili, S. A. Self-Defensive Layer-by-Layer Films with Bacteria-Triggered Antibiotic Release. *ACS Nano* **2014**, *8*, 7733–7745.

(177) Høiby, N.; Bjarnsholt, T.; Givskov, M.; Molin, S.; Ciofu, O. Antibiotic Resistance of Bacterial Biofilms. *Int. J. Antimicrob. Agents* **2010**, *35* (4), 322–332.

(178) Canaparo, R.; Foglietta, F.; Giuntini, F.; Della Pepa, C.; Dosio, F.; Serpe, L. Recent Developments in Antibacterial Therapy: Focus on Stimuli-Responsive Drug-Delivery Systems and Therapeutic Nanoparticles. *Molecules* **2019**, *24*, 1–15.

(179) Wu, Y.; Long, Y.; Li, Q.; Han, S.; Yang, Y.; Gao, H. Layer-by-Layer (LBL) Self-Assembled Biohybrid Nanomaterials for Efficient Antibacterial Applications. *Appl. Mater. Interfaces* 1–33.

(180) Cortese, B.; D'Amone, S.; Testini, M.; Ratano, P.; Palamà, I. E. Hybrid Clustered Nanoparticles for Chemo-Antibacterial Combinatorial Cancer Therapy. *Cancers*

(Basel). **2019**, *11*, 1–18.

(181) Zhao, Q.; Mao, Z.; Gao, C.; Shen, J. Assembly of Multilayer Microcapsules on CaCO3 Particles from Biocompatible Polysaccharides. *J. Biomater. Sci. Polym. Ed.* **2006**, *17*, 997–1014.

(182) Sangfai, T.; Dong, F.; Tantishaiyakul, V.; Jandt, K. D.; Lüdecke, C.; Boonrat, O.; Hirun, N. Layer-by-Layer Gelatin/chitosan Polyelectrolyte Coated Nanoparticles on Ti Implants for Prevention of Implant-Associated Infections. *Express Polym. Lett.* **2017**, *11*, 73–82.

(183) Gnanadhas, D. P.; Ben Thomas, M.; Elango, M.; Raichur, A. M.; Chakravortty, D. Chitosan-Dextran Sulphate Nanocapsule Drug Delivery System as an Effective Therapeutic against Intraphagosomal Pathogen Salmonella. *J. Antimicrob. Chemother.* **2013**, *68*, 2576–2586.

(184) Duan, S.; Zhao, X.; Su, Z.; Wang, C.; Lin, Y. Layer-by-Layer Decorated Nanoscale ZIF-8 with High Curcumin Loading Effectively Inactivates Gram-Negative and Gram-Positive Bacteria. *ACS Appl. Bio Mater.* **2020**, *3*, 3673–3680.

(185) Wang, X.; Cao, W.; Xiang, Q.; Jin, F.; Peng, X.; Li, Q.; Jiang, M.; Hu, B.; Xing, X. Silver Nanoparticle and Lysozyme/tannic Acid Layer-by-Layer Assembly Antimicrobial Multilayer on Magnetic Nanoparticle by an Eco-Friendly Route. *Mater. Sci. Eng. C* **2017**, *76*, 886–896.

(186) Wang, X.; Deng, A.; Cao, W.; Li, Q.; Wang, L.; Zhou, J.; Hu, B.; Xing, X. Synthesis of Chitosan/poly (Ethylene Glycol)-Modified Magnetic Nanoparticles for Antibiotic Delivery and Their Enhanced Anti-Biofilm Activity in the Presence of Magnetic Field. *J. Mater. Sci.* **2018**, *53*, 6433–6449.

(187) Petkova, P.; Francesko, A.; Perelshtein, I.; Gedanken, A.; Tzanov, T. Simultaneous Sonochemical-Enzymatic Coating of Medical Textiles with Antibacterial ZnO Nanoparticles. *Ultrason. Sonochem.* **2016**, *29*, 244–250.

(188) IUPAC. Top ten emerging technologies in Chemistry 2021.

(189) Natan, M.; Edin, F.; Perkas, N.; Yacobi, G.; Perelshtein, I.; Segal, E.; Homsy, A.; Laux, E.; Keppner, H.; Rask-andersen, H.; Gedanken, A.; Banin, E. Two Are Better than One : Combining ZnO and MgF 2 Nanoparticles Reduces Streptococcus Pneumoniae and Staphylococcus Aureus Biofi Lm Formation on Cochlear Implants. *Adv. Funct. Mater.* **2016**, *26*, 2473–2481.

(190) Perelshtein, I.; Applerot, G.; Perkas, N.; Grinblat, J.; Gedanken, A. A One-Step Process for the Antimicrobial Finishing of Textiles with Crystalline TiO 2 Nanoparticles. *Chem. - A Eur. J.* **2012**, *18*, 4575–4582.

(191) Trends, R.; Evidences, C. *Nano Medicine and Nano Safety*; Das M.K., P. Y. V., Ed.; Springer, Singapore, 2020.

(192) Perkas, N.; Amirian, G.; Dubinsky, S.; Gazit, S.; Gedanken, A. Ultrasound-Assisted Coating of Nylon 6,6 with Silver Nanoparticles. *J. Appl. Polym. Sci.* **2007**, *104*, 1423–1430.

(193) Rahn, K.; Diamantoglou, M.; Klemm, D.; Berghmans, H.; Heinze, T. Homogeneous Synthesis of Cellulose P-Toluenesulfonates in N , N-Dimethylacetamidel LiCl Solvent System. *Die Angew. Makromol. Chemie* **1996**,

238, 143–163.

(194) Salman, H. H. A.; Goni Azcarate, I.; Esparza Catalan, I. Nanoparticles Comprising a Vegetable Hydrophobic Protein and a Water Miscible Non-Volatile Organic Solvent and Uses Thereof. WO2013120856, 2013.

(195) Damjanovich, S.; Bähr, W.; Jovin, T. M. The Functional and Fluorescence Properties of Escherichia Coli RNA Polymerase Reacted with Fluorescamine. *Eur. J. Biochem.* **1977**, *72*, 559–569.

(196) Chen, Y.; Zhang, Y. Fluorescent Quantification of Amino Groups on Silica Nanoparticle Surfaces. *Anal. Bioanal. Chem.* **2011**, *399*, 2503–2509.

(197) Abu-Sharkh, B. Stability and Structure of Polyelectrolyte Multilayers Deposited from Salt Free Solutions. *J. Chem. Phys.* **2005**, *123*, 114907−114913.

(198) Arhin, F. F.; McKay, G. A.; Beaulieu, S.; Sarmiento, I.; Parr, T. R.; Moeck, G. Time-Kill Kinetics of Oritavancin and Comparator Agents against Streptococcus Pyogenes. *Int. J. Antimicrob. Agents* **2009**, *34*, 550–554.

(199) Macdonald, T. J.; Wu, K.; Sehmi, S. K.; Noimark, S.; Peveler, W. J.; du Toit, H.; Voelcker, N. H.; Allan, E.; MacRobert, A. J.; Gavriilidis, A.; Parkin, I. P. Thiol-Capped Gold Nanoparticles Swell-Encapsulated into Polyurethane as Powerful Antibacterial Surfaces Under Dark and Light Conditions. *Sci. Rep.* **2016**, *6*, No. 39272.

(200) Hamblin, M. R.; Hasan, T. Photodymamic Therapy: A New Antimicrobial Approach to Infectious Disease? *Photochem Photobiol Sci.* **2004**, *3*, 436–450.

(201) Másson, M.; Holappa, J.; Hjálmarsdóttir, M.; Rúnarsson, Ö. V.; Nevalainen, T.; Järvinen, T. Antimicrobial Activity of Piperazine Derivatives of Chitosan. *Carbohydr. Polym.* **2008**, *74*, 566–571.

(202) Lim, S.-H.; Hudson, S. M. Review of Chitosan and Its Derivatives as Antimicrobial Agents and Their Uses as Textile Chemicals. *J. Macromolacular Sci. Part C Polym. Rev.* **2003**, *43*, 223–269.

(203) Thoma, L. M.; Boles, B. R.; Kuroda, K. Cationic Methacrylate Polymers as Topical Antimicrobial Agents against *Staphylococcus Aureus* Nasal Colonization. *Biomacromolecules* **2014**, *15*, 2933–2943.

(204) Zhang, P.; Lu, H.; Chen, H.; Zhang, J.; Liu, L.; Lv, F.; Wang, S. Cationic Conjugated Polymers-Induced Quorum Sensing of Bacteria Cells. *Anal. Chem.* **2016**, *88*, 2985–2988.

(205) Li, Y.; Xu, Y.; Fleischer, C. C.; Huang, J.; Lin, R.; Yang, L.; Mao, H. Impact of Anti-Biofouling Surface Coatings on the Properties of Nanomaterials and Their Biomedical Applications. *J. Mater. Chem. B* **2018**, *6*, 9–24.

(206) Bračič, M.; Fras-Zemljič, L.; Pérez, L.; Kogej, K.; Stana-Kleinschek, K.; Kargl, R.; Mohan, T. Protein-Repellent and Antimicrobial Nanoparticle Coatings from Hyaluronic Acid and a Lysine-Derived Biocompatible Surfactant. *J. Mater. Chem. B* **2017**, *5*, 3888–3897.

(207) Som, A.; Gregory, N. T. Influence of Lipid Composition on Membrane Activity of Antimicrobial Phenylene Ethynylene Oligomers. *ACS J. Phys. Chem. B* **2008**,

112, 3495–3502.

(208) Lee, P. C.; Melsel, D. Adsorption and Surface-Enhanced Raman of Dyes on Silver and Gold Sols. *J. Phys. Chem.* **1982**, *86*, 3391–3395.

(209) Steindler, L.; Venturi, V. Detection of Quorum-Sensing N -Acyl Homoserine Lactone Signal Molecules by Bacterial Biosensors. *FEMS Microbiol Lett* **2007**, *266*, 1–9.

(210) Rehman, Z. U.; Leiknes, T. Quorum-Quenching Bacteria Isolated From Red Sea Sediments Reduce Biofilm Formation by Pseudomonas Aeruginosa. *Front. Microbiol.* **2018**, *9*, 1354.

(211) Dwivedi, S.; Wahab, R.; Khan, F.; Mishra, Y. K.; Musarrat, J.; Al-khedhairy, A. A. Reactive Oxygen Species Mediated Bacterial Biofilm Inhibition via Zinc Oxide Nanoparticles and Their Statistical Determination. *PLoS One* **2014**, *9*, e111289.

(212) Ali, S. G.; Ansari, M. A.; Khan, H. M.; Jalal, M.; Mahdi, A. A.; Cameotra, S. S. Antibacterial and Antibiofilm Potential of Green Synthesized Silver Nanoparticles against Imipenem Resistant Clinical Isolates of P . Aeruginosa. *Bionanoscience* **2018**, *8*, 544–553.

(213) Shirtliff, M. E.; Mader, J. T.; Camper, A. K. Molecular Interactions in Biofilms. *Chem. Biol.* **2002**, *9*, 859–871.

(214) Paul, D.; Kim, Y. S.; Ponnusamy, K.; Kweon, J. H. Application of Quorum Quenching to Inhibit Biofilm Formation. *Environ. Eng. Sci.* **2009**, *26*, 1319–1324.

(215) Chow, J. Y.; Yang, Y.; Tay, S. B.; Chua, K. L.; Yew, W. S. Disruption of Biofilm Formation by the Human Pathogen Acinetobacter Baumannii Using Engineered Quorum-Quenching Lactonases. *Antimicrob. Agents Chemother.* **2014**, *58*, 1802–1805.

(216) Giri, K.; Yepes, L. R.; Duncan, B.; Parameswaran, P. K.; Yan, B.; Jiang, Y.; Bilska, M.; Moyano, D. M.; Thompson, M.; Rotello, V. M.; Prakash, Y. S. Targeting Bacterial Biofilms via Surface Engineering of Gold Nanoparticles. *RSC Adv.* **2015**, *5*, 105551–105559.

(217) Venkatesh, M.; Barathi, V. A.; Goh, E. T. L.; Anggara, R.; Fazil, M. H. U. T.; Ng, A. J. Y.; Harini, S.; Aung, T. T.; Fox, S. J.; Liu, S.; Yang, L.; Barkham, T. M. S.; Loh, X. J.; Verma, N. K.; Beuerman, R. W.; Lakshminarayanana, R. Antimicrobial Activity and Cell Selectivity of Synthetic and Biosynthetic Cationic Polymers. *Antimicrob Agents Chemother* **2017**, *61*, e00469-17.

(218) Pelgrift, R. Y.; Friedman, A. J. Nanotechnology as a Therapeutic Tool to Combat Microbial Resistance. *Adv. Drug Deliv. Rev.* **2013**, *65*, 1803–1815.

(219) Akter, M.; Sikder, T.; Rahman, M.; Ullah, A. K. M. A.; Fatima, K.; Hossain, K. F. B.; Banik, S.; Hosokawa, T.; Saito, T.; Kurasaki, M. A Systematic Review on Silver Nanoparticles-Induced Cytotoxicity : Physicochemical Properties and Perspectives. *J. Adv. Res.* **2017**, *9*, 1–16.

(220) Das, B.; Tripathy, S.; Adhikary, J.; Chattopadhyay, S.; Mandal, D.; Dash, S. K.; Das, S.; Dey, A.; Dey, S. K.; Das, D.; Roy, S. Surface Modification Minimizes

the Toxicity of Silver Nanoparticles: An in Vitro and in Vivo Study. *J. Biol. Inorg. Chem.* **2017**, *22*, 893–918.

(221) Gagliardi, A.; Paolino, D.; Iannone, M.; Palma, E.; Fresta, M.; Cosco, D. Sodium Deoxycholate-Decorated Zein Nanoparticles for a Stable Colloidal Drug Delivery System. *Int. J. Nanomedicine* **2018**, *13*, 601–614.

(222) Dai, L.; Sun, C.; Wang, D.; Gao, Y. The Interaction between Zein and Lecithin in Ethanol-Water Solution and Characterization of Zein-Lecithin Composite Colloidal Nanoparticles. *PLoS One* **2016**, *11*, e0167172.

(223) Podaralla, S.; Perumal, O. Influence of Formulation Factors on the Preparation of Zein Nanoparticles. *AAPS PharmSciTech* **2012**, *13*, 919–927.

(224) Padua, G. W.; Guardiola, L. V. Microcapsules Produced from Zein. In *Microencapsulation and Microspheres for Food Applications*; Sagis, L. M. C., Ed.; Elsevier Inc., 2015; *Vol. 1*, pp. 3–20.

(225) Escosura-Muniz, A. D. La; Ivanova, K.; Tzanov, T. Electrical Evaluation of Bacterial Virulence Factors Using Nanopores. *ACS Appl. Mater. Interfaces* **2019**, *11*, 13140–13146.

(226) Welch, N. G.; Scoble, J. A.; Muir, B. W.; Pigram, P. J. Orientation and Characterization of Immobilized Antibodies for Improved Immunoassays. *Biointerphases* **2017**, *12*, 02D301.

(227) Chouhan, S.; Sharma, K.; Guleria, S. Antimicrobial Activity of Some Essential Oils — Present Status and Future Perspectives. *Medicines* **2017**, *4*, 58.

(228) Ciandrini, E.; Campana, R.; Federici, S.; Manti, A.; Battistelli, M.; Falcieri, E.; Papa, S.; Baffone, W. In Vitro Activity of Carvacrol against Titanium-Adherent Oral Biofilms and Planktonic Cultures. *Clin. Oral Investig.* **2014**, *18*, 2001–2013.

(229) Alexander, T. E.; Lozeau, L. D.; Camesano, T. A. QCM-D Characterization of Time-Dependence of Bacterial Adhesion. *Cell Surf.* **2019**, *5*, 100024.

(230) Poitras, C.; Tufenkji, N. A QCM-D-Based Biosensor for E. Coli O157:H7 Highlighting the Relevance of the Dissipation Slope as a Transduction Signal. *Biosens. Bioelectron.* **2009**, *24*, 2137–2142.

(231) Kahl, B. C.; Becker, K.; Löffler, B. Clinical Significance and Pathogenesis of Staphylococcal Small Colony. *Am. Soc. Microbiol.* **2016**, *29*, 401–427.

(232) Landis, R. F.; Li, C.-H.; Gupta, A.; Lee, Y.-W.; Yazdani, M.; Ngernyuan, N.; Altinbasak, I.; Mansoor, S.; Khichi, M. A. S.; Sanyal, A.; Rotello, V. M. Biodegradable Nanocomposite Antimicrobials for the Eradication of Multidrug-Resistant Bacterial Biofilms Without Accumulated Resistance. *J Am Chem Soc* **2018**, *140*, 6176–6182.

(233) Singh, K.; Shandilya, M.; Kundu, S.; Kayastha, A. M. Heat, Acid and Chemically Induced Unfolding Pathways, Conformational Stability and Structure-Function Relationship in Wheat α-Amylase. *PLoS One* **2015**, *10*, e0129203.

(234) Blanco, C. D.; Ortner, A.; Dimitrov, R.; Navarro, A.; Mendoza, E.; Tzanov, T. Building an Antifouling Zwitterionic Coating on Urinary Catheters Using an

Enzymatically Triggered Bottom-Up Approach. *Appl. Mater. Interfaces* **2014**, *6*, 11385−11393.

(235) David, C. A.; Galceran, J.; Quattrini, F.; Puy, J.; Rey-Castro, C. Dissolution and Phosphate-Induced Transformation of ZnO Nanoparticles in Synthetic Saliva Probed by AGNES without Previous Solid-Liquid Separation. Comparison with UF-ICP-MS. *Environ. Sci. Technol.* **2019**, *53*, 3823–3831.

(236) Venkatesh, C.; Laurenti, M.; Bandeira, M.; Lanzagorta, E.; Lucherini, L.; Cauda, V.; Devine, D. M. Biodegradation and Antimicrobial Properties of Zinc Oxide–polymer Composite Materials for Urinary Stent Applications. *Coatings* **2020**, *10*, 1–22.

(237) Shimanovich, U.; Perelshtein, I.; Cavaco-Paulo, A.; Gedanken, A. Releasing Dye Encapsulated in Proteinaceous Microspheres on Conductive Fabrics by Electric Current. *ACS Appl. Mater. Interfaces* **2012**, *4*, 2926–2930.

(238) Monteiro, C.; Costa, F.; Pirttilä, A. M.; Tejesvi, M. V.; Martins, M. C. L. Prevention of Urinary Catheter-Associated Infections by Coating Antimicrobial Peptides from Crowberry Endophytes. *Sci. Rep.* **2019**, *9*, 1–14.

(239) Sharma, G.; Sharma, S.; Sharma, P.; Chandola, D.; Dang, S.; Gupta, S.; Gabrani, R. Escherichia Coli Biofilm: Development and Therapeutic Strategies. *J. Appl. Microbiol.* **2016**, *121*, 309–319.

(240) Limoli, D. H.; Jones, C. J.; Wozniak, D. J. Bacterial Extracellular Polysaccharides in Biofilm Formation and Function. *Microbiol. Spectr.* **2015**, *3*, 1–30.

(241) Sirelkhatim, A.; Mahmud, S.; Seeni, A.; Kaus, N. H. M.; Ann, L. C.; Bakhori, S. K. M.; Hasan, H.; Mohamad, D. Review on Zinc Oxide Nanoparticles: Antibacterial Activity and Toxicity Mechanism. *Nano-Micro Lett.* **2015**, *7*, 219–242.

(242) Morris, N. S.; Stickler, D. J.; Mclean, R. J. C. The Development of Bacterial Biofilms on Indwelling Urethral Catheters. *World J. Urol.* **1999**, *17*, 345–350.

(243) Yavari, S. A.; Castenmiller, S. M.; van Strijp, J. A. G.; Croes, M. Combating Implant Infections: Shifting Focus from Bacteria to Host. *Adv. Mater.* **2020**, *25*, 2002962.

(244) Saint, S. Clinical and Economic Consequences of Nosocomial Catheter-Related Bacteriuria. *Am. J. Infect. Control* **2000**, *28*, 68–75.

(245) Karygianni, L.; Ren, Z.; Koo, H.; Thurnheer, T. Biofilm Matrixome: Extracellular Components in Structured Microbial Communities. *Trends Microbiol.* **2020**, *28*, 668–681.

(246) Stepanović, S.; Vuković, D.; Ježek, P.; Pavlović, M.; Švabic-Vlahović, M. Influence of Dynamic Conditions on Biofilm Formation by Staphylococci. *Eur. J. Clin. Microbiol. Infect. Dis.* **2001**, *20*, 502–504.

(247) Fiandra, L.; Bonfanti, P.; Piunno, Y.; Nagvenkar, A. P.; Perlesthein, I.; Gedanken, A.; Saibene, M.; Colombo, A.; Mantecca, P. Hazard Assessment of Polymer-Capped CuO and ZnO Nanocolloids: A Contribution to the Safe-by-Design Implementation of Biocidal Agents. *NanoImpact* **2020**, *17*, 100195.

(248) Mody, L.; Juthani-Mehta, M. Urinary Tract Infections in Older Women: A Clinical Review. *JAMA - J. Am. Med. Assoc.* **2014**, *311*, 844–854.

(249) Xiong, S.; Liu, X.; Deng, W.; Zhou, Z.; Li, Y.; Tu, Y.; Chen, L.; Wang, G.; Fu, B. Pharmacological Interventions for Bacterial Prostatitis. *Front. Pharmacol.* **2020**, *11*, 1–18.

(250) Colodner, R.; Eliasberg, T.; Chazan, B.; Raz, R. Clinical Significance of Bacteriuria with Low Colony Counts of Enterococcus Species. *Eur. J. Clin. Microbiol. Infect. Dis.* **2006**, *25*, 238–241.

(251) Lacerda Mariano, L.; Ingersoll, M. A. The Immune Response to Infection in the Bladder. *Nat. Rev. Urol.* **2020**, *17*, 439–458.

(252) Desalegn, G.; Pabst, O. Inflammation Triggers Immediate rather than Progressive Changes in Monocyte Differentiation in the Small Intestine. *Nat. Commun.* **2019**, *10*, 1–14.

(253) Harcourt-Brown, F. M.; Harcourt-Brown, S. Clinical Value of Blood Glucose Measurement in Pet Rabbits. *Vet. Rec.* **2012**, *170*, 674.

(254) Melillo, A. Rabbit Clinical Pathology. *J. Exot. Pet Med.* **2007**, *16*, 135–145.

(255) Döhrmann, S.; Cole, J. N.; Nizet, V. Conquering Neutrophils. *PLoS Pathog.* **2016**, *12*, 1–8.